



**HAL**  
open science

## Deterministic placement of doping atoms on silanol surfaces for ultimate devices

Laurent Mathey

► **To cite this version:**

Laurent Mathey. Deterministic placement of doping atoms on silanol surfaces for ultimate devices. Other. Université Claude Bernard - Lyon I, 2012. English. NNT : 2012LYO10235 . tel-00908954

**HAL Id: tel-00908954**

**<https://theses.hal.science/tel-00908954>**

Submitted on 25 Nov 2013

**HAL** is a multi-disciplinary open access archive for the deposit and dissemination of scientific research documents, whether they are published or not. The documents may come from teaching and research institutions in France or abroad, or from public or private research centers.

L'archive ouverte pluridisciplinaire **HAL**, est destinée au dépôt et à la diffusion de documents scientifiques de niveau recherche, publiés ou non, émanant des établissements d'enseignement et de recherche français ou étrangers, des laboratoires publics ou privés.

Université Claude Bernard  Lyon 1

N° d'ordre  
235-2012



Année 2012

THESE DE L'UNIVERSITE DE LYON

Délivrée par

L'UNIVERSITE CLAUDE BERNARD LYON 1

ECOLE DOCTORALE

CHIMIE (ED206)

DIPLOME DE DOCTORAT

(arrêté du 7 août 2006)

soutenue publiquement le 5 novembre 2012

par

M. Laurent MATHEY

TITRE :

**Placement déterministe de dopants pour dispositifs ultimes**

Directeur de thèse : M. Christophe COPERET

JURY :  
M. Didier BOURISSOU  
M. Christophe COPERET  
M. Brice GAUTIER  
M. François MARTIN  
M. Dominique MASSIOT  
M. Marc SANQUER  
Mme Chloé THIEULEUX

RAPPORTEURS : M. Didier BOURISSOU  
M. Marc SANQUER



# UNIVERSITE CLAUDE BERNARD - LYON 1

Président de l'Université

M. François-Noël GILLY

Vice-président du Conseil d'Administration

M. le Professeur Hamda BEN HADID

Vice-président du Conseil des Etudes et de

M. le Professeur Philippe LALLE

Vice-président du Conseil Scientifique

M. le Professeur Germain GILLET

Secrétaire Général

M. Alain HELLEU

## **COMPOSANTES SANTE**

Faculté de Médecine Lyon Est – Claude Bernard

Directeur : M. le Professeur J. ETIENNE

Faculté de Médecine et de Maïeutique Lyon Sud – Charles Mérieux  
UFR d'Odontologie

Administrateur provisoire : M. le Professeur G.  
KIRKORIAN

Institut des Sciences Pharmaceutiques et Biologiques

Directeur : M. le Professeur D. BOURGEOIS

Institut des Sciences et Techniques de la Réadaptation

Directeur : Mme la Professeure C. VINCIGUERRA.

Département de formation et Centre de Recherche en Biologie  
Humaine

Directeur : M. le Professeur Y. MATILLON

Directeur : M. le Professeur P. FARGE

## **COMPOSANTES ET DEPARTEMENTS DE SCIENCES ET TECHNOLOGIE**

Faculté des Sciences et Technologies

Directeur : M. le Professeur F. De MARCHI

Département Biologie

Directeur : M. le Professeur F. FLEURY

Département Chimie Biochimie

Directeur : Mme le Professeur H. PARROT

Département GEP

Directeur : M. N. SIAUVE

Département Informatique

Directeur : M. le Professeur S. AKKOUCHE

Département Mathématiques

Directeur : M. le Professeur A. GOLDMAN

Département Mécanique

Directeur : M. le Professeur H. BENHADID

Département Physique

Directeur : Mme S. FLECK

Département Sciences de

Directeur : Mme la Professeure I. DANIEL

UFR Sciences et Techniques des Activités Physiques et Sportives

Directeur : M. C. COLLIGNON

Observatoire de Lyon

Directeur : M. B. GUIDERDONI

Polytech Lyon

Directeur : M. P. FOURNIER

Ecole Supérieure de Chimie Physique Electronique

Directeur : M. G. PIGNAULT

Institut Universitaire de Technologie de Lyon 1

Directeur : M. C. VITON

Institut Universitaire de Formation des Maîtres

Directeur : M. R. BERNARD

Institut de Science Financière et d'Assurances

Directeur : Mme la Professeure V. MAUME-  
DESCHAMPS



## REMERCIEMENTS

---

Les travaux présentés dans cette thèse se sont déroulés d'octobre 2009 à octobre 2012 dans le cadre d'une collaboration entre le CEA Grenoble, CPE Lyon, le CNRS et l'Université Lyon 1 ayant abouti à la mise en place d'une plateforme « Nanochimie » inauguré en janvier 2010. Ce laboratoire est rattaché à l'UMR 5265, C2P2, Chimie, Catalyse, Polymérisation et Procédés, dirigé par Mme Bernadette Charleux.

Je tiens en premier lieu à remercier MM. Bourissou et Sanquer qui ont accepté de juger ce travail en tant que rapporteurs. Je remercie aussi MM. Gautier et Massiot d'avoir accepté de faire partie du jury, témoignant ainsi leur intérêt pour ces travaux.

Merci à mes encadrants, François Martin, qui a su me faire découvrir le monde du CEA et de la microélectronique, à Chloé Thieuleux, toujours prête à discuter de science pour débloquer une situation et toujours dynamique, et enfin Christophe Copéret pour sa disponibilité, son exigence et sa patience à mon égard durant ces trois années, mais aussi pour les discussions, aussi bien scientifiques que « païennes ».

Merci à toute l'équipe du C2P2, en particulier M. Laurent Veyre, véritable Grand Horloger de la plateforme Nanochimie sans qui le laboratoire n'aurait pu être ce qu'il est. Merci aussi à Mmes Anne Baudoin, à présent au laboratoire de RMN de M. Fenet, et Christine Lucas pour leur aide précieuse en RMN. Merci à M. François Bayard pour son aide en informatique.

Du côté isérois, je tiens à remercier MM Hervé Fontaine et Karim Ykache pour m'avoir aidé à effectuer des manipulations précieuses. Un grand merci à Mme Virginie Enyedi et M. Jean Guerrero pour leur disponibilité, leur gentillesse et leur aide indispensable. Merci à MMs Nicolas Chevalier et Denis Mariolle pour leur aide, merci encore à M. Chevalier pour son aide lors de la rédaction. Je tiens encore à remercier MMs Jean-Paul Barnes et Marc Veillerot pour leur expertise en Tof-SIMS. Enfin, merci à M. Carmello Scibetta pour ses mesures d'épaisseurs de couche.

Je souhaite encore remercier MM Maxime Berthe et Bruno Grandidier, de l'Institut d'Electronique, de Microélectronique et de Nanotechnologie (IEMN) de Lille pour les mesures qu'ils ont effectuées et qui permis de donner à cette thèse tout son sens.

Je ne saurais oublier de remercier les étudiants du LCOMS, en particulier mes camarades du Copéret Group Pierre Laurent, gai luron chantant des vendredi après-midi et chef cuistot hors pair, et Arthur Roussey, compagnon de labeur pince-sans-rire. Je tiens bien évidemment à exprimer mes plus vifs remerciements à David Gajan pour m'avoir formé aux techniques COMS et pour son incroyable altruisme, « toujours prêt », et sans lequel j'aurais été incapable de me faire au COMS, à Raphael Wischert pour les calculs qu'il a eu le courage d'effectuer et surtout à Anthony Kermagoret pour ses conseils, son sérieux ainsi que pour son humour ravageur et les fléchettes. Merci à Philippe Arquillière pour m'avoir supporté comme voisin de bureau, à Léa Chancelier pour les balles de squash, à Inga Helgadottir pour les films grecs et les discussions eddiques, Leila Moura pour les cauchemars et les ramens et Yasemin Kaya pour les fous rires.

Merci aussi aux camarades d'études, Morgane pour les concerts les plus violents, Issao pour le whisky, Fneuh pour les discussions et jeux de plateau, Mylène pour le cinéma, James pour son accent, à mes « eurofriends » du MEU, Elena, Jasiiek, Thanos, Callum... pour les bons moments m'ayant permis de me déconnecter quelques heures un peu du monde de la chimie.

Merci enfin et tout particulièrement à mes parents et à mes sœurs pour leur patience à mon égard, l'inflexible capacité à me ramener sur terre et leur indéfectible soutien durant ces trois années.

**RESUME** : Placement déterministe de dopants sur surfaces pour dispositifs ultimes

En raison de la miniaturisation des dispositifs pour semi-conducteurs, le caractère aléatoire de la distribution de dopants dans un dispositif devient un paramètre critique pour les performances de ce dernier. Le but de ce travail est de valider une stratégie de dopage du silicium par un positionnement contrôlé de molécules, alternatif aux implantations, afin de limiter la variabilité de la tension de seuil. Nous avons choisi de contrôler la densité des sites et le positionnement des dopants en combinant le contrôle de la densité des sites d'ancrage et l'utilisation de molécules à fort encombrement stérique. Ceci a été réalisé en étudiant dans un premier temps le greffage de bore sur les silanols de silice amorphe partiellement traitée en température, à partir de molécules porteuses présentant des ligands de différentes tailles et des symétries ; le modèle de greffage a pu être déterminé en utilisant différentes techniques analytiques (IR-DRIFT, multi-core SSRMN et analyses élémentaires). L'élimination des ligands par un traitement thermique a permis de réaliser la fixation du Bore sur la silice avec un rendement supérieur à 96%. Cette méthode a été transférée avec succès à des wafers de silicium recouverts de silice native. Le recuit à haute température permettant la redistribution du bore dans le silicium a été ensuite validé par l'analyse VPD-ICPMS de l'oxyde greffé couplées aux mesures de profil de dopant dans le silicium obtenues par TofSIMS. Ce traitement a conduit à définir un procédé optimal par greffage sur silice mince, donnant des concentrations de dopant dans le silicium équivalentes à celles rapportées par la littérature sur silicium désoxydé, et sans passivation additionnelle de silice pour éviter la volatilisation du Bore greffé. En effet, la taille des ligands permet de contrôler la volatilisation du bore pendant recuit. Les analyses électriques par spectroscopie à effet tunnel ont confirmé l'activation électrique du dopant apporté par greffage et diffusé dans le silicium.

**ABSTRACT**: Deterministic placement of doping atoms on silanol surfaces for ultimate devices

With the everlasting shrinking of semiconductor devices, the randomness of dopant distribution within a device becomes more likely to critically impact the performance of the latter. The aim of this work is to validate a silicon doping strategy through a controlled positioning of molecules in place of conventional implantations in order to limit the variability of the threshold tension. In contrast to previous works, doping atoms were directly grafted onto a thin silica layer and not onto a bare silicon surface. Here, we chose to control both site density and positioning by combining the control of site anchoring density and the use of sterically hindered molecules to yield a finely structured doped surface. This was carried out by first optimizing this approach by studying the grafting of boron compounds with ligands of various sizes and symmetries on the surface silanols of non-porous amorphous silica partially treated at high temperatures (700 °C) as a model system. This allowed obtaining a fully characterization of surface species through combined analytical techniques (IR-DRIFT, solid-state multi-core NMR and elemental analyses). The ligands were then eliminated by a thermal treatment, yielding surface boronic acids characterized by IR-DRIFT and NMR with optimal density (> 96%,  $6.7 \cdot 10^{13}$  B.cm<sup>-2</sup>). This technology was then successfully transferred to silicon wafers covered with native silica as evidenced by ICPMS analyses of the grafted oxide layer removed in HF droplet (VPD). Subsequent high temperature annealing step without capping in order to trigger diffusion of boron was then validated on silicon wafers using ICPMS in HF-dipped oxide and in silicon by TofSIMS profile measurements. Such treatment led to a dopant concentration in the silicon matrix equivalent to that reported in the literature (e.g. direct grafting on silicon and cap during annealing). Electrical analyses by tunnel spectroscopy showed the efficiency of the annealing step and confirmed the dopant amount in the surface layer of the silicon wafer.





## TABLE OF CONTENTS

---

Abbreviations.....	xiii
Introduction .....	1
Chapter 1 : Bibliography .....	5
Summary of the Chapter.....	6
Moore’s Law: the importance of device shrinking and integration .....	7
1. Doping of semiconductors .....	10
1.1. Effect of doping on a semiconductor .....	10
1.2. The interest of doping.....	11
1.3. Doping of the substrate.....	12
1.3.1. Ion implantation .....	12
1.3.2. Possibility of alternative nanomasking methods for deterministic doping.....	16
1.3.2.1. Nanometric stamping .....	16
1.3.2.2. Polymer templating .....	18
1.3.3. Doping by grafting .....	20
2. Silica surface chemistry .....	23
2.1. Properties of amorphous silica.....	23
2.1.1. Surface species on silica .....	23
2.1.2. Dehydration and dehydroxylation of silica .....	24
2.2. Characterisation methods.....	25
2.2.1. Infrared spectroscopy.....	26
2.2.2. Solid-State NMR .....	27
2.2.3. Chemistry of surface silanols .....	28
2.2.3.1. Surface organometallic chemistry .....	28

2.2.3.2. Boron chemistry on silica .....	29
2.2.3.2. Phosphorus chemistry on silica .....	30
2.2.3. Conclusion .....	32
References .....	34
Chapter 2 : Application of the grafting strategy to a P-dopant, the case of boron .....	39
Summary of the Chapter.....	40
Introduction: establishment of a dispersion strategy .....	41
1. Defining a grafting strategy .....	42
1.1. Boranes.....	42
1.2. Oxaboroles.....	47
2. Tuning the molecules .....	49
2.1. Improving the reactivity C <sub>2</sub> oxaboroles .....	49
2.2. Synthesis of an oxy-dioxaborole.....	51
2.3. C <sub>3</sub> tri-coordinated molecules.....	53
2.3.1 Tri-tert-butylborate.....	53
2.3.1. Tri-tert-butylsilanolborate.....	54
2.4.2. Use of a pyrrolidinylborane .....	56
3. Improving grafting by self-positioning of C <sub>3v</sub> molecules .....	58
3.3. Synthesis of a cage-shaped C <sub>3v</sub> molecule .....	58
3.4. Grafting of a cage-shaped borate.....	59
3.5. Determination of the mechanism of grafting .....	62
4. Elimination of the ligands.....	66
4.3. Outcome of the different calcination experiments.....	66
4.4. Determination of the nature of the calcined species.....	70
4.4.1. Determination of the nature of the calcined species.....	70
4.4.2 Determination of the acidity of the formed surface species .....	71

Conclusion.....	73
References .....	74
Chapter 3 : Application of the strategy to N-dopant, the case of Phosphorus, an NMR study.....	77
Summary of the Chapter.....	78
Introduction .....	79
1. Towards a permanent-bonding strategy.....	79
1.1. Grafting of a phosphite.....	79
1.2. Adsorption of phosphonate .....	82
2. Self-positioning as a better placement regulating tool.....	86
2.1. Adsorption of phosphine.....	86
2.2. Improving the umbrella effect: POSS as a sterically hindered ligand .....	88
2.2.1. Grafting and geometry characterisation of POSS-P .....	89
2.2.2. NMR analyses and computational modelling.....	92
2.2.2.1. NMR spectroscopy of surface species of P-POSS on SiO <sub>2-(700)</sub> .....	92
2.2.2.2. Calculating tensors for the grafted compound on SiO <sub>2-(200)</sub> .....	96
2.2.3. Computational structures as a discriminating method .....	99
2.3. Grafting of phosphonium .....	106
3. Elimination of the ligands.....	107
Conclusion.....	111
References .....	112
Chapter 4 : Transposition to silicon wafers: Feasibility, doping amounts and efficiency.....	115
Summary of the Chapter.....	116
Introduction .....	117
1. Transferability of the concept onto Si-wafers .....	117
1.1. Grafting of an organometallic species as a silanol revelator .....	117
2. Diffusion of B within the silicon wafer by annealing .....	118

2.1. Grafting experiments and RTP annealing .....	119
2.2. Analysis of the oxide layer .....	119
2.3. Analysis of the near surface of the silicon matrix.....	121
2.4. Surface imaging and annealing improvement .....	125
3. Diffusion of P within the silicon matrix.....	128
3.1. Phosphorus quantification by ICP-MS after annealing .....	128
3.2. SIMS analysis of the near surface of silicon .....	129
4. Electrical efficiency of the doped wafers.....	131
Conclusion.....	137
References .....	139
Conclusion.....	141
Experimental Part .....	147
Appendices.....	175

## Abbreviations

---

NMR	Nuclear Magnetic Resonance
SSNRM	Solid-State Magnetic Resonance
$\delta$	Chemical shift in NMR downfield from TMS, Hz or ppm
CP	Cross-Polarisation
MAS	Magic Angle spinning
CSA	Chemical Shift Anisotropy
$\Omega$	Span (in ppm)
$\kappa$	Skew
IR	Infrared
DRIFT	Direct Reflectance Infrared Fourier Transform spectroscopy
Tof-SIMS	Time-of-Flight Secondary Ion Mass Spectrometry
$\nu(\text{A-B})$	Deformation frequencies of A-B bond
GC	Gas Chromatography
MS	Mass Spectroscopy
RT	Room Temperature (always specified)
eV	Electron-Volt, $1\text{eV} = 1.60217646 \times 10^{-19} \text{ J}$
MOS-FET	Metal-Oxide-Semiconductor Field-Effect Transistor
$\text{SiO}_2\text{-(700)}$	Silica Aerosil 200 partially dehydroxylated at 700°C in dynamic vacuo ( $1.5 \times 10^{-5}$ mbar)
TEPO	Triethylphosphine oxide
POSS	Polysilsesquioxane (here, hexaisobutyl-)
POSS-P	Phospha-polysilsesquioxane

# Introduction

---

The aim of this PhD thesis was to investigate a chemical way to secure the deterministic positioning of doping atoms, namely boron and phosphorus, in the near surface of silicon wafers. The study was divided into two main steps:

- i) A chemical approach to determine the feasibility of the concept on silica;
- ii) Its application to an oxide-covered silicon wafer.

The model that was experimented on silica proved efficient and led to the formation of new surface species. The transposition of the strategy to silicon wafers allowed thorough investigation of the near surface.

**Chapter I** of this thesis dwells on the state of the art in the field of dopant positioning. It is divided in three main parts. The first one deals with the need to dope semi-conductors for ever-shrinking microelectronic devices and several doping techniques that are used so far. The second part discusses silica as a tunable material, ideal for grafting dopant-containing molecules and dopant implantation.

**Chapter II** will investigate the grafting of well-defined boron-containing compounds on silica surfaces in order to provide a molecular understanding of the chemistry of B with silica surface, which will be used as a model for amorphous silica present on silicon wafers.

**Chapter III** will use the same approach as Chapter II, focussing on phosphorus-containing molecules.

**Chapter IV** describes the transfer of the overall strategy to oxide-covered silicon wafers, a comparison of the surfaces will be provided, and then implantation and diffusion of the doping atoms will be discussed.

**Chapter V** will provide conclusion and perspectives of this work.





## **Chapter 1 : Bibliography**

---

## Summary of the Chapter

---

Moore's Law: the importance of device shrinking and integration.....	7
1. Doping of semiconductors .....	10
1.1. Effect of doping on a semiconductor .....	10
1.2. The interest of doping.....	11
1.3. Doping of the substrate.....	12
1.3.1. Ion implantation .....	12
1.3.2. Possibility of alternative nanomasking methods for deterministic doping.....	16
1.3.2.1. Nanometric stamping .....	16
1.3.2.2. Polymer templating .....	17
1.3.3. Doping by grafting .....	19
2. Silica surface chemistry .....	21
2.1. Properties of amorphous silica.....	23
2.1.1. Surface species on silica .....	23
2.1.2. Dehydration and dehydroxylation of silica .....	24
2.2. Characterisation methods .....	25
2.2.1. Infrared spectroscopy.....	26
2.2.2. Solid-State NMR .....	27
2.2.3. Chemistry of surface silanols .....	27
2.2.3.1. Surface organometallic chemistry .....	27
2.2.3.2. Boron chemistry on silica.....	28
2.2.3.2. Phosphorus chemistry on silica.....	29
2.2.3. Conclusion .....	31
References .....	34

## Moore's Law: the importance of device shrinking and integration

The main focus of the actual race to better performance of microelectronics is deeply related to the shrinking of transistors that are present in devices such as processors or chips. Gordon Moore predicted in 1965 that integration performances would double every year, leading to smaller grid size and an increase in the number of transistors on a chip.<sup>[1]</sup> He predicted this trend would continue “for at least ten years” i.e. until 1975, when the number of transistors on a chip would double every two years, and this prediction proved to be surprisingly accurate.

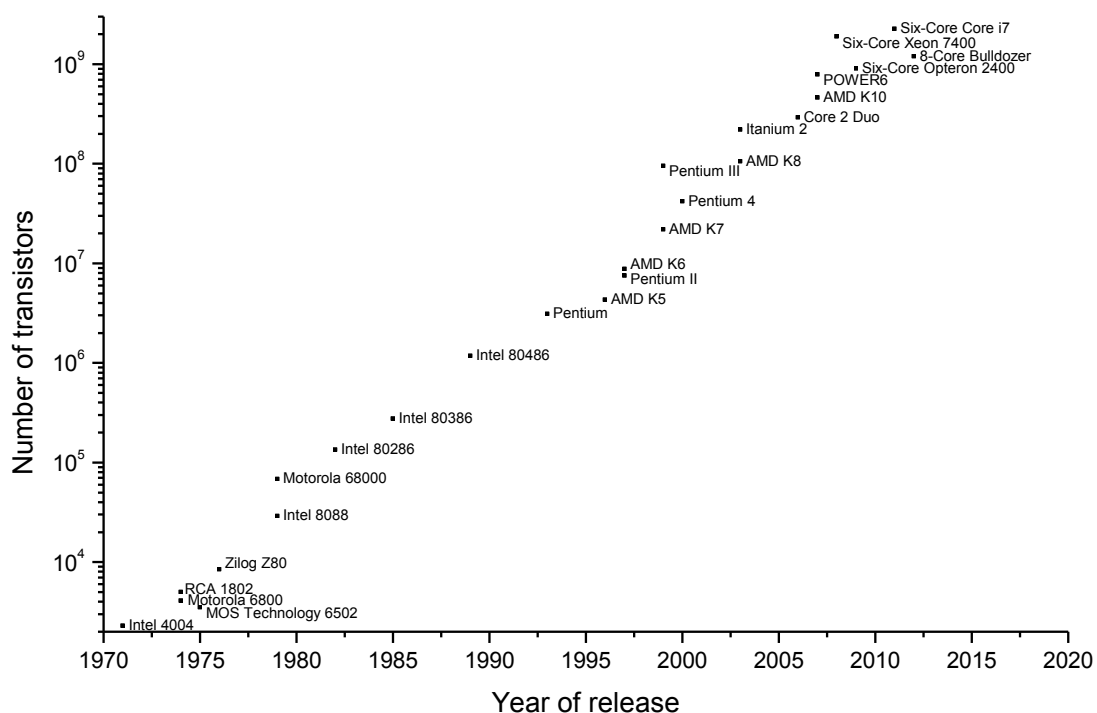


Fig 1. Number of transistor per chip versus year (from the reference found <sup>i</sup>)

The now used MOSFETs (metal-oxide-semiconductor field-effect transistor) have the interesting property of becoming cheaper as they become smaller. Also, they thus consume less power, can work faster, and enable more functions per unit area of silicon. Therefore, denser silicon integrated circuits offer increased performances compared to their ancestors from the 1970's.

Today, this law seem to reach a saturation level, because of the difficulties in controlling the matter properties as well as small fluctuations of technological parameters at this scale. Moreover, it is more complex to achieve optical lithography sources and predict a final return on the huge investments that are required by more complex tools.

<sup>i</sup> Found on <http://www.intel.com/pressroom/kits/quickreffam.htm>

**Fig 2. Shrinking of transistors and the emergence of atom-scale electronics: a) bulk transistor ("FET"); b) 25 nm MOSFET (2008); c) 4 nm MOSFET; d) towards single-atom (from <sup>[2]</sup>)**

Thus, such a decrease in transistors sizes shows especially that a good dopant control at a nanometric scale will become very important. Indeed, as shown in **Fig 2**, the smaller the MOSFET, the more precise the control of dopant implantation should be. Starting from a doped-bulk, (**Fig 2-a**) reducing the size of transistors leads to a bigger importance of dopants' position in the MOSFET, (**Fig 2-b** and **c**) leading, eventually, to single atom devices (**Fig 2-d**).

**Fig 3. Randomness of dopant distribution on a silicon wafer (left) compared to an ordered dopant distribution (right) (reproduced from <sup>[3]</sup>)**

As visible on **Fig 3** hereupon, the randomness of dopant distribution on a wafer would inevitably lead to a variability of the threshold voltage at the terminal of the wafer piece.

**Fig 4. Schematic of gate-edge components that fluctuate along W in MOSFET (reproduced from [4])**

<b>L</b> : gate length	<b>W</b> : gate width
<b>L<sub>SW</sub></b> : sidewall length	<b>L<sub>off</sub></b> : offset spacer length
<b>E<sub>halo</sub></b> : halo implantation energy	<b>D<sub>halo</sub></b> : halo implantation dose
<b>E<sub>ext</sub></b> : extension implantation energy	<b>D<sub>ext</sub></b> : extension implantation dose

As the size of a MOSFET decreases, impurities present in the gate (as shown by darker green spots in **Fig 4**) influence more the variability of the threshold voltage, thus leading to unexpected and unwanted performances.<sup>[5]</sup> Also, it was recently shown that the fluctuations of threshold voltage were also due to different factors, especially the sidewall length (noted LSW above), which would bring even more variability.

The goal of this thesis is to control of the density of dopant at a nanometric level, in order to limit the variability of the threshold voltage.

## 1. Doping of semiconductors

---

### 1.1. Effect of doping on a semiconductor

---

Semiconductors such as silicon, germanium or even aluminium phosphide are called intrinsic semiconductor, as they have no dopant present within their matrices. A lightly or moderately doped semiconductor would be then called extrinsic semiconductor. A semiconductor that was doped so as to act like a conductor would be defined as degenerate.

The energy distribution of the electrons is described by Fermi-Dirac statistics. This distribution determines which of the states are filled and which are empty. It can easily be described by the Fermi-Dirac distribution  $f(E)$  which gives the probability of having a single-particle state of energy  $E$  occupied by an electron (at thermodynamic equilibrium). It is defined as follows:

$$f(E) = \frac{1}{1 + e^{\frac{E-\mu}{k_B T}}}$$

- With:
- $\mu$ : the chemical potential (dependent on T)
  - $k_B$ : Boltzmann's constant
  - T: temperature

Therefore, "Fermi level" is the highest energy level that an electron can reach or occupy in a material at absolute zero temperature since, according to the Pauli exclusion principle,<sup>[6]</sup> electrons cannot exist in identical energy states. Thus, at absolute zero, electrons pack into the lowest available energy states to form the "Fermi sea".<sup>[7]</sup> Above this "sea", the Fermi level can be found, and is the energy level where no electron has enough energy to rise. Typically, the Fermi energies of metals are of the order of a few electron volts.<sup>[8]</sup> In doped semiconductors, the Fermi level is therefore shifted by the impurities (**Fig 5**).

**Fig 5.** Scheme representing the Fermi function on the band of a semiconductor (taken from hyperphysics<sup>ii</sup>)

<sup>ii</sup> The figure can be found on: <http://hyperphysics.phy-astr.gsu.edu/hbase/solids/fermi.html>

As can be seen in **Fig 5** above, at 0 K, no electron is above the valence band, as no electron can have energy above the Fermi level and there are no available energy levels in the band gap. However, it can be seen that, at higher temperature, some electrons may be present in the conduction band, thus participating to the conduction of current. The effect of doping shifts the Fermi level, thus decreasing the energy gap required to let conduction happen.

## 1.2. The interest of doping

---

In order to overcome this band gap in semiconductors, doping is performed to change the electrical properties of the semiconductor. The first semiconductor doping was performed by John Woodyard during World War II.<sup>[9]</sup> Since then, it has become an important topic in semiconductor research and development.<sup>[10, 11]</sup>

Two types of doping exist: n-doping and p-doping. By a controlled addition of impurities, dopants, valence electrons (n-type, n for “negative”) or holes (p-type, p for “positive”) can be added to the semiconductor. Usual p-dopants for Group IV semiconductors as silicon are Group III acceptors such as boron or sometimes gallium they “lack” one valence electron with respects to silicon, and usual n-dopants are Group IV donors as phosphorus or arsenic, having one more valence electron than silicon.

**Fig 6. Schematics of three basic bonds in semiconductors. (a) intrinsic silicon, (b) n-type Si with donor (phosphorus), (c) p-type Si with acceptor (boron) (reproduced from Sze et al.<sup>[12]</sup>)**

The addition of dopants in the semiconductor matrix will change the band diagram of the latter. If the dopant has more valence electrons, (such as P, As...) it will contribute extra electrons to the band. As the valence band is already filled with electrons from the semimetal, a higher-energy band is formed. This will thus reduce the energy gap between the valence band and the conduction band.

Alternatively, if the dopant has fewer valence electrons (such as boron, aluminium...) it will contribute fewer electrons to the valence band, thus generating an electron deficit. This type of dopant creates holes closer to the valence band. Therefore, electrons from the valence band of the semiconductor can move to the newly-formed conducting band, requiring less energy than the



undoped semiconductor. Subsequently, the Fermi level for such doped semiconductors is also shifted.

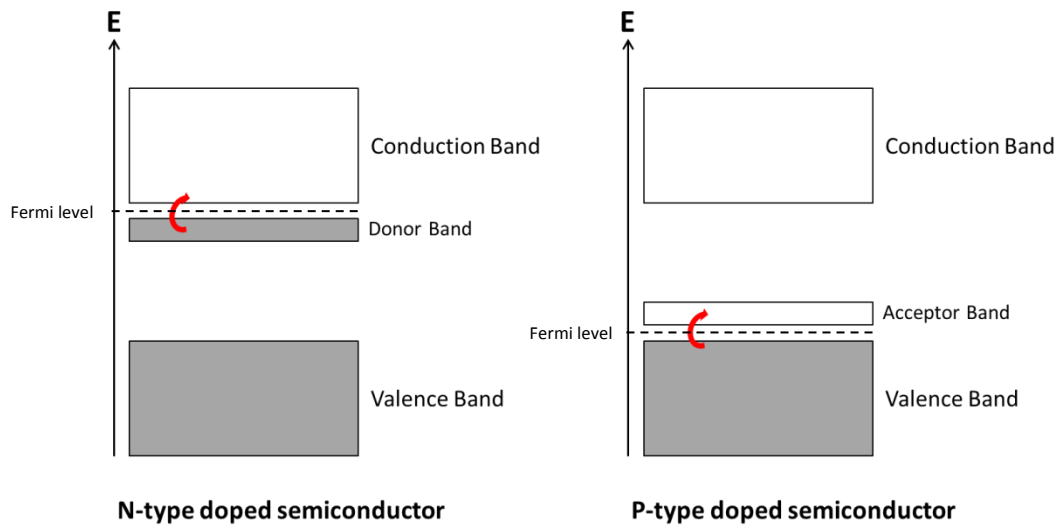


Fig 7. Schematics of the band theory for n- and p-doped semiconductors

### 1.3. Doping of the substrate

Doping of the substrate may take place while the silicon boule is grown. This results in a uniform doping of the wafer.<sup>[11]</sup> Photolithography can also be used as a tool to define more precise elements, like circuits.

Processes such as diffusion and ion implantation can also be used. Nowadays, the latter is more popular thanks to its increased controllability.

#### 1.3.1. Ion implantation

To deliver homogeneous doping<sup>[13]</sup> single-ion implantation techniques<sup>[14-16]</sup> have been developed and have nowadays become the most commonly used techniques to introduce dopants into the semiconductor.<sup>[17, 18]</sup>

Ion implantation can be considered to have appeared in the late 1940's and early 1950's with Shockely's,<sup>[19]</sup> Ohl's<sup>[20]</sup> and Moyer's<sup>[21]</sup> patents that were the first papers reporting ionic bombardment of semiconductors.

In this technique, ionised dopants are accelerated in electric fields and shot into the wafer. The main advantage of this technique is the precision of the control of both position and amount of incorporated dopant.<sup>[22]</sup> Once the dopants are implanted, an annealing step is required to

incorporate the dopants into the crystal lattice.<sup>[23]</sup> This annealing process, known as RTA (Rapid Thermal Annealing), leads to the efficient incorporation of the dopant within the Si matrix, respecting the initial pattern obtained by ion implantation. This result makes therefore this method very important for dopant activation.<sup>[24]</sup> Recently, laser-induced RTP (Rapid Thermal Process, same as RTA) annealing can be performed in less than a second, leading to the annealing of 20 wafers in less than 12s.<sup>[25]</sup>

For instance, for very high doping rates, gas clusters containing dopant gases such as B<sub>2</sub>H<sub>6</sub> or PH<sub>3</sub> are ionised and accelerated. Such clusters are formed when a gas is pressurised to approximately 10 atmospheres (**Fig 8**) and expanded into high vacuum (1x10<sup>-5</sup> atm). Clusters are then ionised by electrons, accelerated and focused into a tight beam right before hitting the Si wafers.<sup>[26, 27]</sup> This allows a good positioning of clusters onto the silicon wafer.

**Fig 8. Schematic layout of a ionized cluster beam apparatus (reproduced from <sup>[27]</sup>)**

However, it was shown that such a gas cluster does not implant dopant atoms on impacting the silicon surface. Indeed, the energy of the atom is not sufficient. In fact, the surface melts upon impact, allowing dopants to either mix or infuse several nanometres into it.<sup>[28]</sup> (**Fig 9**)

**Fig 9. Schematics of the impact of a gas cluster onto a surface and its effect (reproduced from <sup>[26]</sup>)**

As the size of devices in semiconductors is decreasing, such random distribution of individual dopants is yet a critical factor for the performance of the device.<sup>[29]</sup> Recent studies focused on controlling the ion number on a fine semiconductor region, resulting in developing single-ion implantation (SII) as a way to enable one-by-one ion implantation into a fine semiconductor region.<sup>[30]</sup>

Shinada et al. recently reported an efficient way to achieve such a positioning on a 100 nm-scale.<sup>[3]</sup> In the single-ion implantation technique, a small aperture divides a focused beam which then extracts single ions, hence controlling the number of implanted ions one-by-one by single ion incidence. In this case, P ions were implanted every 100nm through a 25nm deep silicon oxide. (**Fig 10**)

**Fig 10. Implantation of P ions at a range of 1  $\mu\text{m}$  by single-ion implantation (reproduced from <sup>[5]</sup>)**

In this method, single ions are extracted by chopping the focused ion beam through an aperture. The number of implanted ions can be precisely controlled by detecting secondary electrons emitted upon implantation. The apparatus displays an excellent micrometric precision, as is shown on **Fig 10**.

Albeit its efficiency on a micrometric scale, this process cannot achieve an implantation down to the nanometre scale.<sup>[31]</sup> Indeed, the implantation of dopants results in clusters and not single-atom, therefore it fails to achieve nanometric precision.

Therefore such a doping presents the inability to yield nanometric precision, but also leads to a longer time of implantation, due to machines' constraints.

Recent experiments carried out by Jamieson *et al.* showed the creation of 10nm-scaled nanodevices by ion implantation and detected by SEM.<sup>[32]</sup>

**Fig 11. Composite image showing the SEM image of the As-implanted device overlaid with another SEM image of the metallisation produced by the same mask in a different device. (reproduced from <sup>[32]</sup>)**

The width of 10 nm seen in **Fig 11** is consistent with the standard deviation of the implant determined by SRIM.

A recently-developed method showed the possibility of creating a single-atom transistor in which an individual phosphorus dopant atom has been deterministically placed by using a combination of scanning tunnelling microscopy (STM) and hydrogen-resist lithography.<sup>[33]</sup>

**Fig 12. Single-atom transistor based on deterministic positioning of a phosphorus atom in epitaxial silicon (reproduced from <sup>[33]</sup>)**

**Fig 12a** hereupon displays an STM image of the device with the hydrogen-desorbed regions defining source (S) and drain (D) leads and two gates (G1, G2). After a subsequent doping with phosphine, these observed regions form highly phosphorus-doped electrodes of monatomic height. **Fig 12b** is a close-up of the inner device area (represented by the dashed box in **Fig 12a**). There, the central bright spot represents the silicon atom ejected by a single phosphorus atom incorporated into the surface. **Fig 12C** is a schematic of the chemical reaction that undergoes the deterministic incorporation of a single phosphorus atom into the surface.

### 1.3.2. Possibility of alternative nanomasking methods for deterministic doping

---

Since two types of dopants are to be studied, many ways of positioning were investigated. Such methods would ensure whether or not these could be of any interest in the forthcoming labwork and research that was going to follow. As it was proven to be easy to graft boron onto silica,<sup>[34-37]</sup> immobilisation of phosphorus-containing species on  $\text{TiO}_2$ <sup>[38]</sup> and  $\text{SiO}_2$ <sup>[39]</sup> was also shown to be effective. Therefore, the initial idea of supporting boron- and phosphorus-containing species onto  $\text{SiO}_2$  is validated.

Knowing that we aimed for the same order of dopant amount per  $\text{nm}^2$  as Ho<sup>[40]</sup>, and, as previously discussed, physical methods have strong drawbacks that hinder their efficiency for submicrometer doping precision, we decided to look further into chemical adsorption onto surfaces. We will here focus on chemical methods suitable for implantation precision down to the atom scale.

#### 1.3.2.1. Nanometric stamping

---

Numerous publications have dealt with the issue of patterning a surface throughout stamping methods.<sup>[41-43]</sup> Such processes were used to locally protect some areas on the surface and generate a patterning mask. The principle of nanoimprint lithography is to create a regular striped mould of that would then be pressed on a resist, an inorganically cross-linked sol-gel (ICSG) such as silica, and heated up to a certain temperature to result in a patterned region.

**Fig 13. Schematics of the imprinting process for inorganically cross-linked sol-gel (reproduced from <sup>[41]</sup>)**

With such a technique, very well-defined areas on a surface can be formed.

**Fig 14. SEM image of a square-island array after two imprints using Peroz's method <sup>[41]</sup>**

The mould goes through a 90° in-plane rotation and the process is repeated once more to create an equally tiled structure on the imprint. A thermal treatment degrades all organic moieties leaving only pure silica. The obtained cross-sections were 340 nm linewidth, 1µm pitch and a depth of about 160nm. The 100-nanometric scale was even attained with such methods. <sup>[44, 45]</sup>

**Fig 15. AFM image of a Pd catalytic stamp with NP diametres of 20 nm and centre-to-centre spacing of 60 nm (reproduced from <sup>[46]</sup>)**

In such a method, a catalytic stamp is “inked” with a solution of terminal alkenes/alkynes and applied on a flat H terminated Si surface. Pressing the stamp on the surface resulted in the duplication of the stamp pattern of alkyl/alkylenyl groups on the surface. The positive point was that the stamp was totally reusable at the end of the reaction. The technique allows a nanoscale patterning of a relatively large surface (~1cm<sup>2</sup>) with a good precision (down to 20nm) in a relatively short time, since the whole process takes less than 30 min to be executed.

### *1.3.2.2. Polymer templating*

---

An easier way to template a surface would be to go through the use of polymer that would either be spin-coated or would self-assemble on a surface.

Block copolymers could be used to generate a template on the surface after etching. Block copolymers such as PS-*v*-PVP have been used on aluminium films<sup>[47]</sup> or on silica surfaces.<sup>[48]</sup> Li et al. report that they polymerised in situ poly(R-methylstyrene-*b*-4-*tert*-butoxystyrene) (later referred to as P $\alpha$ MS-*b*-PtBuOS) before spin-coating in on a silicon surface. The coating polymer would then be masked by a template and be irradiated by a 248nm stepper and be baked to selectively create zones of polymer presence on the surface. The remaining copolymer would then once more be irradiated by a 365nm lamp under vacuum to eliminate all P $\alpha$ MS blocks leaving a patterned surface with nanoporous channels of interesting diameters (18-25nm)<sup>[49]</sup>, selectively giving way to the bare surface, enabling further reactions on these specific spots only. The surface is thus patterned as desired. (**Fig 16** hereafter)

**Fig 16. Example of surface patterning (reproduced from <sup>[49]</sup>)**

SEM images of such etched block-copolymers show the formation of cavities, which size can be tuned by the duration of the etching duration.<sup>[48]</sup>

**Fig 17. SEM images of the etch pits obtained at different etching time using PS-b-P4VP as templates. The etching time from (a-c) is 20, 30, 40, and 50 min, respectively (reproduced from <sup>[48]</sup>)**

Some excellent periodicity have been already obtained via the use of metal-oxide nanopatterns from block copolymers (17-45nm)<sup>[50]</sup> formed of a hydrophilic head and a hydrophobic tail. These block copolymers would be suspended so as to form micelles into a precursor (metal chloride) or ceramic pattern (metal oxide) solution. The surface to be coated would be dipped into this suspension then evaporated. Nanocavities are thus formed after thermal treatments, yielding even 10nm pore diameter.<sup>[50]</sup>

Such pores could be used to channel molecules down to the surface and have them react on precise areas.



### 1.3.3. Doping by grafting

---

In order to circumvent drawbacks of the physical approach described above and the difficulty of nanopatterning surfaces, chemistry based methods were developed. These techniques rely on the formation of highly uniform organic monolayers of dopant-containing molecules.<sup>[51]</sup>

First investigations were performed by grafting molecules on bare silicon surfaces. In this process, the native silica layer on top of the wafer is first etched with HF yielding Si-H surface functions. The thus formed Si-H surface is then reacted with allyl derivatives to create a self-assembled monolayer. (**Fig 18**)

This technique was implemented for dopants into silicon surfaces.<sup>[40]</sup> A naked Si-H surface, obtained by etching the native silicon oxide with a 0.5% HF solution was contacted with allylboronic derivatives creating Si-C bond at the C=C molecular sites. The grafted surface was then capped with a 50nm thick SiO<sub>2</sub> layer using an electron beam evaporator. The surface was finally annealed at different temperatures (950°C, 1000°C and 1050°C) and etched to yield the doped surfaces. (**Fig 18**) The role of silica capping, in this case, permitted a protection of the grafted molecules during RTP annealing.

**Fig 18. Ho's method of deterministic implantation (reproduced from <sup>[40]</sup>)**

The formation of the covalently bonded species is confirmed by X-ray photoelectron spectroscopy (XPS). Secondary-ion mass spectroscopy was performed to draw profiles of the boron diffusion after the RTA. As shown in **Fig 19** below, the annealing temperature influences the resistance, which is explained by the lower diffusivity of boron at lower temperatures.

**Fig 19. Sheet resistance at different annealing temperatures (reproduced from [40])**

The quick decrease from  $10^5$  to  $10^3 \Omega/\square$  shows the rapid diffusion of B atoms within the silicon lattice. An interesting point that is raised by Ho *et al.* is that at a longer annealing time, surface resistance seems to converge to the same point, around  $10^3 \Omega/\square$ , proving the influence of the temperature on the diffusivity of boron.

The limitation of this method is, however, that no control in dopants positioning can be ensured. Therefore, using silica, an oxide layer being present on silicon wafers without etching, would permit us to ensure a new strategy and hopefully fulfil the desired controlled effect.

**Fig 20. Calculated B diffusivity in pure SiO<sub>2</sub> vs. oxide thickness compared with measured data (reproduced from [52])**

As shown by Fair *et al.*,<sup>[52]</sup> boron diffusivity increases with a decreasing oxide thickness so that if the gate oxide was scaled down to 15 Å, the diffusivity of boron in SiO<sub>2</sub> would strongly increase, by a factor of 24.

We will therefore investigate in this project the controlled positioning of boron dopant by a chemical route. The strategy will rely on the controlled grafting or the self-positioning of boron molecules on silicon wafers coated with a silica surface (and not with bare Si-H).

## Chapter 1

Several questions are to be addressed:

- How thin should the silica layer on the wafer be to allow further dopant diffusion?
- Can we graft or self-position B and P molecules onto silica surfaces with an efficient control of both their position and loading?

Thus, we should first examine the chemistry of silica surfaces.

## 2. Silica surface chemistry

---

### 2.1. Properties of amorphous silica

---

Silica, often made from the condensation of  $\text{Si}(\text{OH})_4$  led to the formation of a surface covered by hydroxyl groups, known as silanols.<sup>[53-55]</sup> These surface species are key to understand the reactivity of silica.

We shall here first discuss the surface species of silica, before explaining the modifications strategies that have been used and describe the most interesting techniques to characterize it.

#### 2.1.1. Surface species on silica

---

Silica surface shows different types of silanols (**Fig 21**). First, isolated silanols represent  $\text{SiOH}$  groups that are not in interaction with other silanol groups. Then, germinal silanols, or silanediols are two OH groups carried by a single silicon atom. Vicinal silanols, also called bonded silanols, are H-bonded surface silanols, counting also H-bonded geminal silanols. Siloxane bridges are also found on the surface.

**Fig 21. Representation of the different surface species present on silica (reproduced from Bergna<sup>[56]</sup>)**

These different silicon-containing species can be described as different  $Q^n$  species as proposed by Engelhardt *et al.*<sup>[57]</sup>  $Q^n$  is short for  $\text{Si}(\text{O-Si})_n(\text{O-R})_{4-n}$ , where  $n$  is the number of bridging oxygen and  $4-n$  the number of non-bridging oxygen. ( $R = \text{C}$  or  $\text{H}$ )

To that extent, silicon atoms corresponding to siloxanes ( $Q^4$ ), single silanols ( $Q^3$ ) or geminal silanols ( $Q^2$ ) can be distinguished<sup>[58]</sup> (**Fig 22** hereafter).

**Fig 22. Schematic showing the different silicon atom species according to their environment (reproduced from <sup>[58]</sup>)**

It is noteworthy that water can also be coordinated, or physisorbed, onto the surface.<sup>[59]</sup> Removal of part or all of this water, as well as thermal rearrangement of the surface will be tackled in the next part.

### 2.1.2. Dehydration and dehydroxylation of silica

The removal of absorbed water can be achieved between 110 and 180°C depending on the porosity of silica.<sup>[59-62]</sup>

From 200°C, no water is physisorbed at the surface of silica any longer, dehydration is complete, according to Bergna.<sup>[56]</sup> Therefore, the surface is made of silanol groups and siloxane bridges only. Above this temperature, dehydroxylation processes, which lead to the condensation of silanols into siloxane bridges, will take place. Depending on the dehydroxylation temperature and the atmospheres (vacuum, inert gas...), the surface OH density can be finely tuned<sup>[63]</sup> (**Fig 23**).

**Fig 23. Relationship between the silanol number  $\alpha_{OH}$  and the treatment temperature for various silica samples (specific surface areas from 9.5 to 945m<sup>2</sup>.g<sup>-1</sup> and accessible pore diameters from 1.0 to 1000 nm and higher)(reproduced from <sup>[63]</sup>)**

Values for the number of silanols  $\alpha_{\text{OH}}$  decrease rapidly in the IIa (AB) segment, from 190°C to 400°C then more slowly in the IIb' (BC) segment. In the BC segment, silanols become mostly isolated. In the last segment IIb'', or segment DE, no geminal silanols are present anymore and the condensation is due to interaction between sparsely distributed silanol groups only. This observation was corroborated by Vansant who performed an ATG analysis of silica.<sup>[64]</sup> (**Fig 24** hereafter) It is also important to add that, above 700 °C, loss of surface area becomes important because of sintering and eventually the formation of quartz is observed above 1100 °C.

**Fig 24. Thermogravimetric analysis of silica (reproduced from <sup>[64]</sup>)**

Two spectra were obtained by such an analysis. Spectrum 1 is a DTA (Differential Thermogravimetric Analysis) displaying a very sharp peak between 30°C and about 150°C. This was attributed to the aforementioned decoordination of water from the silica surface. Spectrum 2 is a TGA (Thermogravimetric Analysis) showing the loss of weight (in percents) versus temperature. Both spectra 1 and 2 tend to show the loss of water ends at about 150°C. Then, the weight loss displayed by the TGA spectrum denotes the dehydroxylation of the surface, as mentioned earlier.<sup>[59, 63]</sup>

Thus, temperature treatment of the silica surfaces is an efficient way to yield a statistics of reactive surface silanols. This key point would then be implemented to the strategy in order to try and ensure a better positioning of dopants on the surface, by grafting. However, this would only yield a statistic positioning of dopants. Therefore, this statistics should be balanced by another one.

## 2.2. Characterisation methods

---

Different techniques can be used to characterise silica surfaces. These may help characterising either the type of silica that is studied, for instance after a thermal treatment, or to characterise modified surfaces and determine the adsorbed or grafted species.

### 2.2.1. Infrared spectroscopy

First, the most common and straightforward method that can be used to characterise silica surface is infrared spectroscopy. This can be performed by either FTIR (Fourier Transform Infrared) in transmission IR, or DRIFT (Diffuse Reflectance Infrared Fourier Transform) which is often used for the characterisation of powder catalysts.<sup>[65, 66]</sup>

IR spectroscopy is a very sensitive tool to assess the surface chemistry of silica treated at various temperatures under secondary vacuum ( $10^{-5}$  mBar - dehydroxylation process)(Fig 25).

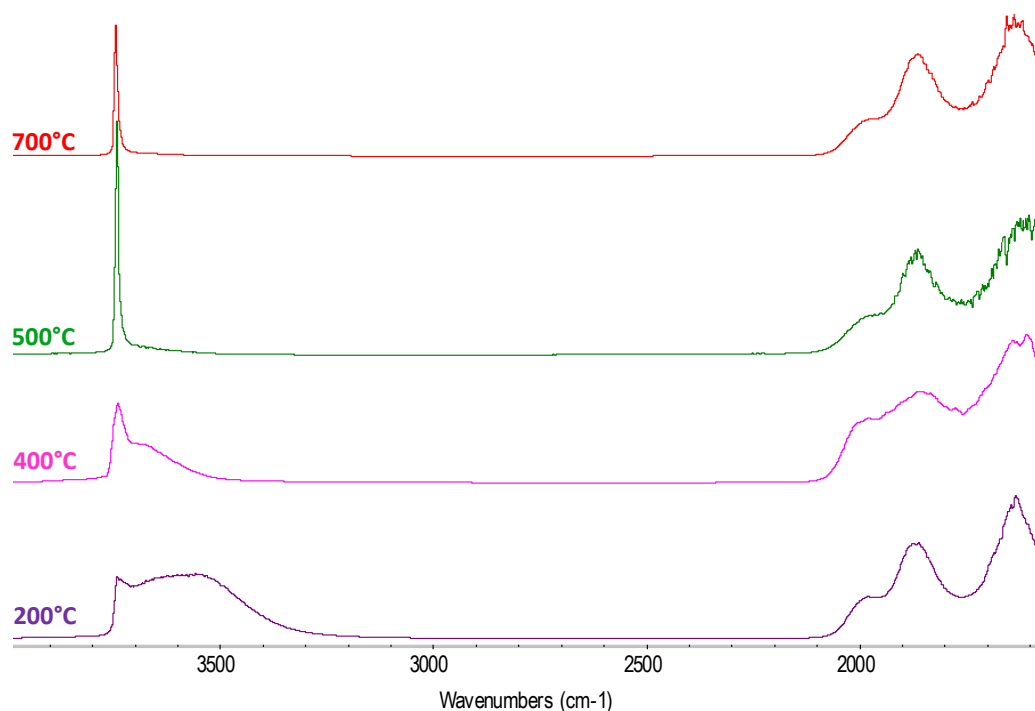


Fig 25. Comparison of silica treated at different temperatures by DRIFT

The above Fig 25 displays four spectra, each representing a DRIFT analysis of thermally treated silica. It was reported that the peak at  $3747\text{ cm}^{-1}$  was characteristic of free silanols.<sup>[67-69]</sup> Likewise, the broad peak between  $3200\text{ cm}^{-1}$  and  $3740\text{ cm}^{-1}$  was reported to be consistent with bonded silanol, namely geminal and vicinal silanols.<sup>[67-69]</sup> The bands between  $1600\text{ cm}^{-1}$  and  $2100\text{ cm}^{-1}$  were reported as Si-O-Si combination bands, i.e. they are relevant to the bulk of silica, made of siloxane bonds.<sup>[70]</sup>

Also, it is noteworthy that the results shown in the previous part can be immediately observed here: geminal and vicinal silanols disappear with increasing temperature to yield isolated silanols only. IR spectroscopy can also help determine the modification of the surface, either by the passivation of surface species, by the grafting of organic species<sup>[71, 72]</sup> or organometallic species.<sup>[73]</sup>

**Fig 26. Infrared spectra of the grafting reaction of  $[\text{W}(=\text{N}(2,6\text{-}i\text{PrC}_6\text{H}_3))(\text{=CH}t\text{Bu})(\text{CH}_2t\text{Bu})_2]$  (blue) onto thermally treated silica at 700°C for 15h (red) (reproduced from <sup>[73]</sup>)**

As was described by Rhers et al., peaks around 3000  $\text{cm}^{-1}$  showed the presence of the organic chain, as well as the peaks in the 1300-1500  $\text{cm}^{-1}$  region, representing stretching vibrations of C-H bonds and scissoring (in-plane bending) vibrations of the same C-H bonds, respectively. They also attributed the peaks at 3710 and 3607  $\text{cm}^{-1}$  to two different interactions of the grafted species with the surface silanols.<sup>[73]</sup>

### 2.2.2. Solid-State NMR

---

Solid-state NMR (Nuclear Magnetic Resonance) is nowadays commonly used for supports<sup>[74]</sup> and especially silica.<sup>[74-77]</sup>

<sup>1</sup>H-NMR and <sup>13</sup>C-NMR can prove to be efficient for characterising surface species, as it is a way to recover the moiety of the grafted species.<sup>[78, 79]</sup>

**Fig 27. <sup>13</sup>C CP/MAS NMR spectrum of partially dehydroxylated silica treated with ethanol (reproduced from <sup>[80]</sup>)**



Other nuclei may also be studied. Therefore,  $^{11}\text{B}$  or even  $^{31}\text{P}$ , both being frequently studied on surfaces,<sup>[69, 80-82]</sup> can be tackled through this analytical method. As both boron and phosphorus are the chosen dopants we wish to study, such NMR techniques would be an important asset in the characterisation of the silica-supported species.

Also,  $^{29}\text{Si}$ -NMR allows differentiating the different  $\text{Q}^n$  substructures that are present on silica.<sup>[75, 76]</sup> In the case of a wet silica, Sindorf et al., showed that  $\text{Q}^2$ ,  $\text{Q}^3$  and  $\text{Q}^4$  could be separated as shown in **Fig 28**.<sup>[83]</sup> Indeed,  $^{29}\text{Si}$  NMR spectroscopy shows that isotropic chemical shifts vary as a function of the silicate structure,<sup>[76]</sup> therefore different chemical shifts range appear according to Si-O-Si (siloxane) bridges.

**Fig 28. CP/MAS  $^{29}\text{Si}$  NMR spectrum of wet silica (Fisher S-157) (reproduced from<sup>[83]</sup>) with the  $\text{Q}^n$  attribution for each peak**

### 2.2.3. Chemistry of surface silanols

---

#### 2.2.3.1. Surface organometallic chemistry

---

Surface organometallic chemistry (SOMC)<sup>[84, 85]</sup> has been developed in order to bridge the gap between homogeneous catalysis, which is molecularly in nature, and heterogeneous catalysis, which is more empirical but better suited for industrial processes. This approach dwells on the generation of well-defined active sites by the reaction of an organometallic complex or cluster with a support, one of the most commonly used being partially dehydroxylated silica.<sup>[84]</sup>

This yields a solid supported species in which the support can assume the role of a macromolecular ligand. In the case of oxide supports (silica, alumina, ceria...) the reacted metal is

permanently bonded to the surface to yield a ( $\equiv\text{EO}$ )-M bond where E = Si, Al, Ti, Mg... Such prepared supported organometallic complexes can undergo many further steps as thermal treatments, chemical reactions, photoreactions in order to yield the desired surface species. (**Scheme 1**)

**Scheme 1. Preparation and reactivity of surface organometallic complexes.** (a) Grafting of organometallic complex  $\text{R}_x\text{ML}_n$  onto an oxide support. (b) Reactivity of the surface species (reproduced from <sup>[84]</sup>)

Nowadays, a large range of catalysts has been prepared following this scheme in order to be used in different reactions (polymerisation,<sup>[86, 87]</sup> hydrogenation,<sup>[88]</sup> oxidation<sup>[89]</sup> and alkene metathesis<sup>[90, 91]</sup>).

### *2.2.3.2. Boron chemistry on silica*

---

Recent studies in the field of catalysis showed that boron species were successfully grafted onto silica supports in order to yield co-catalysts that could be efficient in olefin polymerisation.<sup>[92]</sup> The grafting of  $\text{BAr}_{\text{F}_3}$  onto silica was thus proven to be performed in the presence of pyridine, which would enhance the surface acidity and thus react with boron, forming a surface anion. (**Scheme 2**)

**Scheme 2. Reaction of  $\text{SiO}_2$  with  $\text{BAr}_{\text{F}_3}$  (reproduced from <sup>[92]</sup>)**

More recent studies showed the grafting of such a species could be performed in the absence of a Brønsted base under non-anhydrous conditions.<sup>[93]</sup> This led to the formation of a neutrally charged surface species.

**Scheme 3. Grafting of  $\text{BAR}_{\text{F}_3}$  onto Silica yielding a neutrally charged surface species (reproduced from <sup>[93]</sup>)**

The difficulty of grafting this compound was reported as due to the very low electrophilic nature of the boron centre.<sup>[93, 94]</sup> However, knowing the reaction of boron derivatives such as boranes with alcohol groups, extension of the strategy of grafting could be undertaken following the principle developed by Zheludov *et al.* (**Scheme 4**).<sup>[95]</sup>

**Scheme 4. Formation of diethylmethoxyborane as described by Zheludov *et al.***

### 2.2.3.2. Phosphorus chemistry on silica

---

Likewise, the grafting of phosphorus-containing compounds on oxide supports has been widely reported.<sup>[96, 97]</sup> However, grafting on silica did not involve the reactivity of phosphorus, the latter being attached to the support by a tether.<sup>[96]</sup>

**Fig 29. Phosphonate modified silica (reproduced from <sup>[96]</sup>)**

Phosphites, thanks to their reactivity, were shown to react quickly with silica and form surface phosphonates that could ensure further transformations.<sup>[68]</sup> The reaction was assumed to involve a Michaelis-Arbuzov rearrangement<sup>[98]</sup> as shown below. The formed phosphonate was shown to further react with the surface.

**Scheme 5. Mechanism of reaction of trimethylphosphite with silica (reproduced from <sup>[68]</sup>)**

Reactivity of phosphonates has been reported as reacting with ROH groups<sup>[99]</sup> (**Scheme 6**) which makes them eligible components to be grafted onto a silica surface.

**Scheme 6. Formation of a phosphonate (from <sup>[99]</sup>)**

Therefore, the grafting of both boron-containing and phosphorus-containing species on silica could potentially be achieved by transferring their reactivity onto surface oxides.

### 2.2.3. Conclusion

---

The urge to yield smaller devices in microelectronics is nowadays a burning issue. Single-atom dopant in devices seems to be the ultimate goal to reach. In order to do so, dopants must be well ordered on silicon in order to avoid any variability of the threshold tension.

The analysis of literature on the topic of silicon doping leads to an immediate conclusion: a better controlled positioning of dopants onto silicon wafers cannot be achieved through the classical way, i.e. by using single ion-implantation. Methods of direct grafting onto silicon surfaces showed an important dopant amount but failed to control the positioning of such implanted dopants. The main goal for silicon doping is thus to yield a doping as controlled as with single-ion implantation and as dense as that obtained by direct grafting of boron-containing species on silicon. It could also be possible to dilute such molecules to yield a surface concentration of  $1.0 \times 10^{13}$  at.cm<sup>-2</sup> for dopants, by using techniques described above.

Arranging molecules onto a surface can yield very precise results. Yet, the difficulty of creating monolayers was so demanding in terms of feasibility that it was rejected.

Knowing that the silica surface can exhibit different properties according to thermal treatment, especially in terms of silanol density, the reacting sites, it was decided to dwell on this feature to try and arrange dopant-containing molecules onto the silica surface. Yet, the repartition of grafting sites by such a treatment remains statistical, which led us to choose to balance this site density method by a steric approach. All dopant-containing molecules would then be sterically bulky.

In this thesis, we shall apply the strategy discussed above: regulating the statistics of silanol distribution on partially dehydroxylated silica by grafting sterically hindered dopant-containing molecules. Once this step is confirmed on silica particles, it will be transferred onto silicon wafers with native oxide. The implantation step would then be performed by annealing.

**Chapter II** will investigate the grafting of well-defined boron-containing compounds on silica surfaces in order to provide a molecular understanding of the chemistry of B with silica surface, which will be used as a model for amorphous silica present on silicon wafers.

**Chapter III** will use the same approach as Chapter II, focussing on phosphorus-containing molecules.

**Chapter IV** describes the transfer of the overall strategy to oxide-covered silicon wafers, a comparison of the surfaces will be provided, and then implantation and diffusion of the doping atoms will be discussed.

**Chapter V** will provide conclusion and perspectives of this work.

## References

- [1] G. E. Moore, *Electronics* **1965**, 38.
- [2] A. Asenov, A. R. Brown, J. H. Davies, S. Kaya, G. Slavcheva, *Electron Devices, IEEE Transactions on* **2003**, 50, 1837
- [3] T. Shinada, S. Okamoto, T. Kobayashi, I. Ohdomari, *Nature* **2005**, 437, 1128.
- [4] A. T. Putra, A. Nishida, S. Kamohara, T. Hiramoto, *Applied Physics Express* **2009**, 2.
- [5] T. Shinada, M. Hori, Y. Ono, K. Taira, A. Komatsubara, T. Tanii, T. Endoh, I. Ohdomari, in *Electron Devices Meeting (IEDM), 2010 IEEE International*, **2010**, pp. 26.5.1.
- [6] P. B. a. M. B. G. Constantin, *Journal of High Energy Physics* **1998**, 1998, 015.
- [7] F. d. r. Chevy, *Physics* **2009**, 2, 48.
- [8] C. A. Mead, W. G. Spitzer, *Physical Review* **1964**, 134, A713.
- [9] J. R. Woodyard, *Vol. 2530110* (Ed.: USPTO), The Sperry Corporation, US, **1944**.
- [10] P. M. Koenraad, M. E. Flatté, *Nature Materials* **2011**, 10, 91.
- [11] R. A. Levy, *Microelectronic Materials and Processes, Vol. 164*, Proceedings of the NATO Advanced Study Institute, Il Ciocco, Castevecchio Pascoli, **1986**.
- [12] S. M. Sze, K. K. Ng, *Physics of Semiconductor Devices, 3rd Edition*, Wiley, **2006**.
- [13] R. W. Keyes, *Appl. Phys.* **1975**, 8, 251.
- [14] T. Matsukawa, *Appl. Surf. Sci.* **1997**, 117/118, 677.
- [15] T. Shinada, A. Ishikawa, C. Hinoshita, M. Koh, I. Ohdomari, *Jpn J. Appl. Phys.* **2000**, 39, L265.
- [16] T. Shinada, H. Koyama, C. Hinoshita, K. Imamura, I. Ohdomari, *Jpn. J. Appl. Phys.* **2002**, 41, L287.
- [17] J. F. Ziegler, *Ion Implantation: Science and Technology*, 2nd sub ed., Academic Press, **1988**.
- [18] R. Doering, Y. Nishi, *Handbook of Semiconductor Manufacturing Technology*, 2nd ed., CRC Press, **2007**.
- [19] W. Shockley, (Ed.: U. P. Office), US, **1949**.
- [20] R. S. Ohl, (Ed.: U. P. Office), US, **1950**.
- [21] J. W. Moyer, (Ed.: U. P. Office), US, **1954**.
- [22] G. Dearnaley, *Nature* **1975**, 256, 701.
- [23] J. W. Mayer, L. Eriksson, J. A. Davies, *Ion implantation in semiconductors, silicon and germanium*, Academic Press, New York and London, **1970**.
- [24] P. Kohli, R. Wise, G. Braithwaite, M. T. Currie, A. Lochtefeld, M. Rodder, J. Bennett, M. Gostowski, B. Nguyen, R. Cleavelin, S. Yu, M. Pas, J. Gelpey, S. McCoy, A. Champion, M. Chaumont, in *SiGe: Materials, Processing, And Devices*, Electrochemical Society, Honolulu, **2004**, p. 1113.
- [25] R. Paetzel, J. Brune, F. Simon, L. Herbst, M. Machida, J. Shida, in *Advanced Thermal Processing of Semiconductors (RTP), 2010 18th International Conference on* (Ed.: IEEE), Gainesville, FL, **2010**, pp. 98.
- [26] I. Yamada, J. Matsuo, N. Toyoda, A. Kirkpatrick, *Materials Science and Engineering: R: Reports* **2001**, 34, 231.
- [27] P. H. Rose, G. Ryding, *Rev. Sci. Instrum.* **2006**, 77, 1.
- [28] M. E. Mack, *Nuclear Instruments and Methods in Physics Research Section B: Beam Interactions with Materials and Atoms* **2005**, 237, 235.
- [29] P. Ebert, N. D. Jäger, K. Urban, E. R. Weber, *J. Vac. Sci. Technol. B* **2004**, 22, 2018.
- [30] T. Matsukawa, T. Fukai, S. Suzuki, K. Hara, M. Koh, I. Ohdomari, *Applied Surface Science* **1997**, 117-118, 677.
- [31] P. S. Peercy, *Nature* **2000**, 406, 1023.

- [32] D. N. Jamieson, V. Chan, F. E. Hudson, S. E. Andresen, C. Yang, T. Hopf, S. M. Hearne, C. I. Pakes, S. Prawer, E. Gauja, A. S. Dzurak, R. G. Clark, *Nuclear Instruments and Methods in Physics Research Section B: Beam Interactions with Materials and Atoms* **2006**, 249, 221.
- [33] M. Fuechsle, J. A. Miwa, S. Mahapatra, H. Ryu, S. Lee, O. Warschkow, L. C. L. Hollenberg, G. Klimeck, M. Y. Simmons, *Nat Nano* **2012**, 7, 242.
- [34] M. Nicolas, C. Andrew, C. S. Catherine, M. Yann, B. Jean-Marie, *Chemistry - A European Journal* **2002**, 8, 1438.
- [35] R. J. Kwaan, C. J. Harlan, J. R. Norton, *Organometallics* **2001**, 20, 3818.
- [36] S. Charoenchaidet, S. Chavadej, E. Gulari, *Journal of Molecular Catalysis A: Chemical* **2002**, 185, 167.
- [37] M. Bochmann, G. J. Pindado, S. J. Lancaster, *Journal of Molecular Catalysis A: Chemical* **1999**, 146, 179.
- [38] A. A. S. Alfaya, Y. Gushikem, S. C. de Castro, *Chemistry of Materials* **1998**, 10, 909.
- [39] Z. Elbhiri, Y. Chevalier, J.-M. Chovelon, N. Jaffrezic-Renault, *Talanta* **2000**, 52, 495.
- [40] J. C. Ho, R. Yerushalmi, Z. A. Jacobson, Z. Fan, R. L. Alley, A. Javey, *Nat Mater* **2008**, 7, 62.
- [41] C. Peroz, V. Chauveau, E. Barthel, E. Søndergård, *Advanced Materials* **2009**, 21, 555.
- [42] X.-M. Li, M. Peter, J. Huskens, D. N. Reinhoudt, *Nano Letters* **2003**, 3, 1449.
- [43] S. Casimirus, E. Flahaut, C. Laberty-Robert, L. Malaquin, F. Carcenac, C. Laurent, C. Vieu, *Microelectronic Engineering* **2004**, 73-74, 564.
- [44] E. Menard, M. A. Meitl, Y. Sun, J.-U. Park, D. J.-L. Shir, Y.-S. Nam, S. Jeon, J. A. Rogers, *Chemical Reviews* **2007**, 107, 1117.
- [45] F. Zhang, H. Y. Low, *Nanotechnology* **2006**, 17, 1884.
- [46] H. Mizuno, J. M. Buriak, *Journal of the American Chemical Society* **2008**, 130, 17656.
- [47] J. C. Meiners, H. Elbs, A. Ritzi, J. Mlynek, G. Krausch, *Journal of Applied Physics* **1996**, 80, 2224.
- [48] Y. Qiao, D. Wang, J. M. Buriak, *Nano Letters* **2007**, 7, 464.
- [49] M. Li, K. Douki, K. Goto, X. Li, C. Coenjarts, D. M. Smilgies, C. K. Ober, *Chemistry of Materials* **2004**, 16, 3800.
- [50] M. Kuemmel, C. Boissière, L. Nicole, C. Laberty-Robert, C. Sanchez, D. Grosso, *Journal of Sol-Gel Science and Technology* **2008**, 48, 102.
- [51] A. B. Sieval, V. Vleeming, H. Zuilhof, E. J. R. Sudhölter, *Langmuir* **1999**, 15, 8288.
- [52] R. B. Fair, *IEDM* **1995**, 85.
- [53] U. Hofmann, K. Endell, D. Wilm, *Angewandte Chemie* **1934**, 47, 539.
- [54] E. K. Rideal, *Transactions of the Faraday Society* **1936**, 32, 3.
- [55] A. V. Kiselev, *Kolloidnyi zhurnal* **1936**, 2, 17.
- [56] H. E. Bergna, in *The Colloid Chemistry of Silica*, American Chemical Society, Washington DC, **1994**, pp. 1.
- [57] G. Engelhardt, D. Zeigan, H. Jancke, D. Hoebbel, W. Weicker, *Zeitschrift für anorganische und allgemeine Chemie* **1975**, 418, 17.
- [58] F. Kleitz, in *Nanoscale Materials in Chemistry, 2nd Edition* (Eds.: K. J. Klabunde, R. M. Richards), Wiley, **2009**, p. 257.
- [59] L. T. Zhuravlev, *Colloids and Surfaces A: Physicochemical and Engineering Aspects* **2000**, 173, 1.
- [60] R. K. Iler, *The Chemistry of Silica Solubility, Polymerization, Colloid and Surface Properties and Biochemistry of Silica*, John Wiley & Sons, **1979**.
- [61] C. Okkerse, in *Physical and Chemical aspects of adsorbents and catalysts* (Ed.: B. G. Linsen), Academic Press, London, **1970**.
- [62] V. M. Bermudez, *The Journal of Physical Chemistry* **1971**, 75, 3249.
- [63] L. Zhuravlev, V. Potapov, *Russian Journal of Physical Chemistry A, Focus on Chemistry* **2006**, 80, 1119.



- [64] E. F. Vansant, P. Van der Voort, K. C. Vrancken, *Characterization and Chemical Modification of the Silica Surface*, Elsevier, Amsterdam, **1996**.
- [65] T. Armaroli, T. Bécue, S. Gautier, *Oil & Gas Science and Technology - Rev. IFP* **2004**, *59*, 215.
- [66] B. Mitchell Mark, in *Structure-Property Relations in Polymers*, Vol. 236, American Chemical Society, **1993**, pp. 351.
- [67] C. P. Tripp, M. L. Hair, *Langmuir* **1992**, *8*, 1120.
- [68] I. D. Gay, A. J. McFarlan, B. A. Morrow, *The Journal of Physical Chemistry* **1991**, *95*, 1360.
- [69] S. J. Lang, I. D. Gay, B. A. Morrow, *Langmuir* **1995**, *11*, 2534.
- [70] V. M. Gun'ko, M. S. Vedomuthu, G. L. Henderson, J. P. Blitz, *Journal of Colloid and Interface Science* **2000**, *228*, 157.
- [71] O. François, V. Charlotte, W. Marcel, D. Thomas, P. Maxime, C. Jean-Noël, *The Canadian Journal of Chemical Engineering* **1998**, *76*, 1020.
- [72] V. Dugas, Y. Chevalier, *Journal of Colloid and Interface Science* **2003**, *264*, 354.
- [73] B. Rhers, A. Salameh, A. Baudouin, E. A. Quadrelli, M. Taoufik, C. Copéret, F. Lefebvre, J.-M. Basset, X. Solans-Monfort, O. Eisenstein, W. W. Lukens, L. P. H. Lopez, A. Sinha, R. R. Schrock, *Organometallics* **2006**, *25*, 3554.
- [74] *NMR Techniques in Catalysis*, M. Dekker, New York, **1994**.
- [75] G. Engelhardt, D. Michel, *High-Resolution solid-state NMR of silicates and zeolites*, John Wiley and sons, New York, **1987**.
- [76] E. Lippmaa, M. Maegi, A. Samoson, G. Engelhardt, A. R. Grimmer, *Journal of the American Chemical Society* **1980**, *102*, 4889.
- [77] E. Lippmaa, M. Maegi, A. Samoson, M. Tarmak, G. Engelhardt, *Journal of the American Chemical Society* **1981**, *103*, 4992.
- [78] J. Bluemel, *Journal of the American Chemical Society* **1995**, *117*, 2112.
- [79] A. G. Stepanov, *Russian Chemical Reviews* **1999**, *68*, 563.
- [80] J. Bluemel, *Inorganic Chemistry* **1994**, *33*, 5050.
- [81] L. Baltusis, J. S. Frye, G. E. Maciel, *Journal of the American Chemical Society* **1987**, *109*, 40.
- [82] J. H. Lunsford, P. N. Tutunjian, P. J. Chu, E. B. Yeh, D. J. Zalewski, *The Journal of Physical Chemistry* **1989**, *93*, 2590.
- [83] D. W. Sindorf, G. E. Maciel, *Journal of the American Chemical Society* **1983**, *105*, 3767.
- [84] C. Copéret, M. Chabanas, R. Petroff Saint-Arroman, J.-M. Basset, *Angewandte Chemie International Edition* **2003**, *42*, 156.
- [85] J. M. Basset, A. Choplin, *Journal of Molecular Catalysis* **1993**, *21*, 95.
- [86] J. Amor Nait Ajjou, S. L. Scott, *Journal of the American Chemical Society* **2000**, *122*, 8968.
- [87] M. Jezequel, V. r. Dufaud, M. J. Ruiz-Garcia, F. Carrillo-Hermosilla, U. Neugebauer, G. P. Niccolai, F. d. r. Lefebvre, F. o. Bayard, J. Corker, S. Fiddy, J. Evans, J.-P. Broyer, J. Malinge, J.-M. Basset, *Journal of the American Chemical Society* **2001**, *123*, 3520.
- [88] M. S. Eisen, T. J. Marks, *Journal of Molecular Catalysis* **1994**, *86*, 23.
- [89] D. Meunier, A. Piechaczyk, A. de Mallmann, J.-M. Basset, *Angewandte Chemie International Edition* **1999**, *38*, 3540.
- [90] W. A. Herrmann, A. W. Stumpf, T. Priermeier, S. Bogdanović, V. Dufaud, J.-M. Basset, *Angewandte Chemie International Edition in English* **1996**, *35*, 2803.
- [91] A. Salameh, C. Copéret, J.-M. Basset, V. P. W. Böhm, M. Röper, *Advanced Synthesis & Catalysis* **2007**, *349*, 238.
- [92] N. Millot, C. C. Santini, F. d. r. Lefebvre, J.-M. Basset, *Comptes Rendus Chimie* **2004**, *7*, 725.
- [93] Y.-J. Wanglee, J. Hu, R. E. White, M.-Y. Lee, S. M. Stewart, P. Perrotin, S. L. Scott, *Journal of the American Chemical Society* **2012**, *134*, 355.
- [94] N. Millot, C. C. Santini, F. Lefebvre, J.-M. Basset, *Comptes Rendus Chimie* **2004**, *7*, 725.
- [95] E. A. Zheludov, B. A. Seljakov, O. V. Suchkova, M. A. Uljantsev, Vol. RU2102397, **1998**.
- [96] M. Jurado-Gonzalez, A. C. Sullivan, J. R. H. Wilson, *Tetrahedron Letters* **2003**, *44*, 4283.
- [97] B. C. Vicente, Z. Huang, M. Brookhart, A. S. Goldman, S. L. Scott, *Dalton Transactions* **2011**, *40*, 4268.

- [98] A. K. Bhattacharya, G. Thyagarajan, *Chemical Reviews* **1981**, *81*, 415.  
[99] A. Munoz, C. Hubert, J.-L. Luche, *The Journal of Organic Chemistry* **1996**, *61*, 6015.



## **Chapter 2 : Application of the grafting strategy to a P-dopant, the case of boron**

---

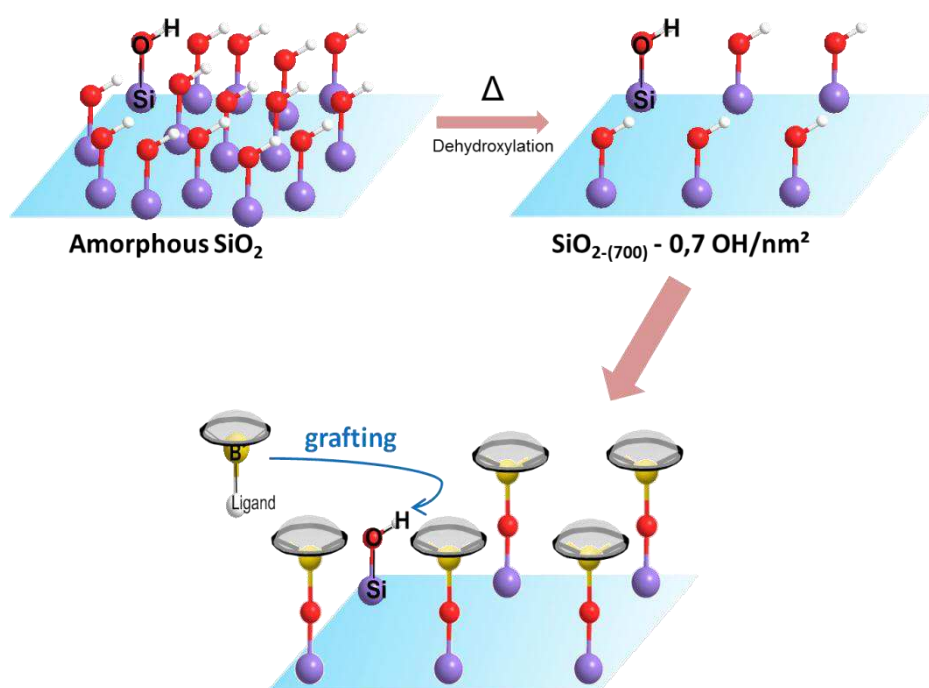
## Summary of the Chapter

---

Introduction: establishment of a dispersion strategy .....	41
1. Defining a grafting strategy .....	42
1.1. Boranes.....	42
1.2. Oxaboroles.....	47
2. Tuning the molecules .....	49
2.1. Improving the reactivity $C_2$ oxaboroles .....	49
2.2. Synthesis of an oxy-dioxaborole.....	51
2.3. $C_3$ tri-coordinated molecules.....	53
2.3.1 Tri-tert-butylborate.....	53
2.3.1.1. Tri-tert-butylsilanolborate.....	54
2.4.2. Use of a pyrrolidinyborane.....	56
3. Improving grafting by self-positioning of $C_{3v}$ molecules .....	58
3.3. Synthesis of a cage-shaped $C_{3v}$ molecule .....	58
3.4. Grafting of a cage-shaped borate.....	59
3.5. Determination of the mechanism of grafting .....	62
4. Elimination of the ligands.....	66
4.3. Outcome of the different calcination experiments.....	66
4.4. Determination of the nature of the calcined species.....	70
4.4.1. Determination of the nature of the calcined species.....	70
4.4.2. Determination of the acidity of the formed surface species .....	71
Conclusion.....	73
References .....	74

## Introduction: establishment of a dispersion strategy

The implantation of boron atoms into silicon wafers was successfully performed in the past years<sup>[1]</sup> using a chemical route for grafting onto Si-H surfaces thus yielding a dopant surface density of  $10^{14}$  at.cm<sup>-2</sup>. However, no controlled positioning was evidenced. Here, the strategy was to control the surface density by combining a controlled concentration of surface anchoring sites (silanols) present at the surface of partially oxidized silicon wafers and a self-positioning of molecules at the surface through steric control between adsorbed molecules (“umbrella effect”, **Fig 30**).



**Fig 30.** Illustration of the strategy and the concept of “Umbrella Effect”

Controlling the OH density on silica materials has been well established over the years on silica particles, and it can be tuned between 0.7-4.0 OH.nm<sup>-2</sup> by thermal treatment under vacuum.<sup>[2]</sup> For the control based on steric, the size and the symmetry of the adsorbed molecules ought to be important. Molecules with high symmetry (C<sub>2</sub> and C<sub>3v</sub>) and a functional group, which can react or interact with surface functionalities, on the principal axis are particularly adapted to control the surface packing.<sup>[3]</sup> Additionally, it is also important for these molecules to be readily accessible in view of their application to microelectronics. For B, two main strategies have been considered depending on the anchoring mode. The B-containing molecule can contain a reactive B-X bond, which will serve to anchor B by reaction on a surface silanol. This X ligand can be chosen from

hydride, alkoxide or amides. The alternative approach is to exploit the Lewis acidity of B, which will interact with O surface functionalities of silica. This latter approach would have the advantage of allowing the possibility of molecules self-assembly at the surface and thus providing a better control of the density, since anchoring *via* grafting is limited by the statistical distribution of OH groups at the surface or silica.

Here, we explore the surface chemistry of boranes, aza- and oxa-boroles and the stability of the grafted boron atom upon calcination.

## 1. Defining a grafting strategy

---

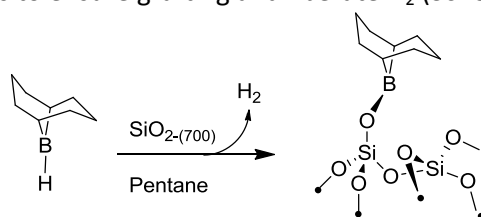
Boranes are one of the most used boron-containing molecules in organic chemistry,<sup>[4],[5]</sup> and are commercially available or easily synthesised through few steps.<sup>[6]</sup>

### 1.1. Boranes

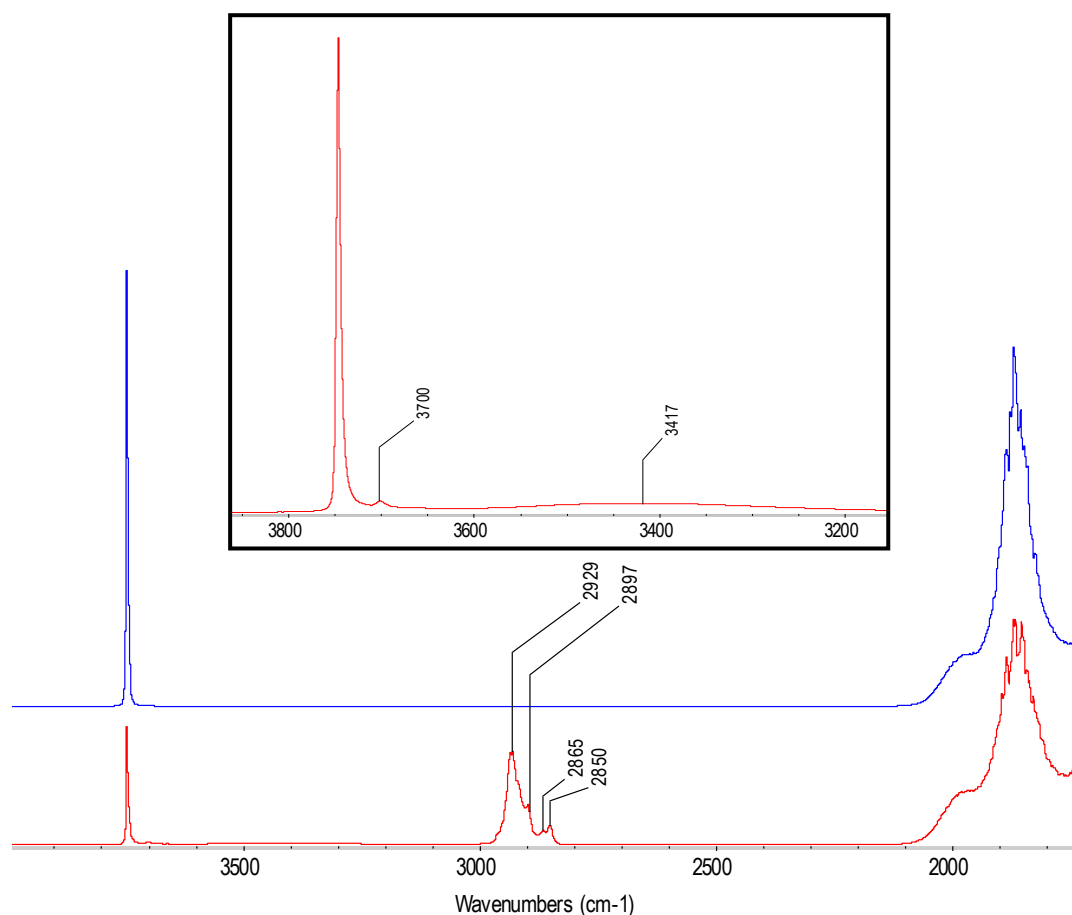
---

A commercially available molecule with a C<sub>2</sub> symmetry, 9-BBN,<sup>[7, 8]</sup> which has been vastly used in organic chemistry<sup>[9-12]</sup> was used to test the grafting possibility.

9-BBN (9-borabicyclo[3.3.1]nonane) presents a very reactive hydride moiety, which should readily react with surface silanols to ensure grafting and liberate H<sub>2</sub> (**Scheme 7**).



**Scheme 7.** Grafting of 9-BBN on SiO<sub>2</sub>-(700)

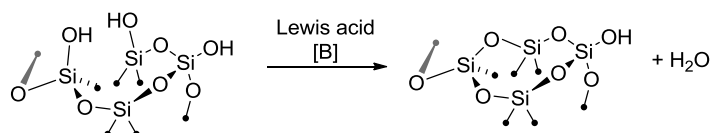


**Fig 31. IR-DRIFT of the grafted 9-BBN on  $\text{SiO}_2(700)$**

9-BBN in a pentane solution was contacted with  $\text{SiO}_2(700)$  and the reaction was monitored by IR-DRIFT spectroscopy. The spectra of silica dehydroxylated at 700°C (blue) before and after reaction with 9-BBN (red) are presented in **Fig 31**. Upon grafting, a partial disappearance of the peak at 3745  $\text{cm}^{-1}$  associated with surface silanols is observed. This is accompanied by the appearance of peaks at 2929  $\text{cm}^{-1}$  and 2866  $\text{cm}^{-1}$  associated with  $\nu_{\text{sym}}(\text{C-H})$  and  $\nu_{\text{asym}}(\text{C-H})$  of the  $\text{CH}_2$  groups respectively. Additionally, two peaks appear at 2898  $\text{cm}^{-1}$  and 2850  $\text{cm}^{-1}$ , associated with the  $\nu_{\text{sym}}(\text{C-H})$  and  $\nu_{\text{asym}}(\text{C-H})$  of the CH groups respectively. Note also the appearance of a broad peak around 3417  $\text{cm}^{-1}$ , which can be tentatively attributed to water, as well as a peak of weak intensity at 3700  $\text{cm}^{-1}$ , consistent with the formation of BOH.<sup>[13, 14]</sup>

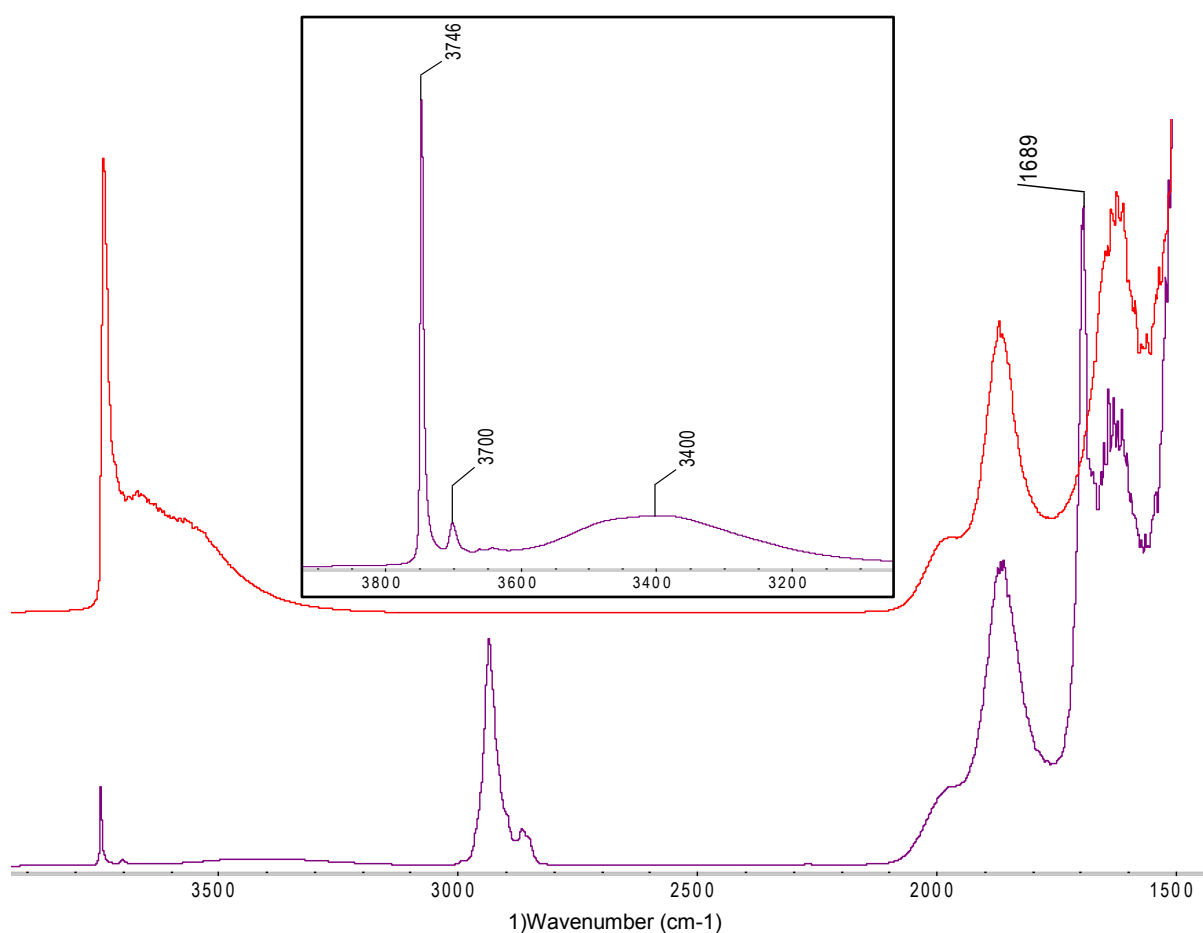
The presence of IR signals associated with formation of water coupled with the presence of BOH groups are reproducible, and does not result from contamination or technical problems. One possible interpretation is that upon contacting the 9-BBN with the surface, grafting is slow and surface rearrangement is catalysed by the Lewis acid property of B.<sup>[15]</sup> (**Scheme 8**) This would yield water, which upon reaction with 9-BBN or B-containing surface compounds can lead to B-OH formation.





Scheme 8. Condensation of silanols catalyzed by a Lewis acid

In order to test this hypothesis, we explored the reaction of 9-BBN with a partially dehydroxylated silica at lower temperature to increase the density of OH group.  $\text{SiO}_{2-(200)}$  was chosen; it displays an OH density of  $2.4 \text{ OH}\cdot\text{nm}^{-2}$  versus  $0.7 \text{ OH}\cdot\text{nm}^{-2}$  for  $\text{SiO}_{2-(700)}$ .<sup>[2]</sup> The IR-DRIFT spectra are presented in **Fig 32** hereafter for  $\text{SiO}_{2-(200)}$  (red) after reaction with 9-BBN on  $\text{SiO}_{2-(200)}$  (dark purple).

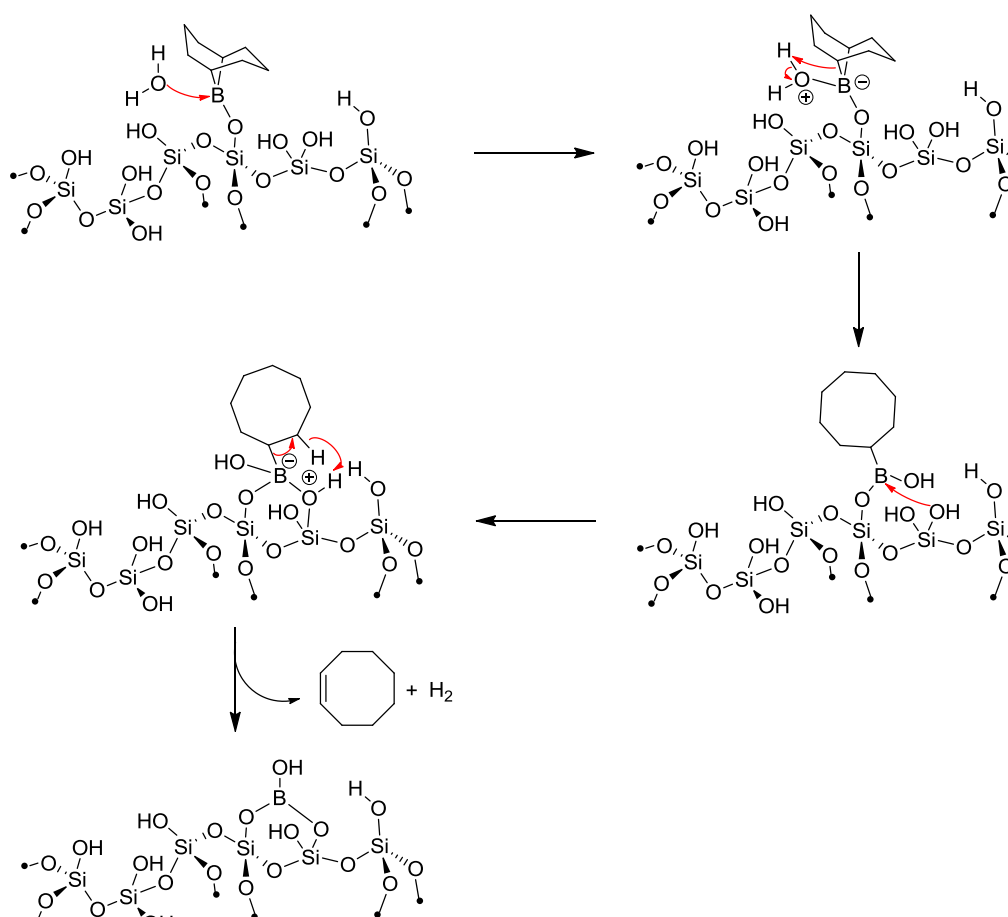
Fig 32. IR-DRIFT of the grafting of 9-BBN on  $\text{SiO}_{2-(200)}$ 

First, as previously found on  $\text{SiO}_{2-(700)}$  (cf **Fig 30**), isolated silanols are partially consumed, signals associated with alkyl ligand appear as well as a peak at  $3700 \text{ cm}^{-1}$  characteristic of B-OH.<sup>[13, 14]</sup> However, it is noteworthy that the broad and rather intense signal associated with bonded silanols

also disappears, while a large peak at  $3400\text{ cm}^{-1}$  appears. The latter probably corresponds to adsorbed water. Moreover, an intense peak at  $1692\text{ cm}^{-1}$  appears, which is characteristic of an alkenyl C=C stretching vibration, although no trace of any alkene C-H stretching band can be seen around  $3100\text{-}3000\text{ cm}^{-1}$ .

Here, with a higher density of surface silanols, water is probably formed in larger amount according to the large and intense band observed in IR. This is consistent with the proposed surface restructuration catalysed by a Lewis acid;<sup>[16]</sup> the formed water can further oxidise the B-H bond of 9-BBN or B-containing surface species to generate species with BO-H functionalities.

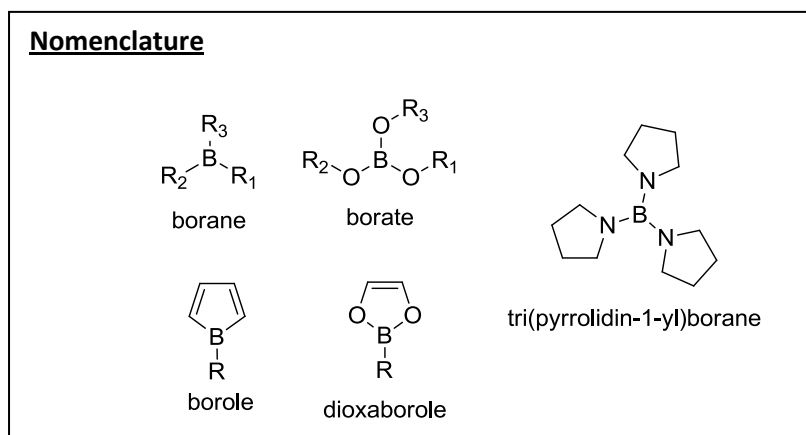
Moreover, GC and GC-MS analysis shows that 0.8 equiv. of  $\text{H}_2$  is formed per initial surface OH and that cyclooctene was formed during the grafting process. The former is consistent with the chemical grafting of 9-BBN by protonolysis of the B-H bond, and the latter, which is consistent with the appearance of alkenyl group by IR, could be indicating that the grafted species is unstable and further decomposes quickly.<sup>[17, 18]</sup> One possibility would be that hydrolysis of the B-C bond generate a non-B-containing cyclic compound. A scheme is proposed hereafter.<sup>[19, 20]</sup> (**Scheme 9**)



**Scheme 9.** B-elimination on the grafted borane, leading to the formation of cyclooctene

In view of the complexity of the surface reactivity with borane reagents, we decided to study the surface chemistry of other B-containing molecules as boroles and boronates.

Knowing that oxaboroles were more stable than boranes,<sup>[21]</sup> the whole ligand screening was then oriented towards bulky B-O ligands type.

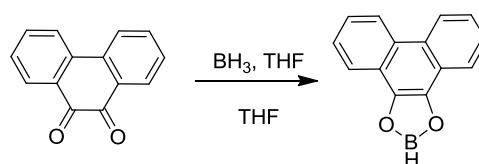


## 1.2. Oxaboroles

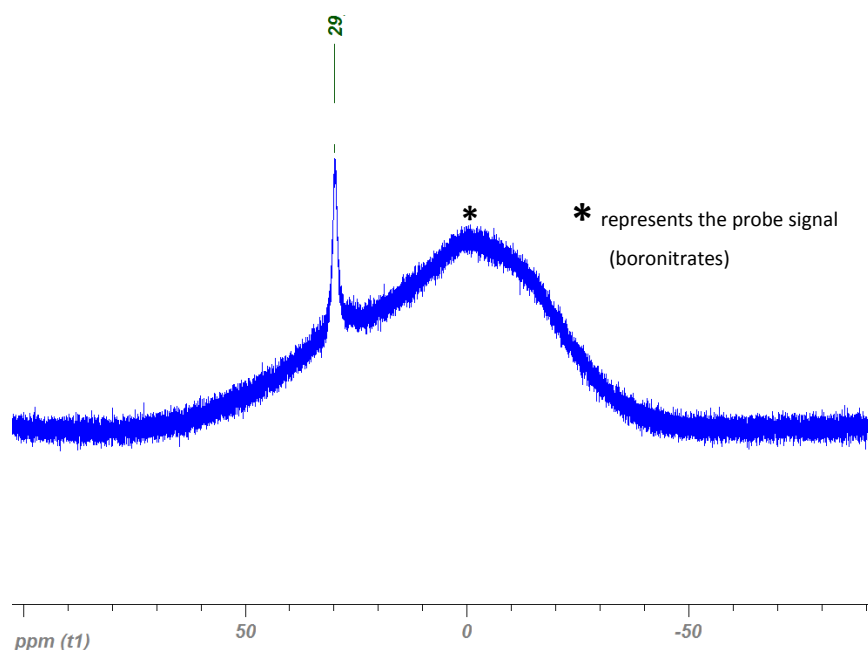
Because of the high stability of B-O bonds,<sup>[21-27]</sup> (RO)<sub>2</sub>B-X species were then used, in order to ensure both a good reactivity through their B-X bond but also, as previously, prevent any kind of side-reaction as previously described.

Also, such species are easily tuned<sup>[28-30]</sup> which is an important asset for the implementation of the chosen strategy.

The dioxaborole was prepared by reacting phenanthrene-9,10-dione with BH<sub>3</sub>, THF (1M) in THF. The <sup>11</sup>B-NMR spectrum of the formed product (**Fig 33**) displays a peak at 29,8 ppm, characteristic of (RO)<sub>2</sub>BH.<sup>[29]</sup> The absence of peak at -1,1ppm<sup>[31]</sup> and ca. 50-55ppm<sup>[32]</sup> show the absence of residual BH<sub>3</sub> and no formation of hydrolysed by-product [(RO)<sub>2</sub>BOH], respectively.



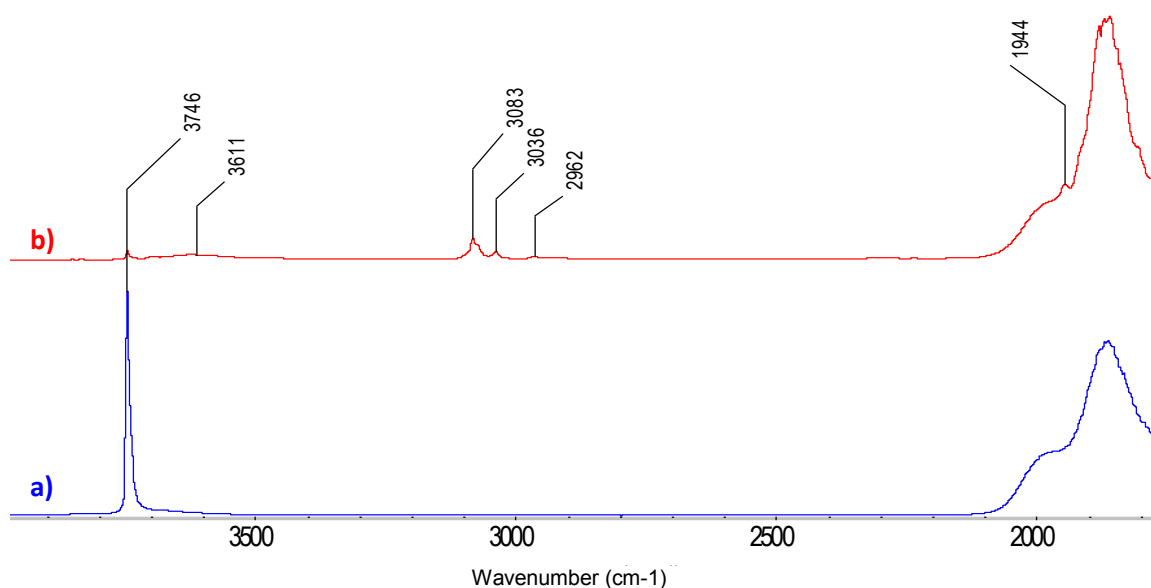
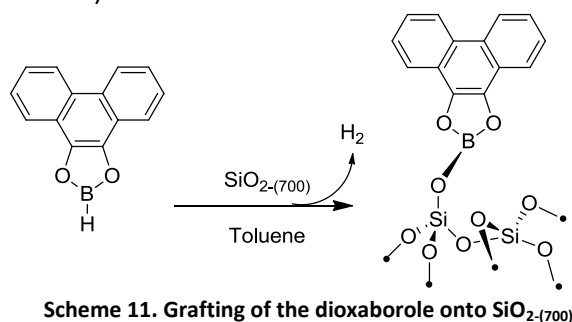
**Scheme 10. Synthesis of the dioxaborole**



**Fig 33. <sup>11</sup>B-NMR of the C<sub>2</sub> dioxaborole**

Grafting of the dioxaborole on SiO<sub>2-(700)</sub> (0.7 OH.nm<sup>-2</sup>) leads to the evolution of 0.9 equiv. of H<sub>2</sub> per surface silanol. This is consistent with elemental analysis with the presence of 0.23% of B, which corresponds to 0.6 B.nm<sup>-2</sup> and thereby 90% grafting. Moreover, IR-DRIFT analysis (**Fig 33**) showed that most isolated silanols (80%) are consumed upon grafting. It also shows the appearance of peaks

at  $3083\text{cm}^{-1}$  and  $3037\text{cm}^{-1}$ , both of which witness the presence of aromatic functionalities as these peaks correspond respectively to  $\nu_{\text{sym}}(\text{C}_{\text{sp}2}\text{-H})$  and  $\nu_{\text{asym}}(\text{C}_{\text{sp}2}\text{-H})$ . The presence of a peak at  $2962\text{ cm}^{-1}$  of weak intensity and characteristic of alkyl functionalities is most consistent with the presence of residual toluene. One can also stress the appearance of a peak at  $1944\text{ cm}^{-1}$ . While this has been subject to a number of controversial interpretations,<sup>[33-35]</sup> it can be assigned to  $\nu_{\text{sym}}(\text{B-H})$  band.<sup>[36]</sup> This band must stem from the presence of residual oxaborole, which is also corroborated by the results from Klanberg et al.<sup>[35]</sup> (**Scheme 11**)



**Fig 34. IR-DRIFT of the starting  $\text{SiO}_2\text{-(700)}$  (a) and after grafting of the dioxaborole (b)**

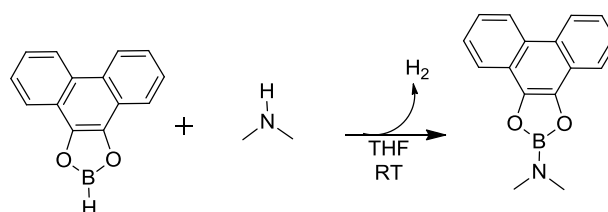
Overall, these data are consistent with a chemical grafting of the dioxaborole on the surface silanols of silica as shown in **Scheme 14**, where the aromatic ligands interact with residual silanols, probably not accessible to the reagent. It also shows that residual dioxaborole is probably present at the surface as evidenced by the presence of a weak signal at  $1944\text{ cm}^{-1}$ .

## 2. Tuning the molecules

### 2.1. Improving the reactivity C<sub>2</sub> oxaboroles

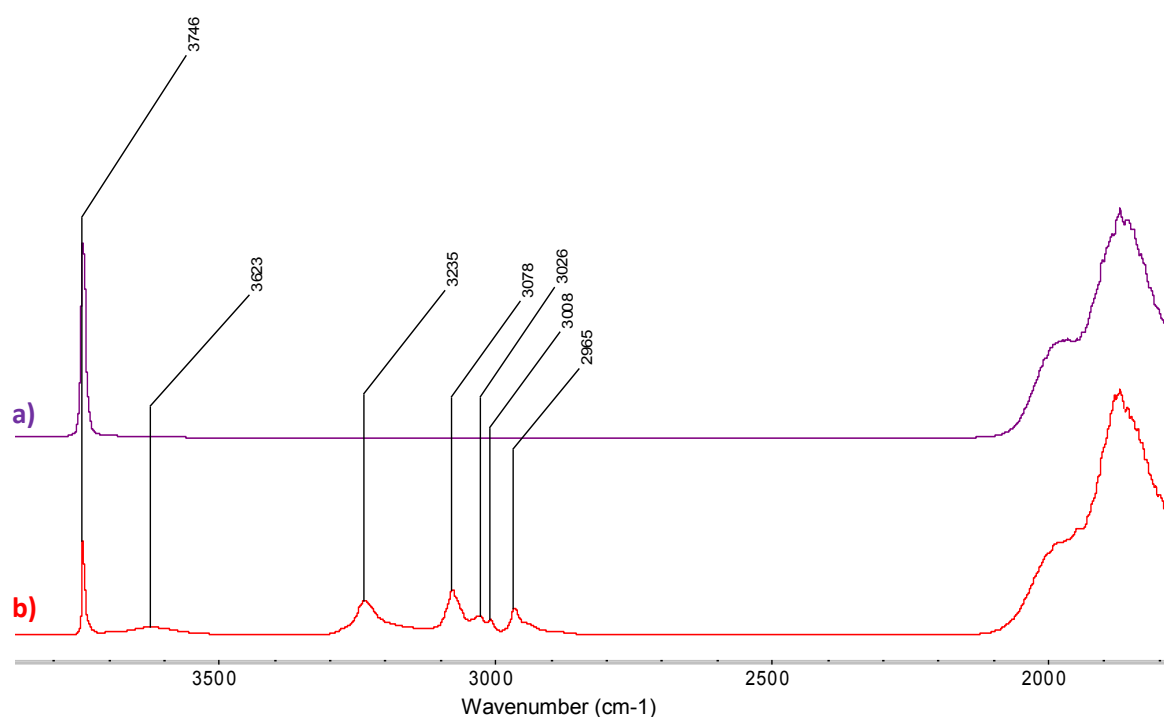
Further molecules such as amino-dioxaborole were synthesized following existing procedures<sup>[37]</sup> and tested, knowing that B-N bonds were more reactive than B-O bonds.<sup>[22, 38, 39]</sup>

We first prepare the isoelectronic aminodioxaborole. (**Scheme 12**)



**Scheme 12.** Synthesis of the dimethylamino-dioxaborole

A DRIFT spectrum of the outcome of the reaction can be seen on **Fig 35** hereafter.



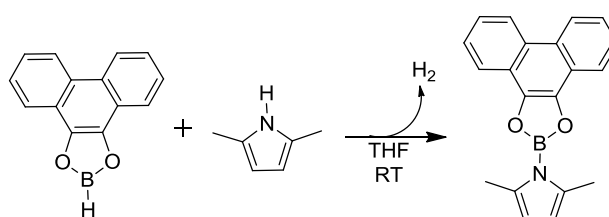
**Fig 35.** IR-DRIFT of the starting SiO<sub>2</sub>-(700) (a) and after grafting of the dimethylamino-dioxaborole (b)

The presence of peaks between 3078 cm<sup>-1</sup> ( $\nu_{\text{sym}}(\text{C}_{\text{sp}^2}\text{-H})$ ) and 3008 cm<sup>-1</sup> ( $\nu_{\text{asym}}(\text{C}_{\text{sp}^2}\text{-H})$ ) is consistent with the presence of aromatic compounds. The peak at 2965 cm<sup>-1</sup> is characteristic of an alkyl C-H stretching (symmetrical), the asymmetric stretching vibration being the shoulder at 2936 cm<sup>-1</sup>. The

broad peak at  $3235\text{ cm}^{-1}$  is characteristic of an amine N-H hydrogen-bonded stretching. Also, the very large peak at  $3623\text{ cm}^{-1}$  corresponds to bonded O-H vibration bands.

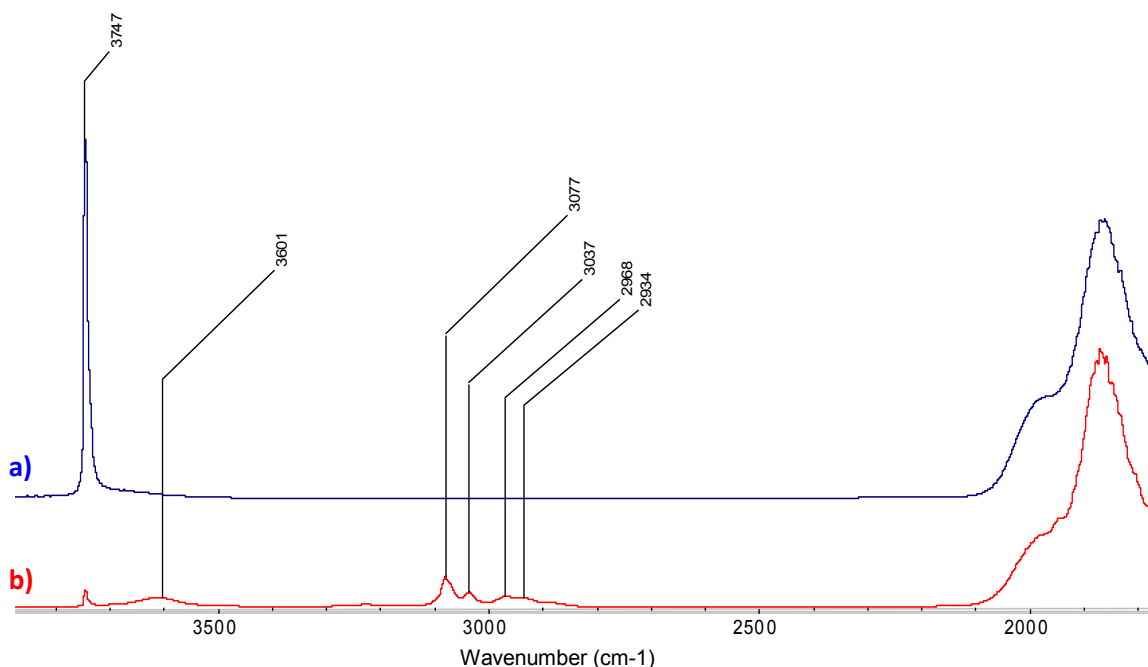
As could be expected, the formed amine remained stacked onto the surface, as proved both by the peak at  $2936\text{ cm}^{-1}$  but also by the N-H stretching band at  $3235\text{ cm}^{-1}$ . Some bonded silanols appear as well, being either interacting with the amine or the grafted borole.

Based on this encouraging result, we examined a B-compound with a 2,5-dimethylpyrrolyl ligand, which liberates upon grafting 2,5-dimethylpyrrole, a molecule less basic and less prompt to remain at the surface,<sup>[40]</sup> upon grafting. The molecule was synthesised following the same methodology as published:<sup>[37]</sup>



**Scheme 13.** Synthesis of the pyrrolyl-dioxaborole

The molecule was contacted with  $\text{SiO}_{2-(700)}$ , and an IR-DRIFT analysis was then performed to confirm the grafting.



**Fig 36.** IR-DRIFT of the starting  $\text{SiO}_{2-(700)}$  (a) and after grafting of the pyrrolyl-dioxaborole (b)

As can be seen in **Fig 36** above, the peak at  $3747\text{ cm}^{-1}$ , characteristic of isolated silanols, decreases drastically and the next broad peak appearing at  $3601\text{ cm}^{-1}$  is coherent with bonded OH

groups. Both peaks at  $3077\text{ cm}^{-1}$  and  $3037\text{ cm}^{-1}$  are significant of the alkene  $\nu_{\text{sym}}(\text{C-H})$  and  $\nu_{\text{asym}}(\text{C-H})$  respectively. Then, the two last peaks are characteristic of alkyl  $\nu_{\text{sym}}(\text{C-H})$  and  $\nu_{\text{asym}}(\text{C-H})$  respectively.

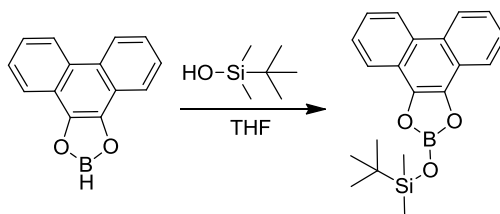
The peak at  $3601\text{ cm}^{-1}$  is consistent with H-bonded O-H stretching, which may stem from the unreacted SiOH in interaction with the aromatic rings of the borole. The presence of the two peaks at  $2968\text{ cm}^{-1}$  and  $2934\text{ cm}^{-1}$  associated with symmetrical and asymmetrical  $\text{sp}^3$  C-H bond vibration are consistent with the release of 2,5-dimethylpyrrolyl from the grafted species.

An elemental analysis was performed and gave a B-loading of  $0.24\%_{\text{wt}}$ , hence a surface density of  $0.6\text{ B.nm}^{-2}$  which corresponds to a grafting yield of 90%. The result is comparable to that of the initial borole.

## 2.2. Synthesis of an oxy-dioxaborole

A third grafting way was investigated using B-OR containing precursors.

Trying to find good leaving groups, trans-esterification reactions had were performed<sup>[41]</sup> using dioxaborole and dimethyltert-butylsilanol as follows:



**Scheme 14.** Reaction between the usual dioxaborole and a silanol

The synthesized species was grafted on  $\text{SiO}_{2-(700)}$  and the reaction was monitored by IR-DRIFT. (**Fig 37**)



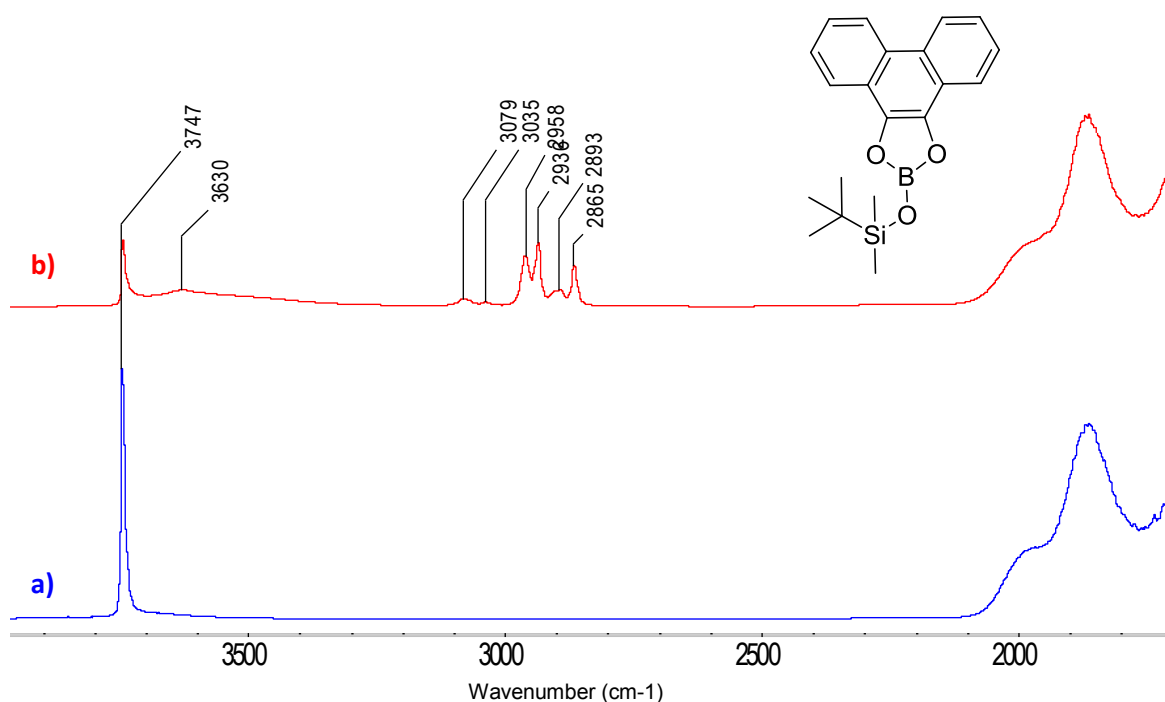


Fig 37. IR-DRIFT of the starting SiO<sub>2</sub>-(700) (a) and after grafting of the oxy-dioxaborole (b)

The top spectrum (red) is the IR-DRIFT of the grafting of the oxy-dioxaborole. The bottom one (blue) is the standard for SiO<sub>2</sub>-(700). Peaks between 2893 cm<sup>-1</sup> and 2958 cm<sup>-1</sup> refer to the  $\nu_{\text{asym}}(\text{C-H})$  and  $\nu_{\text{sym}}(\text{C-H})$  from the alkyl chain respectively. Peaks at 3079 cm<sup>-1</sup> and 3035 cm<sup>-1</sup> are characteristic of the  $\nu_{\text{sym}}(\text{C-H})$  and  $\nu_{\text{asym}}(\text{C-H})$  of the aromatic ring respectively. The broad peak at 3630 cm<sup>-1</sup> is characteristic of bonded OH groups. The remaining peak at 3747 cm<sup>-1</sup> shows remaining isolated surface silanols.

From the latter peak, it can easily be concluded that all surface silanols did not react. The aromatic C-H stretching bands prove that the molecules could effectively be found on the surface. However, more interestingly, the presence of alkyl chains shows that the silanol could not be eliminated, despite strong washing with toluene and pentane. This can be easily explained by the fact that this silanol may easily condense onto the surface and generate water<sup>[42-44]</sup> (*vide supra*).

Then, the presence of the peak at 3630 cm<sup>-1</sup> may represent two things: First, it may be due to surface silanols in interaction with the aromatic cycle of the molecule. It could also be due to the presence of formed water.

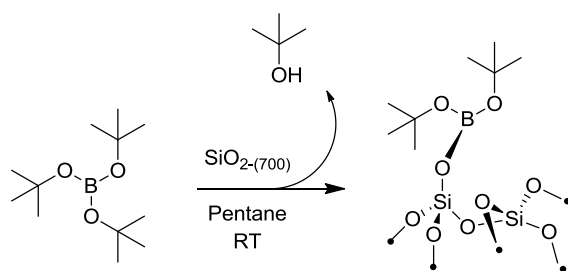
### 2.3. C<sub>3</sub> tri-coordinated molecules

In order to find simple, straightforward useable molecules, an interesting choice was to use C<sub>3</sub> molecules with homoleptic ligands; such geometry being able to favour good coverage of the surface and ensure the desired umbrella effect.

#### 2.3.1 Tri-tert-butylborate

As transesterifications of borates with silanols were reported to be easily feasible,<sup>[45]</sup> the strategy was implemented to the synthesis of C<sub>3</sub>-symmetry molecules. Indeed, due to sterics, the hopefully formed tert-butanol will be less likely to condense onto the surface than, say, methanol or ethanol.

The compound was reacted with the surface as shown hereafter.



Scheme 15 .Grafting of tri-tert-borate onto SiO<sub>2-(700)</sub>

An IR-DRIFT analysis of the resulting powder was then performed. (Fig 38)

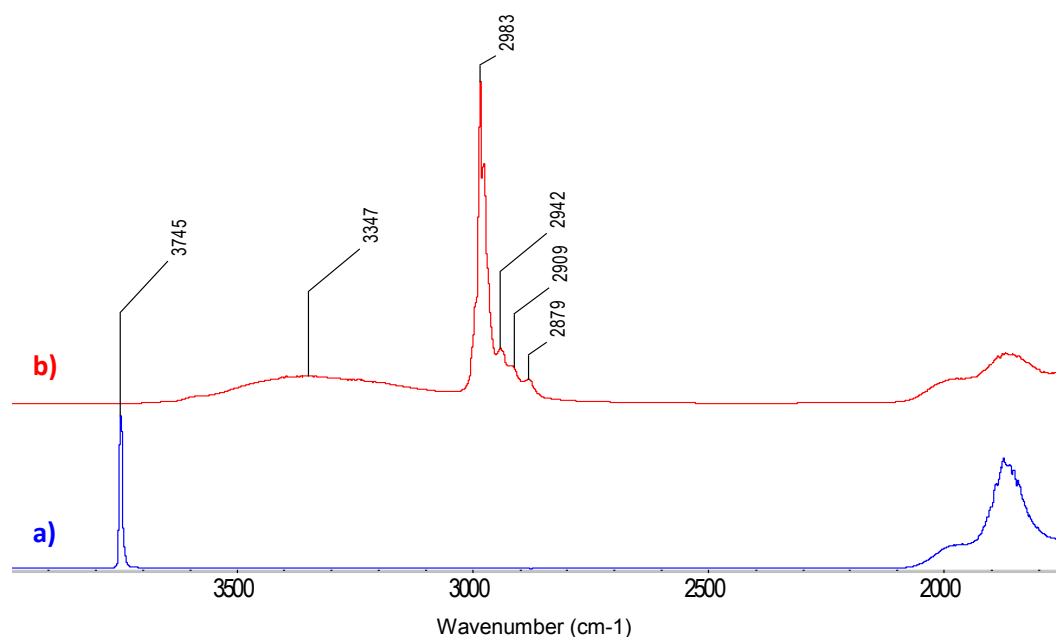
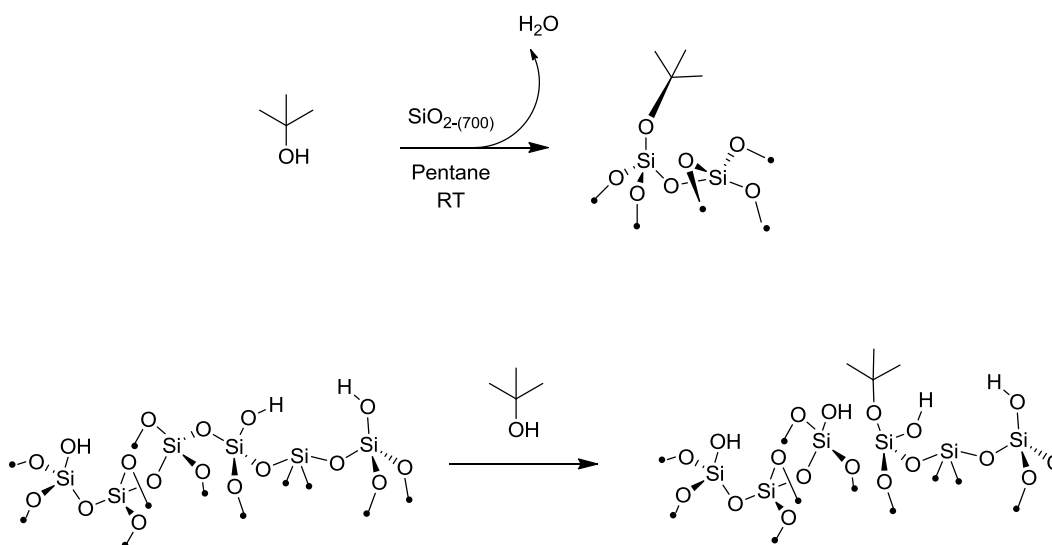


Fig 38. IR-DRIFT of the starting SiO<sub>2-(700)</sub> (a) and after grafting of tert-butylborate (b)

As can be seen on the IR spectrum, the C-H  $sp^3$  vibrations appear quite clearly: peaks between  $2982\text{ cm}^{-1}$  and  $2942\text{ cm}^{-1}$  refer to the  $\nu_{\text{asym}}(\text{C-H})$  and peaks between  $2942\text{ cm}^{-1}$  and  $2879\text{ cm}^{-1}$  to  $\nu_{\text{sym}}(\text{C-H})$  from the alkyl chain respectively. Also, the absence of the peak at  $3745\text{ cm}^{-1}$  proves that there is no residual surface silanol. However one may note the appearance of a broad peak at  $3347\text{ cm}^{-1}$ .

This broad peak at  $3347\text{ cm}^{-1}$  is most likely due to adsorbed tBuOH or water released during the grafting. Indeed, the grafting of the borate releases one equivalent of tert-butanol which may further react with the surface. Tert-butanol can react with either surface silanols or siloxane bridges to give  $\text{SiOtBu}$  and  $\text{H}_2\text{O}$  or  $\text{SiOH}$  respectively (**Scheme 16**).



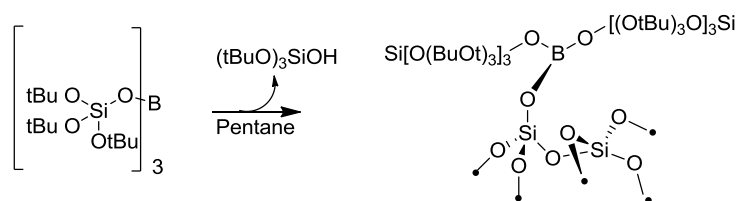
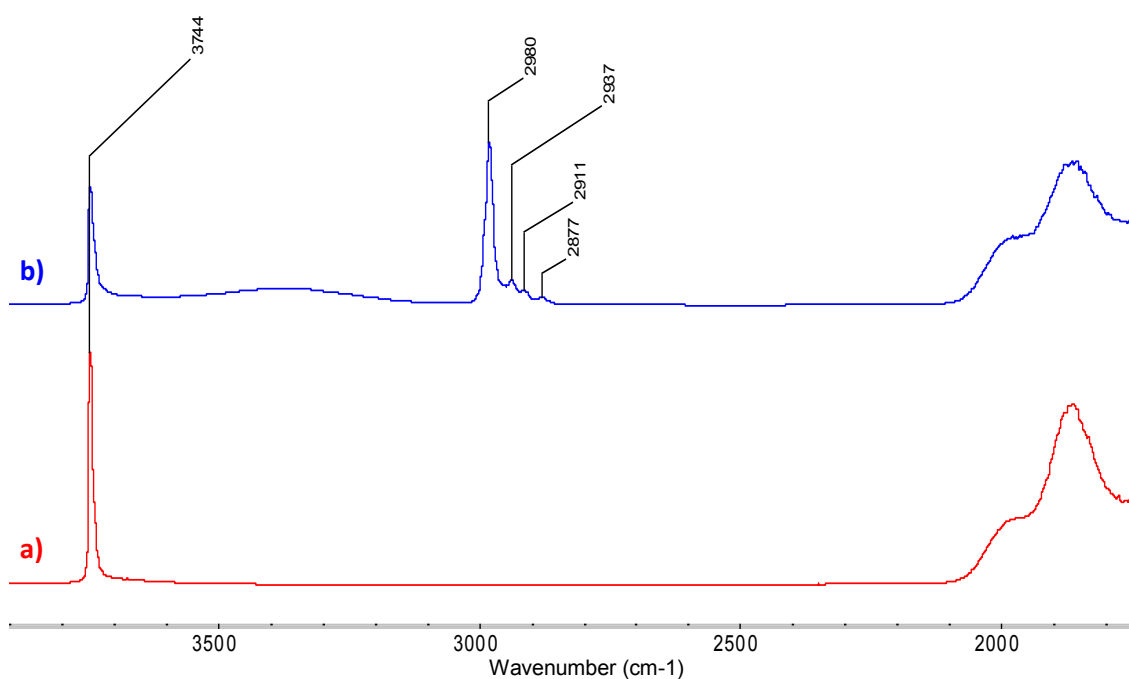
**Scheme 16. Condensation of tert-butanol with silica**

This likely precludes a full control of the grafting process, and therefore the necessity of finding B-precursors, which avoid such side reaction.

### 2.3.1. Tri-tert-butylsilanolborate

Tilley et al. have shown over the years that silanolate ligand can readily be introduced around metal centers and released selectively upon grafting  $(\text{tBuO})_3\text{SiOH}$ , which does not react with the surface or itself to release water and can be readily desorbed from the surface by washing steps.<sup>[46]</sup> Moreover the use of tri-silylborates would also be a promising approach as it will provide silica upon calcination helping the insertion of B into silica. (*vide infra*)

The silanolborate was prepared according to literature procedures<sup>[47]</sup> and then grafted onto silica (**Scheme 17**). An IR-DRIFT analysis of the grafted species was performed. (**Fig 39**)

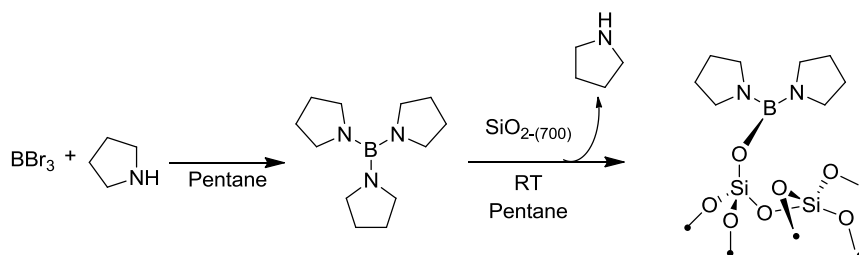
Scheme 17. Grafting of tri-tert-butylsilanol borate onto  $\text{SiO}_{2-(700)}$ Fig 39. IR-DRIFT of the starting  $\text{SiO}_{2-(700)}$  (a) and after grafting of tri-tert-butylsilanolborate (b)

The spectrum of the grafted species (top) shows two peaks at  $2937\text{ cm}^{-1}$  and  $2877\text{ cm}^{-1}$ , which are characteristic of  $\nu_{\text{sym}}(\text{C-H})$  and  $\nu_{\text{asym}}(\text{C-H})$  of  $\text{sp}^3$  alkyl groups. The large band at  $3400\text{ cm}^{-1}$  is characteristic of bonded OH and may result from  $\text{tBuO}_3\text{SiOH}$  adsorbed on the surface. It is noteworthy that, the peak characteristic of isolated silanols at  $3744\text{ cm}^{-1}$  is still present, which shows that grafting is not quantitative.

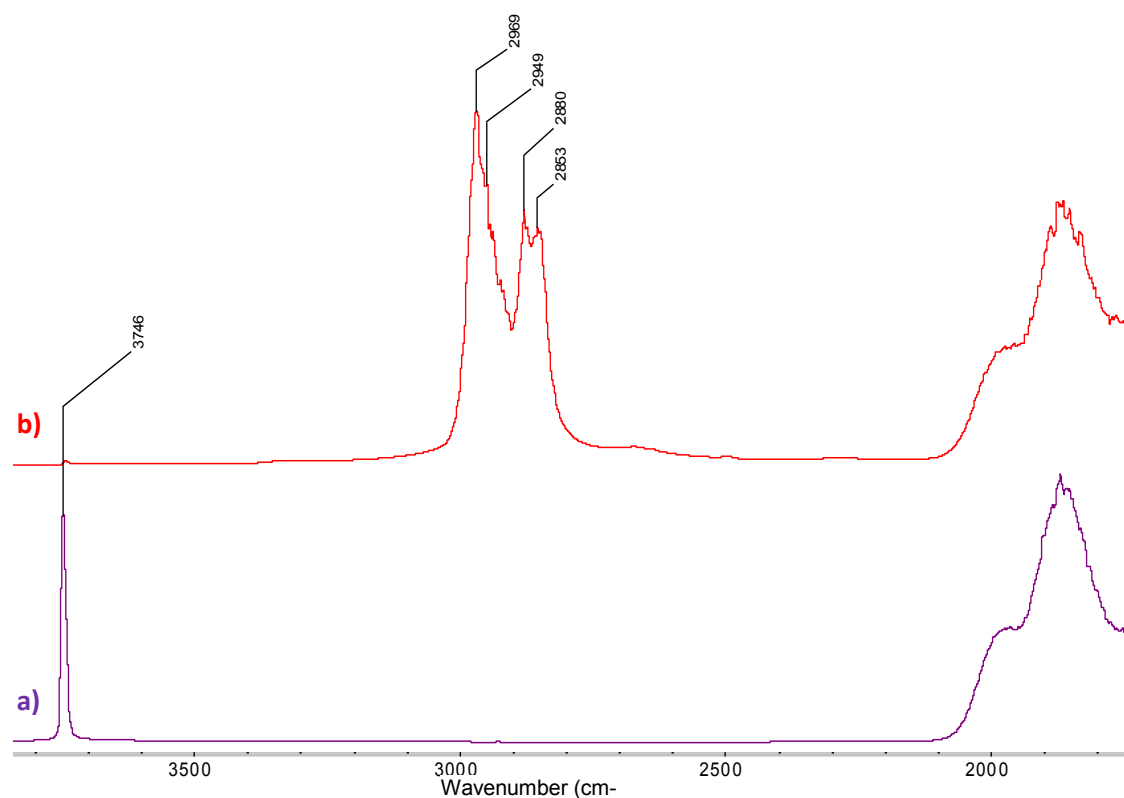
The low yield of grafting may result from the lower reactivity of this compound or to the formation of water, which could inhibit grafting.

## 2.4.2. Use of a pyrrolidinyborane

In order to avoid the formation of water, we also used tri-pyrrolidinyborane (**tPB**) for grafting. The molecule was synthesized as described in the literature<sup>[48]</sup> then grafted onto SiO<sub>2</sub>. The grafting step was performed in pentane (**Scheme 18**) and the thus formed grafted species was analysed through IR-DRIFT (**Fig 40**)



Scheme 18. Synthesis and grafting of tPB

Fig 40. IR-DRIFT of the starting SiO<sub>2</sub>(700) (a) and after grafting of tPB (b)

According to the IR-DRIFT spectrum, the peak at 3746 cm<sup>-1</sup>, characteristic of isolated surface silanols disappeared almost entirely, showing that only little or no silanol remained (no additional broad feature associated with bonded OH). This disappearance is associated with the appearance of peaks at 2969 cm<sup>-1</sup> and 2880 cm<sup>-1</sup> referring to the  $\nu_{\text{asym}}(\text{C-H})$  and  $\nu_{\text{sym}}(\text{C-H})$  of the CH<sub>2</sub> in  $\alpha$  of the N

atom as well as peaks at  $2949\text{ cm}^{-1}$  and  $2853\text{ cm}^{-1}$  referring to the  $\nu_{\text{asym}}(\text{C-H})$  and  $\nu_{\text{sym}}(\text{C-H})$  of the  $\text{CH}_2$  in the  $\beta$  position of N atom respectively.

Elemental analyses showed a B-loading of  $0.25\%_{\text{wt}}$ , which gives a grafting yield of 94%, showing that the grafting was indeed quasi quantitative.

A short conclusion can be drawn from these experiments. First, the  $\text{C}_2$ -borole could be easily grafted in a quasi-quantitative yield ( $>90\%$ ). The changes in side-chain ligands, replacing the initial hydrogen by a pyrrolyl group proved to be efficient in terms of grafting yield and avoiding of side-reactions. The latter pyrrolylborole could also be a good choice as it is slightly more stable towards air than its borole counterpart. Also, as pyrrole does not coordinate to the surface, grafting of the targeted molecule onto the surface should be observed. As for the  $\text{C}_3$ -symmetrical molecules, the sole pyrrolylborate was indeed the only one that proved to be a very interesting molecule, achieving apparent quantitative grafting (as seen on the DRIFT spectrum, **Fig 40**).

### 3. Improving grafting by self-positioning of $C_{3v}$ molecules

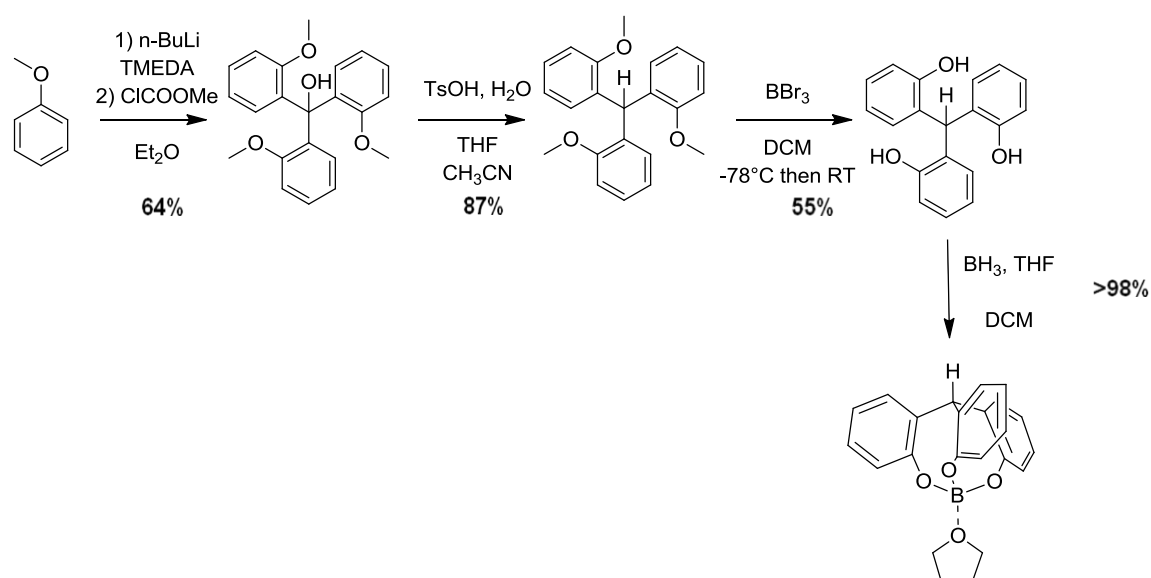
In order to ensure a better and more homogeneous surface coverage and to prevent any interaction of the organic chain with the surface as seen with  $C_2$  molecules, another strategy was to focus on the adsorption of molecular precursors by interaction of the Lewis Acid B site with the Lewis basic oxygen sites without making a covalent bond between B and the support, thus allowing surface self-organisation of the B-containing precursor on the substrate.

#### 3.3. Synthesis of a cage-shaped $C_{3v}$ molecule

Because of its strong Lewis-acid centre imbedded in a sterically hindered  $C_3$  symmetric cage-molecule, the selected molecule, a borate,<sup>[49]</sup> was synthesised.

Such compound requires several steps, but is straightforward leading to an overall yield of 30%.

(Scheme 19)



Scheme 19. Synthesis of the cage-shaped borate ester

### 3.4. Grafting of a cage-shaped borate

The borate was then reacted with  $\text{SiO}_{2-(700)}$  in toluene. Elemental analyses gave a B loading of 0.22%<sub>wt</sub> which corresponds to a grafting yield of 88%. The reaction was also monitored by IR-DRIFT. (Fig 41)

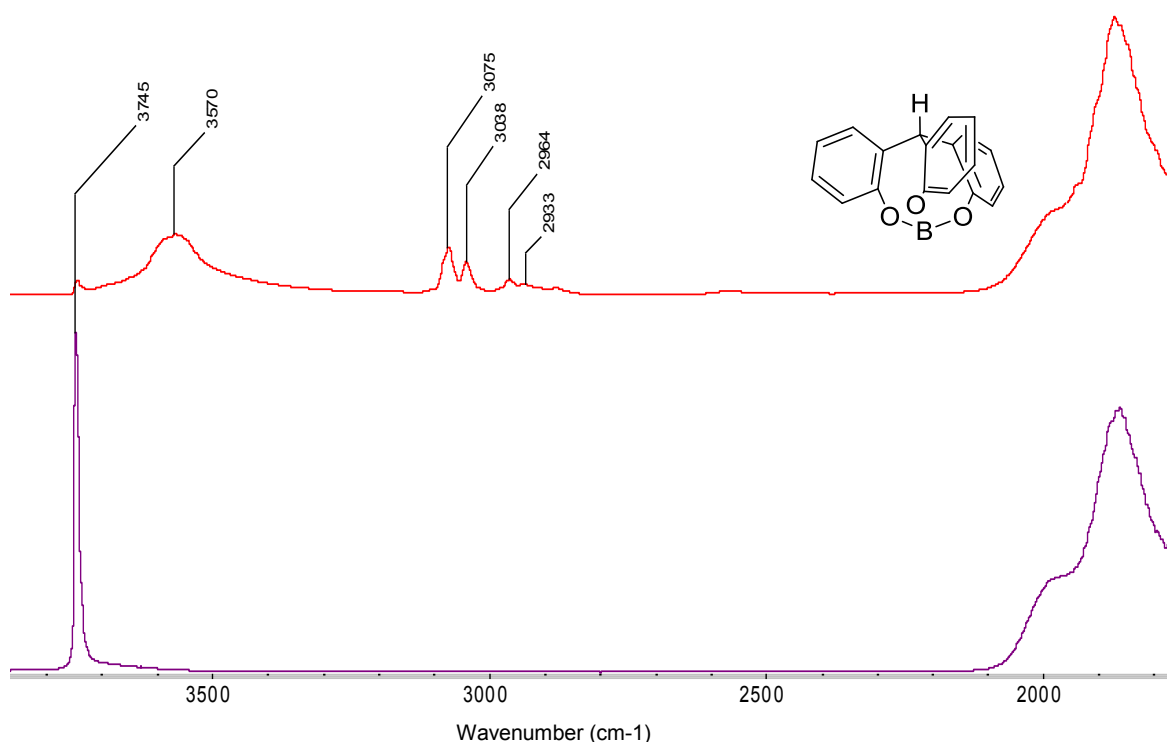
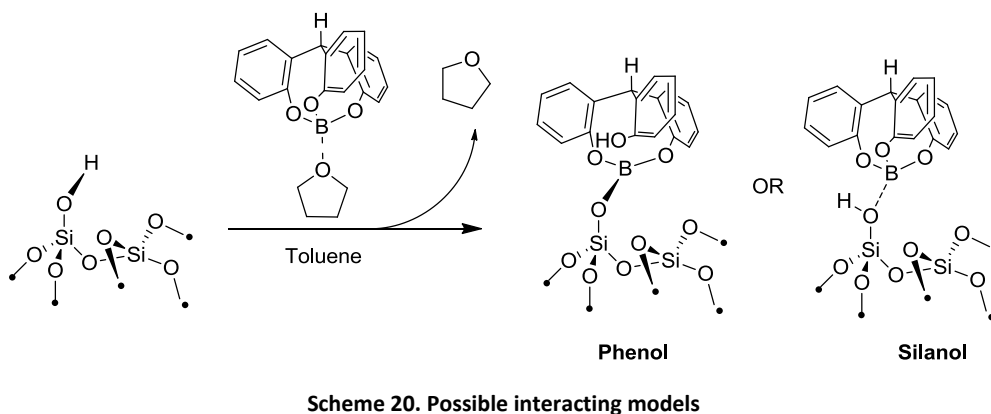


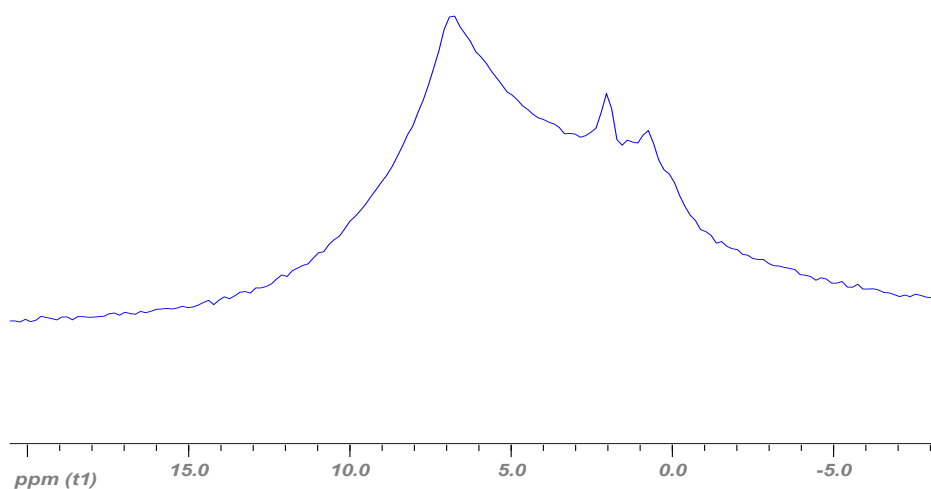
Fig 41. IR-DRIFT of the reacted cage-shaped borate

Most importantly, the IR spectrum shows that the peak at  $3745\text{ cm}^{-1}$ , characteristic of isolated surface silanols, almost disappeared, while a broad broad peak appeared at  $3570\text{ cm}^{-1}$ . Additionally, the appearance of peaks at  $2964\text{ cm}^{-1}$  [ $\nu_{\text{sym}}(\text{C}_{\text{Alk}}\text{-H})$ ],  $2933\text{ cm}^{-1}$  [ $\nu_{\text{asym}}(\text{C}_{\text{Alk}}\text{-H})$ ],  $3075\text{ cm}^{-1}$  [ $\nu_{\text{sym}}(\text{C-H})$ ] and  $3038\text{ cm}^{-1}$  [ $\nu_{\text{asym}}(\text{C-H})$ ], respectively, were consistent with the presence of new surface species having hydrocarbonyl ligands. While there was clearly adsorption of the dioxaborocine on silica, it is not clear how this molecule is bound to the surface, i.e. by coordination of the B atom on the surface oxygen functionalities or by opening the B-O bond from the cage molecule; the latter hypothesis would lead to the formation of a phenol and thus a shift of the OH vibration. (Scheme 20).





Solid-state NMR was then performed on the sample. Using a spinning rate at the magic angle of 10 kHz, the proton NMR remains very broad and did not provide much information besides the presence of aromatic protons (large peak centred at 6.8 ppm), associated with aromatic protons (**Fig 42**)



**Fig 42.**  $^1\text{H}$ -SSNMR of the grafted cage-shaped borate (zg, 10kHz, d1=2s, ns=8, lb=0Hz)

$^{13}\text{C}$  SSNMR (**Fig 43**) confirmed the presence of the aromatic carbon associated with the phenoxy group. In particular, the peak at 150 ppm is characteristic of a phenolic carbon ( $\text{C}_b$  on **Fig 43**). The signal at 128 ppm can be attributed to  $\text{C}_a$ ,  $\text{C}_d$  and  $\text{C}_f$ , the one at 121 ppm to  $\text{C}_d$  and finally, the one at 116 ppm to  $\text{C}_c$ . It has to be noted that the alkyl C-H, expected at 20 ppm, is not observed.<sup>[49]</sup> However, it does not allow to distinguish between the two precedent hypotheses (vide supra, **Scheme 20**).<sup>[50]</sup> The absence of peak at 26 ppm and 68 ppm proved that all THF coming from the initial coordinated THF was removed upon contact of the cage-shaped borate with the surface.

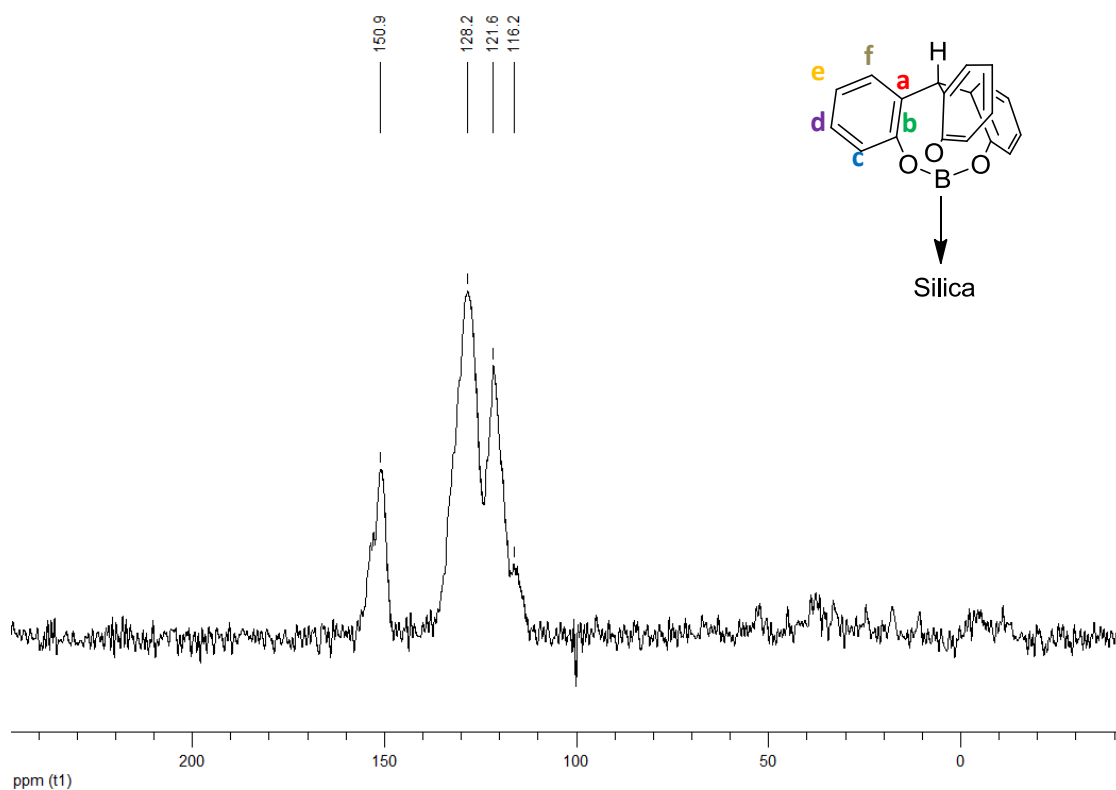


Fig 43.  $^{13}\text{C}$ -SSNMR of the grafted cage-shaped borate (CPMAS, 10 kHz,  $d_1=10\text{s}$ ,  $ns=30000$ ,  $lb=50\text{Hz}$ )

The absence of peak in  $^{11}\text{B}$ -SSNMR (Fig 44) is consistent with the presence of a B atom of low symmetry, such as this expected for planar trigonal geometry. This could indicate that the cage opened while grafting and led to the formation of the phenol species.

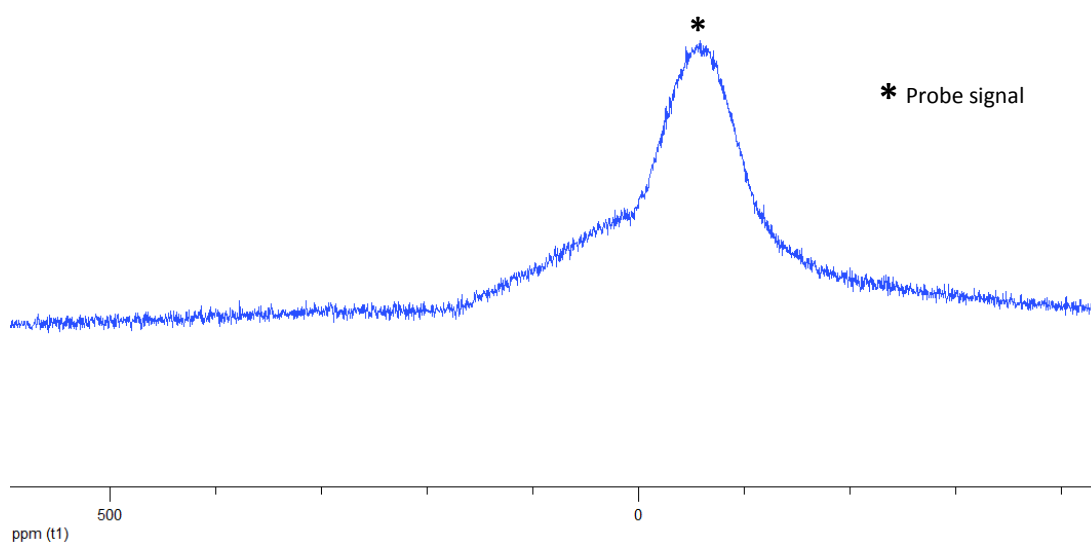


Fig 44.  $^{11}\text{B}$ -SSNMR of the grafted cage-shaped borate (MAS, 10kHz,  $d_1=2\text{s}$ ,  $ns=219$ ,  $lb=0\text{Hz}$ )

### 3.5. Determination of the mechanism of grafting

According to these spectroscopic data, it is not clear whether the borate is just coordinated to surface functionalities or if it reacted with SiOH to give a ring opened product. The latter implies the formation of a phenol and the transfer of protons from the surface oxygen to an oxygen-bound to an aromatic ring. Thus, we decided to investigate the grafting on  $^{18}\text{O}$ -doped support in order to discriminate the species by IR-DRIFT since grafting should lead either to proton bound to an  $^{18}\text{O}$ -H (simple interaction/coordination of SiOH on the dioxaborocine) or to a proton bound to  $^{16}\text{O}$ -H if proton transfer occurred. (Fig 45)

The difference between both mechanisms should result in a shift of the  $^{18}\text{O}$ -H vibration band to lower wavenumbers. As  $(\text{Si})^{16}\text{O}$ -H is expected at  $3745\text{cm}^{-1}$ , we would await the  $(\text{Si})^{18}\text{O}$ -H at  $3733\text{cm}^{-1}$ . Similarly the peak observed at  $3560\text{cm}^{-1}$  could be shifted to  $3548\text{cm}^{-1}$ .

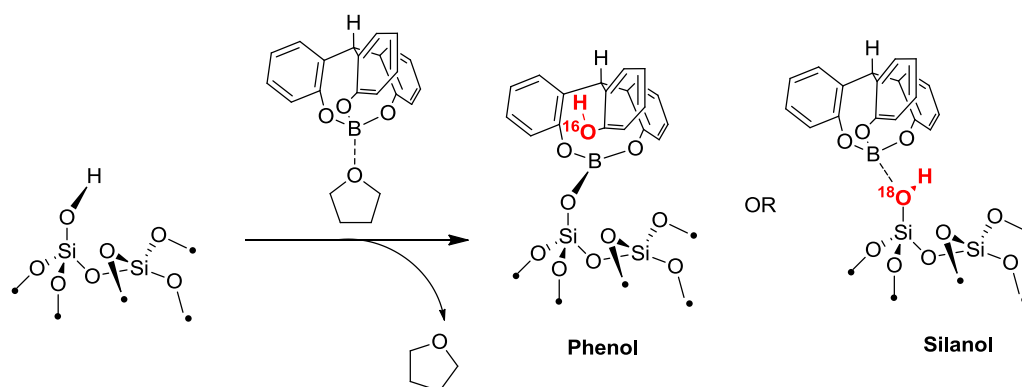
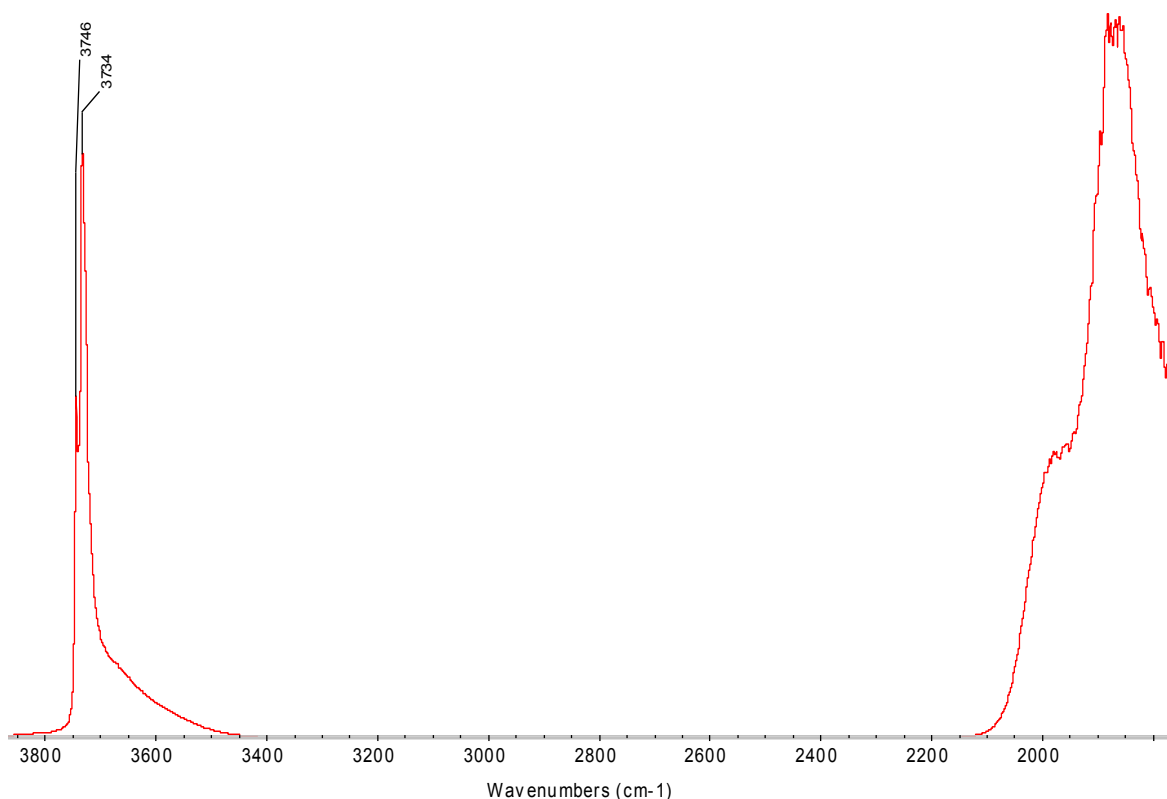


Fig 45. Comparison between the two possible obtainable products

Thus,  $^{18}\text{O}$ -doped silica was synthesized as described in the literature.<sup>[51]</sup>

The IR-DRIFT spectrum of the  $^{18}\text{O}$ -doped  $\text{SiO}_{2-(700)}$  shows a major peak at  $3734\text{ cm}^{-1}$ , consistent with a very good labelling of the surface.



**Fig 46.**IR-DRIFT of the  $^{18}\text{O}$ -labelled  $\text{SiO}_{2-(700)}$

The OH signal was decomposed in two features to evaluate the ratio of  $^{18}\text{O}/^{16}\text{O}$  on the surface of  $^{18}\text{O}$ -doped silica. (**Fig 47**) The respective areas of the  $^{16}\text{O}$ -H and  $^{18}\text{O}$ -H peaks are 305 and 5617 (as calculated by OMNIC), which is consistent with a 95% labelling by  $^{18}\text{O}$  of the surface silanols.

## Chapter 2

Component peak centered at 3732.906 cm<sup>-1</sup>

Component peak centered at 3746.721 cm<sup>-1</sup>

LM097

Composite result spectrum: LM097

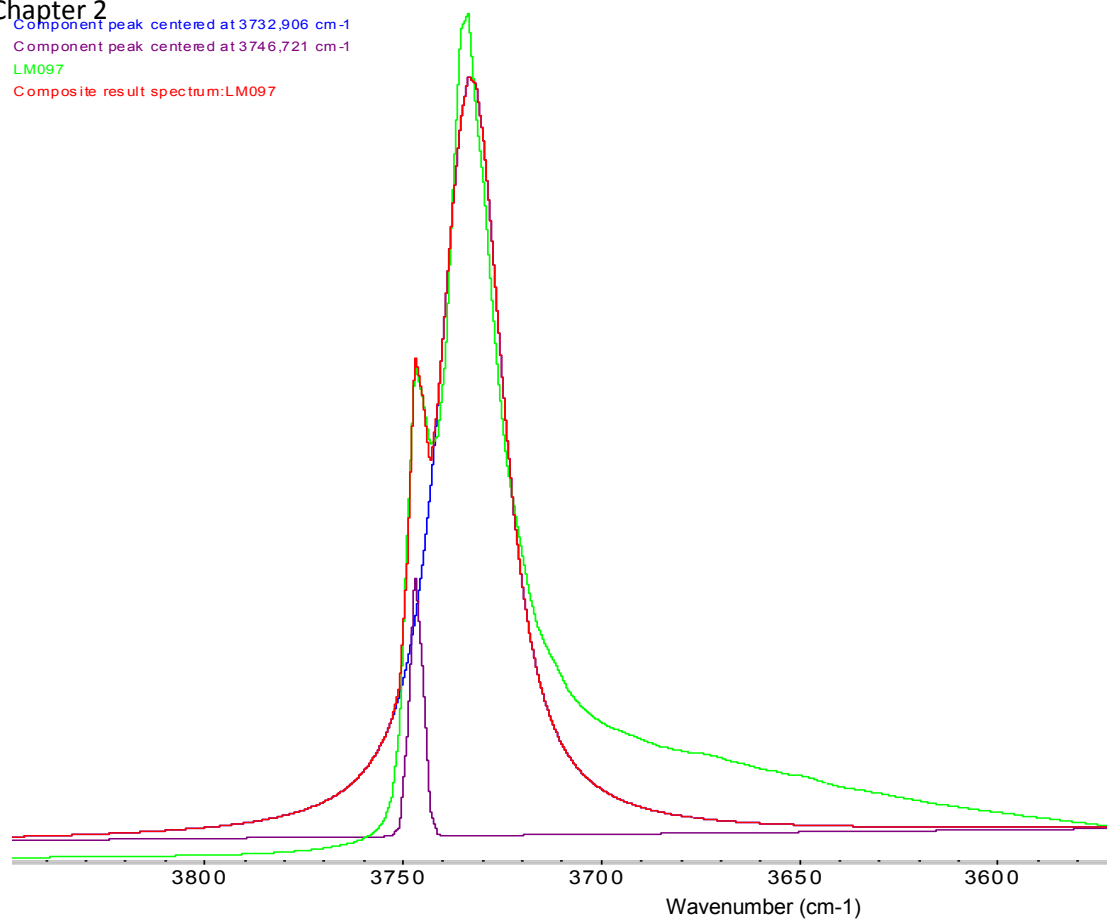


Fig 47. Peak resolve of the <sup>18</sup>O-labelled silica surface

The next step was to perform the grafting of the cage-shaped borate with the <sup>18</sup>O-labeled silica and to record an IR spectrum (**Fig 47**). After grafting the cage-shaped borate onto the surface, a similar spectrum to that observed in **Fig 41** is obtained. However, two peaks are noteworthy at 3745 cm<sup>-1</sup> and 3732 cm<sup>-1</sup>. As shown above, they are coherent with the <sup>18</sup>O-doped surface. The two peaks between 3100 cm<sup>-1</sup> and 3000 cm<sup>-1</sup> represent the aromatic asymmetrical and symmetrical C-H stretching bands respectively. They are unchanged compared to the previous result on non-doped silica along with the peaks between 3000 cm<sup>-1</sup> and 2860 cm<sup>-1</sup>, characteristic of the alkyl C-H stretching.

Also, the peak at 3570 cm<sup>-1</sup> was not shifted despite the use of <sup>18</sup>O-doped silica.

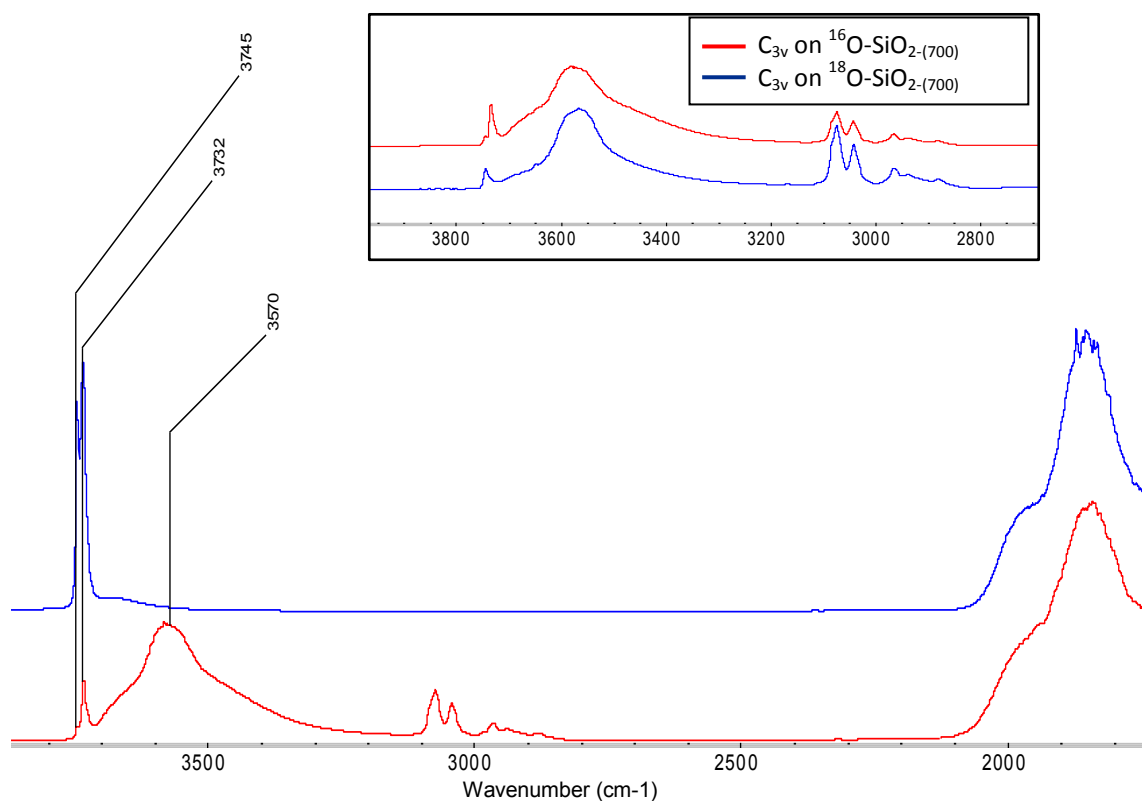


Fig 48. IR-DRIFT of the grafted cage-shaped borane onto  $^{18}\text{O}$ -doped silica

Since the peak at  $3570\text{ cm}^{-1}$  was not shifted, it was therefore attributed to  $^{16}\text{O-H}$ , from the cage-shaped borate, thus proving that grafting occurred *via* opening of this cage. (Fig 49)

In conclusion, the cage-shaped molecule reacted with the surface silanols, by opening by cleavage of an O-B bond and thus generating a phenol moiety. Therefore, grafting was observed versus self-assembly.

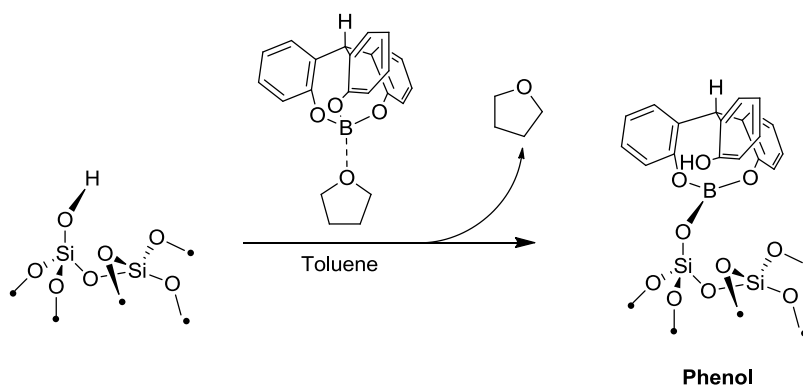


Fig 49. Conclusive scheme for the grafting of the  $\text{C}_{3v}$ -borate

## 4. Elimination of the ligands

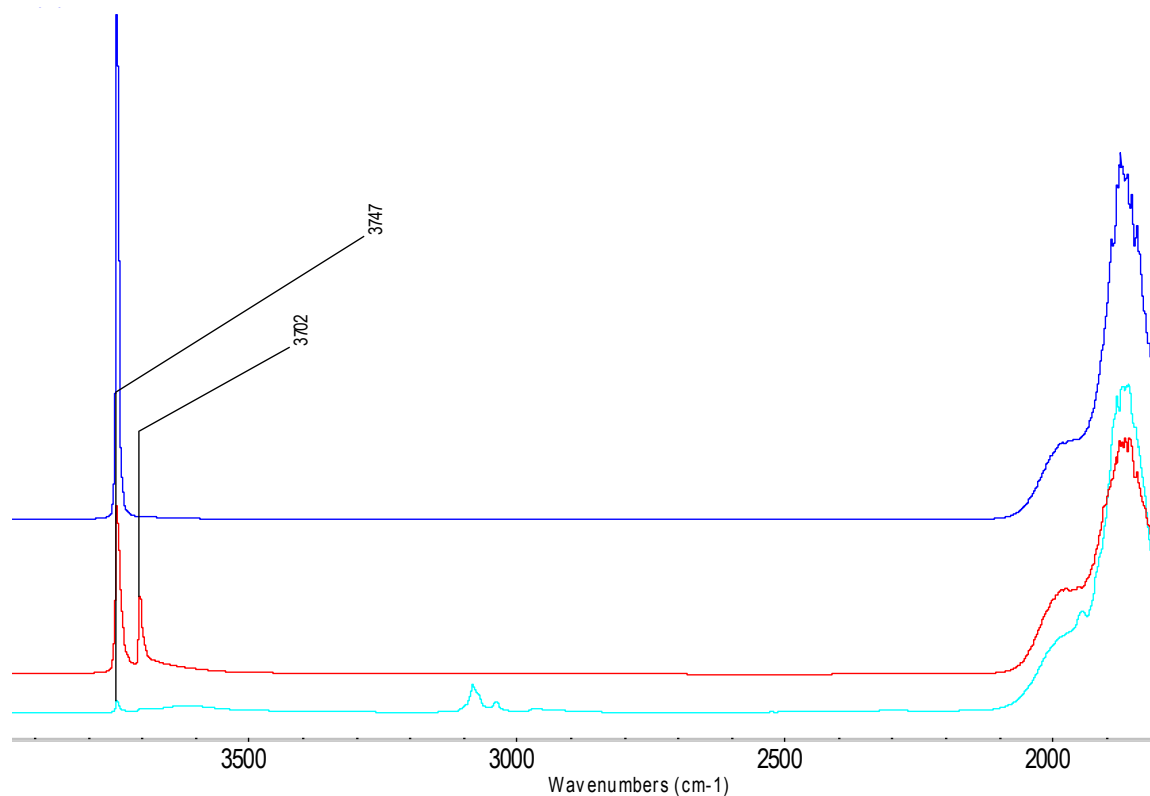
---

Before implementing the grafting procedures from silica to 2D wafer surfaces, the ligands from the grafted molecule was studied in order to secure the B content at the surface or inside the material in the silica materials. Calcination was used to address this point.<sup>[52-55]</sup>

### 4.3. Outcome of the different calcination experiments

---

All grafted species were calcined for 2h under a flow of dry air ( $50 \text{ mL}\cdot\text{min}^{-1}$ ) at  $500^\circ\text{C}$  (ramp:  $6^\circ\text{C}\cdot\text{min}^{-1}$ ). This step was performed using all previously grafted molecules. We first examined the case of the grafted  $\text{C}_2$  species as an illustrative exemple of all other species. (see **Table 1**)



**Fig 50.** IR-DRIFT of the calcined grafted  $\text{C}_2$  species (red) compared to the initial  $\text{SiO}_2-(700)$  (blue) and the grafted  $\text{C}_2$ -species (cyan)

As can be seen on the previous **Fig 50**, the following features can be drawn from the spectrum after calcination:

- Disappearance of all peaks associated with the organic ligands,
- Reappearance of the peak at  $3747 \text{ cm}^{-1}$  associated with isolated silanols,

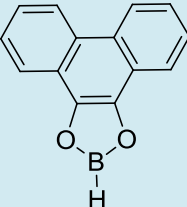

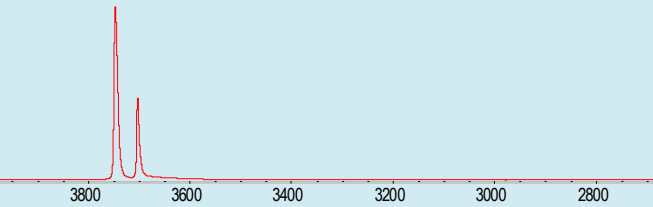
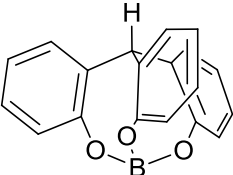

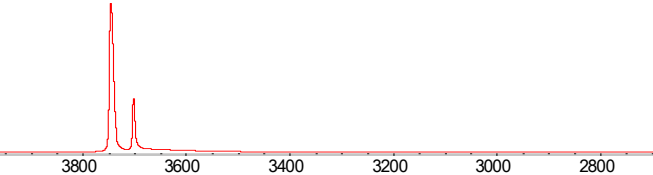
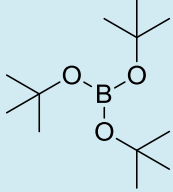
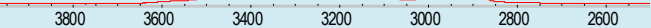
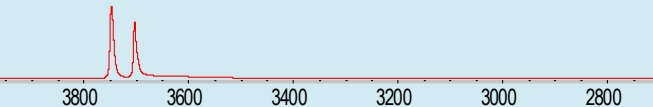
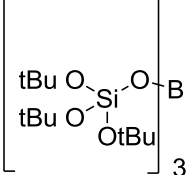

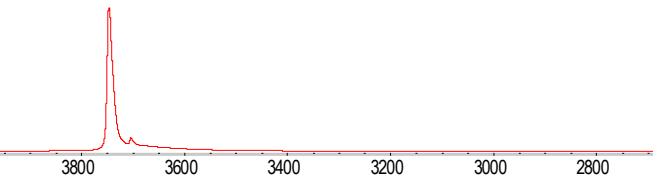
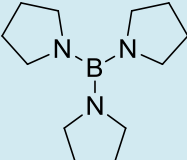
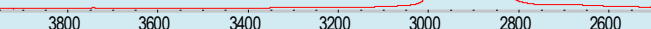
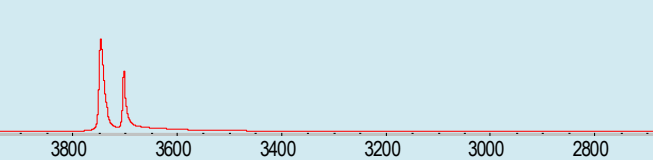
- Appearance of a new peak at  $3702\text{ cm}^{-1}$  attributed to a hydroxyl group according to its position in the spectrum.

While the peak at  $3747\text{ cm}^{-1}$  typical of surface silanols, the peak at  $3702\text{ cm}^{-1}$  is in agreement to formation of an isolated BOH group.<sup>[13, 14]</sup> This is consistent with the fact that boron is known to easily diffuse through silica<sup>[56]</sup>. Many different boron-silicon matrices were reported in the literature, such as potential BOH<sup>[13]</sup> which appear at  $3702\text{ cm}^{-1}$  (vs  $3747\text{ cm}^{-1}$  for actual SiOH) and B(OH)Si that appear at  $3725\text{ cm}^{-1}$ .<sup>[14]</sup> Moreover, elemental analysis showed a B loading of 0.24%<sub>wt</sub> after calcination which shows that boron remains in the silica support upon calcination (96% surface coverage of all surface silanols and equal to the surface loading before calcination).

In the following **Table 1**, it is noteworthy that these features arise for every initial grafted compound: recovery of the isolated SiOH and appearance of the peak at  $3702\text{ cm}^{-1}$ , coherent with the formation of BOH species.



Table 1. Comparison of the effect of calcination on each grafted precursor

Precursor	IR-DRIFT spectrum of the grafted species (wavenumbers $\text{cm}^{-1}$ )	IR-DRIFT spectrum of the calcined species (wavenumbers $\text{cm}^{-1}$ )	%wtB before calcination	%wtB after calcination
			0.24	0.24
			0.22	0.22
			X	X
			X	X
			0.25	0.24

Several conclusions stem from these observations. First, upon calcination, organic chains were removed in all cases. Elemental analyses on the C<sub>3v</sub> cage-shaped borate reported a decrease from 4.46%<sub>wt</sub> of C in the non-calcined supported species to 0.68%<sub>wt</sub> in the calcined species. This proves that only 15% of the original organic moiety remained on the surface, the rest being removed by calcination.

It is interesting to note that, for the tri-tertbutylborate and tri-pyrrolidinylborane, the amount of species which are represented by the peak at 3702 cm<sup>-1</sup> is higher than for the other precursors. Also, in the case of tri-tert-butoxysilanolborate, the amount of the newly-formed surface species is lower than for all others.

The loading of B remains at 0.24%<sub>wt</sub> before and after calcination for the C<sub>2</sub> grafted species and at 0.22%<sub>wt</sub> for the C<sub>3v</sub> grafted one. The only weak decrease in boron loading can be seen for the grafted tri-pyrrolidinylborane, as the elemental analyses show a loading of 0.25%<sub>wt</sub> before calcination and 0.24%<sub>wt</sub> after calcination. This proves that the calcination step does not influence the boron loading, and is suitable for removing the organic chain of the grafted species.

The next step of this analysis is to determine the nature of the newly formed species.

#### 4.4. Determination of the nature of the calcined species

##### 4.4.1. Determination of the nature of the calcined species

To further confirm the attribution to B-OH and to understand how it was formed, a sample of grafted tri-pyrrolidinylborane on  $^{18}\text{O}$ -doped silica was prepared. If this newly formed OH group is specific of a surface boronic acid, then, as boron diffuses through  $\text{SiO}_2$ , this would lead to a peak shifting at  $3700\text{ cm}^{-1}$  with the same amplitude as shown before.

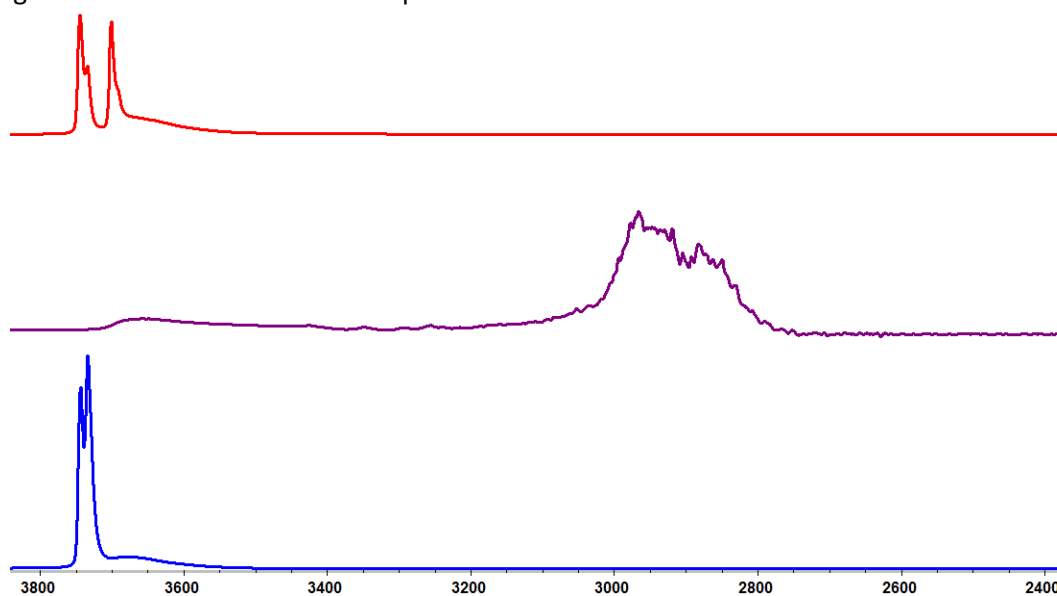


Fig 51. IR-DRIFT of the calcined tri-pyrrolidinylborane (red) versus the non-calcined species (purple) and original  $^{18}\text{O}$ -doped  $\text{SiO}_{2-(700)}$  (blue)

As can be seen on Fig 51, calcinations lead to the formation of both types of OH groups, O-16 or O-18 labelled, either bound to Si or B.

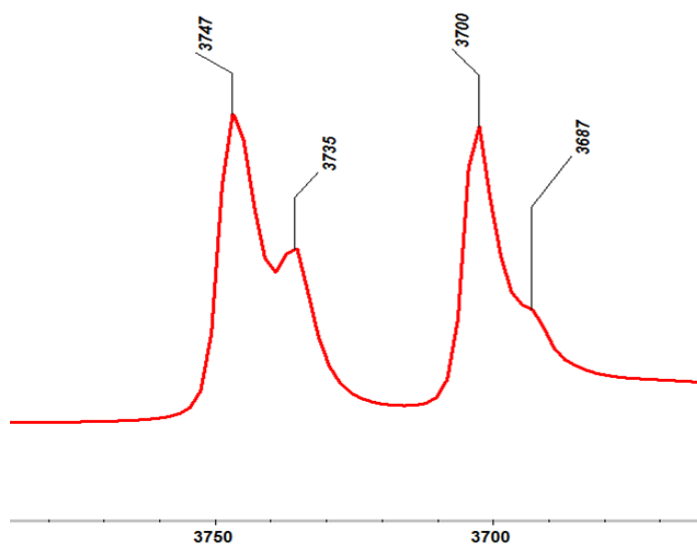


Fig 52. Close-up of the OH region of the calcined tri-pyrrolidinylborane on  $^{18}\text{O}$ -doped  $\text{SiO}_{2-(700)}$

As can be seen on the above **Fig 52** all peaks are duplicated, because of the  $^{18}\text{O}$ -doping. Yet, concerning the newly obtained peak at  $3700\text{ cm}^{-1}$ , a shoulder appears at  $3693\text{ cm}^{-1}$  which is coherent with the expected shift due to a change of isotopical oxygen. It is thus indeed a surface OH and it can be attributed to BOH, as literature reported.<sup>[13, 14]</sup>

The calcination of supported boron-containing species therefore eliminates all organic chains without removing any of the boron content, as shown by elemental analyses. Also, the diffusion of boron within the silica matrix yields a new BOH species which still contain O from the original SiOB bond.

A general trend can be drawn from these observations. First, the different ligands yield different loadings, due to their various sterics. Therefore, it was expected to have a lower loading by grafting the  $\text{C}_{3v}$  molecule onto silica. Calcination did not eliminate any boron, which confirmed the accuracy of the chosen strategy of ligand elimination.

### 4.4.2 Determination of the acidity of the formed surface species

---

In order to estimate the acidity strength of the newly-formed surface species, the adsorption of triethylphosphine oxide (TEPO) was investigated.<sup>[57]</sup>

The interaction between the phosphine basic site and the surface acidic site induces a delocalisation of the P=O bond electronic density to the acidic site. The P=O bond is then weakened, and the resonance of phosphorus is thus shifted downfield. As a consequence, the stronger the acidic site, the higher the chemical shift. This method is however insensitive to the Brønsted or Lewis nature of the site. Some studies in 2D  $^1\text{H}$ - $^{31}\text{P}$  SSNMR with TEPO as a probe could resolve Brønsted acid sites on silica-alumina.<sup>[58]</sup>

The previously formed doped solid was contacted with an excess of TEPO and a  $^{31}\text{P}$ -SSNMR spectrum was recorded after elimination of the excess of TEPO. (**Fig 53**)

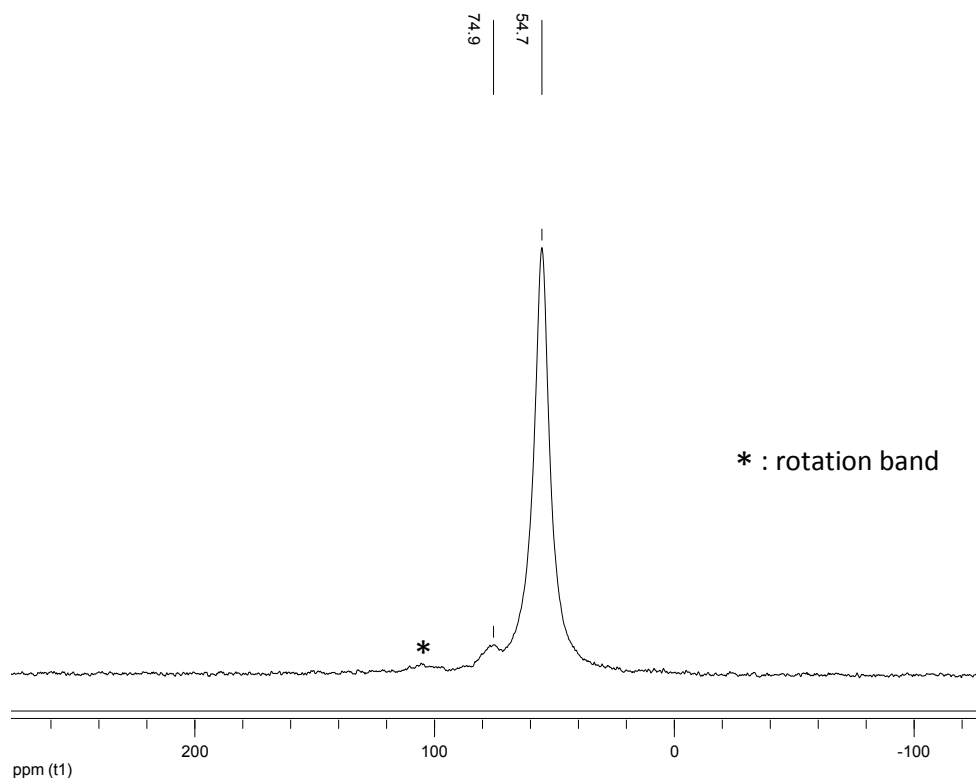


Fig 53.  $^{31}\text{P}$ -SSNMR spectrum of adsorbed TEPO on a formed SiOH-BOH species (CPMAS, 10kHz, d1= 30s, ns=1024, lb=150Hz)

The  $^{31}\text{P}$  solid-state NMR spectrum shows two signals at 74.9 and 54.7 ppm, corresponding to chemi- and physisorbed TEPO respectively. The chemical shift difference, related to the acidic strength, is  $\Delta(\delta) = 20.2$  ppm, thus showing that the formed species is quite acidic.

Table 2. Difference in chemical shifts after chemisorption of TEPO on different supports

Support	Sulfated silica-gel <sup>[a]</sup>	Silica-alumina <sup>[b]</sup>	Silica-gel <sup>[a]</sup>	Aerosil silica <sup>[b]</sup>	$\gamma$ -alumina <sup>[a]</sup>	NaOH <sup>[a]</sup>
$\Delta(\delta)$ (ppm)	35.9	25.5	6.0	1.9	-1.35	-1.36

[a] As reported by Osegovic *et al.*<sup>[57]</sup>

[b] As reported by Rataboul *et al.*<sup>[59]</sup>

It is noteworthy that the new surface is more acidic than Aerosil silica. This is coherent with the fact that boron increases surface acidity.<sup>[60]</sup>

## Conclusion

---

In this chapter, we defined a strategy in order to position boron atoms on a silica surface by a chemical method. This strategy consists in controlling the surface silanol density of thermally treated silica by using sterically hindered molecules, thus balancing the statistics of silanol repartition.

Therefore, simple molecules were synthesised, yielding both a good reactivity with surface silanols, allowing us to implement the chosen strategy. Different ligands on the boron atom were investigated. It could be drawn from these screening experiments that the most suitable molecules for this work would be the  $C_2$ -borole with the H ligand, as it was easily formed and yielded excellent grafting yields. The  $C_{3v}$  molecule, thanks to its geometry and its carbon loading, was selected as a good molecule to be further used for the grafting onto silicon wafers, while other  $C_3$ -symmetrical molecules, although achieving high yields, lacked an improved steric hindrance. Therefore, two main symmetries were finally accepted as good candidates:  $C_2$  and  $C_{3v}$  symmetries seemed to be the best compromise between easiness of synthesis and interesting sterics for our strategy.

It was also demonstrated that, contrarily to our primary expectations, the  $C_{3v}$  cage-shaped borate did not self-position onto the surface but performed a grafting as all other precursors.

Then, the removal of organic chains pointed out that the formation BOH surface species upon calcination with the quantitative removal of the organic ligands while keeping the boron content unchanged was performed. Such species formed species show a higher acidity than Aerosil silica.

As the strategy was thus approved on the silica model support, we could then move on and apply it to silica-covered silicon wafers.

## References

---

- [1] J. C. Ho, R. Yerushalmi, Z. A. Jacobson, Z. Fan, R. L. Alley, A. Javey, *Nat Mater* **2008**, *7*, 62.
- [2] L. T. Zhuravlev, *Colloids and Surfaces A: Physicochemical and Engineering Aspects* **2000**, *173*, 1.
- [3] R. B. Shirts, *Journal of Chemical Education* **2007**, *84*, 1882.
- [4] M. M. Midland, *Chemical Reviews* **1989**, *89*, 1553.
- [5] Y. N. Bubnov, M. E. Gurskii, S. Y. Erdyakov, O. A. Kizas, G. D. Kolomnikova, N. Y. Kuznetsov, T. V. Potapova, O. A. Varzatskii, Y. Z. Voloshin, *Journal of Organometallic Chemistry* **2009**, *694*, 1754.
- [6] K. Smith, *Chemical Society Reviews* **1974**, *3*, 443.
- [7] J. A. Soderquist, H. C. Brown, *The Journal of Organic Chemistry* **1981**, *46*, 4599.
- [8] J. A. Soderquist, A. Negron, *Organic Syntheses* **1992**, *70*, 169.
- [9] S. Kotha, K. Lahiri, D. Kashinath, *Tetrahedron* **2002**, *58*, 9633.
- [10] S. Masamune, W. Choy, A. J. Kerdesky Francis, B. Imperiali, *Journal of the American Chemical Society* **1981**, *103*, 1566.
- [11] H. C. Brown, U. R. Khire, G. Narla, U. S. Racherla, *The Journal of Organic Chemistry* **1995**, *60*, 544.
- [12] N. Miyaoura, T. Ishiyama, M. Ishikawa, A. Suzuki, *Tetrahedron Letters* **1986**, *27*, 6369.
- [13] H. Michael L, *Journal of Non-Crystalline Solids* **1975**, *19*, 299.
- [14] C. Carteret, A. Burneau, *Physical Chemistry Chemical Physics* **2000**, *2*.
- [15] Y.-J. Wanglee, J. Hu, R. E. White, M.-Y. Lee, S. M. Stewart, P. Perrotin, S. L. Scott, *Journal of the American Chemical Society* **2012**, *134*, 355.
- [16] B. C. Scott , B. H. Peter , F. L. Michael , G. M. Philippe , F. N. John , N. László, *Chemistry - A European Journal* **2007**, *13*, 7121.
- [17] B. Bilinski, *Powder Technology* **1994**, *81*, 241.
- [18] Z. Suprynowicz, B. Buszewski, R. Lodkowski, L. Dawidowicz, *Journal of Chromatography A* **1988**, *446*, 347.
- [19] M. E. Gurskii, S. V. Baranin, B. M. Mikhailov, *Journal of Organometallic Chemistry* **1984**, *270*, 9.
- [20] J. A. Soderquist, H. C. Brown, *The Journal of Organic Chemistry* **1980**, *45*, 3571.
- [21] P. R. Rablen, J. F. Hartwig, *Journal of the American Chemical Society* **1996**, *118*, 4648.
- [22] P. R. Rablen, J. F. Hartwig, S. P. Nolan, *Journal of the American Chemical Society* **1994**, *116*, 4121.
- [23] K. Severin, *Dalton Transactions* **2009**, 5254.
- [24] D. S. Matteson, *Tetrahedron* **1989**, *45*, 1859.
- [25] A. P. Cote, A. I. Benin, N. W. Ockwig, M. O'Keeffe, A. J. Matzger, O. M. Yaghi, *Science* **2005**, *310*, 1166.
- [26] K. E. Maly, N. Malek, J.-H. Fournier, P. Rodríguez-Cuamatzi, T. Maris, J. D. Wuest, *Pure Appl. Chem.* **2006**, *78*, 1305.
- [27] R. R. Haynes, H. R. Snyder, *The Journal of Organic Chemistry* **1964**, *29*, 3229.
- [28] H. C. Brown, S. K. Gupta, *Journal of the American Chemical Society* **1971**, *93*, 1816.
- [29] H. C. Brown, S. K. Gupta, *Journal of the American Chemical Society* **1975**, *97*, 5249.
- [30] G. Wulff, A. Hansen, *Angewandte Chemie* **1986**, *98*, 552.
- [31] D. E. Young, G. E. McAchran, S. G. Shore, *Journal of the American Chemical Society* **1966**, *88*, 4390.
- [32] G. W. Kramer, H. C. Brown, *Journal of Organometallic Chemistry* **1974**, *73*, 1.

- [33] N. Davies, B. D. James, M. G. H. Wallbridge, *Journal of the Chemical Society A: Inorganic, Physical, Theoretical* **1969**, 2601.
- [34] H. Nöth, R. Hartwimmer, *Chemische Berichte* **1960**, 93, 2238.
- [35] F. Klanberg, E. L. Muetterties, L. J. Guggenberger, *Inorganic Chemistry* **1968**, 7, 2272.
- [36] T. J. Marks, W. J. Kennelly, J. R. Kolb, L. A. Shimp, *Inorganic Chemistry* **1972**, 11, 2540.
- [37] E. S. Sattely, G. A. Cortez, D. C. Moebius, R. R. Schrock, A. H. Hoveyda, *Journal of the American Chemical Society* **2005**, 127, 8526.
- [38] R. W. Hoffman, U. Weidmann, *Journal of Organometallic Chemistry* **1980**, 195, 137.
- [39] R. W. Hoffmann, H. J. Zeiss, *The Journal of Organic Chemistry* **1981**, 46, 1309.
- [40] F. Blanc, J. Thivolle-Cazat, J.-M. Basset, C. Copéret, A. S. Hock, Z. J. Tonzetich, R. R. Schrock, *Journal of the American Chemical Society* **2007**, 129, 1044.
- [41] G. Villa, L. Ford, D. Pozzi, C. H. Schiesser, P. Renaud, *Chemical Communications* **2010**, 46, 803.
- [42] E. Wanek, Y.-M. Pai, W. P. Weber, *Synthetic Communications* **1985**, 15, 185.
- [43] S. Enthaler, B. r. Spilker, G. Erre, K. Junge, M. K. Tse, M. Beller, *Tetrahedron* **2008**, 64, 3867.
- [44] H. Nishiwaki, A. Kiyomori, T. Kubota, C07F7/08; C07F7/18; (IPC1-7): C07F7/08; C07F7/21 ed., US, **2003**.
- [45] V. F. A. Henglein, R. Lang, K. Scheinoet, *Die Makromolekulare Chemie* **1955**, 15, 177.
- [46] K. L. Furdala, A. G. Oliver, F. J. Hollander, T. D. Tilley, *Inorganic Chemistry* **2003**, 42, 1140.
- [47] K. L. Furdala, A. G. Oliver, F. J. Hollander, T. D. Tilley, *Inorganic Chemistry* **2003**, 42, 1140.
- [48] Hijazi A. Ali, I. Goldberg, M. Srebnik, *European Journal of Inorganic Chemistry* **2002**, 2002, 73.
- [49] M. Yasuda, S. Yoshioka, S. Yamasaki, T. Somyo, K. Chiba, A. Baba, *Organic Letters* **2006**, 8, 761.
- [50] P. K. Agrawal, H.-J. Schneider, *Tetrahedron Letters* **1983**, 24, 177.
- [51] G. L. Rice, S. L. Scott, *Journal of Molecular Catalysis A: Chemical* **1997**, 125, 73.
- [52] R. Jelinek, B. F. Chmelka, Y. Wu, P. J. Grandinetti, A. Pines, P. J. Barrie, J. Klinowski, *Journal of the American Chemical Society* **1991**, 113, 4097.
- [53] S. Hosokawa, K. Shimamura, M. Inoue, *Materials Research Bulletin* **2011**, 46, 1928.
- [54] H. Peng, L. Xu, H. Wu, Z. Wang, Y. Liu, X. Li, M. He, P. Wu, *Microporous and Mesoporous Materials* **2011**, 153, 8.
- [55] J. Patarin, *Angewandte Chemie International Edition* **2004**, 43, 3878.
- [56] M. Ghezzo, D. M. Brown, *Journal of The Electrochemical Society* **1973**, 120, 146.
- [57] J. P. Osegovic, R. S. Drago, *The Journal of Physical Chemistry B* **1999**, 104, 147.
- [58] B. Alonso, I. Klur, D. Massiot, *Chemical Communications* **2002**, 804.
- [59] F. Rataboul, A. Baudouin, C. Thieuleux, L. Veyre, C. Copéret, J. Thivolle-Cazat, J.-M. Basset, A. Lesage, L. Emsley, *Journal of the American Chemical Society* **2004**, 126, 12541.
- [60] E. F. Vansant, P. Voort, K. C. Vrancken, *Characterization and Chemical Modification of the Silica Surface, Vol. 93*, Elsevier, **1995**.





## **Chapter 3 : Application of the strategy to N-dopant, the case of Phosphorus, an NMR study**

---

## Summary of the Chapter

---

Introduction .....	77
1. Towards a permanent-bonding strategy.....	77
1.1. Grafting of a phosphite.....	77
1.2. Adsorption of phosphonate .....	82
2. Self-positioning as a better placement regulating tool.....	84
2.1. Adsorption of phosphine.....	86
2.2. Improving the umbrella effect: POSS as a sterically hindered ligand .....	88
2.2.1. Grafting and geometry characterisation of POSS-P .....	87
2.2.2. NMR analyses and computational modelling.....	92
2.2.2.1. NMR spectroscopy of surface species of P-POSS on $\text{SiO}_{2-(700)}$ .....	92
2.2.2.2. Calculating tensors for the grafted compound on $\text{SiO}_{2-(200)}$ .....	96
2.2.3. Computational structures as a discriminating method.....	97
2.3. Grafting of phosphonium .....	106
3. Elimination of the ligands.....	107
Conclusion.....	111
References .....	112

## Introduction

---

The main target of this study is the control of P-site density, dwelling on two levels:

- i) The thermal treatment of the surface leading to defined density of OH groups and thus of surface anchoring sites,
- ii) Using interactions between P-containing surface species, which will further contribute to the control of the placement of doping atoms.

The search for possible P-sources was focused on two different aspects: the P-precursor should either react or strongly interact with the surface, the advantage of the latter being the possible self-organisation on the surface.<sup>[1, 2]</sup> We have thus investigated various types of P-containing molecules, by varying the basicity of the P centre and the size of its surrounding ligands. The surface chemistry of P-containing molecules has already been explored. For instance, phosphines and phosphine oxides have been widely used as surface acidity probes in NMR spectroscopy.<sup>[3-6]</sup> Also, in order to graft phosphorus-containing species onto the surface, reactions with phosphites<sup>[7]</sup> or phosphonates<sup>[8]</sup> were studied.

Here we compare the controlled surface chemistry of phosphines, phosphites, phosphonates and phosphoniums and their stability upon calcination in view of generating well-distributed P-doping on the surface of silica particles and 2D silicon wafers. We shall first describe a grafting strategy through transesterification reactions, then switch to a self-placement strategy through adsorption of tricoordinated phosphorus onto the surface, as well as ionic interaction with the surface.

## 1. Towards a permanent-bonding strategy

---

In order to keep the phosphorus precursor attached to the silica surface and be able to sustain high temperatures without desorption, we first focused on the use of highly reactive molecules, that could strongly interact with the surface.

### 1.1. Grafting of a phosphite

---

Knowing that phosphites undergo trans-esterification with silanols<sup>[9]</sup>, triethylphosphite was first used and the grafting step was monitored by IR-DRIFT (**Fig 54**).

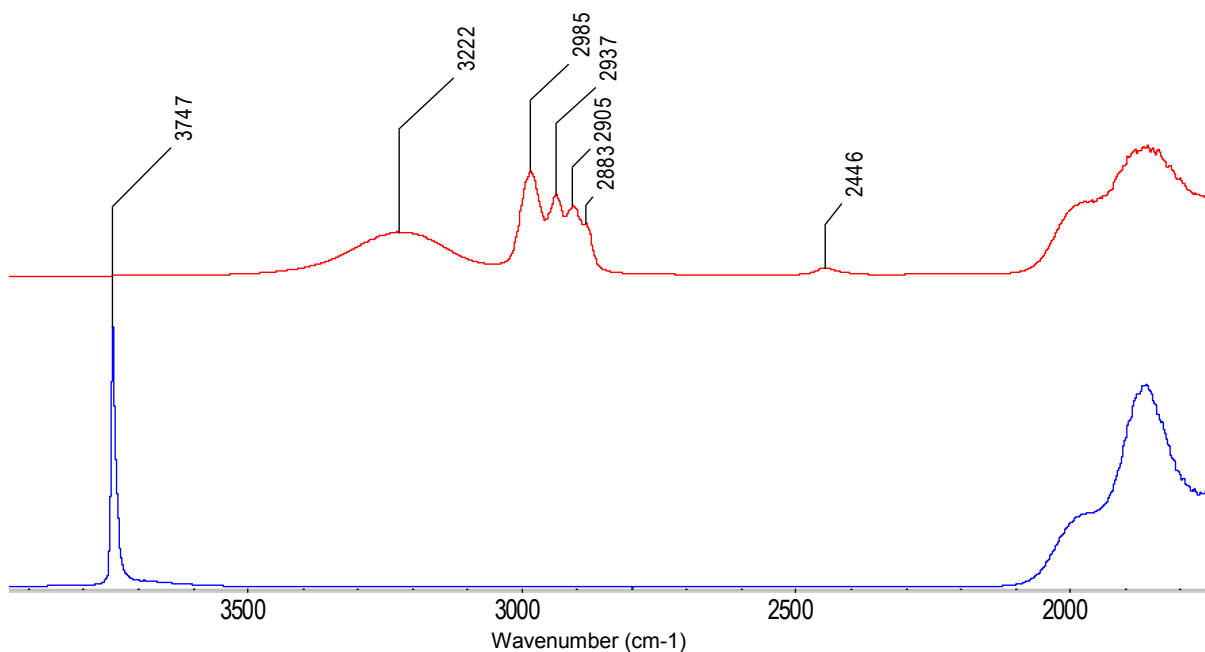
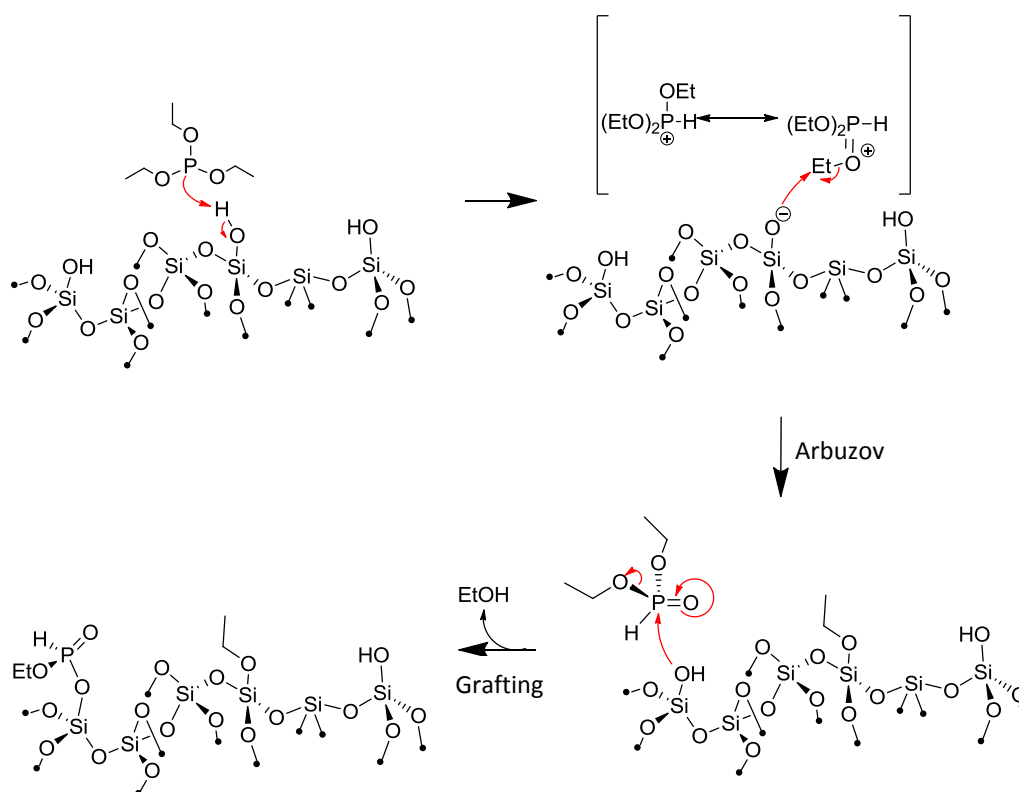


Fig 54. IR-DRIFT of the grafted tri-ethylphosphite onto  $\text{SiO}_{2-(700)}$

As shown on the spectrum above, peaks between  $2985\text{ cm}^{-1}$  and  $2883\text{ cm}^{-1}$ , respectively attributed to  $\nu_{\text{sym}}(\text{C-H})$  and  $\nu_{\text{asym}}(\text{C-H})$ , are present. In addition, a broad peak at  $3222\text{ cm}^{-1}$  appears, which could be due to the presence of adsorbed species, likely P-containing species, in interaction with surface OH<sup>[7, 10]</sup>. It is noteworthy that all isolated silanols associated with a peak at  $3747\text{ cm}^{-1}$  disappeared. One can also notice the presence of a small and broad peak at  $2446\text{ cm}^{-1}$ , which is consistent with a  $(\text{P}^{\text{V}}(=\text{O})\text{-H})$  stretching vibration.<sup>[11]</sup> These observations are fully explained by a two-step reaction between the phosphites and silanols, as already reported. **(Scheme 21)**.<sup>[9, 12]</sup>



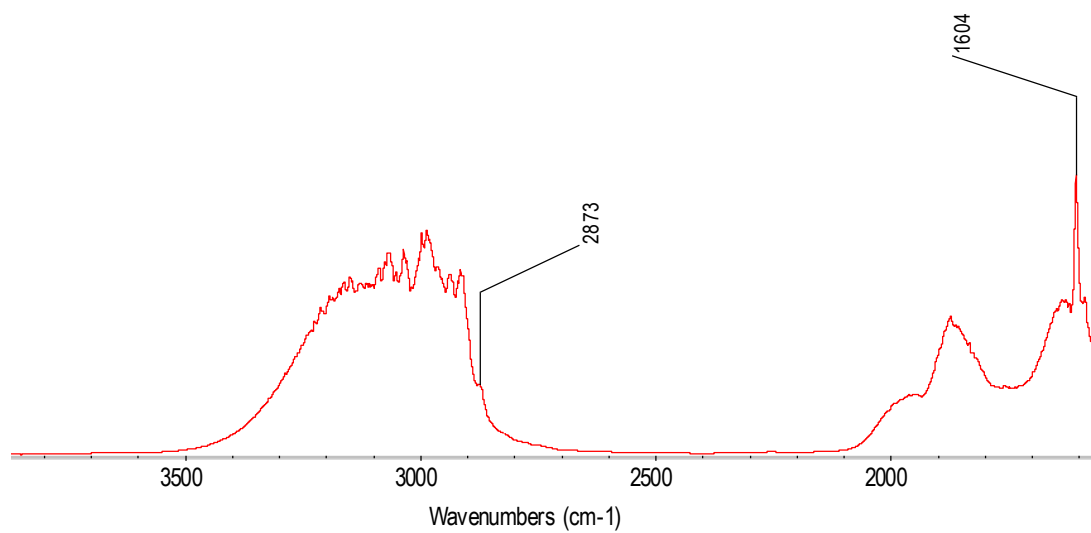
**Scheme 21.** Proposed mechanism of the reaction between a phosphite and a surface silanol (inspired by <sup>[13]</sup>)

Therefore, the formation of  $(\text{SiO})(\text{EtO})\text{P}^{\text{V}}(=\text{O})\text{H}$  implies that for every grafted P on a silanol group, the latter is converted into a surface  $\equiv\text{SiOEt}$  species, so that overall chemisorption of phosphite cannot yield more than 50% grafting via this route (**Scheme 21**).

Elemental analyses gave a P loading of 0.28%<sub>wtr</sub> (0.30 P.nm<sup>-2</sup>) which is lower than silanol density (0.7 OH.nm<sup>-2</sup> on SiO<sub>2-(700)</sub>). This indicates a grafting yield of 42%.

## 1.2. Adsorption of phosphonate

In order to avoid “Arbusov” type chemistry making the grafting of phosphite very complex, we focused on phosphonates, which are known to readily undergo transesterification with alcohol groups, such as silanols.<sup>[8, 14, 15]</sup> Here, we selected diethylbenzylphosphonate as a test substrate in order to yield higher P surface densities, not obtainable with phosphites, as shown before. After grafting, the solid was analysed by IR-DRIFT. (**Fig 55**)



**Fig 55.** IR-DRIFT of the grafted diethylbenzylphosphonate onto SiO<sub>2</sub>-(700)

The spectrum on **Fig 55** shows that all isolated surface silanols have disappeared, (no peak at 3747 cm<sup>-1</sup>) and that most of the expected signals associated with the organic functionalities are blinded by a broad peak around 3100cm<sup>-1</sup>; the latter being attributed in the literature to a P--OH interaction.<sup>[7]</sup> However, the C=C stretching vibration at 1604 cm<sup>-1</sup> can be seen. Additionally, the peak at 2873 cm<sup>-1</sup> can be attributed to the  $\nu_{\text{asym}}(\text{C-H})$  of sp<sup>3</sup> CH<sub>2</sub> of the ethoxy ligands.

Elemental analyses gave a P loading of 0.60%<sub>w/w</sub>, (0.64 P.nm<sup>-2</sup>), i.e. a grafting yield of 90%.

In order to characterise the formed solid further, SSNMR analyses were performed on the product. (**Fig 56**)

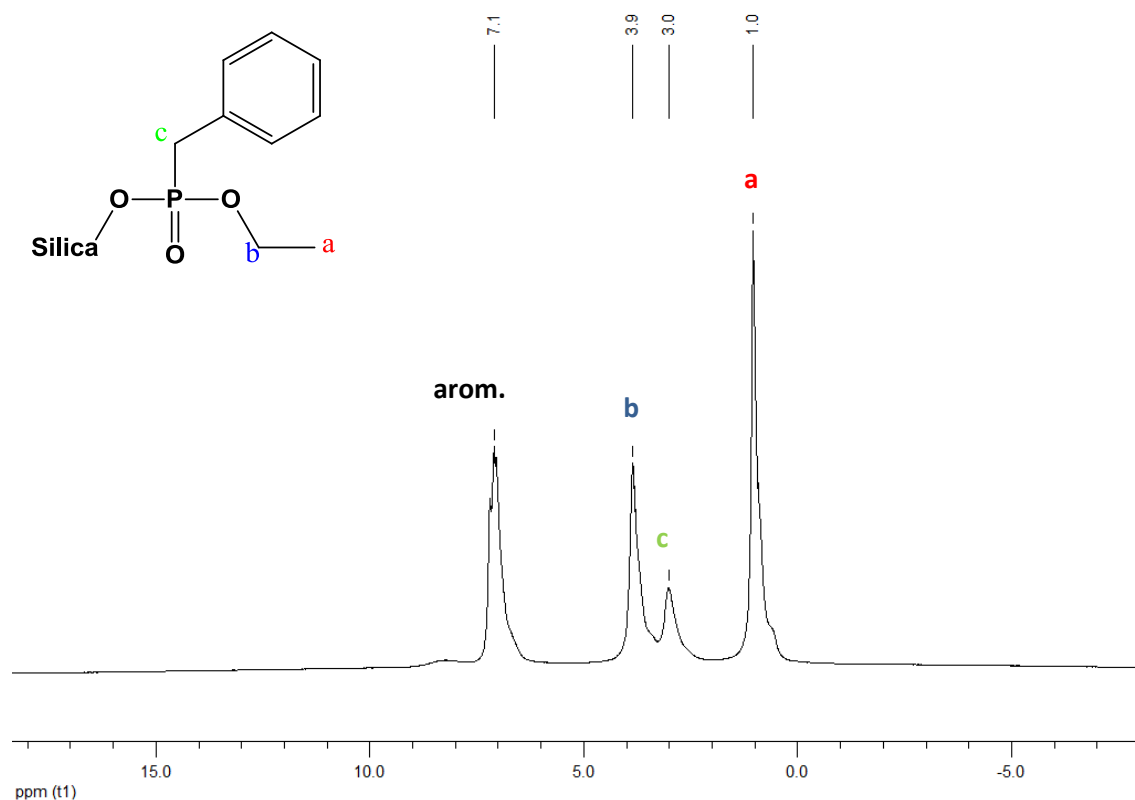
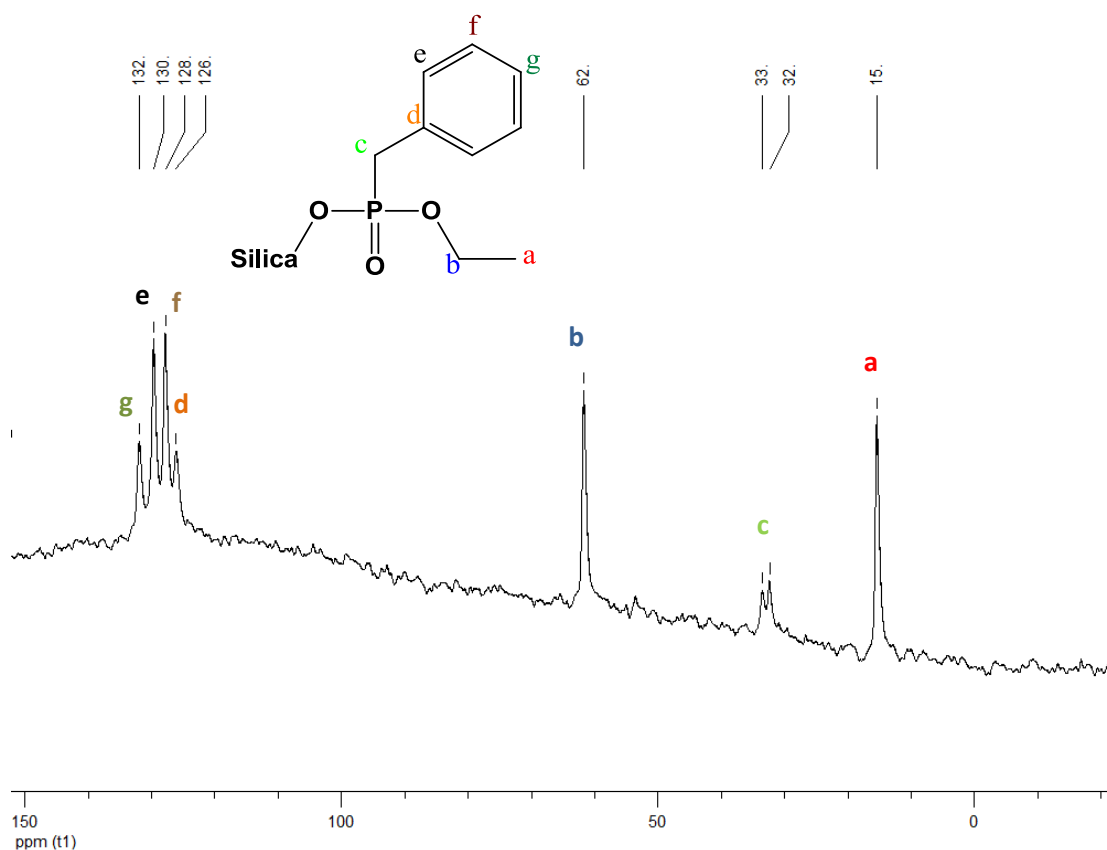


Fig 56.  $^1\text{H}$ -SSNMR of the grafted diethylbenzylphosphonate onto  $\text{SiO}_{2-(700)}$  (zg, 10kHz, d1=5s, ns=8, lb=0Hz)

The proton MAS NMR spectrum shows peaks at 1.0, 3.0, 3.9 and 7.1 ppm, which can be attributed respectively to  $-\text{OCH}_2\text{CH}_3$ , benzylic  $-\text{CH}_2\text{Ph}$ ,  $-\text{OCH}_2\text{CH}_3$  and the aromatic protons. Note that the relative intensity of “H<sub>b</sub>” and “H<sub>c</sub>” is not one-to-one as it would be expected for a single surface species like  $\equiv\text{SiO-P(O)}(\text{CH}_2\text{Ph})(\text{OEt})$ , this probably indicates the presence of surface ethoxy group obtained by condensation of EtOH with surface silanols. Also, a very weak peak appears around 8 ppm, probably resulting from interacting aromatic protons.





**Fig 57.**  $^{13}\text{C}$ -SSNMR of the grafted diethylbenzylphosphonate onto  $\text{SiO}_2\text{-(700)}$  (hpdec, 10kHz, d1=50s, ns=1024, lb=50Hz)

Both  $^{13}\text{C}$ -SSNMR and  $^{31}\text{P}$ -SSNMR were also performed.

In the  $^{13}\text{C}$ -NMR spectrum, all peaks were attributed as follows:

- peaks between 132 ppm and 126 ppm are attributed to the aromatic C, the most deshielded peak at 132 ppm being attributed to  $\text{C}_g$  (para), then peaks at 130 ppm, 128 ppm and 126 ppm are attributed to  $\text{C}_e$ ,  $\text{C}_f$  and  $\text{C}_d$  respectively;
- the peak at 62 ppm is attributed to  $\text{C}_b$ , from the ethyl chain;
- the two peaks at 33 and 32 ppm are in fact a doublet resulting from the coupling of the carbon atom with the directly bonded phosphorus atom; this signal is thus associated with  $\delta_{\text{iso}} = 32.5$  ppm and  $J_{\text{C-P}} = 558$  Hz;
- Finally, the peak at 15 ppm is attributed to  $\text{C}_a$ .

Finally, a  $^{31}\text{P}$ -NMR spectrum was recorded and displayed a single peak at 26.2 ppm, which could be readily assigned to a phosphonate (**Fig 58**).<sup>[16-18]</sup>

Overall, the IR-DRIFT spectrum showed that grafting occurred “quantitatively” as all surface silanols disappeared. This result was further corroborated by  $^1\text{H}$ -SSNMR, which shows no peak characteristic of surface silanols. Moreover, the presence of a single surface monografted phosphonate species was evidenced from  $^{13}\text{C}$ - and  $^{31}\text{P}$ -SSNMR spectra, the latter displaying a peak at

26.2 ppm as published.<sup>[16-18]</sup> Also, according to the IR-DRIFT spectrum, nothing can be concluded about potential traces of water, as they would appear under the P-OH broad peak. However, the  $^1\text{H}$  SSNMR proved that no water can be seen, as no peak can be seen around 4 ppm, apart from the one corresponding to  $\text{H}_b$ .

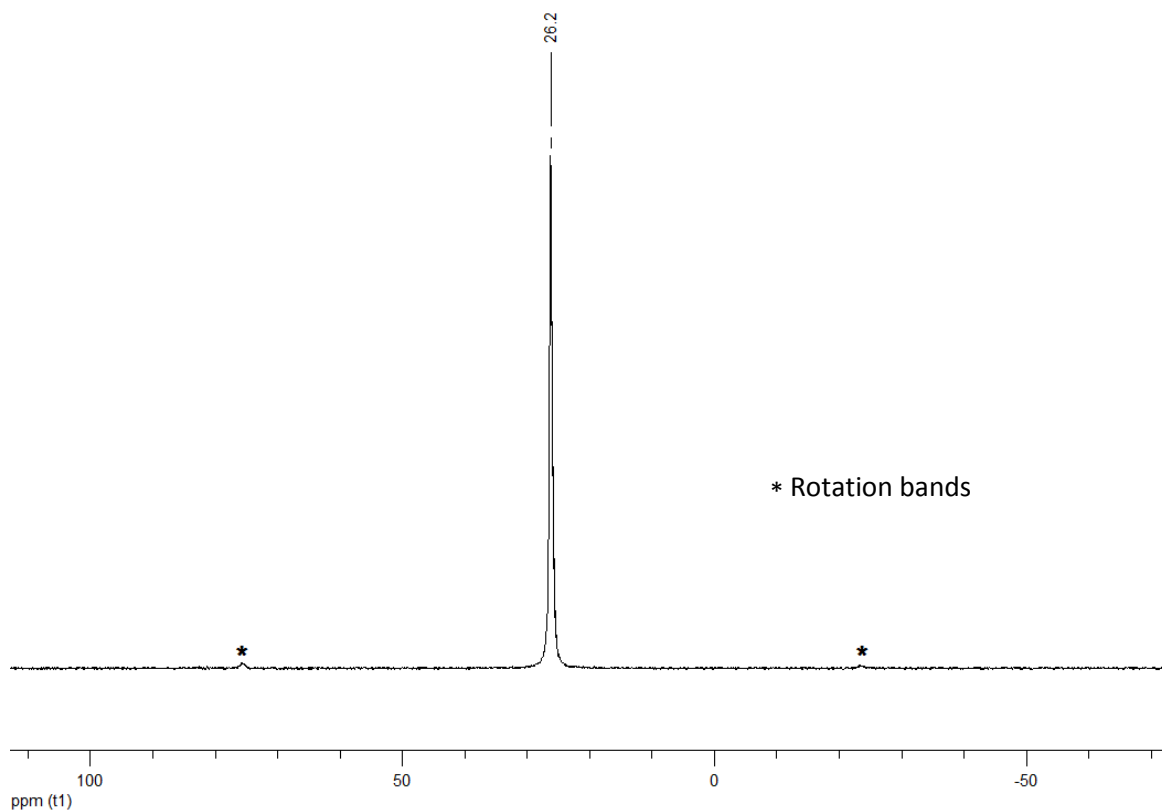


Fig 58.  $^{31}\text{P}$ -SSNMR of the grafted diethylbenzylphosphonate onto  $\text{SiO}_{2-(700)}$  (hpdec, 10kHz, d1=30s, ns=157, lb=50Hz)

## 2. Self-positioning as a better placement regulating tool

### 2.1. Adsorption of phosphine

The first molecule to be studied was a large and basic phosphine, namely tricyclohexylphosphine ( $\text{PCy}_3$ ).  $\text{PCy}_3$  was sublimed onto a silica pellet in a closed reactor under vacuum. The pellet was then treated at  $50^\circ\text{C}$  (ramp of  $6^\circ\text{C}\cdot\text{min}^{-1}$ ) for 2h under argon to allow a better homogeneity of the adsorbed phosphine. To remove the excess of phosphine, the pellet was further heated up by  $50^\circ\text{C}$  increment until the temperature reached  $200^\circ\text{C}$ , which appeared to be the lowest temperature before desorption. (Fig 59)

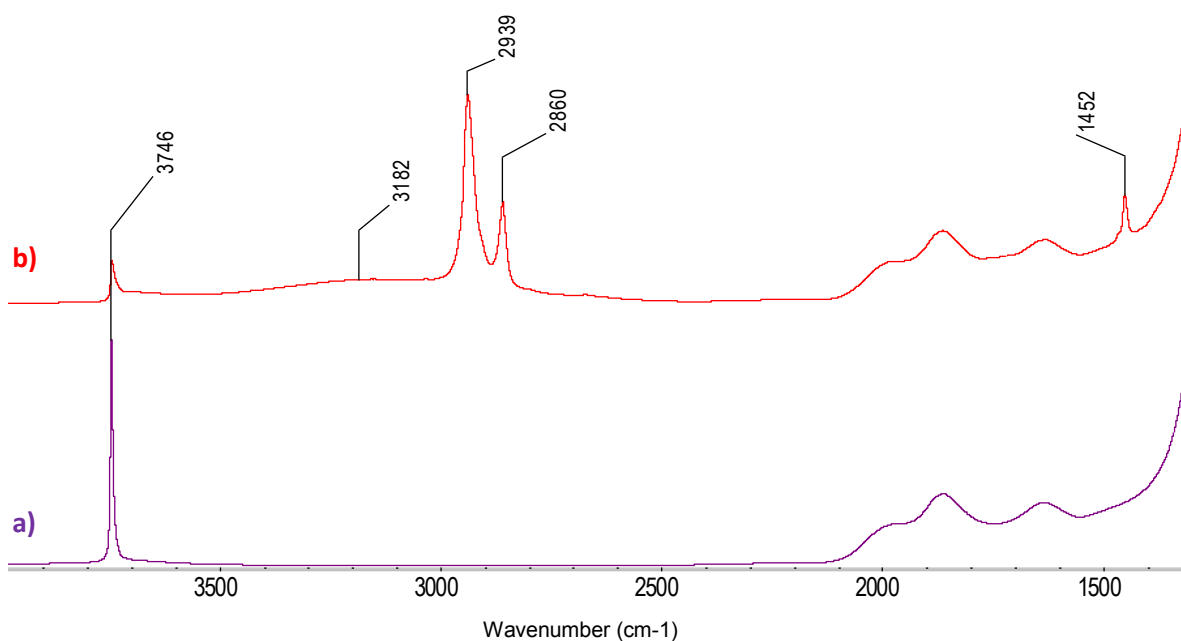


Fig 59. Sublimation of  $\text{PCy}_3$  onto a  $\text{SiO}_{2-(700)}$  pellet a)  $\text{SiO}_{2-(700)}$ , b) phosphine adsorbed onto  $\text{SiO}_{2-(700)}$

The spectrum of the adsorbed species shows two peaks at  $2939\text{ cm}^{-1}$  and  $2860\text{ cm}^{-1}$ , which are characteristic of  $\nu_{\text{sym}}(\text{C-H})$  and  $\nu_{\text{asym}}(\text{C-H})$  of  $\text{sp}^3$  alkyl groups. Additionally, one peak appears at  $1452\text{ cm}^{-1}$  attributed to  $\delta_{\text{asym}}(\text{P-CH})$ .<sup>[11, 19]</sup> The broad peak at  $3182\text{ cm}^{-1}$  can be attributed to a P-OH interaction.<sup>[7]</sup> The peak at  $3746\text{ cm}^{-1}$ , characteristic of silanols does not disappear completely, showing that all surface silanols are not coordinated to phosphine after the reaction.

According to this observation, it can be concluded that  $\text{PCy}_3$  is strongly adsorbed to silica which is coherent with reported studies.<sup>[3]</sup> In view of the need to make the phosphorus atom diffuse into the silica matrix prior to desorption of the P-precursor, the thermal stability of the P-surface species under vacuum was further investigated (Fig 60).

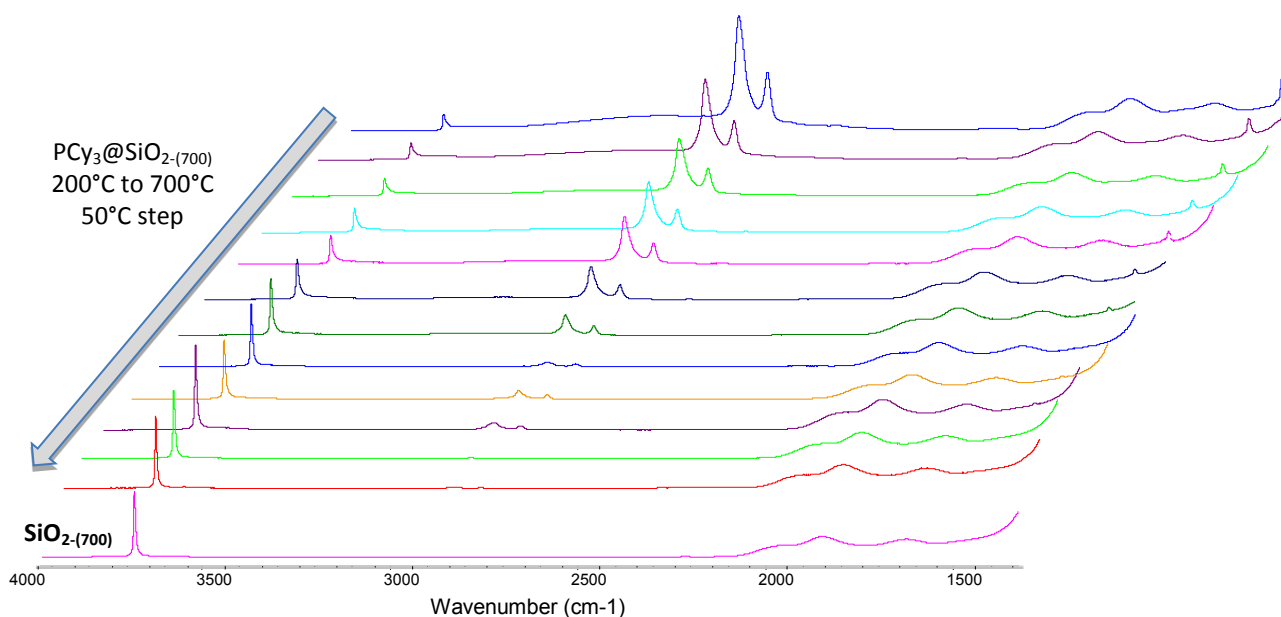


Fig 60. Thermal study of the coordinated PCy<sub>3</sub> onto an SiO<sub>2-(700)</sub> pellet

The solid was therefore treated under vacuum using 50°C increments from 200°C to 700°C. The sample was kept under dynamic vacuum for thirty minutes at each temperature before spectrum acquisition.

From 200°C to 700°C, SiOH groups are regenerated (increase of the 3747 cm<sup>-1</sup> peak), alkyl groups (2937 cm<sup>-1</sup> and 2858 cm<sup>-1</sup>) and P-C signal (1452 cm<sup>-1</sup>) disappeared, thus showing the removal of organic chains from the surface. The integration of all peaks leads to a coherent mass balance (Fig 61) which further confirms the quantitative carbon removal.

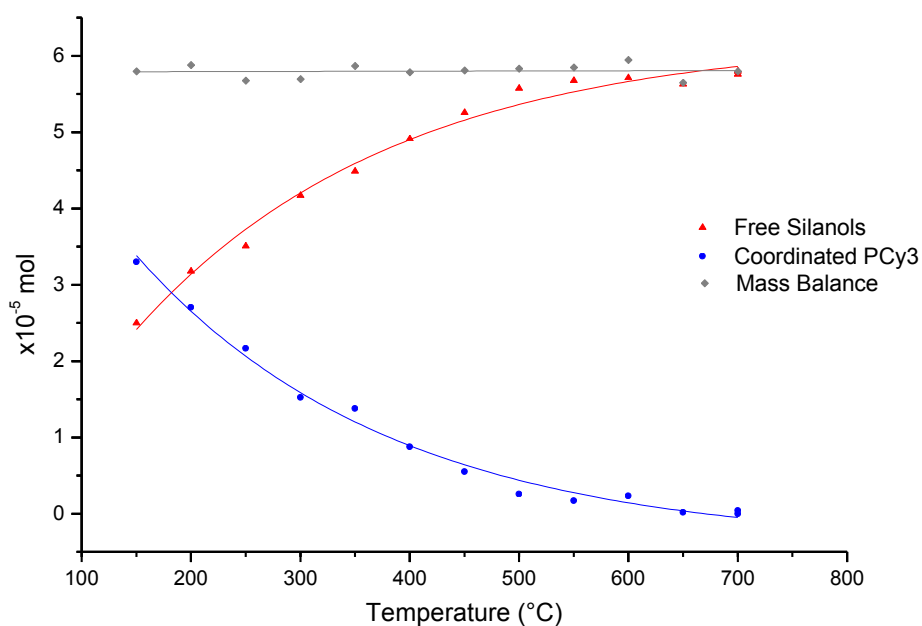


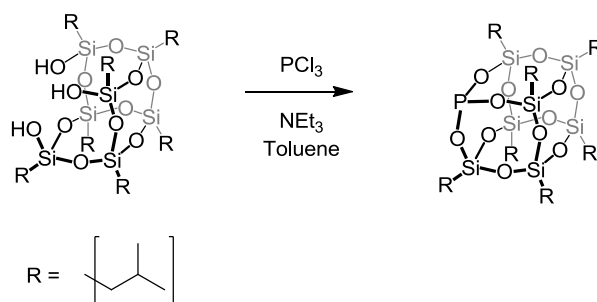
Fig 61. Evolution of the number of free silanols and coordinated PCy<sub>3</sub> through thermal treatment

Knowing that P diffusivity in SiO<sub>2</sub> is weak (under N<sub>2</sub> inert ambient in pure SiO<sub>2</sub>:  $D_{1100^{\circ}\text{C}} = 3 \times 10^{-18} \text{ cm}^2 \cdot \text{s}^{-1}$  [20-22],  $E_a = 4.4 \text{ eV}$  [20]), we can assume that PCy<sub>3</sub> was completely desorbed from SiO<sub>2</sub>.

At 700 °C, the P-surface interaction between P and SiO<sub>2</sub> is probably not strong enough to secure P immobilisation during calcination, a mandatory step for further P-doping.

## 2.2. Improving the umbrella effect: POSS as a sterically hindered ligand

Knowing that phosphorus diffuses with difficulty into silica, [22, 23] one approach could rely on the grafting a P-containing precursor first and then to deposit a first silica layer to disfavour the desorption of P and thereby favour its diffusion into the solid. An alternative approach could consist in grafting a P-containing precursor that already contains a silica component, such as in siloxide. Moreover, in view of the possibility to exploit steric interaction and self-assembly, an interesting candidate is the P-silsesquioxane (**POSS-P**) (Scheme 22). [24]



**Scheme 22.** Synthesis of the used P-silsesquioxane

This compound was prepared according to the literature procedure; it displays a characteristic signal in <sup>31</sup>P-NMR at 84.8 ppm as previously reported [24] (Fig 62). No peaks around 217 ppm and 4ppm were observed, which is consistent with the absence of PCl<sub>3</sub> and POCl<sub>3</sub> respectively, the starting reagent and the oxide. [25-28] More importantly, no peak at -45 ppm corresponding to POSS-P oxide appeared. [24] The peak at 130 ppm is an artefact resulting from the spectral window size.

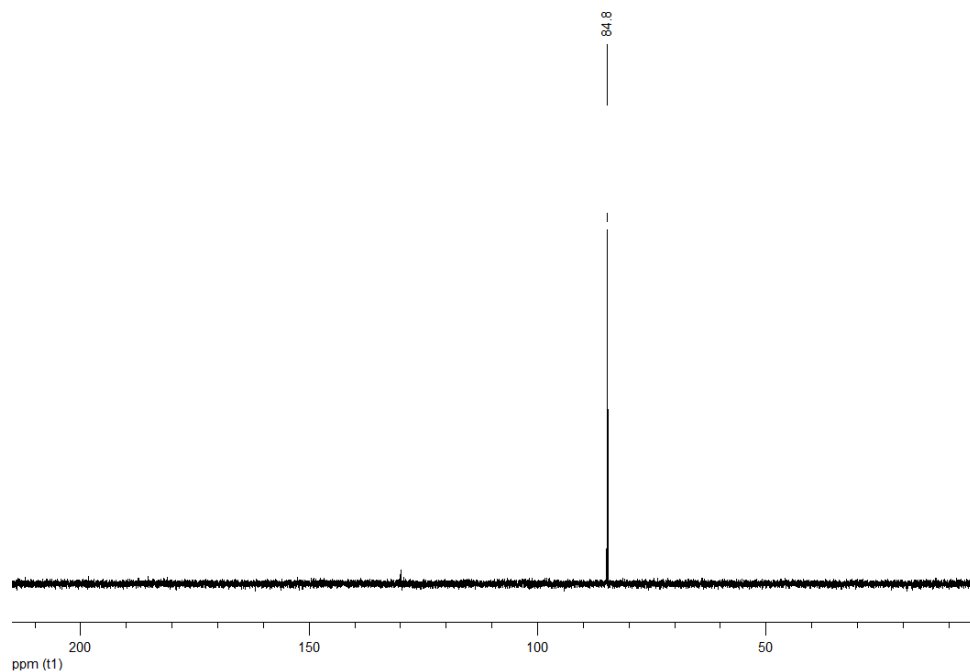
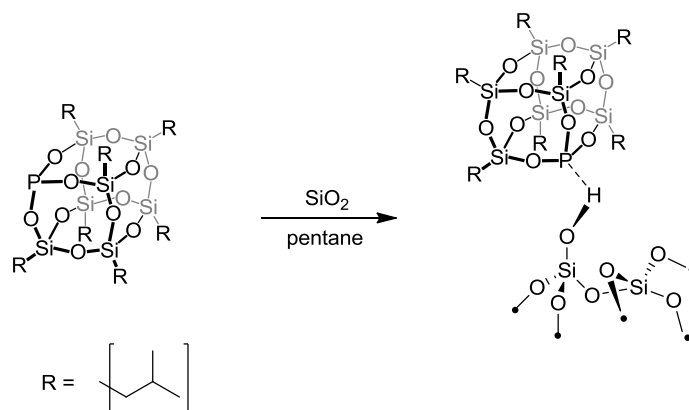


Fig 62.  $^{31}\text{P}$ -NMR spectrum of the synthesized POSS-P (in  $\text{C}_6\text{D}_6$ )

### 2.2.1. Grafting and geometry characterisation of POSS-P

POSS-P was then contacted with  $\text{SiO}_{2-(700)}$  by impregnation in pentane (**Scheme 23**). After washing and drying, elemental analysis, IR-DRIFT (**Fig 63**) and NMR spectroscopy were performed.



Scheme 23. Expected outcome of impregnation of  $\text{SiO}_{2-(700)}$  by POSS-P

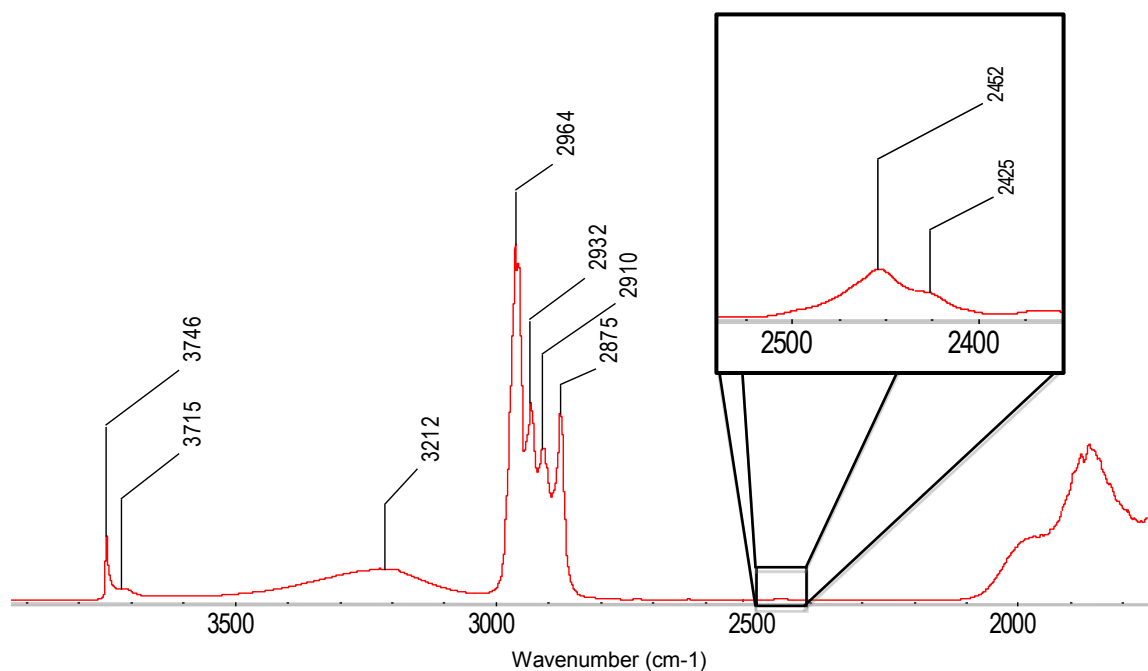


Fig 63. IR-DRIFT spectrum of the grafted POSS-P

We observe that most of surface isolated surface silanols at  $3746\text{ cm}^{-1}$  disappeared, and that new peaks appeared:

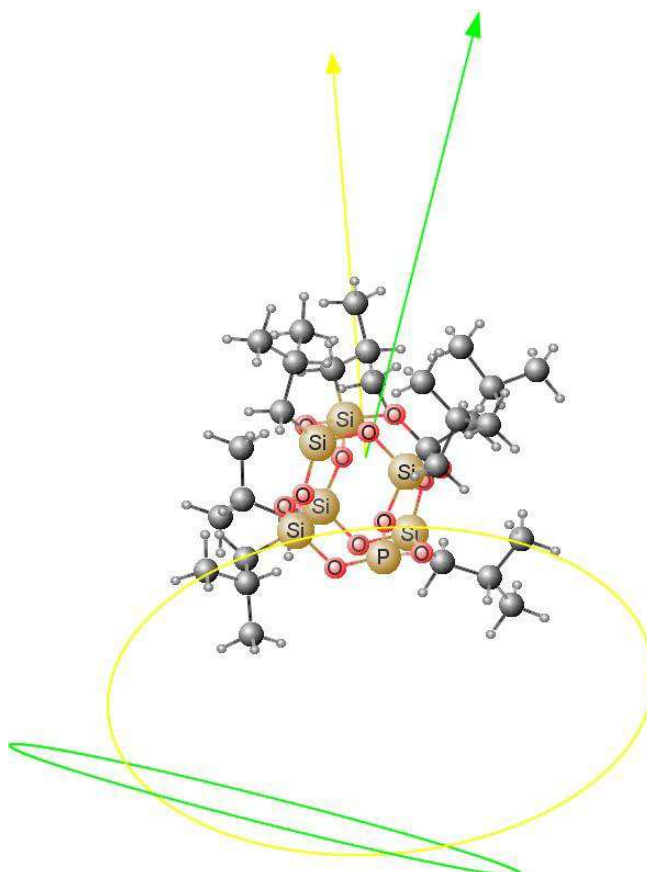
- A signal at  $3715\text{ cm}^{-1}$ , which is consistent with the presence of Si-OH in interaction with surrounding ligands;
- A large and broad peak at  $3212\text{ cm}^{-1}$ , which is associated with H-bonded OH groups, to the P atom,<sup>[10]</sup>
- Peaks at  $2964\text{ cm}^{-1}$  and  $2910\text{ cm}^{-1}$ , which corresponds to the  $\nu_{\text{asym}}(\text{C-H})$  and  $\nu_{\text{sym}}(\text{C-H})$  of  $\text{CH}_3$  group respectively as well as these at  $2932\text{ cm}^{-1}$  and  $2875\text{ cm}^{-1}$  to  $\nu_{\text{asym}}(\text{C-H})$  and  $\nu_{\text{sym}}(\text{C-H})$  of  $\text{CH}_2$  group respectively;
- A peak of weak intensity at  $2452\text{ cm}^{-1}$  along with a peak of weaker intensity at  $2425\text{ cm}^{-1}$ . Both are consistent with the presence of  $(\text{P}^{\text{V}}(=\text{O})\text{H})$  species (vide supra, Section on phosphites)<sup>[19]</sup> probably in a slightly different environment hence the appearance of two bands.

The presence of unreacted silanols and silanols in interactions probably indicate that the P-POSS is likely too large to interact with all surface silanols.

In fact, elemental analyses on the resulting solid showed the presence of  $\%_{\text{wt}}\text{C} = 3.17\%$ ;  $\%_{\text{wt}}\text{H} = 0.52\%$  and  $\%_{\text{wt}}\text{P} = 0.36\%$ . This amount represents a surface density equal to 0.6 P per surface silanol. Also, it is noteworthy that a C/P ratio of 23 is consistent with the amount of C in the POSS-P molecule (28 C for 1 P).

**Determination of the POSS-P surface area**

We determined the projected surface area using Marvin software.<sup>‡</sup> One can notice that both the geometrically calculated projection area and the maximal projection area are similar (154.95 Å<sup>2</sup> vs 147.77 Å<sup>2</sup>, i.e. **150 Å<sup>2</sup>**).



**Fig 64. Projection areas as calculated with Marvin**

Minimal projection area = 123,71 Å<sup>2</sup> (green projection)

Maximal projection area = 147,77 Å<sup>2</sup> (yellow projection)

Using this value and the surface area per gram of a silica Aerosil 200 (200 m<sup>2</sup>.g<sup>-1</sup>), a maximum of 0.88 P.nm<sup>-2</sup> is possible, which is greater than the density of surface silanols (0.7 OH.nm<sup>-2</sup>) and the final coverage in P (0.6 P.nm<sup>-2</sup>). Since a maximum coverage of 0.88 is possible and since not all surface silanols are consumed, this shows that the latter are likely not evenly distributed at the surface of the nanoparticles.

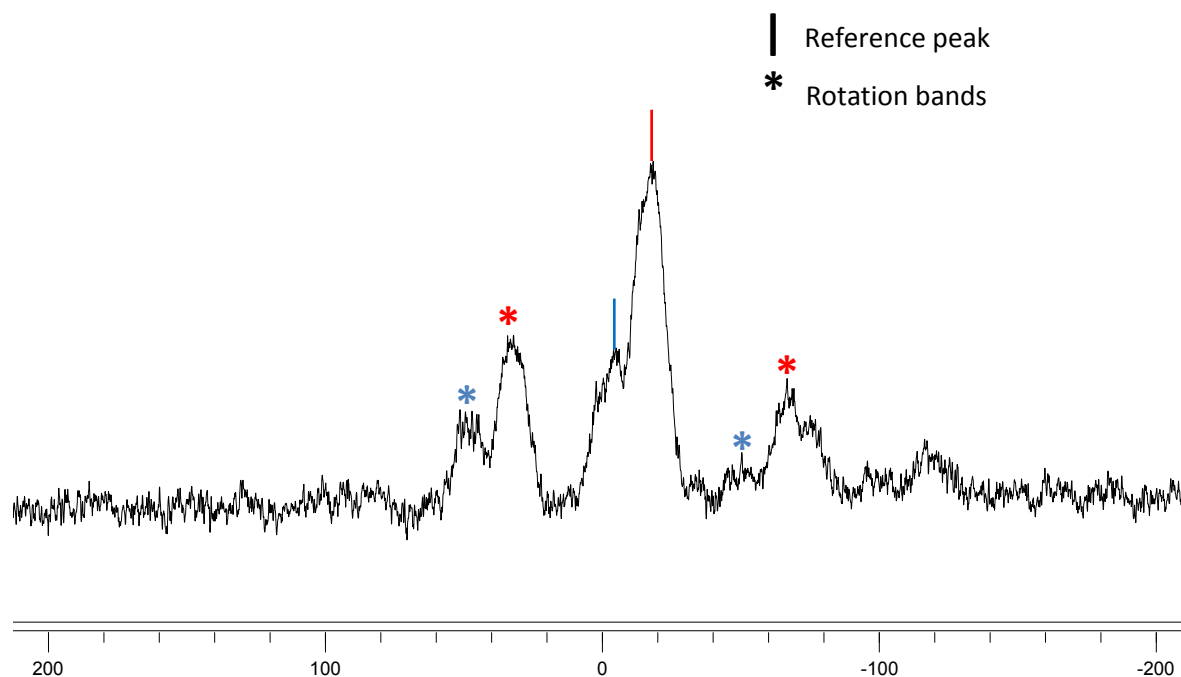
<sup>‡</sup> ChemAxon : <http://www.chemaxon.com/marvin/sketch/index.php>



## 2.2.2. NMR analyses and computational modelling

### 2.2.2.1. NMR spectroscopy of surface species of P-POSS on SiO<sub>2</sub>-(700)

A <sup>31</sup>P-SSNMR spectrum of the grafted compound was acquired, in order to characterise the structure(s) of P-containing surface species. (**Fig 65**)



**Fig 65.** <sup>31</sup>P-SSNMR of the grafted POSS-P on SiO<sub>2</sub>-(700) (MAS, 10kHz, d1= 40s, ns=1972, lb=50Hz)

First, the solid-state phosphorus-31 NMR spectrum displays several signals, which can be decomposed into two very different sites in a 80:20 ratio with isotropic chemical shifts of -18 ppm and -3 ppm (**Fig 65** above and **Fig 66** hereafter for the decomposition spectrum). The first site with an isotropic chemical shift  $\delta_{\text{iso}}$  of -3 ppm is associated with the following chemical shift anisotropy parameters (CSA):  $\delta_{11} = \delta_{22} = 55.2$  ppm and  $\delta_{33} = -119.0$  ppm, which corresponds to an axially symmetrical tensor ( $\Omega = 174$  ppm and  $\kappa = 1.00$ ). The second site of isotropic chemical shift  $\delta_{\text{iso}} = -18$  ppm, has the following CSA values:  $\delta_{11} = 68.0$  ppm,  $\delta_{22} = -2.7$  ppm and  $\delta_{33} = -118.9$  ppm, which corresponds to an asymmetrical tensor ( $\Omega = 186.9$  ppm and  $\kappa = 0.24$ ). The CSA parameters and the associated simulated static spectra are given in **Table 3**.

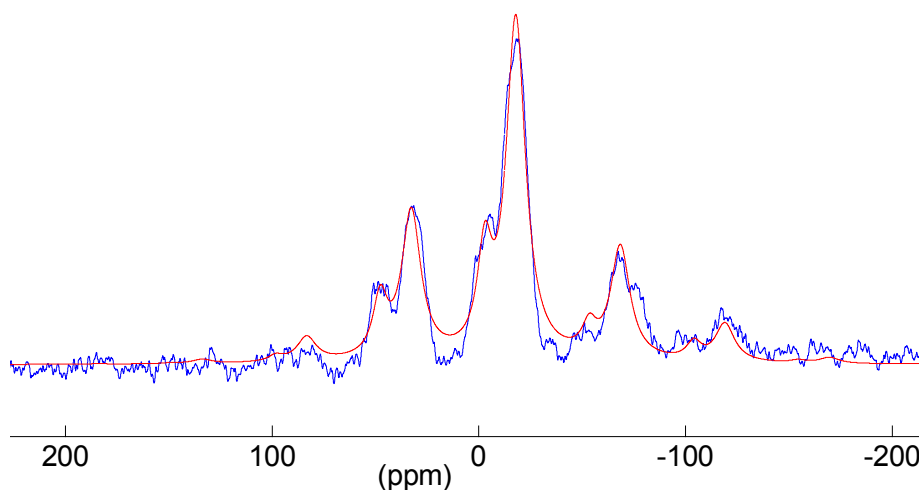


Fig 66. Decomposition of the  $^{31}\text{P}$ -SSNMR spectrum using DMFit (as before,  $l_b = 150\text{Hz}$ )

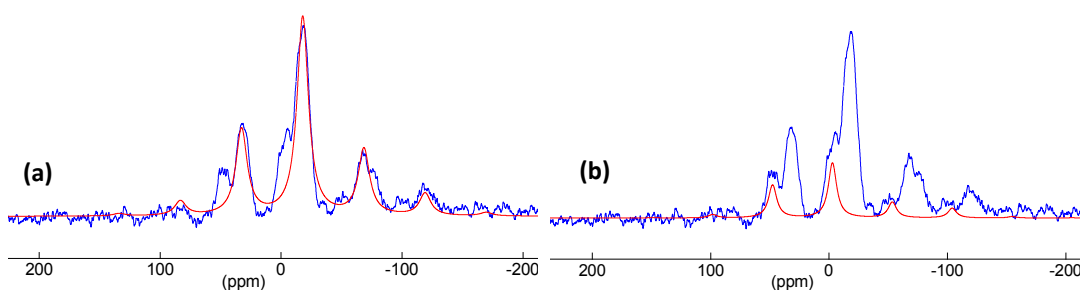


Fig 67. Decomposition of the  $^{31}\text{P}$ -SSNMR spectrum using DMFit (as before,  $l_b = 150\text{Hz}$ ) of each peak: (a) -18 ppm, (b) -3 ppm

Table 3. Templating of the calculated tensors for the spectrum at 10kHz

Measured $\delta$ (ppm)	Calculated $\delta_{ii}$ (ppm)	Calculated $\Omega$ and $\kappa$	Tensor shape (no rotation)	Tensor symmetry
-18	$\delta_{11} = 68.0$ $\delta_{22} = -2.7$ $\delta_{33} = -118.9$	$\Omega = 187$ $\kappa = 0.24$		asymmetrical
-3	$\delta_{11} = 55.2$ $\delta_{22} = 55.2$ $\delta_{33} = -119.0$	$\Omega = 174$ $\kappa = 1.00$		Axially symmetrical

As shown in **Table 3** above, the NMR spectrum acknowledges the presence of two different species. The starting POSS-P being  $C_{3v}$  bears an axial symmetry and is expected to have an axially

symmetric tensor (vide infra, **Table 6**). Therefore, the species at -18 ppm associated with an asymmetrical tensor must result from a profound change of symmetry around P, while the other species at -3 ppm, which still bears an axially symmetrical tensor, probably conserves a similar  $C_{3v}$  symmetry. However, in view of the large change of chemical shift, ( $\delta = 85$  ppm for molecular POSS-P) this species must have also changed upon interaction of POSS-P with the silica surface. In order to have a clearer understanding of the structure of surface species, it is thus important to test the proposed models by investigating the influence of spinning rates on the shape of CSA and the influence of OH density of the silica surface on the resulting surface species, and finally to confront potential structures of surface species with their calculated NMR signatures.

First, a  $^{31}\text{P}$ -SSNMR spectrum of the grafted POSS-P was recorded at a lower spinning rate (5kHz) (**Fig 68**). As expected, more rotation bands appeared. While the decomposition of the spectrum was more difficult (proximity of rotation bands), it was possible to extract two signals in an 80:20 ratio; at -18 and 0 ppm, respectively. For instance, the peak at ca. 0 ppm (-3 ppm in the previous spectrum) is almost completely hidden by the peak at  $\delta_{\text{iso}} = -18$  ppm and its first rotation band, making the extraction of the CSA values difficult. The different tensor parameters were then extracted and summed up in the following table. (**Table 4**)

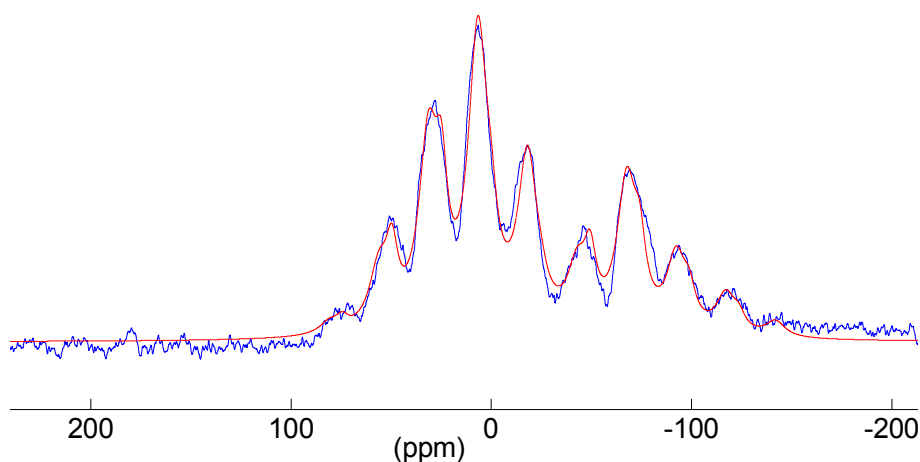


Fig 68. Decomposition of the  $^{31}\text{P}$ -SSNMR spectrum using DMFit (5kHz, lb = 150Hz)

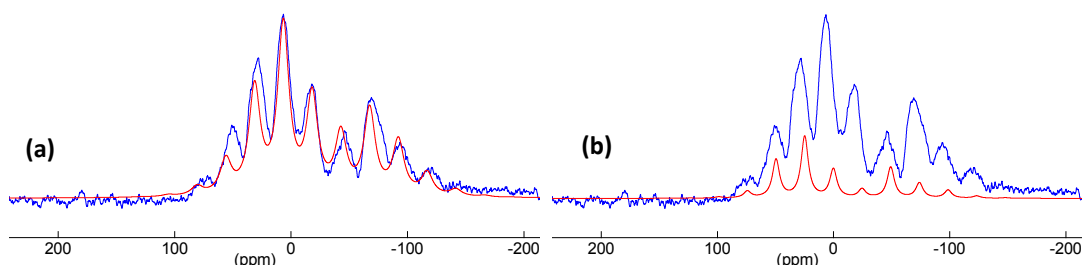
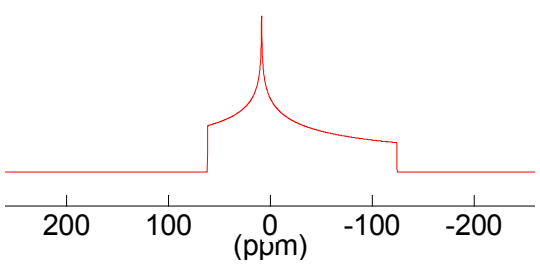
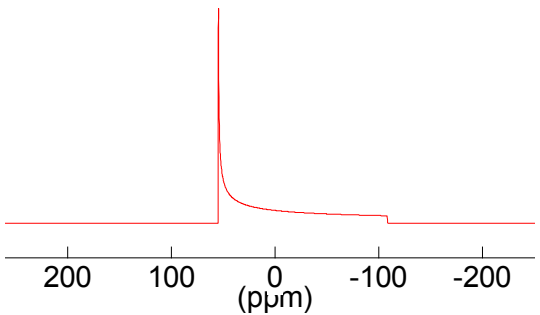


Fig 69. Decomposition of the  $^{31}\text{P}$ -SSNMR spectrum using DMFit (5kHz, lb = 150Hz) of each peak: (a) -18 ppm, (b) 0 ppm

Table 4. Templating of the calculated tensors for the spectrum at 5kHz

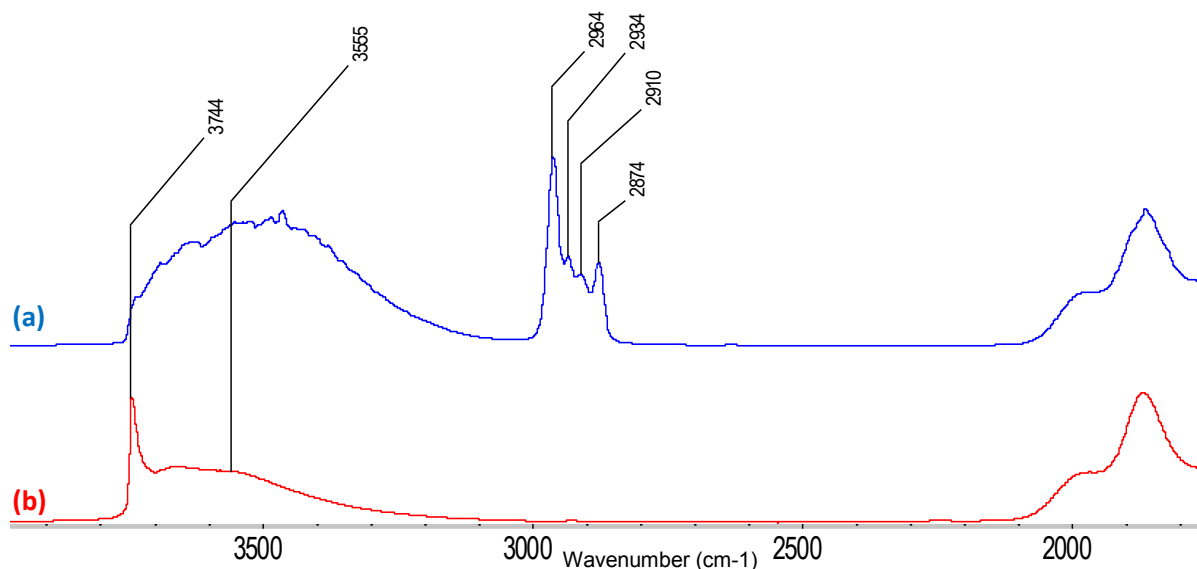
Measured $\delta$ (ppm)	Calculated $\delta_{ii}$ (ppm)	Calculated $\Omega$ and $\kappa$	Tensor shape (no rotation)	Tensor symmetry
-18	$\delta_{11} = 61.6$ $\delta_{22} = 8.5$ $\delta_{33} = -124.3$	$\Omega = 186$ $\kappa = 0.42$		Asymmetrical
0	$\delta_{11} = 54.5$ $\delta_{22} = 54.5$ $\delta_{33} = -108.5$	$\Omega = 163$ $\kappa = 1.00$		Axially symmetrical

Both signals displays similar isotropic chemical shift and CSA, which further support the consistency of the simulated parameters. The slight decrease of spans at higher spinning rate could be due to the slightly higher temperature at higher spinning rates, which could induce dynamic of the adsorbed species and thus a decrease of the apparent CSA.

While the first peak, at ca. -18 ppm, corresponds to POSS-P having likely reacted with the surface, thus breaking the original axial symmetry of the molecular species, the second peak, at ca. -3 ppm, would correspond to a coordinated POSS-P onto the surface, since there is no change in the tensor's symmetry (vide infra for final assignment).

### 2.2.2.2. Calculating tensors for the grafted compound on $\text{SiO}_{2-(200)}$

Grafting was then performed on  $\text{SiO}_{2-(200)}$ , which has a density of surface silanols of  $2.5 \text{ OH.nm}^{-2}$  (vs  $0.7 \text{ OH.nm}^{-2}$  for  $\text{SiO}_{2-(700)}$ ),<sup>[29]</sup> and it was monitored by IR-spectroscopy (**Fig 70**).



**Fig 70.** IR-DRIFT spectrum of  $\text{POSS-P}$  grafted onto  $\text{SiO}_{2-(200)}$  (a)  $\text{SiO}_{2-(200)}$  (b)  $\text{POSS-P}$  onto  $\text{SiO}_{2-(200)}$

The spectrum of the original  $\text{SiO}_{2-(200)}$  displays a peak at  $3744 \text{ cm}^{-1}$  corresponding to free  $\text{SiOH}$  and a broad peak between  $3500 \text{ cm}^{-1}$  and  $3744 \text{ cm}^{-1}$  corresponding to bonded silanol groups.

After grafting, no remaining free silanol peak at  $3744 \text{ cm}^{-1}$  can be observed, and a very broad peak at  $3555 \text{ cm}^{-1}$ , characteristic of  $\text{OH}$  interacting with a  $\text{P}$  atom, was observed.<sup>[7, 10]</sup> Note that bonded silanols present in  $\text{SiO}_{2-(200)}$  are still visible indicating their lower reactivity towards grafting compared to isolated silanols. The characteristic peaks of the isobutyl ligand were again observed ( $\nu_{\text{asym}}(\text{C-H})$  and  $\nu_{\text{sym}}(\text{C-H})$  of  $\text{CH}_3$  group at  $2964 \text{ cm}^{-1}$  and  $2910 \text{ cm}^{-1}$  and the  $\nu_{\text{asym}}(\text{C-H})$  and  $\nu_{\text{sym}}(\text{C-H})$  of  $\text{CH}_2$  group at  $2934 \text{ cm}^{-1}$  and  $2874 \text{ cm}^{-1}$ ).

Then, a  $^{31}\text{P}$ -SSNMR spectrum was recorded and decomposed by DMFit (**Fig 71** and **Table 5**). In this case, two sites were found in a ca. 50:50 ratio, and they have the following CSA parameters:

- One site associated with an isotropic chemical shift of  $-17 \text{ ppm}$  and characterized by a span  $\Omega$  of  $215 \text{ ppm}$  and a skew  $\kappa$  of  $0.04$ . This corresponds to an asymmetrical tensor, though tending towards spherical symmetry.
- A second site associated with an isotropic shift  $-1 \text{ ppm}$ , characterised with a span  $\Omega$  of  $170 \text{ ppm}$  and a skew  $K$  of  $1.0$ . This corresponds to an axially symmetrical tensor.

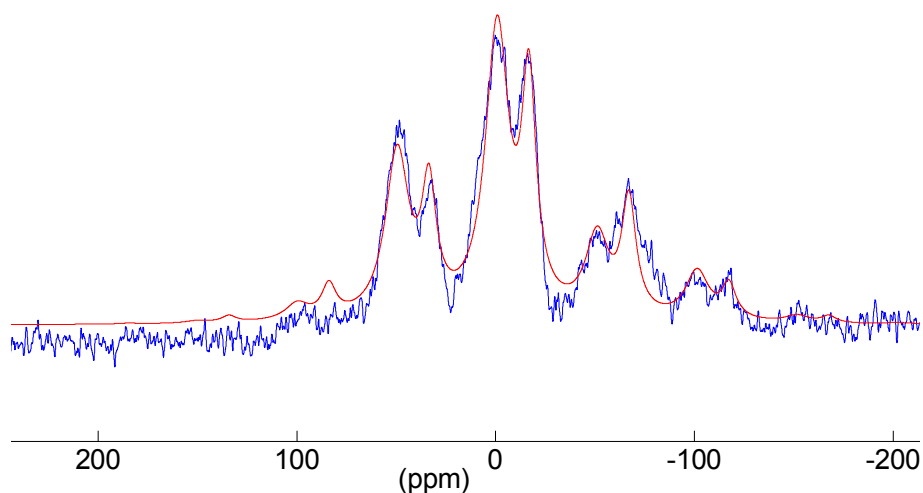


Fig 71. <sup>31</sup>P-SSNMR of grafted POSS-P onto SiO<sub>2-(200)</sub> (blue) and its decomposition using DMFit (red) (HPDEC, 10kHz, d1= 40s, ns=532, lb=150Hz)

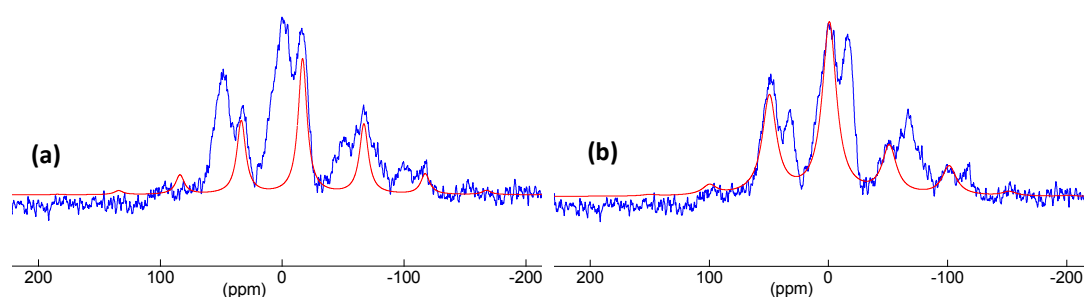
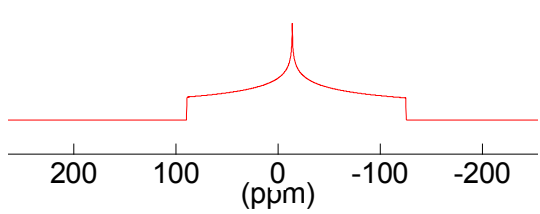
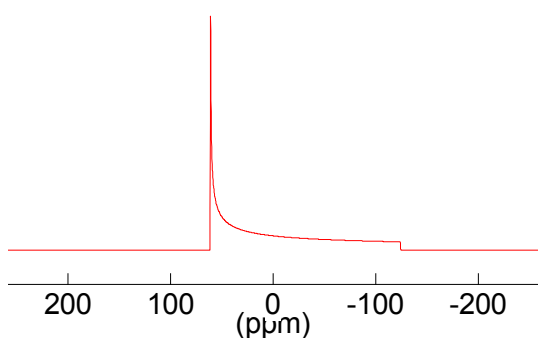


Fig 72. Decomposition of the <sup>31</sup>P-SSNMR spectrum using DMFit (10kHz, lb = 150Hz) of each peak: (a) -17 ppm, (b) -1ppm

Table 5. Templating of the calculated tensors for the spectrum at 10kHz for SiO<sub>2-(200)</sub>

Measured $\delta$ (ppm)	Calculated $\delta_{ii}$ (ppm)	Calculated $\Omega$ and $\kappa$	Tensor shape (no rotation)	Tensor symmetry
-17	$\delta_{11} = 89.2$ $\delta_{22} = -14.0$ $\delta_{33} = -125.4$	$\Omega = 215$ $\kappa = 0.04$		Asymmetrical (tending towards spherical symmetry)
-1	$\delta_{11} = 56.0$ $\delta_{22} = 56.0$ $\delta_{33} = -114.3$	$\Omega = 170$ $\kappa = 1.00$		Axially symmetrical

As can be seen in **Table 5** above, the two surface species are observed again in a different ratio, but, importantly, the surface species corresponding to the peak at -17 ppm has similar CSA parameters as that this obtained on  $\text{SiO}_{2-(700)}$  with a slightly different asymmetry ( $\kappa$  of 0.04 vs. 0.24). In contrast, the signal at -1 ppm displays a closer resemblance with almost the same  $\Omega$  and exactly the same  $\kappa$  as that observed on  $\text{SiO}_{2-(700)}$ .

In order to have further insight into the nature of surface species, DFT calculations were performed on POSS-P and possible surface species resulted from the interaction of POSS-P with the surface functionalities of silica, namely silanols and siloxane bridges.<sup>§</sup> This was performed by using the full model of POSS-P with all its ligands and a simplified model for silica,  $(\text{MeO})_3\text{SiOH}$ , which represents already quite well the electronic features of silica.<sup>[30-32]</sup>

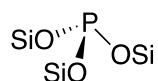
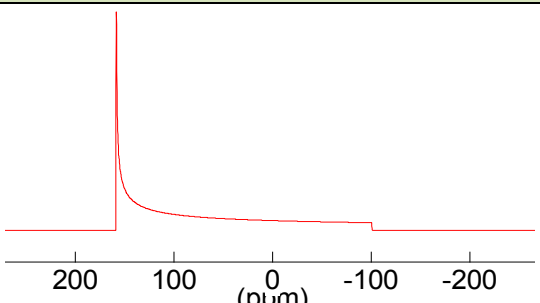
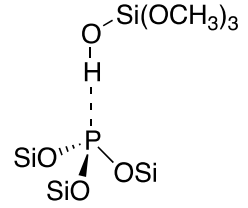
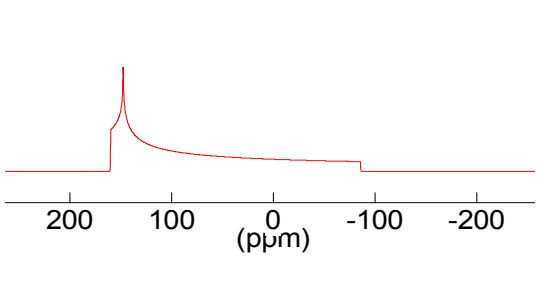
---

<sup>§</sup> Calculations performed at ETH Zürich by Dr Wischert.

## 2.2.3. Computational structures as a discriminating method

All calculations were performed according to the Herzfeld-Berger convention and are transcribed here in Haeberlen convention, in order to match the software's standard.<sup>5</sup>

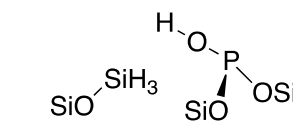
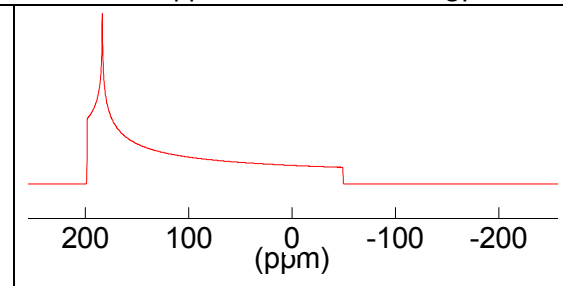
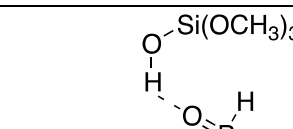
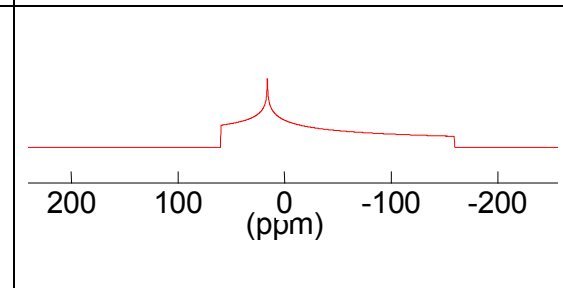
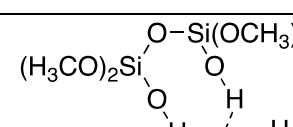
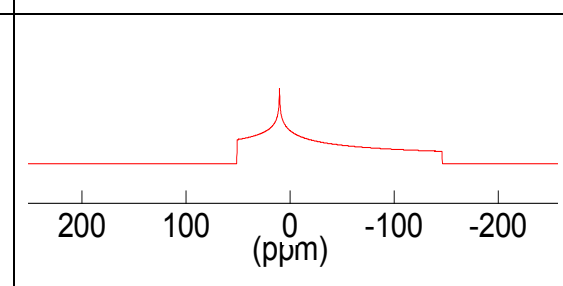
Table 6. Calculated species depending on POSS-P geometry and reactivity

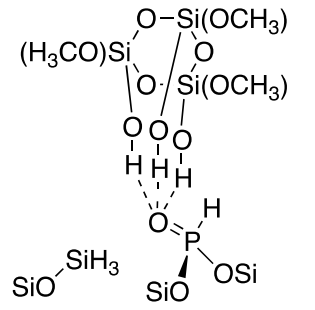
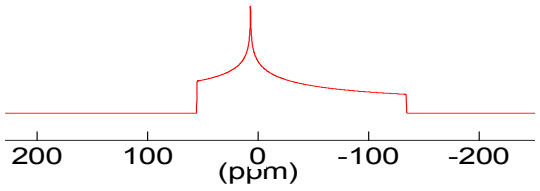
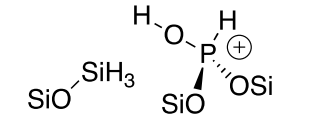
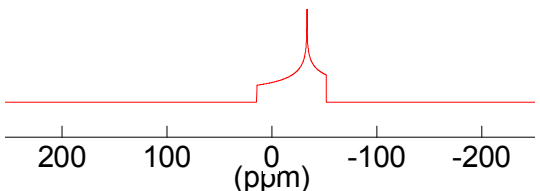
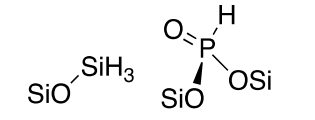
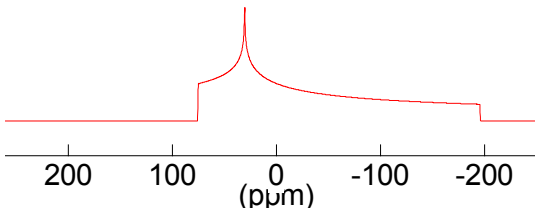
	#	Structure	Calculated $\delta_{\text{iso}}$ (ppm)	Calculated $\delta_{\text{ii}}$ (ppm)	Calculated $\Omega$ and $\kappa$	Tensor shape (no rotation)	Tensor symmetry
Phosphites	<b>A</b>	 <p>Molecular methyl-terminated POSS-P</p>	72.0 $\delta_{\text{exp}}=84.8\text{ppm}$	$\delta_{11} = 159$ $\delta_{22} = 158.4$ $\delta_{33} = -100.4$	$\Omega = 259$ $\kappa = 1.00$		Axially symmetrical
	<b>B</b>	 <p>POSS-P + <math>\text{Si}(\text{OMe})_3\text{OH}</math>, H-bound</p>	73.6	$\delta_{11} = 159.9$ $\delta_{22} = 147.4$ $\delta_{33} = -86.0$	$\Omega = 245.5$ $\kappa = 0.90$		Asymmetrical

<sup>5</sup> Conversions were done using the online tools of the University of Tübingen: <http://anorganik.uni-tuebingen.de/klaus/nmr/index.php?p=conventions/csa/csa>



<b>Phosphites</b>	<b>C</b>	<p>POSS-P + R(SiOH)<sub>2</sub>, H-bound</p>	75.8	$\delta_{11} = 162.1$ $\delta_{22} = 148.5$ $\delta_{33} = -83.1$	$\Omega = 245.2$ $\kappa = 0.89$		Asymmetrical
	<b>D</b>	<p>POSS-P + R(SiOH)<sub>3</sub>, H-bound</p>	84.8	$\delta_{11} = 166.8$ $\delta_{22} = 161.3$ $\delta_{33} = -73.6$	$\Omega = 240.5$ $\kappa = 0.95$		Asymmetrical (tends to axial symmetry)
	<b>E</b>	<p>POSS-P, protonated</p>	-43.0	$\delta_{11} = -9.8$ $\delta_{22} = -60.0$ $\delta_{33} = -60.2$	$\Omega = 50$ $\kappa = -0.99$		Axially symmetrical
	<b>F</b>	<p>POSS-P + SiH<sub>3</sub>OH, dissociated, H-bound</p>	113.4	$\delta_{11} = 202.9$ $\delta_{22} = 192.7$ $\delta_{33} = -55.5$	$\Omega = 258$ $\kappa = 0.92$		Asymmetrical

Phosphonates	<b>G</b>	 <p>POSS-P + SiH<sub>3</sub>OH inserted POH</p>	110.7	$\delta_{11} = 198.2$ $\delta_{22} = 183.4$ $\delta_{33} = -49.5$	$\Omega = 247.8$ $\kappa = 0.88$		Asymmetrical
	<b>H</b>	 <p>POSS-P phosphonate + Si(OMe)<sub>3</sub>OH inserted, H bound</p>	-27.8	$\delta_{11} = 59.9$ $\delta_{22} = 16.1$ $\delta_{33} = -159.3$	$\Omega = 219.2$ $\kappa = 0.60$		Asymmetrical
	<b>I</b>	 <p>POSS-P phosphonate + bis- Si(OMe)<sub>3</sub>OH inserted, H bound</p>	-28.4	$\delta_{11} = 50.9$ $\delta_{22} = 10.0$ $\delta_{33} = -146.2$	$\Omega = 197.0$ $\kappa = 0.59$		Asymmetrical

Phosphonates	<b>J</b>	 <p>POSS-P phosphonate + tri-Si(OMe)<sub>3</sub>OH inserted, H bound</p>	-24.1	$\delta_{11} = 55.1$ $\delta_{22} = 7.0$ $\delta_{33} = -134.3$	$\Omega = 189.3$ $\kappa = 0.49$		Asymmetrical
	<b>K</b>	 <p>POSS-P phosphonate + SiH<sub>3</sub>OH inserted, protonated</p>	-23.7	$\delta_{11} = 14.3$ $\delta_{22} = -33.6$ $\delta_{33} = -51.9$	$\Omega = 66.2$ $\kappa = -0.45$		Asymmetrical
	<b>L</b>	 <p>POSS-P phosphonate + SiH<sub>3</sub>OH inserted</p>	-30.0	$\delta_{11} = 75.3$ $\delta_{22} = 30.4$ $\delta_{33} = -195.8$	$\Omega = 271.1$ $\kappa = 0.67$		Asymmetrical

*Validity of the model*

Calculations made on simple molecules (**Appendix 6**) showed an average variability of 20 ppm between calculated and experimental isotropic chemical shift, with  $\delta_{\text{calc}} > \delta_{\text{exp}}$ .

Calculated  $\delta_{\text{iso}}$  for a model of POSS-P, for which iBu was replaced by Me, is 72.0 ppm, which is comparable with the one observed in solution for the molecular species,  $\delta_{\text{iso}} = 84.8$  ppm. For the corresponding oxide, the calculated  $\delta_{\text{iso}}$  for POSS-P oxide is -70.4 ppm, but the experimental value  $\delta_{\text{iso}}$  is -44.9 ppm.<sup>[24]</sup> This important difference is found for all P(V)-oxide compounds, and probably results from difficulty to describe the P-O bond.

Therefore, it can be concluded that calculated chemical shifts should be tolerable within a 25 ppm variation.

*Discussion on the calculated species*

The CSA of **POSS-P** (Entry **A**, **Table 6**) is characterised by its isotropic chemical shift (72.0 ppm), a large span ( $\Omega = 259$  ppm) and an axially symmetric tensor ( $\kappa = 1$ ), which shows that the two experimentally observed signals cannot correspond to free POSS-P. In view of the basicity of phosphorus, the interaction of **POSS-P** with the proton of a model surface silanol was investigated, (Entry **B**, **Table 6**), with increasing number of interacting SiOH (Entries **C** and **D**). The higher the number of interactions, the higher  $\delta_{\text{iso}}$ , (from 72.0 ppm to 84.8 ppm) with both span and skew remaining similar. It is noteworthy that POSS-P interacting with three silanols (Entry **D**) bears similar CSA parameters ( $\delta_{\text{iso}} = 84.8$  ppm,  $\Omega = 240.5$  ppm and  $\kappa = 0.95$ ) as molecular **POSS-P** ( $\delta_{\text{iso}} = 84.8$  ppm,  $\Omega = 259$  ppm and  $\kappa = 1.00$ ).

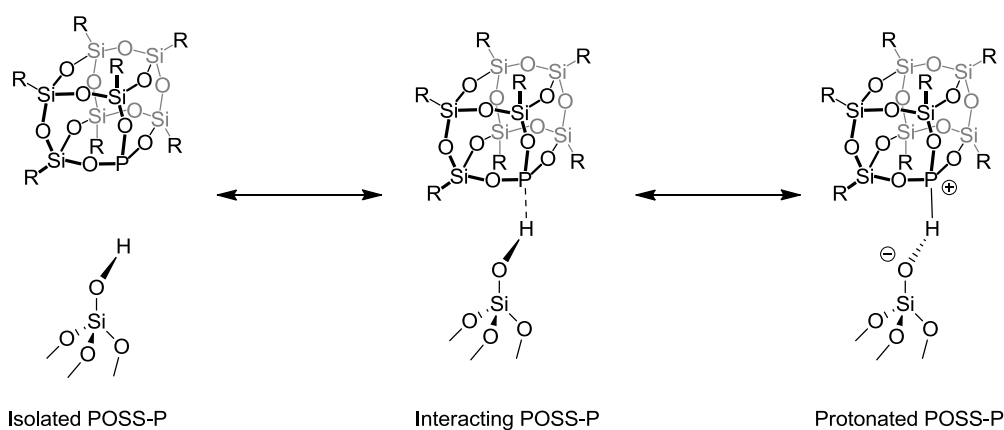
A fully protonated **POSS-P** was also studied as an extreme model (Entry **E**, **Table 6**). While all H-bonded POSS-P exhibit CSA values similar to that of molecular POSS-P,  $\delta_{\text{iso}}$  being slight shifted upfield, this structure displays values ( $\delta_{\text{iso}} = -43.0$  ppm,  $\Omega = -60.2$  ppm and  $\kappa = 0.5$ ) with a strong upfield shift, bringing  $\delta_{\text{iso}}$  to a highly negative value (see below for further comment).

Moreover, in view of the chemistry of phosphites with surface silanols,<sup>[7]</sup> (see **Appendix 7** for proposed mechanisms) we decided to investigate species resulting from the cleavage of a P-O bond of POSS-P by a silanol and leading to the cage-opening of the phosphite structures (Entries **F-G**, **Table 6**) as well as the corresponding phosphonates (Entries **H to K**, **Table 6**). All opened phosphite structures display a strongly deshielded  $\delta_{\text{iso}}$  and large  $\Omega$ , with asymmetrical tensor, showing they are inconsistent with the experimental values. On the other hand, the phosphonates have negative  $\delta_{\text{iso}}$  close to the experimental values (within 30 ppm), an asymmetrical tensor, and a  $\Omega$  in the same order of magnitude as experimental values. Yet, it is noteworthy that interaction with a silanol leads to a downfield shift and a narrower  $\Omega$  (Entry **H to J**, **Table 6**), and the more interacting silanols, the

smaller the span (Entries **I** and **J**, **Table 6**). Protonation of the P=O bond leads to a structure whose chemical shift and skew are close to the experimental value ( $\delta_{\text{iso}} = 23$  ppm,  $\kappa = 0.45$ ) but with a very small span ( $\Omega = -66.2$  ppm) inconsistent with the experimental data.

From these calculations, the signal at  $\delta_{\text{iso}} \approx -18$  ppm would be compatible with a phosphonate surface species stabilized by H-bonding with the more interaction the better the agreement, suggesting that interaction with adjacent OH group is probably important. In particular, the CSA parameters ( $\delta_{\text{iso}} = -24$ ,  $\Omega = 189.3$  ppm and  $\kappa = 0.49$ ) for Entry **J**, **Table 6** are in close agreement with the experimental value ( $\delta_{\text{iso}} = -18$ ,  $\Omega = 185$  ppm and  $\kappa = 0.3$ ).

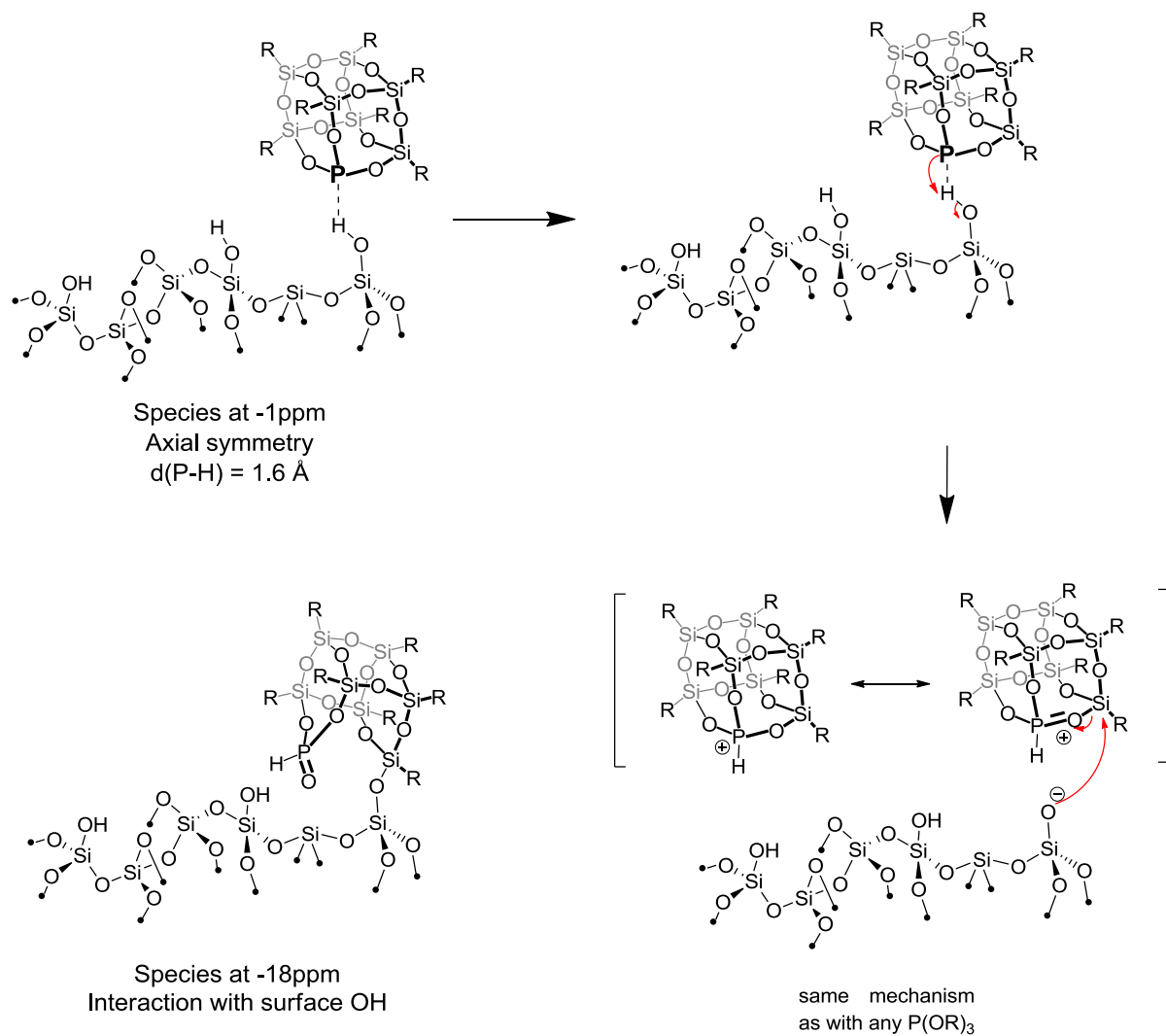
For the surface species associated with  $\delta_{\text{iso}} \approx -1$  ppm, there is no clear agreement with a specific surface species, but it is most consistent with a POSS-P H-bonded to the surface, because its experimental CSA parameters lies in between two extreme models, a fully protonated POSS-P (Entry **E**, **Table 6**) and a POSS-P having a weak H-bond with a silanol: they all display the same skew (0.90 for the calculated single H-bond, -0.99 for the protonated POSS-P), while  $\delta_{\text{iso}}$  and the span of these extreme models lie in between (72.0 ppm and -43 ppm). We are currently investigating in more details the effect of van der Waals interaction and the associated stronger H-bonding on the CSA parameters of P since the model used so far corresponds to POSS-P in interaction with  $\text{HOSi}(\text{OMe})_3$  (Entry **B**, **Table 6**). We can so far assume the species to correspond to an intermediate species as shown in **Scheme 24** below, with one or several silanol interactions.



**Scheme 24.** Description of the model applied for P-H distance

**Scheme 25** hereafter sums up the obtained results, showing that the species at -18 ppm is most probably a phosphonate interacting with the surface, whereas the species at -1 ppm is a coordinated POSS-P.

Application of the strategy to N-dopants, the case of Phosphorus

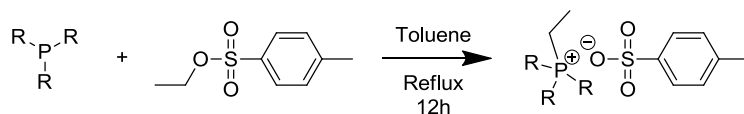


Scheme 25. Summary of the observed species and proposed formation of each

### 2.3. Grafting of phosphonium

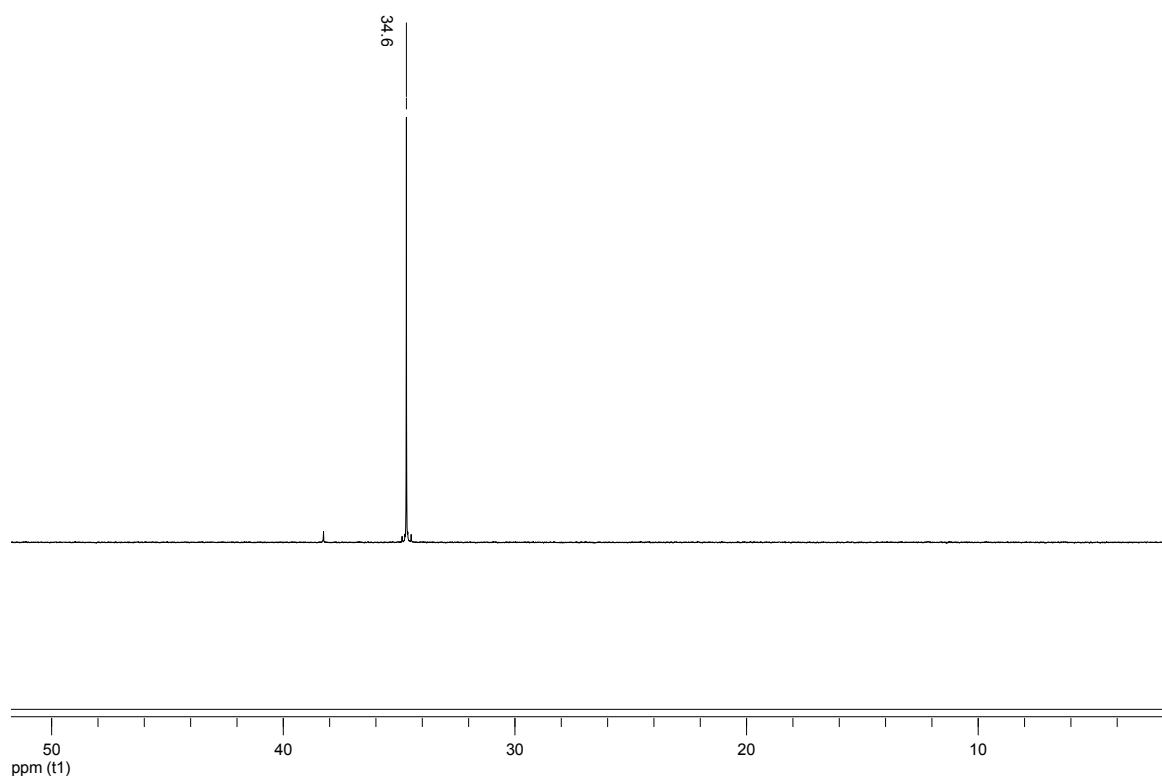
Following our strategy which aims at controlling surface P density *via* steric interaction and self-assembly, the exchange of proton by large phosphonium cations was investigated. It has to be stressed that phosphonium salts have both a good reactivity and tuneable geometry,<sup>[33]</sup> and exist as a wide variety of compounds having various counter-ion. A sulfonate counter-ion was used here as it is highly important to avoid potential halide contamination of the surface, detrimental for electronic applications.<sup>[34]</sup>

The following ionic liquid was thus synthesised as follows (**Scheme 26**):<sup>[33]</sup>



**Scheme 26.** Phosphonium salt synthesised and used for further reactions with the silanol surface, R=n-Bu

The <sup>31</sup>P-NMR spectrum shows a peak at 34.6 ppm (the small peak at 38 ppm being an artefact resulting from the spectral window size), which is different from tributylphosphine (-31.2 ppm)<sup>[35-37]</sup> and consistent with the formation of phosphonium salt.<sup>[38]</sup> (**Fig 73**)



**Fig 73.** <sup>31</sup>P liquid state NMR spectrum of the obtained molten salt

This previous phosphonium salt was then contacted with silica  $\text{SiO}_{2-(700)}$  in dry and degassed toluene and an IR-DRIFT analysis of the resulting powder was performed.

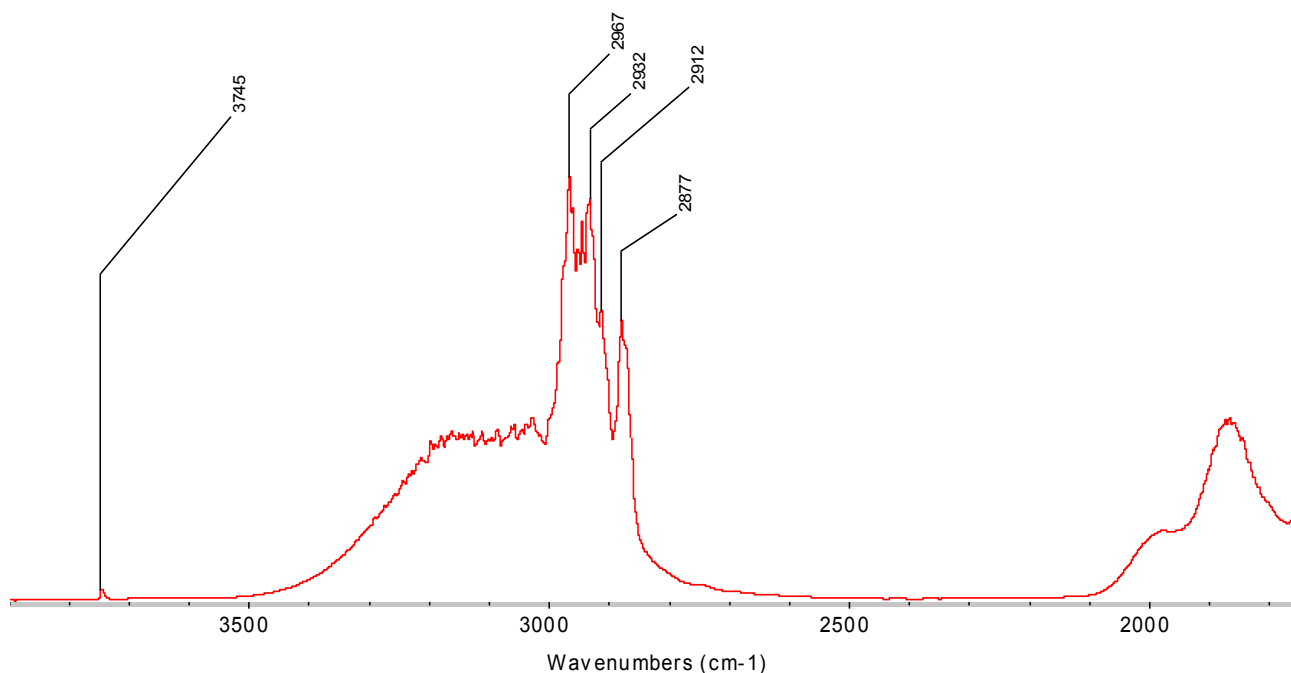


Fig 74. IR-DRIFT of the grafted phosphonium salt

Beside the peaks between  $2967\text{ cm}^{-1}$  and  $2877\text{ cm}^{-1}$  attributed to  $\nu_{\text{sym}}(\text{C-H})$  and  $\nu_{\text{asym}}(\text{C-H})$ , there is a weak peak at  $3745\text{ cm}^{-1}$  associated with residual silanols. Note however the presence of a broad peak at  $3200\text{ cm}^{-1}$ , which is consistent with phosphorus-OH interaction. Although no peak around  $2300\text{ cm}^{-1}$  appeared for the sulfonic acid derivative, elementary analyses showed the presence of  $0.68\%_{\text{wt}}$  sulfur and thus that there is still one S per P. The tosylate anion was therefore not removed as hoped.

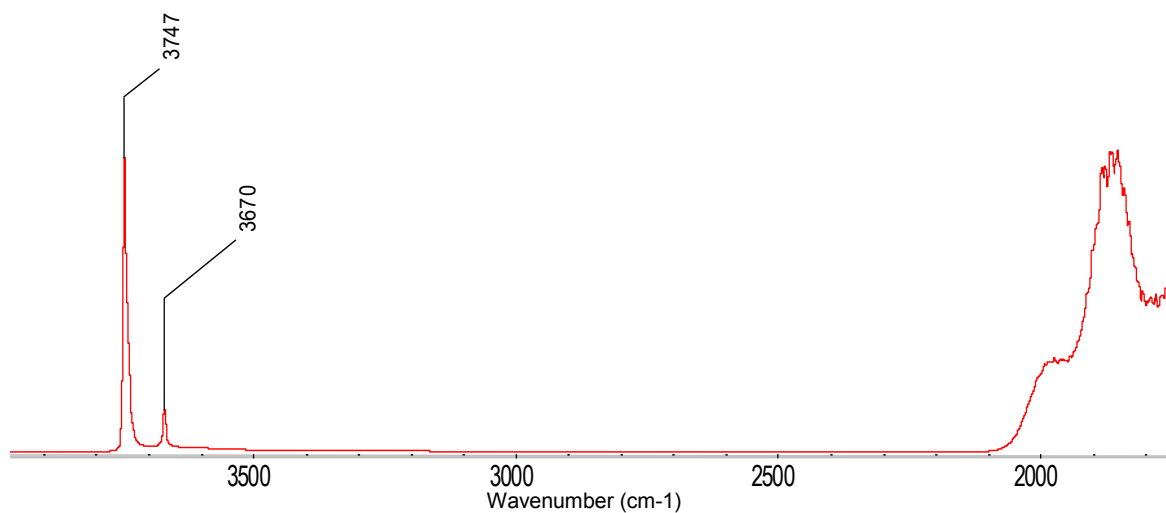
Overall, the phosphonium salt is probably only adsorbed at the surface via electrostatic interaction.

### 3. Elimination of the ligands

As with boron, further calcinations of the grafted species were performed in order to eliminate the organic chains and try to make the phosphorus atom diffuse into silica. Similar treatments were performed as described for boron with a calcination step of 2h at  $500^{\circ}\text{C}$  under dry air (ramp of  $6^{\circ}\text{C}\cdot\text{min}^{-1}$  from  $24^{\circ}\text{C}$  to  $500^{\circ}\text{C}$  under a flow of  $50\text{ mL}\cdot\text{min}^{-1}$  of dry air) on the grafted phosphorus-containing species. The IR-DRIFT spectrum was then recorded (**Table 7**).



We shall first tackle the example of the calcined phosphonium species, which displayed a very clean spectrum and can be used as an illustrative example of all other calcined species. (**Fig 75**)



**Fig 75.** IR-DRIFT of the calcined grafted phosphonium

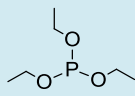
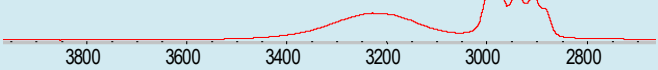
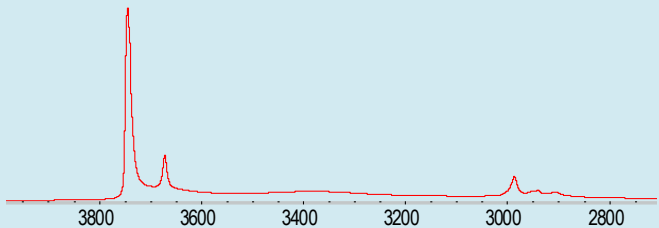
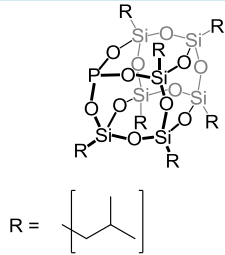
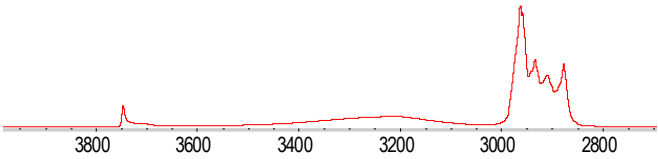
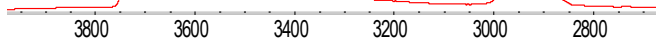
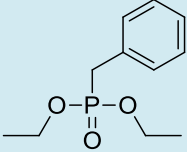
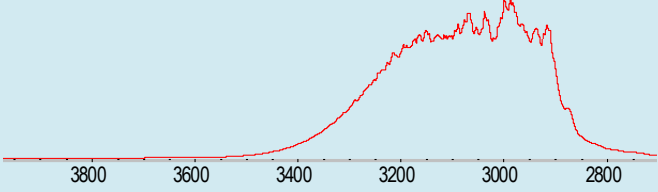
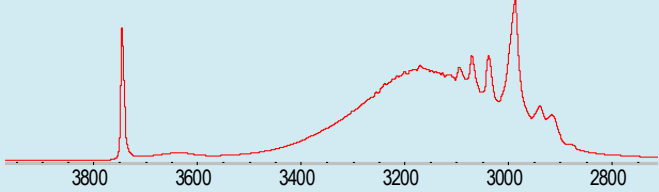
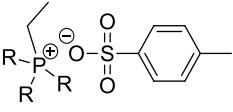
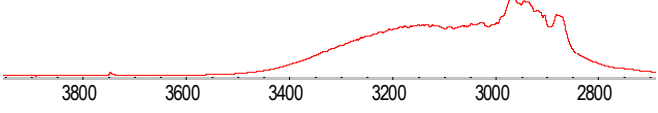
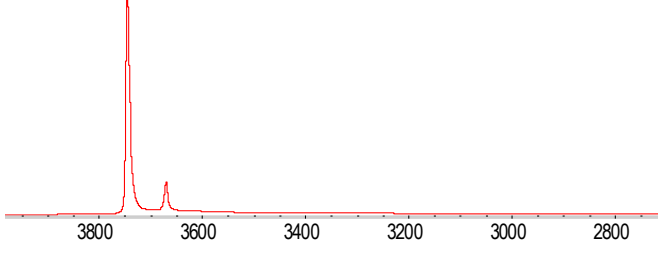
As can be seen on **Fig 75**, the following features can be drawn:

- Disappearance of all peaks associated with the organic ligands,
- Reappearance of the peak at  $3747\text{ cm}^{-1}$  associated with isolated silanols,
- Appearance of a new peak at  $3670\text{ cm}^{-1}$  which can be attributed to P-OH as reported.<sup>[39]</sup>

Moreover, elemental analysis showed a P loading of  $0.25\%_{\text{wt}}$  after calcination which shows that a large proportion of the phosphonium was eliminated ( $> 60\%$ ).

In **Table 7** hereafter, it is noteworthy that these features appear clearly for two species only: the grafted triethylphosphite and phosphonium.

Table 7. Comparison of the effect of calcination on each grafted precursor

Precursor	IR-DRIFT spectrum of the grafted species (wavenumbers $\text{cm}^{-1}$ )	IR-DRIFT spectrum of the calcined species (wavenumbers $\text{cm}^{-1}$ )	%wtP	%wtP
			before calcination	after calcination
			0.28	0.25
			0.77	0.74
			0.60	0.56
			0.65	0.25

It is noteworthy that, in all cases, a recovery of SiOH is observed. After calcination, it is shown that P recovery is higher for all grafted species (above 90%) while the interaction phosphonium displays only a 40% recovery yield.

Also, it appears that the bigger the organic chain of the grafted species, the lesser the loss: 10% for triethylphosphite, 6% for phosphonate, 3% for POSS-P. Such a decrease may result from a “capping” of the dopant by the organic chain. In the case of POSS-P, it may be thought that phosphorus could be embedded in a silica layer formed from the siloxy chains, as discussed for borosilicates.<sup>[40]</sup>

Then, both phosphites and the phosphonate still exhibit peaks around  $3000\text{ cm}^{-1}$ . This proves that all organic chains were not removed during calcination, contrarily to the grafted phosphonium. In the case of grafted phosphonate, the region around  $3000\text{ cm}^{-1}$  is also less saturated.

Grafted triethylphosphite and phosphonium both show the appearance of a peak at  $3670\text{ cm}^{-1}$ , attributed to P-OH.<sup>[39]</sup> This peak is weak and quite broad in the case of the calcined phosphonate. Calcined POSS-P does not exhibit this species.

## Conclusion

---

In this chapter, we transposed the same strategy we used with boron to phosphorus-doping. As before, two main ways for surface doping the surface were studied:

- i) A grafting strategy, starting from phosphites and phosphonate,
- ii) A self-positioning strategy using phosphines, a POSS-P and a phosphonium.

It appeared that the POSS-P actually grafted onto the surface. The permanent bonding strategy was then proven to be majoritary. Interestingly, the removal of organic chains by calcination of grafted compounds showed an excellent phosphorus recovery: for all grafted species, the recovery yield was above 90%. As for self-positioned molecules, it was shown that  $\text{PCy}_3$  desorbed from the surface when treated at temperatures above  $200^\circ\text{C}$ , forbidding any kind of further calcination, while the phosphonium species was simply adsorbed at the silica surface, not yielding the expected silanolate-phosphonium species. Subsequent calcination of the phosphonium-supported species eliminated about 60% of the amount of phosphorus.

Amongst the grafted species, different surface coverages were obtained, depending on the chemistry of grafting. Triethylphosphite was proven to have a maximum yield of 50% because of the initial formation of  $\equiv\text{SiOEt}$ . The used phosphonate showed an excellent surface coverage, as well as POSS-P, despite being a phosphite.

Yet, only two supported species, triethylphosphite and the phosphonium, would yield a newly formed surface POH species after calcination.

Also, an NMR study was performed for the POSS-P molecule, as it showed an interesting behaviour: the formation of two species, one having reacted with the surface to yield an opened cage and the other being in a close coordination to the surface silanols. This study combined computational chemistry with tensor shaping of the experimental species.

In the course of events, however, only the phosphonium species was studied on silicon wafers, as it was the first one to be obtained and fully characterised.

## References

- [1] G. S. Irmukhametova, B. J. Fraser, J. L. Keddie, G. A. Mun, V. V. Khutoryanskiy, *Langmuir* **2012**, *28*, 299.
- [2] J. Bould, J. Macháček, M. G. S. Londesborough, R. Macías, J. D. Kennedy, Z. Bastl, P. Rupper, T. Baše, *Inorganic Chemistry* **2012**, *51*, 1685.
- [3] L. Baltusis, J. S. Frye, G. E. Maciel, *Journal of the American Chemical Society* **1986**, *108*, 7119.
- [4] L. Baltusis, J. S. Frye, G. E. Maciel, *Journal of the American Chemical Society* **1987**, *109*, 40.
- [5] J. H. Lunsford, P. N. Tutunjian, P. J. Chu, E. B. Yeh, D. J. Zaleski, *The Journal of Physical Chemistry* **1989**, *93*, 2590.
- [6] J. P. Osegovic, R. S. Drago, *The Journal of Physical Chemistry B* **1999**, *104*, 147.
- [7] I. D. Gay, A. J. McFarlan, B. A. Morrow, *The Journal of Physical Chemistry* **1991**, *95*, 1360.
- [8] A. I. D. Dalá€Maso, F. d. r. Legendre, C. Blonski, P. Hoffmann, *Synthetic Communications* **2008**, *38*, 1688.
- [9] O. Sakatsume, H. Yamane, H. Takaku, N. Yamamoto, *Tetrahedron Letters* **1989**, *30*, 6375.
- [10] S. J. Lang, I. D. Gay, B. A. Morrow, *Langmuir* **1995**, *11*, 2534.
- [11] R. A. Nyquist, *Spectrochimica Acta Part A: Molecular Spectroscopy* **1969**, *25*, 47.
- [12] G. A. Olah, C. W. McFarland, *The Journal of Organic Chemistry* **1971**, *36*, 1374.
- [13] R. Weiss, L. J. Vande Griend, J. G. Verkade, *The Journal of Organic Chemistry* **1979**, *44*, 1860.
- [14] J. CieÅłak, M. Sobkowski, A. Kraszewski, J. StawiÅłski, *Tetrahedron Letters* **1996**, *37*, 4561.
- [15] S. Berte-Verrando, R. Diziere, M. Samadi, P. Savignac, *Journal of the Chemical Society, Perkin Transactions 1* **1995**.
- [16] L. Ernst, *Organic Magnetic Resonance* **1977**, *9*, 35.
- [17] T. Bottin-Strzalko, J. Seyden-Penne, M.-J. Pouet, M. P. Simonnin, *The Journal of Organic Chemistry* **1978**, *43*, 4346.
- [18] B. Iorga, F. d. r. Eymery, P. Savignac, *Tetrahedron* **1999**, *55*, 2671.
- [19] R. A. Nyquist, *Spectrochimica Acta* **1966**, *22*, 1315.
- [20] K. Shimakura, T. Suzuki, Y. Yadoiwa, *Solid-State Electronics* **1975**, *18*, 991.
- [21] R. B. Allen, H. Bernstein, A. D. Kurtz, *Journal of Applied Physics* **1960**, *31*, 334.
- [22] B. Kalkofen, M. Lisker, E. P. Burte, *Materials Science and Engineering: B* **2005**, *124*–*125*, 288.
- [23] M. Ghezzi, D. M. Brown, *Journal of The Electrochemical Society* **1973**, *120*, 146.
- [24] F. J. Feher, T. A. Budzichowski, *Organometallics* **1991**, *10*, 812.
- [25] K. B. Dillon, M. G. Craveirinha Dillon, T. C. Waddington, *Journal of Inorganic and Nuclear Chemistry* **1976**, *38*, 1149.
- [26] B. W. Tattershall, N. L. Kendall, *Polyhedron* **1994**, *13*, 1517.
- [27] S. Patchkovskii, T. Ziegler, *The Journal of Physical Chemistry A* **2002**, *106*, 1088.
- [28] M. J. Robins, B. Uznański, *Can. J. Chem* **1981**, *59*, 2601.
- [29] L. T. Zhuravlev, *Colloids and Surfaces A: Physicochemical and Engineering Aspects* **2000**, *173*, 1.
- [30] F. Musso, P. Ugliengo, X. Solans-Monfort, M. Sodupe, *The Journal of Physical Chemistry C* **2005**, *114*, 16430.
- [31] A. Poater, X. Solans-Monfort, E. Clot, C. Coperet, O. Eisenstein, *Dalton Transactions* **2006**, 3077.
- [32] X. Solans-Monfort, J.-S. Filhol, C. Coperet, O. Eisenstein, *New Journal of Chemistry* **2006**, *30*, 842.
- [33] A. Kermagoret, P. Braunstein, *Dalton Transactions* **2008**, 822.
- [34] N. Karodia, X. Liu, P. Ludley, D. Pletsas, G. Stevenson, *Tetrahedron FIELD Full Journal Title:Tetrahedron* **2006**, *62*, 11039.
- [35] R.-H. Fan, X.-L. Hou, *Tetrahedron Letters* **2003**, *44*, 4411.
- [36] E. Vedejs, S. T. Diver, *Journal of the American Chemical Society* **1993**, *115*, 3358.

- [37] V. Zagumennov, N. Sizova, E. Nikitin, *Russian Journal of General Chemistry* **2009**, *79*, 1473.
- [38] C. J. Bradaric, A. Downard, C. Kennedy, A. J. Robertson, Y. Zhou, *Green Chemistry* **2003**, *5*, 143.
- [39] J. Chen, P. A. Wright, J. M. Thomas, S. Natarajan, L. Marchese, S. M. Bradley, G. Sankar, C. R. A. Catlow, P. L. Gai-Boyes, *The Journal of Physical Chemistry* **1994**, *98*, 10216.
- [40] K. L. Furdala, A. G. Oliver, F. J. Hollander, T. D. Tilley, *Inorganic Chemistry* **2003**, *42*, 1140.



## **Chapter 4 : Transposition to silicon wafers: Feasibility, doping amounts and efficiency**

---



## Summary of the Chapter

---

Introduction .....	117
1. Transferability of the concept onto Si-wafers .....	117
1.1. Grafting of an organometallic species as a silanol revelator .....	117
2. Diffusion of B within the silicon wafer by annealing .....	118
2.1. Grafting experiments and RTP annealing .....	119
2.2. Analysis of the oxide layer .....	119
2.3. Analysis of the near surface of the silicon matrix.....	121
2.4. Surface imaging and annealing improvement .....	125
3. Diffusion of P within the silicon matrix.....	128
3.1. Phosphorus quantification by ICP-MS after annealing .....	128
3.2. SIMS analysis of the near surface of silicon .....	129
4. Electrical efficiency of the doped wafers.....	131
Conclusion.....	137
References .....	139

## Introduction

---

As shown in the previous chapters, the initial work was focused on the synthesis and characterization of boron-containing molecules which geometry (symmetry  $C_2$  and  $C_{3v}$ ) that would allow the control of the positioning of B and P: Following the work done on silica nanoparticles, we will here transpose this methodology towards the grafting of P and B containing molecules onto silicon wafers.

After the deterministic placement operated by Shinada et al.<sup>[1, 2]</sup> where a controlled positioning of dopants was performed at a scale of a hundred nanometres, and following the chemical grafting onto as performed by Ho et al.,<sup>[3]</sup> this chapter tackles the application of the chosen strategy onto silicon wafers, instead of the conventional implantation.<sup>[4, 5]</sup> This should lead to a doping in the range of  $10^{13}$  to  $10^{14}$  atoms per  $cm^2$  on the silicon surface while verifying the feasibility of the chosen strategy from 3D (silica particles) onto 2D surfaces. Then, implementation of the grafted species into the silicon matrix will be studied.

## 1. Transferability of the concept onto Si-wafers

---

In order to investigate whether what is observed on silica nanoparticles can be transferred onto the amorphous oxide surface present on silicon wafers, we decided to check the number of silanol sites on the oxide layer of the used silicon wafers.

### 1.1. Grafting of an organometallic species as a silanol revelator

---

The underlying idea of this concept is to dose surface silanols by retro-dosing of previously grafted organometallic species, namely by dosing tantalum grafted the surface oxide layer.

As highly reported in the literature<sup>[6-9]</sup>, trisneopentyl-neopentene-tantalum (later written **Ta(CH<sup>t</sup>Bu)(CH<sub>2</sub><sup>t</sup>Bu)<sub>3</sub>**) reacts rapidly and quantitatively with surface OH groups and it will therefore be used here to determine the amount of surface silanols of a thermally treated silicon wafer is to graft one equivalent of **Ta(CH<sup>t</sup>Bu)(CH<sub>2</sub><sup>t</sup>Bu)<sub>3</sub>** onto each silanol and have an elemental analysis of the surface afterwards.

Two silicon wafers will be studied, one N-doped and one P-doped.

The loadings of Ta onto the wafer pieces was determined by ICPMS and the results are summed up hereafter. (**Table 8**)

**Table 8. Summary of the ICPMS analysis in Tantalum of the prepared silicon wafers.**

<b>Tantalum ICPMS Analysis</b>	
Sample	[Ta](at.cm <sup>-2</sup> )
N-doped	$1.5 \times 10^{14}$
P-doped	$1.5 \times 10^{14}$

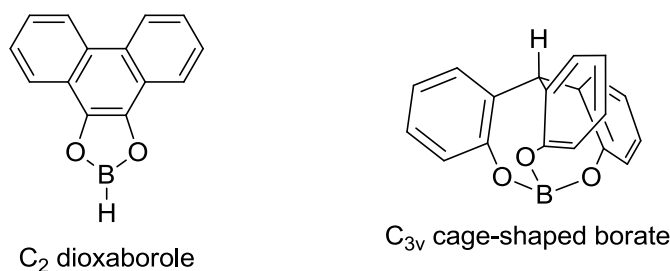
The surface concentration of tantalum is, for wafers,  $1.5 \times 10^{14}$  at.cm<sup>-2</sup> in all cases. It is noteworthy that this value is very close to that of amorphous and non-porous silica (Degussa 200) which has  $1.4 \times 10^{14}$  sites per cm<sup>2</sup>.<sup>[10-12]</sup>

It thus seems that what has been developed on silica nanoparticles is transferrable to silicon wafers covered with native silica.

## 2. Diffusion of B within the silicon wafer by annealing

Knowing that boron diffuses quite fast in silica at high temperature<sup>[13-15]</sup> (under N<sub>2</sub> in pure SiO<sub>2</sub>:  $D_{1100^\circ\text{C}} = 3 \times 10^{-17} \text{ cm}^2 \cdot \text{s}^{-1}$ <sup>[16-18]</sup>,  $E_a = 3.5 \text{ eV}$ <sup>[19]</sup>) the next step was to graft boron onto silicon wafers and to make the doping atom diffuse into both the silica layer and the silicon matrix. The characteristic length of diffusion should be close to that of the oxide layer, hopefully leading to high doping yields. To validate the chosen strategy, the use of a quick thermal annealing was chosen, to allow the doping atom penetration into the wafer and diffusion into its surface.

Because of their good reactivity, two molecules from **Chapter 2** with interesting symmetries were used, as shown below. (**Scheme 27**)



**Scheme 27. Presentation of the two candidate molecules chosen for the study on silicon wafer**

Grafting and annealing are performed as described in **Appendix 8** and **9** and the **experimental section**; the following sub-chapters will deal with all the analyses that were run on the wafer pieces.

## 2.1. Grafting experiments and RTP annealing

---

A n-doped double polished silicon wafer was used for this step, in order to minimise the influence of the fore-existing doping and prepare p-n junctions. To overcome the absence of stirring, the silicon wafer piece was placed in a more concentrated solution of dopant than the one used with silica as described before (about 100 eq). Indeed, due to the reactor that was used, and to prevent any damage that would be caused by a magnetic stirrer on the wafer, the wafer pieces were simply dipped in the solution of dopant.

Here, we decided not to resort to silica-capping as described by Ho<sup>[3]</sup>, and therefore not to passivate the surface. Two ways were investigated:

- The wafers were annealed by RTP to eliminate the ligands and make the dopant diffuse at the same time;
- Based on **Chapter 2** results concerning with the creation of BOH groups; one sample was calcined annealing, expecting a better boron diffusion.

## 2.2. Analysis of the oxide layer

---

As previously explained in **1.1**, the wafers were submitted to an ICPMS analysis in order to assess the quantity of B within the silica layer of each sample. A reference was used in all cases to check the reproducibility of the measurements.

The results are summarised in **Table 9** hereafter.

Table 9. Summary of the ICPMS analysis in Boron of the prepared silicon wafers.

<b>Boron ICPMS analysis</b>			
Sample	[B] <sup>b)</sup> (x10 <sup>13</sup> at.cm <sup>-2</sup> )	RSD <sup>c)</sup> (%)	B count <sup>d)</sup> (x10 <sup>14</sup> atoms)
Reference wafer	1.3	0,25	2.6
C <sub>2</sub> grafted	29.0	0,53	58.0
C <sub>2</sub> RTP 1000°C	2.0	1,18	4.0
C <sub>2</sub> RTP 1050°C	2.9	0,06	5.8
C <sub>2</sub> RTP 1100°C	3.3	0,79	6.6
C <sub>3v</sub> grafted	20.0	-	40.0
C <sub>3v</sub> RTP 1000°C	18.0	0,91	36.0
C <sub>3v</sub> RTP 1050°C	3.3	0,13	6.6
C <sub>3v</sub> RTP 1100°C	4.4	0,18	8.8
C <sub>3v</sub> Calc. 500°C + RTP 1050°C	1.9	0,80	3.8

a) LLD (Low Detection Limit):  $1.0 \times 10^{13}$  at.cm<sup>-2</sup>

b) C (at/cm<sup>2</sup>) is calculated with the size of the sample i.e.20cm<sup>2</sup>. Reference was subtracted from all values

c) RSD represents the Relative Standard Deviation of the measurements

d) For one wafer piece of 20cm<sup>2</sup>

For all analyses, it is noteworthy that the RTP-annealing step led to a decrease in dopant amount. This result can be explained by either the evaporation of dopant during the annealing step or its diffusion through the silica layer into the silicon matrix of the wafer. The RTP temperature was also found to be a key factor for the resulting presence of boron within the silica layer after the annealing step. Then, three main trends can be observed.

First, it is noteworthy that grafting occurred with all precursors, demonstrating the efficient transfer of silica surface chemistry onto the native silica layer capping wafers.

Second, it is noteworthy that the reference wafer has a B density of  $1.3 \times 10^{13}$  at.cm<sup>-2</sup> even though there should not be any presence of boron on the initial wafer. This is explained by the fact that all filters in the clean room are made of borosilicates. This issue was already known and quantified by the CEA.

We also notice that the amounts of boron on the non-annealed pieces are higher than actually expected: a surface concentration of  $2.9 \times 10^{14}$  at.cm<sup>-2</sup> is found for the C<sub>2</sub>-grafted wafer piece and  $2.0 \times 10^{14}$  at.cm<sup>-2</sup> for the C<sub>3v</sub> molecule, versus  $1.5 \times 10^{14}$  OH.cm<sup>-2</sup> as measured earlier. Knowing that the used molecules are prone to  $\pi$ -bonding, because of the aromatic rings, we deduce from this that in addition to grafting there is a strong physisorption of the initial molecules on the surface. This may result from the higher concentration used when grafting onto wafers.

#### *Results after annealing*

It is important to stress that about 90% of all C<sub>2</sub>-grafted species onto the silicon wafer are not recovered, whatever the temperature. For the C<sub>3v</sub>-grafted pieces, RTP at 1000°C barely removed any boron from the silica layer, whereas treatments at 1050°C and 1100°C leave between 16 and 22% of

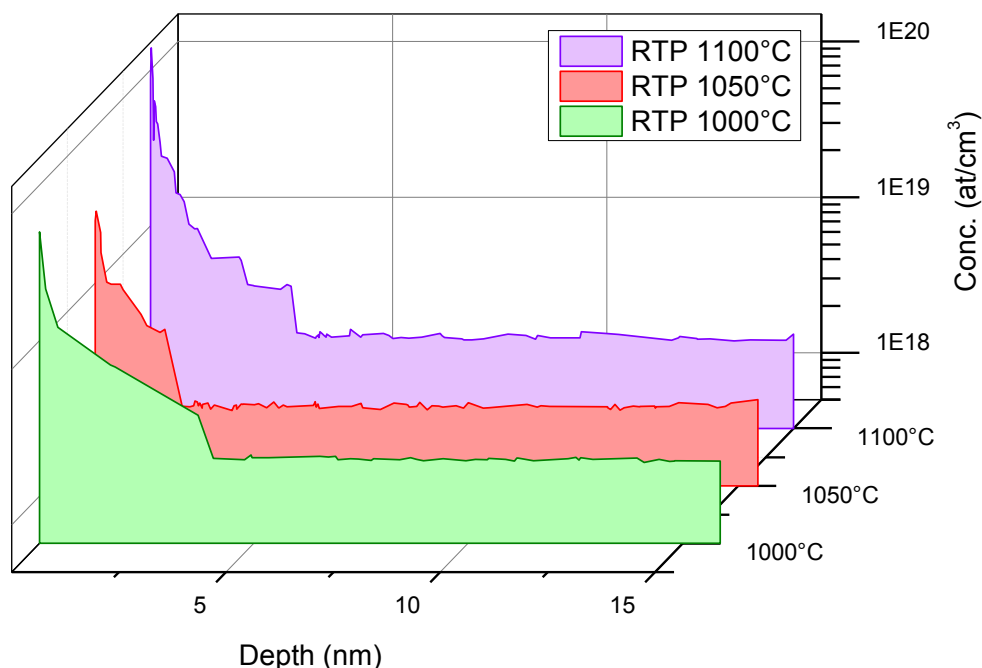
the initial grafted boron. Also, it is noteworthy that the amount of boron recovered from the annealed C<sub>3v</sub>-grafted sample at 1000°C is of the same order as the reference. ( $1.8 \times 10^{14}$  at.cm<sup>-2</sup> versus  $2.9 \times 10^{14}$  at.cm<sup>-2</sup> for the reference).

Further analyses of the near surface of the silicon wafer will help determine the effect of the B ligands.

### 2.3. Analysis of the near surface of the silicon matrix

After each ICPMS analysis, the piece of silicon wafer was analysed by SIMS in order to determine the amount of boron atoms that diffused through the silica layer and into the silicon matrix.

Secondary Ion Mass Spectrometry (SIMS) is a technique that is mostly used in surface and materials science to analyse the composition of solid surfaces and characterise the doping profiles of the thermally diffused boron atoms. (**Appendix 9**) The advantage of using SIMS is that it is a very sensitive technique for surface analysis, determining amounts of elements close the Part Per Billion (ppb).



**Fig 76.** Comparison of the diffusion profiles of the C<sub>2</sub> wafer-grafted species after the different treatments

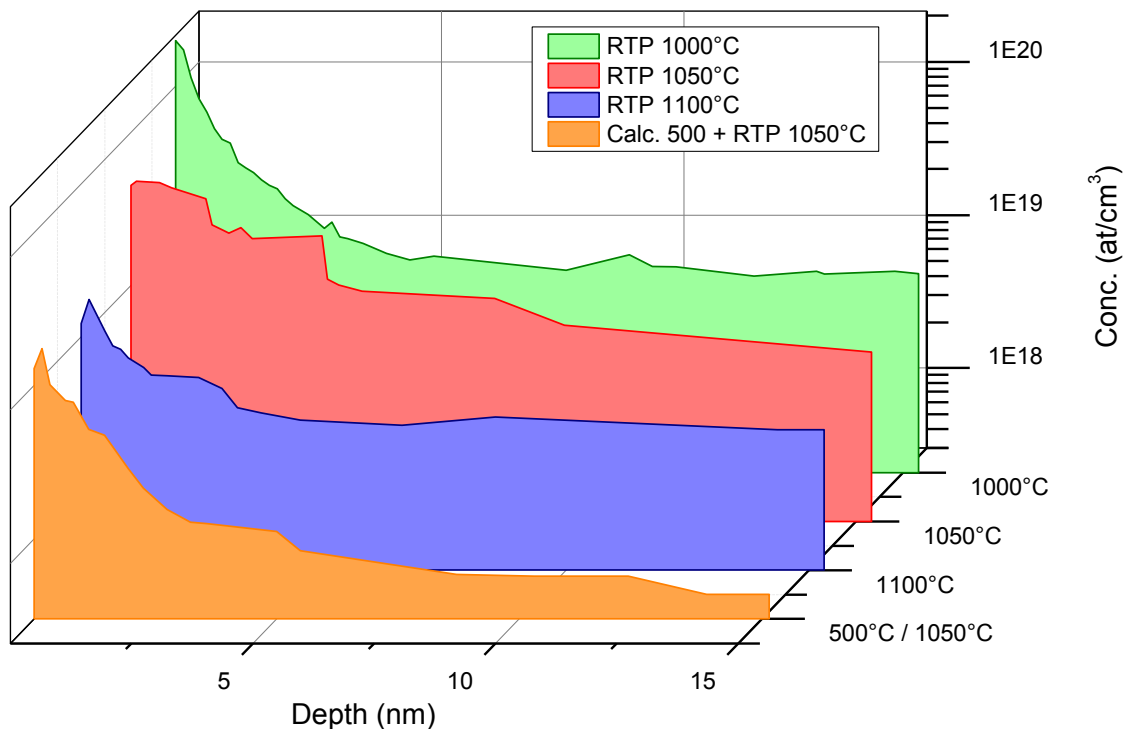
The diffusion profile after each annealing treatment (1000, 1050 and 1100°C) can be seen on **Fig 76** above.

After annealing at the chosen temperature for 1s (see **Appendix 9**) the obtained doping profiles exhibit a boron concentration between  $5.0 \times 10^{19}$  and  $1.0 \times 10^{20}$  at.cm<sup>-3</sup> near the surface, which sharply decreases to  $1.0 \times 10^{18}$  at.cm<sup>-3</sup> at depths below 5 nm. As a comparison, Ho et al. obtained a similar kink-and-tail feature, with a diffusion profile from  $1.0 \times 10^{20}$  at.cm<sup>-3</sup> at the surface to  $1.0 \times 10^{17}$

at.cm<sup>-3</sup> at depths around 40 nm.<sup>[3]</sup> The results obtained here on thin oxide are encouraging as they show similar behaviours as those published with grafting on silica-etched silicon wafers. These results are very close to that obtained by Kalkofen et al. after atomic layer deposition (ALD) of boron oxide<sup>[20]</sup> leading to a similar conditions in integrated doses:

Two main trends can be observed. First, it can be seen than after annealing at 1000°C, boron seems to be found deeper (until almost 4 nm) than for the two other temperatures, thus leading to higher doping yield, *vide infra*.

The following **Fig 77** shows the diffusion profiles of all experiments performed on the C<sub>3v</sub> species grafted on silicon wafers.



**Fig 77.** Comparison of the diffusion profiles of the C<sub>3v</sub> grafted species

As shown with C<sub>2</sub> species, it is noteworthy that boron actually diffused within the silica layer. Then it seems that more boron diffused through silicon at 1000°C than at higher temperatures.

Likewise, the wafers that went through calcination at 500°C for 2h and annealing at 1050°C display a very small amount of diffused boron. The reason could be that, having formed surface BOH species, the annealing of the wafer would generate boron oxide which volatilities more easily.<sup>[21, 22]</sup> Diffusion profiles for the three other wafers correspond well to the usual kink-and-tail profile displayed in such a doping measurement experiments. It is also noticeable that, the higher the annealing temperature, the lower the apparent diffusion.

**Table 10** next page sums up the diffusion profiles for each precursor as well as the mass balance for boron for both C<sub>2</sub> and C<sub>3v</sub> species at the three different annealing temperatures.

Table 10. SIMS analysis and diffusion comparison between the two chosen precursors

ICPMS and SIMS boron analysis

T°C	Diffusion profile comparison	Type	B in SiO <sub>2</sub> (x10 <sup>14</sup> at) <sup>a)</sup>	B in Si (x10 <sup>14</sup> at.) <sup>b)</sup>	Total B recovered (x10 <sup>14</sup> at.)	Yield (%) <sup>c)</sup>
RTP 1000°C		<b>C<sub>2</sub></b>	4.0	0.87	4.87	8.4
		<b>C<sub>3v</sub></b>	36.0	4.54	40.5	101.3
RTP1050°C		<b>C<sub>2</sub></b>	5.8	0.93	6.73	11.6
		<b>C<sub>3v</sub></b>	6.60	3.12	9.72	24.3
RTP 1100°C		<b>C<sub>2</sub></b>	6.6	1.13	7.73	13.3
		<b>C<sub>3v</sub></b>	8.80	0.93	9.73	24.3

a) Obtained by ICPMS at CEA Grenoble

b) Obtained by ToF-SIMS at CEA Grenoble

Integrations obtained for diffusion between 0 and 17 nm as the SIMS experiment for C2-1000°C was truncated at this depth

c) C<sub>2</sub>: 2.9 x 10<sup>14</sup> at.cm<sup>-2</sup> for a 20cm<sup>2</sup> wafer hence an overall number of B atoms B<sub>totC2</sub> = 5.8 x 10<sup>15</sup> at

C<sub>3v</sub>: 2.0 x 10<sup>14</sup> at.cm<sup>-2</sup> for a 20cm<sup>2</sup> wafer hence an overall number of B atoms B<sub>totC3v</sub> = 4.0 x 10<sup>15</sup> at



**Table 10** also shows the different amounts of recovered boron atoms after both ICP-MS and SIMS analyses.

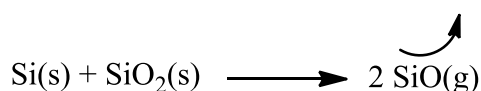
Also, in the case of the  $C_{3v}$ -grafted wafer annealed at 1000°C, the yield of diffusion is slightly higher than 100%, which could be tentatively explained from:

- The pollution of the silicon wafers in the clean room (as stated before);
- The noise on the SIMS spectra.

It is then noteworthy that precursors have different behaviours towards annealing. Indeed, after annealing at 1000°C, about 100% of boron is recovered for the  $C_{3v}$  species, versus only 8.4% in the case of the grafted  $C_2$  species. Also, the boron recovery plummets from 100% recovery of boron after annealing at 1000°C to only 24.3% after annealing at 1050°C and 1100°C. Despite this huge loss, boron recovery remains always higher in the case of the  $C_{3v}$  molecule than  $C_2$ . Two conclusions may be drawn:

- the  $C_{3v}$  ligand helps boron diffuse into silica whereas the  $C_2$  ligand lacks this “protection” against high temperature;
- the  $C_{3v}$  shows a better tolerance to temperature in terms of boron recovery, being able to sustain at least 1000°C.

Annealing was performed under an inert atmosphere in order to impede any regrowth of the oxide layer. Yet, it is known that a pitting effect occurs under inert ambient and consists in silicon volatilising at high temperatures by reacting with silica to form some gaseous silicon oxide,<sup>[23, 24]</sup> (Scheme 28) thus generating such holes in both the silica layer and the silicon matrix. This reaction can be prevented by adding a small partial pressure of oxygen or by reversing the equilibrium with oxygen.



**Scheme 28. Formation of SiO from solid silicon**

A straightforward experiment to check whether this reaction occurs or not is the AFM acquisition of the surface image after the different annealing procedures.

## 2.4. Surface imaging and annealing improvement

---

In order to check the uniformity of the surface, we tried some surface images analyses by atomic force microscope (AFM), which is a high-resolution kind of scanning probe microscopy that can show a resolution close to the nanometre.<sup>[25, 26]</sup> As we doped the very top layer of the silicon matrix of the wafer, should the surface be damaged at any step that was performed at all, this could have some drastic repercussion on the efficiency of the final object (junction leakage).

Four samples were studied: one reference before and after HF etching which removes the oxide layer, and three samples from the above batch with C<sub>2</sub> precursor annealed at 1000°C, 1050°C and 1100°C respectively. (**Table 11** hereafter)

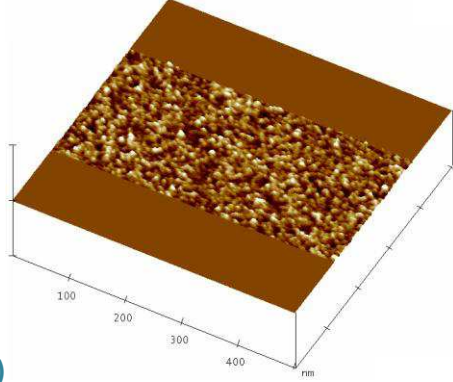
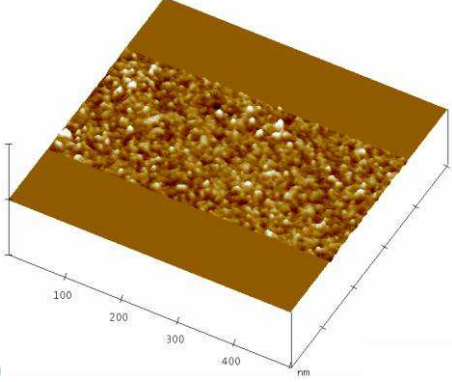
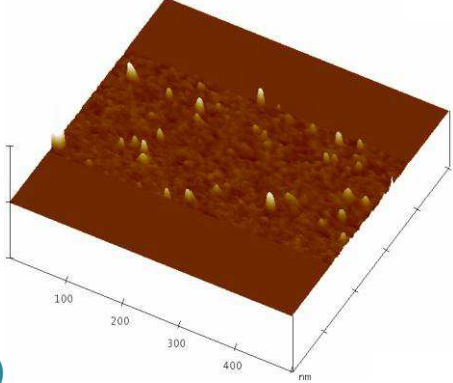
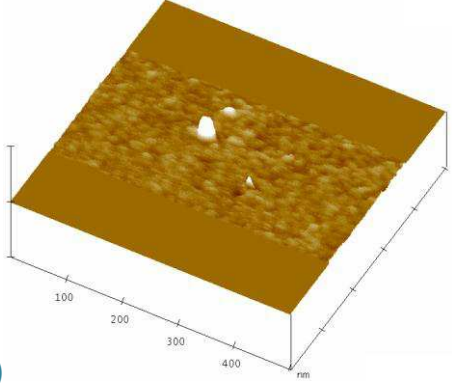
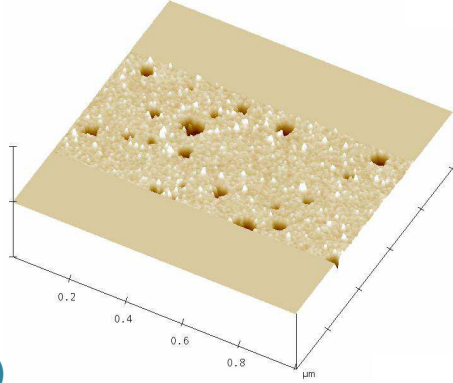
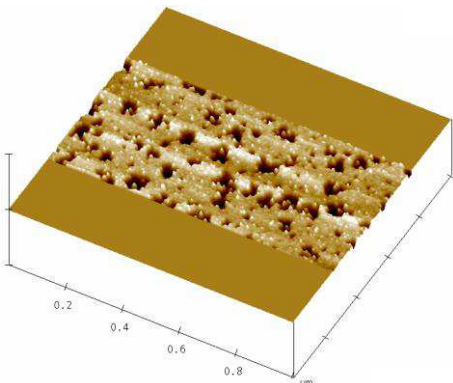
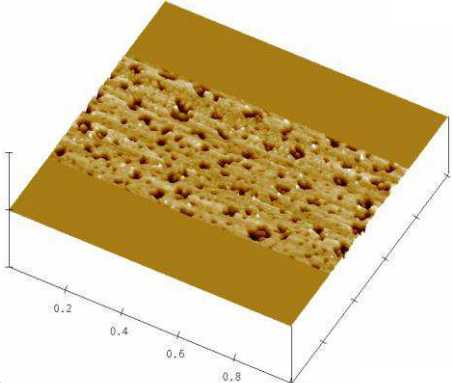
On the reference, it appears that both before and after the HF treatment, the wafer remains flat and with a very low roughness, as expected. There are a few uniformities due to traces of possible adsorbed impurities.

After annealing at 1000°C, as seen on **Table 11-c**), and before the HF etching step, many surface impurities or remaining calcined organics appear. After the HF etching step, on **Table 11-d**), only one big peak of such remains on a pristine surface, which is most certainly due to a particle pollution resulting from the HF-etching step.

Annealing at higher temperatures showed the appearance of holes in the silica layer (**Table 11-e** and **f**) which even pierced the silicon matrix (**Table 11-g**). An increase in temperature leads to even bigger holes in the silica layer.

Knowing that such a pitting effect as described in **2.3** exists, the creation of such holes at higher temperatures is a further justification to the loss of boron in the substrate after annealing at higher temperatures.

Table 11. AFM images of the studied wafers  
*Surface analysis of the grafted wafers*

		AFM images	
		<i>Before HF etching</i>	<i>After HF etching</i>
<b>Reference wafer</b>			
	a)	b)	
<b>C<sub>3v</sub> RTP 1000°C</b>			
	c)	d)	
<b>C<sub>3v</sub> RTP 1050°C</b>		<b>No AFM was recorded for the etched surface of the annealed silicon wafer at 1050°C.</b>	
	e)		
<b>C<sub>3v</sub> RTP 1100°C</b>			
	f)	g)	

An investigated method to counter this pitting effect is to anneal with a trace of O<sub>2</sub>.<sup>††</sup> However, such a technique increases the thickness of the oxide layer except when annealing is performed under very diluted O<sub>2</sub> ambient.<sup>[27]</sup>

Since the tool in LETI cannot perform very diluted O<sub>2</sub> annealing, we have characterised the effect of oxygen at the limits of the apparatus (2.5%). An ellipsometry measurement of the oxide layer is then performed before and after two different annealing steps: one at 1000°C without any O<sub>2</sub> and one at 1050°C with diluted O<sub>2</sub>.

**Table 12. Measurement of the wafer oxide layer thickness by ellipsometry**

Ellipsometric measurement of the oxide layer

	Oxide thickness (Å)	MSE (%)
Reference	13	3
RTP 1000°C – N <sub>2</sub>	19	4
RTP 1050°C – N <sub>2</sub> + 2.5% O <sub>2</sub>	32	3

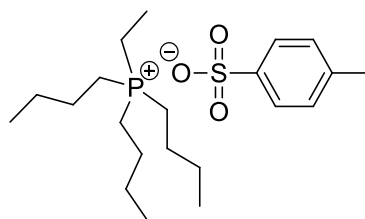
MSE: Mean Squared Error

According to the results of the analyses on the wafer, it confirms that the annealing step makes the oxide grows. If the difference in oxide thicknesses between the reference and the wafer annealed under N<sub>2</sub> only is very little, the addition of 2.5% of O<sub>2</sub> almost triples the oxide thickness. Since a thick oxide layer would be a hindrance to straightforward boron diffusion into silica, we decided to only focus on annealing steps at 1000°C without oxygen which is a good compromise between boron diffusivity and SiO evaporation.

<sup>††</sup> N<sub>2</sub> + 2.5% O<sub>2</sub> as an atmosphere within the RTP oven as was deduced from a screening made at the CEA. The oxygen amount is the minimal that was applicable for such an annealing on the apparatus in the LETI's cleanroom, leading to the results shown afterwards.

### 3. Diffusion of P within the silicon matrix

Knowing that phosphorus diffuses very slowly in silica, ten times slower than boron and requires a higher energy (under N<sub>2</sub> inert ambient in pure SiO<sub>2</sub>:  $D_{1100^{\circ}\text{C}} = 3 \times 10^{-18} \text{ cm}^2 \cdot \text{s}^{-1}$  [28-30],  $E_a = 4.4 \text{ eV}$  [28]) the phosphonium precursor was grafted upon a silicon wafer and sent to CEA for analysis to determine whether it was possible to influence the diffusion of phosphorus within the silicon matrix. The chosen strategy to have the dopant diffuse was to resort to rapid annealing processes and then to measure the diffusion of P throughout the whole wafer thickness. One readily available phosphorus-containing molecule was the “ionic liquid” phosphonium one. (**Fig 78**)



**Fig 78.** Presentation of the candidate molecule for the study on silicon wafer

#### 3.1. Phosphorus quantification by ICP-MS after annealing

A VPD (Vapour Phase Decomposition) experiment was performed and immediately followed by an ICPMS analysis in order to assess the quantity of P within the silica layer of each sample, as described before. The set of samples had one reference and two “grafted samples”, one of which having undergone a RTP annealing.

The different studied samples are listed in the following table (**Table 13**) along with the results of the analysis.

**Table 13.** Outcome of the ICPMS analysis of the phosphorus-grafted samples

<b>Phosphorus analysis</b>		
Label	Concentration (at.cm <sup>-2</sup> ) <sup>a)</sup>	RSD in % <sup>b)</sup>
REFERENCE	$2.06 \times 10^{12}$	1.03
GRAFTED WITHOUT RTP	$1.38 \times 10^{14}$	0.13
GRAFTED+RTP @ 1050°C	$<1.47 \times 10^{12}$	-

LLD (Lower Limit of Detection) for phosphorus =  $1.47 \times 10^{12} \text{ at/cm}^2$

a) C (at/cm<sup>2</sup>) is calculated with the size of the sample i.e. 20cm<sup>2</sup>.

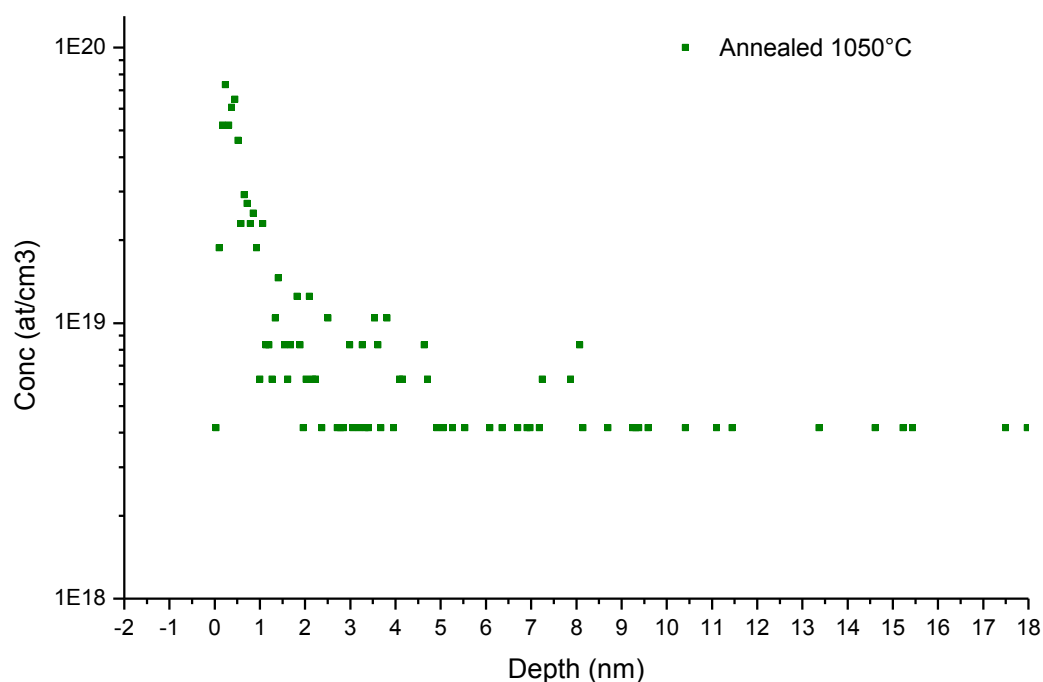
b) RSD represents the Relative Standard Deviation (in %)

It is noteworthy that the amount of grafted species onto the surface is close to that of the surface silanol density ( $1.5 \times 10^{14} \text{ SiOH.cm}^{-2}$  as seen in 1.). There is therefore apparently no or very little physisorption on the surface.

Also, it seems that all of the grafted phosphorus atoms were removed by the RTP annealing step as the measured concentration of P atoms in the silica layer by ICP-MS after the RTP step is below the detection limit. Therefore, SIMS analyses will determine the behaviour of Phosphorus: either diffusion inside Silicon, which has a low probability since diffusivity is low, or desorption. Indeed Contrarily to boron-containing species which were grafted onto the surface, the phosphonium species is physisorbed as shown in Chapter 2.

### 3.2. SIMS analysis of the near surface of silicon

The Phosphorus profile obtained by SIMS analysis after annealing at  $1050^\circ\text{C}$  is shown on **Fig 79**.



**Fig 79.** Diffusion profile for phosphorus after RTP at  $1050^\circ\text{C}$

After integration of the phosphorus profile, the amount of phosphorus in the silicon matrix, can be compared with the previous ICPMS data (**Table 14**)

**Table 14. Summary of Phosphorus equivalent surface concentration after each process step**

<b>Recovered amount of phosphorus</b>				
	Amount of phosphorus		Total amount	Recovery yield
	in SiO <sub>2</sub>	in Si-matrix	recovered	(%)
	(x 10 <sup>14</sup> at)	(x10 <sup>14</sup> at)	(x10 <sup>14</sup> at)	
<b>GRAFTED WITHOUT RTP</b>	27.6	-	27.6	100 (ref)
<b>GRAFTED+RTP @ 1050°C</b>	<0.3	2.39	2.39	4

Integrations obtained for diffusion between 0 and 17 nm

Without annealing, all the phosphorus is recovered within the HF solution obtained from etching by VPD. This amount of phosphorus may be either into or on the initial silica layer.

The recovered amount of phosphorus in silicon is comparable to those obtained with boron in the same conditions (2.39x10<sup>14</sup> at here versus 3.12x10<sup>14</sup> at for C<sub>2</sub>@1050°C). This is a rather surprising result in view of the low diffusivity of phosphorus. One possible reason for such a recovery would be sorption of phosphorus after the HF etching step, which would then be detected by SIMS. Such a low result can be explained by the diffusivity of phosphorus in silica.

Also, only 4% of all grafted phosphorus is recovered after annealing at 1050°C. One reason for such an important loss of phosphorus may come from three main reasons:

- Phosphonium is not grafted onto the surface as seen in Chapter 2, resulting in a weaker interaction, leaving phosphorus more prone to desorb;
- The stability of the molecules towards RTP is an inherent parameter, as seen previously with boron;
- It was shown that pitting occurred during RTP at 1050°C under inert atmosphere.

#### 4. Electrical efficiency of the doped wafers

In order to determine whether the doping of the silicon wafers was electrically efficient, two samples were sent to IEMN, (Institut d'Electronique, de Microélectronique et de Nanotechnologies) Lille, through a collaboration between IEMN (Dr Grandidier) and CEA (Dr Chevalier) to perform tunnelling spectroscopy experiments on pieces of silicon wafer etched with HF before analysis.

The chosen process was, as stated before, n-doped wafers grafted with B-containing species ( $C_{3v}$  species) and annealed at  $1000^{\circ}\text{C}$  to avoid any pitting on the surface.

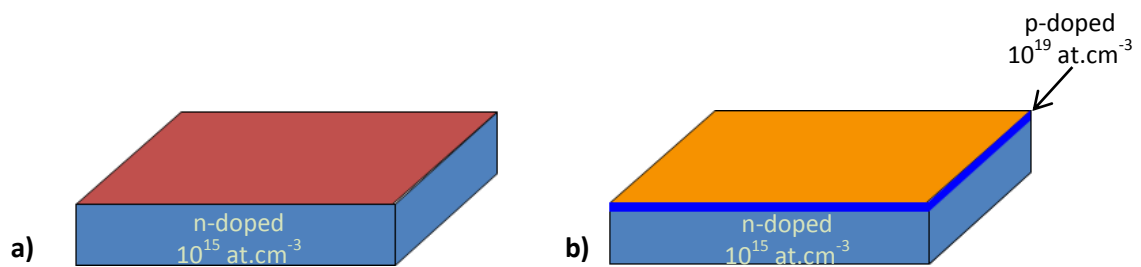


Fig 80. Presentation of the two studied samples: a) reference, n-doped silicon wafer; b) p-doped sample

The first measurements were performed with a single tip in tunnel mode as shown in **Fig 81**. In this case, the sample was grounded and the bias voltage was applied to the tip. The distance between the tip and the surface is defined by the tunnelling current setpoint: the higher the current, the lower the distance. In this mode, the position Fermi level of the tip may vary.

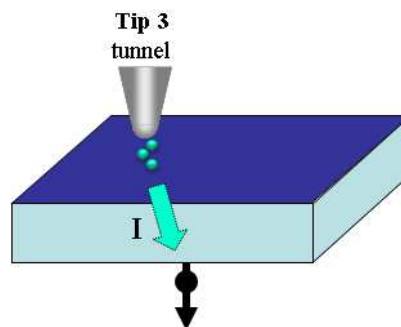
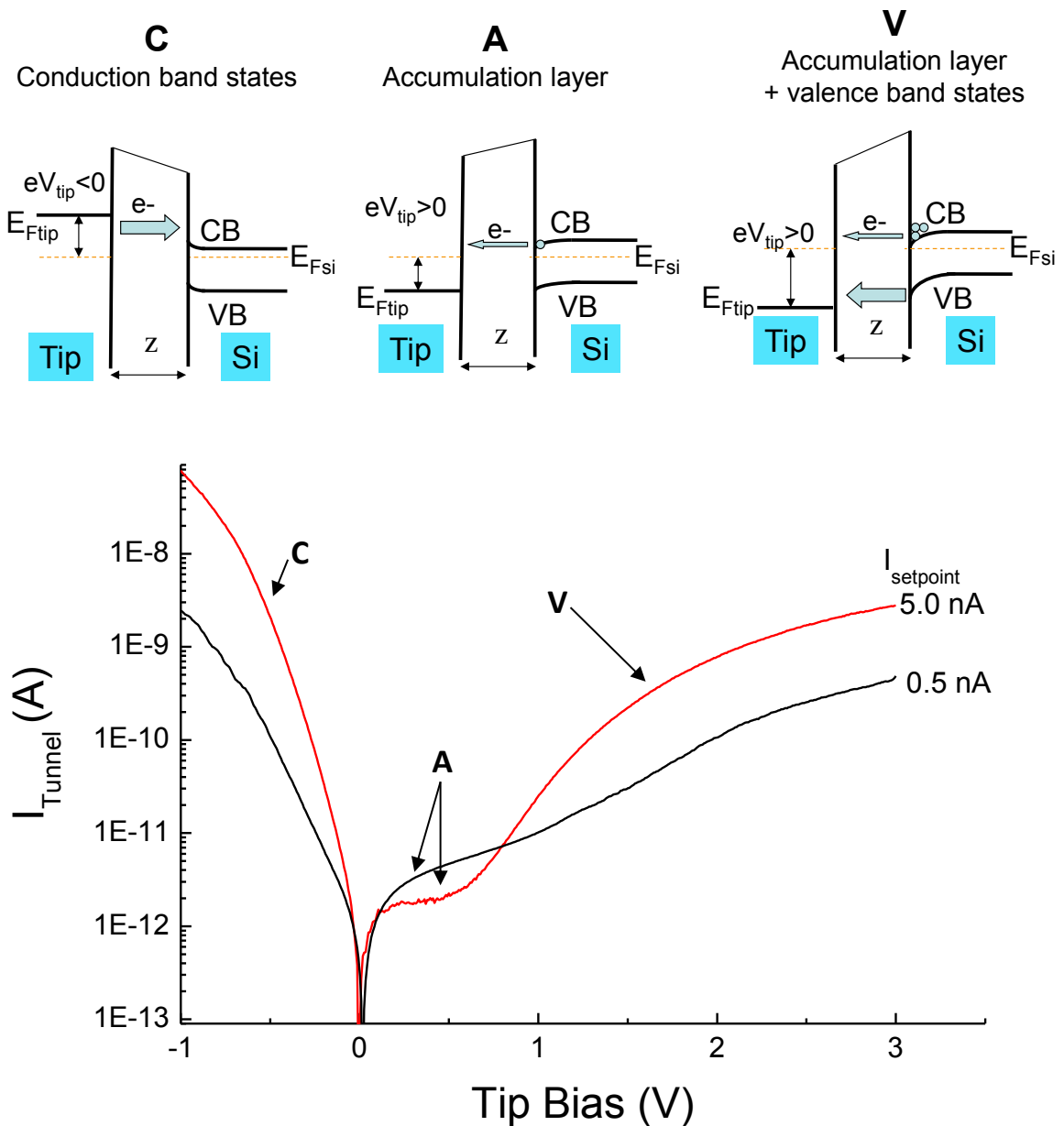


Fig 81. Tunnelling spectroscopy with a single tip on Si-wafer

The first sample to be analysed was the reference, a piece of untreated silicon wafer, n-doped, while the other piece was the same wafer grafted with the  $C_2$  precursor and annealed at  $1000^{\circ}\text{C}$ . **Fig 82** hereafter shows the current-tension (I-V) curve of the reference sample at different feedback conditions.





**Fig 82.** Current vs voltage for the reference sample at different feedback conditions. The various components of the current are shown in the inset (C: conduction band; A: Accumulation layer; V: Valence band)

**Fig 82** hereupon shows three different curves obtained for different distances. It is noteworthy that all three curves should show the same general trend. Three regimes can be observed as noted on the figure.

The first regime, labelled C, corresponds to the tunnelling of electrons from the tip to the conduction band, and appears at  $E_{Ftip} > E_{Fsi}$ . It displays a quick decrease in the tunnel current for a tip bias voltage inferior to 0 V. Therefore, at  $V < 0$ , there is a high level of current, which is expected for an n-doped silicon substrate.

The second component of the voltage represents the accumulation zone, labelled A, when  $E_{VB} < E_{Ftip} < E_{Fsi}$ . It appears for a tip bias between 0 and 1V. This corresponds to the electron tunnelling from the conduction band to the tip.

The third and last regime, V, corresponds to both the accumulation layer and valence band states, and appears when  $E_{Ftip} < E_{VB}$ . In this case, electrons are tunnelling out of the valence band and from the conduction band to the tip.

This result confirms the fact that the bare silicon wafer is slightly n-doped, at the order of  $10^{15}$  at.cm<sup>-3</sup>.

The second measurements were performed with two tips: one in tunnel mode and one in contact (Fig 83). In this case, the setpoint is fixed, and the distance between both tips is varied. This experiment allows the observation of the doped surface.

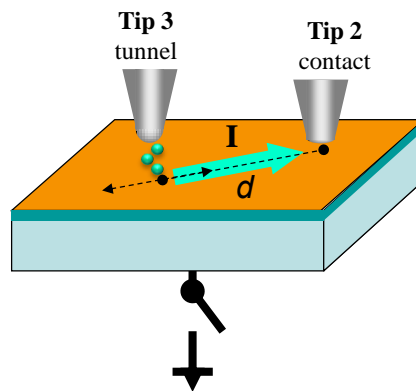


Fig 83. Tunnelling spectroscopy with two tips on Si-wafer

The obtained  $I=f(V)$  spectrum (Fig 84) displays symmetrical curves. This proves a very high doping level. In this case, as shown on the schematic, the Fermi level of the wafer is within the valence band. There is therefore only a tunnelling through the valence band. For a negative polarisation, the states of the valence band above  $E_{Fsi}$  are filled. At a positive polarisation, these states are emptied. Electrons, in this case, are unlikely to go to the conduction band.

Short distances were used in order not to go through the substrate and stay in the doped surface of the wafer.

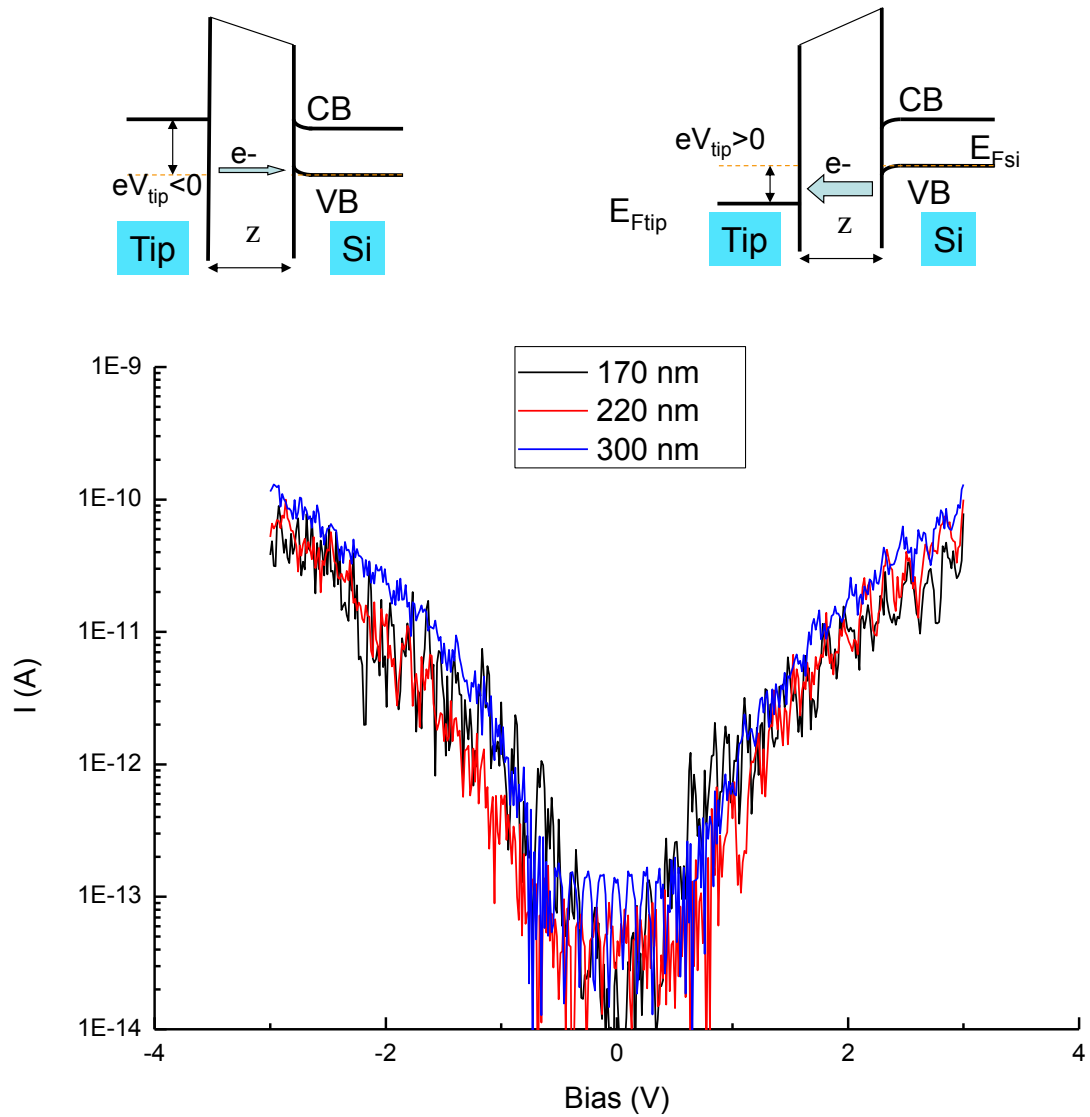


Fig 84. Current vs voltage for the doped sample with increasing distance between tips

This experiment was an excellent way of showing the important doping of the surface. Yet, it cannot give any further information on the type of dopant that is observed.

To verify that the surface was indeed highly p-doped, a third experiment was performed on the boron-doped piece of silicon wafer, with a single tip as shown earlier (**Fig 81**).

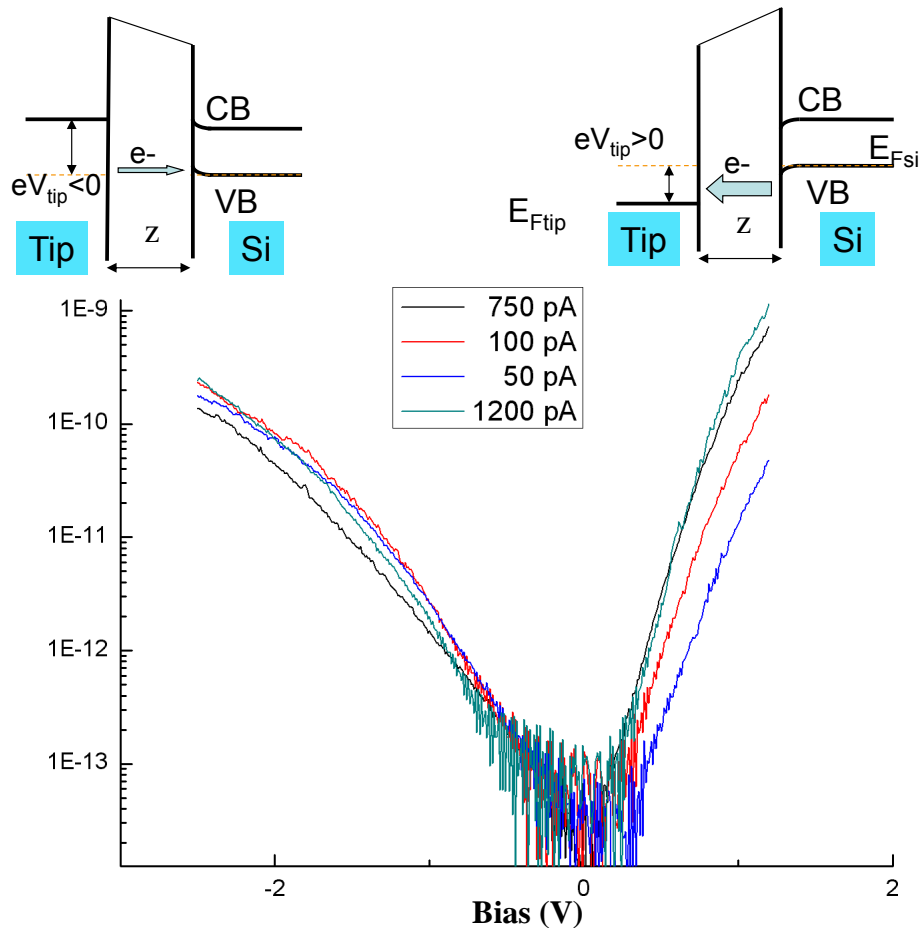


Fig 85. Current vs voltage for p-doped Si wafer at different feedback conditions

On Fig 85 above, two main trends can be observed. For all distances, there is a slow decrease in current for a bias voltage beneath 0V. Then, for all curves, for a positive polarisation of the tip, the current increases quickly.

This shows that, at a positive polarisation of the tip, valence bands are emptied quicker. Also, the slope of all curves for a positive polarisation of the tip is greater than that obtained for a negative polarisation, showing that the studied silicon wafer is indeed p-doped. Also, this proves the existence of a p-n junction.

The fact that the increase in current is quicker for a closer tip to the surface shows that the valence band empties very quickly, showing a strong p-doping. Therefore, the asymmetry of the curve is due to the p-n junction and to the different amounts of each dopant.

Both samples can be compared for a same tip-surface distance as shown on Fig 86 hereafter.

It shows two I-V curves for the two studied samples. It is noteworthy that, at a positive polarisation, current increases quicker in the p-doped wafer than in the reference. This proves indeed that the doping was efficient. Moreover, the increase of current at a more negative

polarisation is weaker in the case of the p-doped wafer. This corroborates the existence of a p-n junction within the wafer.

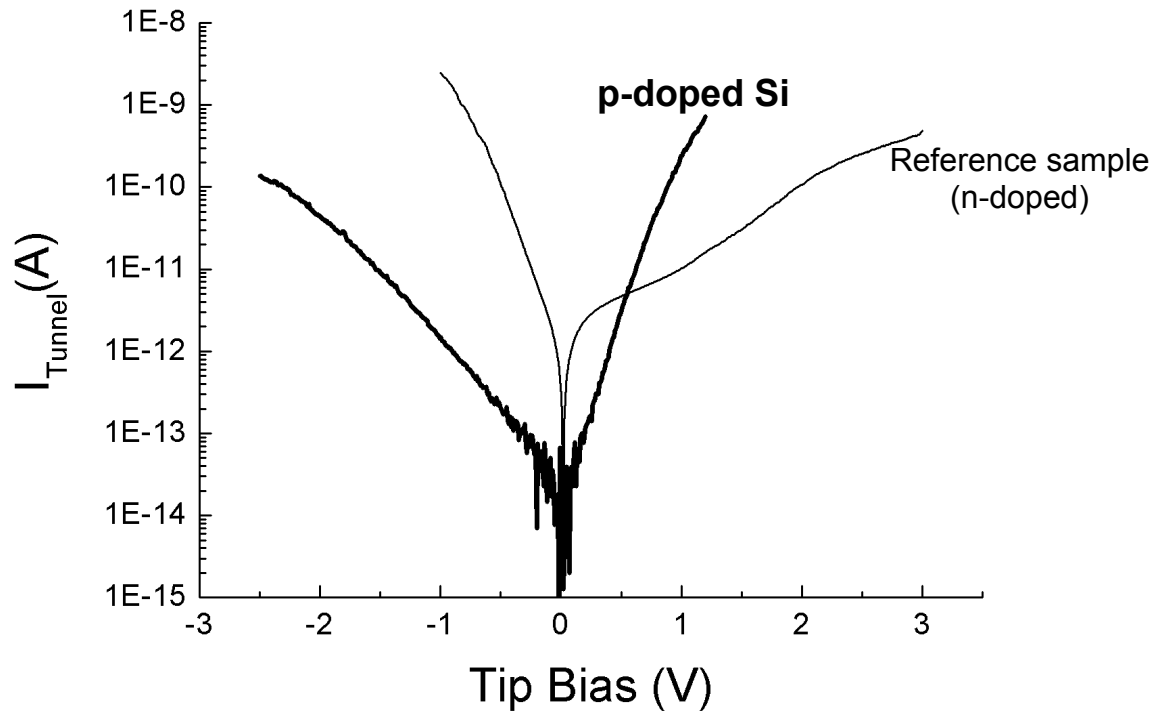


Fig 86. Current vs voltage for the reference wafer (Ref Si) and the p-doped Si wafer (p-doped Si) at 750 pA

## Conclusion

---

In this chapter, we have demonstrated that boron diffused into the silicon matrix from the grafted Boron molecules through the thin native oxide. It was evidenced that the type and therefore the size of the organic moiety influenced the diffusion of the doping atom, i.e. boron, through both the silica layer and then into the silicon matrix.

The only experiment that was performed on a phosphorus-grafted silicon wafer proved that phosphorus weakly diffused within the silica layer, as expected. However, as it was shown with Boron, the weak diffusion of Phosphorus may be due to the annealing temperature.

It has thus been demonstrated that the influence of the organic chain linked on boron led to different diffusion profiles. To that extent, the bigger the structure, the more hindered engaged the boron atom, the better the penetration of boron within silica.

However, too high RTP annealing temperatures in inert atmosphere causes a formation of holes into the substrate – silicon wafer – also called “pitting”, and due to the formation of SiO at the interface of the silicon matrix and the silica layer. This phenomenon is probably also at the origin of boron loss during the RTP steps. Experiments to overcome this problem proved to be inadequate with the strategy, as they led to a thick silica regrowth.

However, it was proven by electrical measurements that the doping was effective, revealing an effective doping of the surface of the silicon wafer (about 5 nm) and an expected p-n junction. Such encouraging results proved the doping strategy to be accurate. The obtained results showed a very thin and highly-doped surface on the silicon matrix of the wafer ( $10^{19}$ - $10^{20}$  at.cm<sup>-3</sup> on a thickness of less than 5 nm) comparable, in terms of amount, to that published by Ho et al in 2008.<sup>[3]</sup> However, it is important to stress that the strategy that was developed here relies on the grafting onto the native silica layer and not directly onto bare silicon, and did not involve any capping of the grafted species. In our case, the “molecular capping” due to the ligand proved to be efficient until 1000°C only with the sterically hindered C<sub>3v</sub> molecule.

Regarding Phosphorus, there seems to be a competition between evaporation of phosphorus during annealing and the diffusivity of P in SiO<sub>2</sub>.

Diffusion needs to be however tamed and improved, in order to increase the yield of dopant incorporation within the silica layer. An idea would be to reduce the oxide layer to a minimum in order to prevent the loss of dopant within the silica. Creating a SiOH monolayer on silicon would reduce the distance between the dopant and silicon and therefore hopefully yield a better doping. Phosphorus remains also a great issue as it hardly diffuses in silica, and reducing the thickness of the silica layer could be a way improve its diffusion in silicon. Capping the grafted molecule with, for

instance, SiN, which is a diffusion barrier for both B and P, would also be a promising way for RTP treatments at temperatures above 1000°C.

In order to reduce the surface amount of dopant, the initial solution could be to dilute with a non-doping reactive species, such as carboxylic acid derivatives, that could occupy some grafting sites and thus reduce the amount of grafted dopant on the surface. Dilution from 1:10 to 1:100 could therefore be investigated.

## References

---

- [1] T. Shinada, M. Hori, Y. Ono, K. Taira, A. Komatsubara, T. Tanii, T. Endoh, I. Ohdomari, in *Electron Devices Meeting (IEDM), 2010 IEEE International*, pp. 26.5.1.
- [2] T. Shinada, S. Okamoto, T. Kobayashi, I. Ohdomari, *Nature* **2005**, *437*, 1128.
- [3] J. C. Ho, R. Yerushalmi, Z. A. Jacobson, Z. Fan, R. L. Alley, A. Javey, *Nat Mater* **2008**, *7*, 62.
- [4] T. Shinada, A. Ishikawa, C. Hinoshita, M. Koh, I. Ohdomari, *Jpn J. Appl. Phys.* **2000**, *39*, L265.
- [5] T. Shinada, H. Koyama, C. Hinoshita, K. Imamura, I. Ohdomari, *Jpn. J. Appl. Phys.* **2002**, *41*, L287.
- [6] R. R. Schrock, *Journal of the American Chemical Society* **1974**, *96*, 6796.
- [7] R. R. Schrock, J. D. Fellmann, *Journal of the American Chemical Society* **1978**, *100*, 3359.
- [8] F. d. r. Lefebvre, J. Thivolle-Cazat, V. r. Dufaud, G. P. Niccolai, J.-M. Basset, *Applied Catalysis A: General* **1999**, *182*, 1.
- [9] D. Soulivong, S. b. Norsic, M. Taoufik, C. Coperet, J. Thivolle-Cazat, S. Chakka, J.-M. Basset, *Journal of the American Chemical Society* **2008**, *130*, 5044.
- [10] J. Fripiat J, in *Soluble Silicates, Vol. 194*, AMERICAN CHEMICAL SOCIETY, **1982**, pp. 165.
- [11] L. T. Zhuravlev, *Colloids and Surfaces A: Physicochemical and Engineering Aspects* **2000**, *173*, 1.
- [12] L. Zhuravlev, V. Potapov, *Russian Journal of Physical Chemistry A, Focus on Chemistry* **2006**, *80*, 1119.
- [13] R. B. Fair, *Journal of Applied Physics* **1980**, *51*, 5828.
- [14] D. Mathiot, J. C. Pfister, *Journal of Applied Physics* **1984**, *55*, 3518.
- [15] M. Ghezzi, D. M. Brown, *Journal of The Electrochemical Society* **1973**, *120*, 146.
- [16] D. M. Brown, P. R. Kennicott, *Journal of The Electrochemical Society* **1971**, *118*, 293.
- [17] R. B. Fair, *IEDM* **1995**, 85.
- [18] R. O. Schwenker, *J. Electrochem. Soc.* **1971**, *118*, 313.
- [19] Y. Shacham-Diamand, W. Oldham, *Journal of Electronic Materials* **1986**, *15*, 229.
- [20] B. Kalkofen, E. P. Burte, *ECS Meeting Abstracts* **2010**, *MA2010-01*, 943.
- [21] F. J. Buchanan, J. A. Little, *Corrosion Science* **1993**, *35*, 1243.
- [22] F. Peng, R. F. Speyer, *Journal of the American Ceramic Society* **2008**, *91*, 1489.
- [23] G. K. Celler, L. E. Trimble, *Applied Surface Science* **1989**, *39*, 245.
- [24] H. Neergaard Waltenburg, J. T. Yates, *Chemical Reviews* **1995**, *95*, 1589.
- [25] S. Xu, G.-y. Liu, *Langmuir* **1997**, *13*, 127.
- [26] D. Wang, S. G. Thomas, K. L. Wang, Y. Xia, G. M. Whitesides, *Applied Physics Letters* **1997**, *70*, 1593.
- [27] T. Yoshitomi, M. Saito, T. Ohguro, M. Ono, H. S. Momose, H. Iwai, in *Symposium on VLSI Technology Digest of Technical Papers*, **1955**.
- [28] K. Shimakura, T. Suzuki, Y. Yadoiwa, *Solid-State Electronics* **1975**, *18*, 991.
- [29] R. B. Allen, H. Bernstein, A. D. Kurtz, *Journal of Applied Physics* **1960**, *31*, 334.
- [30] B. Kalkofen, M. Lisker, E. P. Burte, *Materials Science and Engineering: B* **2005**, *124*–125, 288.
- [31] R. M. Feenstra, J. A. Stroscio, *Journal of Vacuum Science & Technology B: Microelectronics and Nanometer Structures* **1987**, *5*, 923.

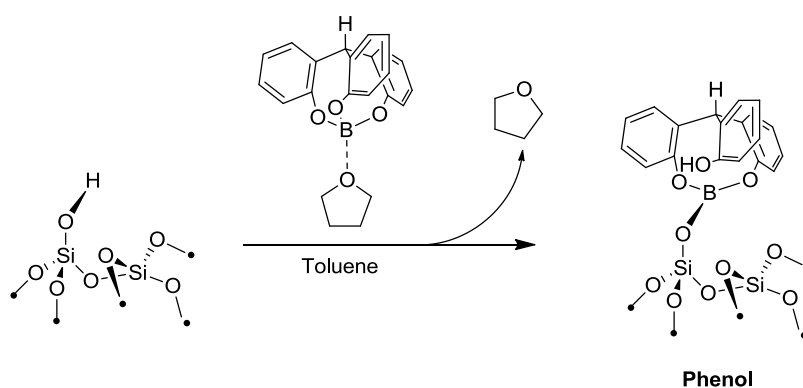


# **Conclusion**

---

In this work, we have defined a strategy for positioning doping atoms to silica surfaces by a chemical method. We have then shown that the strategy was transferable to silicon wafers. Finally, the chosen strategy was found to be suitable for implantation of doping atoms into the silicon wafer.

First, we discriminated amongst different boron-containing bulky molecules to select those with both a large steric hindrance and an interesting symmetry. Amongst these, we selected two molecules whose symmetries,  $C_2$  and  $C_{3v}$ , could yield both the desired effect on the surface and the easiness of synthesis. It was also shown that, contrarily to what we initially expected, the  $C_{3v}$  borate grafted onto the surface and not simply adsorbed, thus creating a phenolic species.

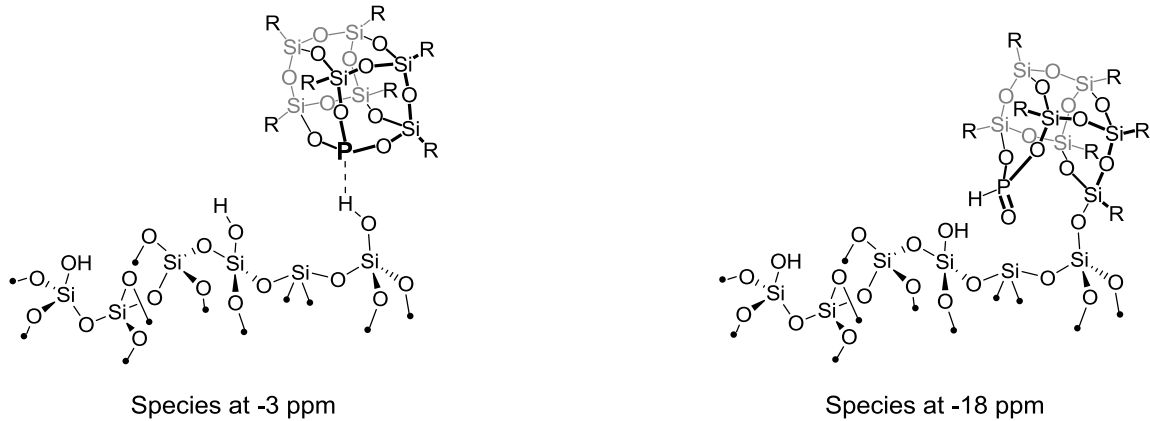


Calcination of the resulting surface species proved to generate surface BOH and to eliminate all organic ligands without losing any trace of boron. Therefore, elimination of the organics by a temperature treatment was validated as inherent to the strategy.

Such surface species were also shown to exhibit quite strong acidic properties, in accordance to published results about the role of boron in silica.

Likewise, the strategy we used with boron was transferred to phosphorus. The urge of using sterically hindered molecules made us study the case of POSS-P. From four different P sources, the latter exhibited interesting traits, as it adopted two different behaviours upon contact with the silica surface: part of the contacted POSS-P being physisorbed and the other one being covalently bonded to silica, as a phosphonate species.

## Conclusion

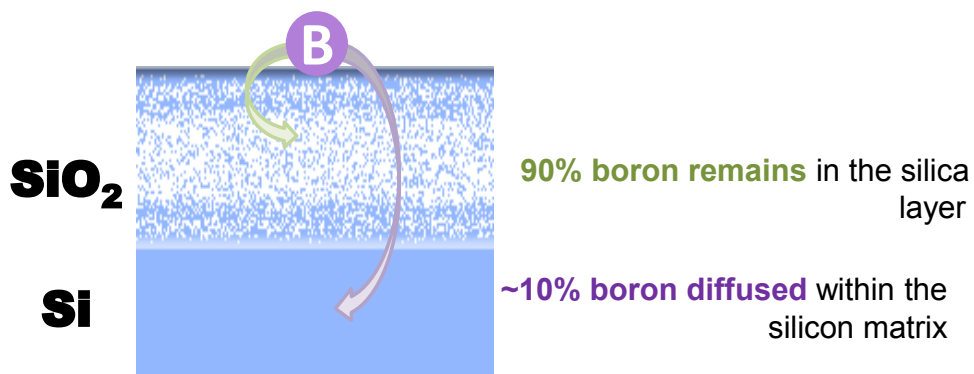


Then, the removal of organic chains by calcination from the different chosen P-sources (phosphine, phosphite, phosphonate, phosphonium) showed that two of them resulted in the formation POH surface species whereas it did not allow the quantitative elimination of organic ligands for the two other P-precursors.

It was then demonstrated that the strategy was fully transferrable to silicon wafers coated with native silica. The same strategy as described before was thus transferred from the 3D model to the 2D silicon wafer. It was shown that both boron- and phosphorus-containing species were successfully grafted to silicon wafers.

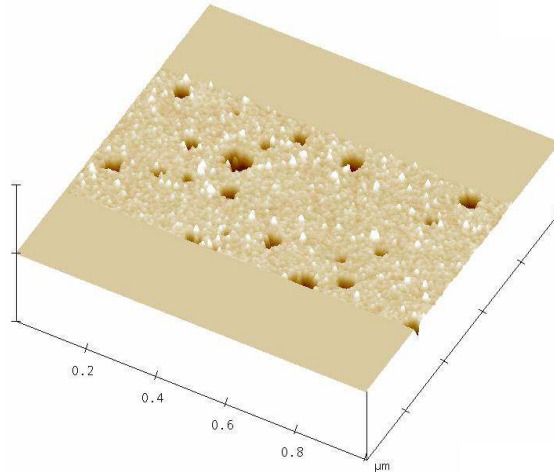
For boronated compounds, it was shown that the diffusion of the doping atom by RTP was quite heavily influenced by the nature of the precursor organic chain. Indeed, it was evidenced that the amount of recovered boron after annealing at 1000°C was almost total for the C<sub>3v</sub> grafted species, versus only a 10% recovery yield for the C<sub>2</sub> molecule. Annealing at higher temperatures also showed an important loss of boron for both grafted species.

## Annealing 1000°C C<sub>3v</sub>



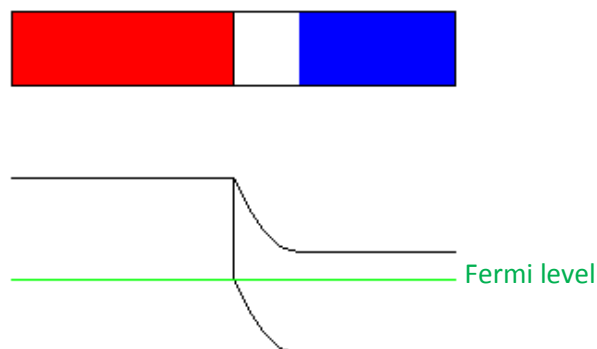
Many reasons could explain such a fact:

- Desorption or evaporation of the ligands during annealing;
- Formation of SiO from Si and SiO<sub>2</sub> (pitting) proved by AFM.



**Annealed wafer at 1050°C under inert ambient**

Then, the key point of the PhD thesis was made possible by tunnelling spectroscopy, proving not only the strong doping of the wafer surface but also the appearance of a p-n junction, with amounts of the order of  $10^{15}$  at.cm<sup>-3</sup> for the n-dopant (initially present in the wafer) and  $10^{19}$ - $10^{20}$  at.cm<sup>-3</sup> on a thickness of less than 5 nm. The latter are similar to the results of Ho *et al.* in 2008,<sup>[1]</sup> but here the diffusion was effective without silica capping of the boron precursor.



**Representation of the junction with  $1.0 \times 10^{19}$  B and  $1.0 \times 10^{15}$  P<sup>++</sup>**

<sup>\*\*</sup> Band Diagram made using <http://www.acsu.buffalo.edu/~wie/applet/pnformation/pnformation.html>

## Conclusion

However, diffusion still needs to be improved, in order to increase the yield of dopant incorporation within the silica layer. An idea would be to reduce the oxide layer to a minimum in order to prevent the loss of dopant within the silica. Creating a SiOH monolayer on silicon would reduce the distance between the dopant and silicon and therefore hopefully yield a better doping. Phosphorus remains also a great issue as it hardly diffuses in silica. Thus a reduction of the silica layer could be the key for its better diffusion into the silicon wafer. Capping the grafted molecule with, for instance, SiN, which is a diffusion barrier for both B and P, could also be a promising alternative when using temperatures above 1000°C.

Also, one of the most important questions raised by the PhD thesis remained unanswered: was the doping actually deterministic? An excellent way to determine such an issue would be to resort to STEM measurements.<sup>[2]</sup> Such analyses could then be performed on species containing atoms whose size would allow their detection by STEM and whose reactivity would be similar to that of boron. Gallium would, for instance, be an excellent choice to perform such an analysis and determine once and for all whether the doping was, indeed, deterministic.

---

**AC-STEM image of a silicon crystal doped with arsenic, viewed from [001] direction. Intensities along the columns are shown in colours, red being highest density (reproduced from <sup>[2]</sup>)**

### References:

- [1] J. C. Ho, R. Yerushalmi, Z. A. Jacobson, Z. Fan, R. L. Alley, A. Javey, *Nat Mater* **2008**, 7, 62.
- [2] K. Takayanagi, Y. Oshima, T. Tanaka, Y. Tanihshiro, H. Sawada, F. Hosokawa, T. Tomita, T. Kaneyama, Y. Kondo, *JEOL News* **2010**, 45, 2.

## **Experimental Part**

---

## Experimental Part

All experiments were carried out under dry and oxygen free Ar using either standard Schlenk or glovebox techniques for the organometallic synthesis. For the syntheses and the treatments of the surface species, reactions were carried out using high vacuum lines ( $10^{-5}$  mbar) and glove-box techniques. Elemental analyses were performed at the Mikroanalytisches Labor Pascher or at the Service Central Analyse in Solaize (Mo). Pentane, toluene, diethylether and dichloromethane were dried using an MBraun solvent purification system, contacted with MS 4 Å and degassed under vacuum. THF and benzene (Aldrich) were distilled and stored in rotaflos under dry and oxygen-free Ar over Na/K in benzophenone.

*In situ IR spectroscopy.* Infrared spectra were recorded on a Nicolet 550-FT by using an infrared cell with CaF<sub>2</sub> windows, allowing in situ studies. Typically 16 scans were accumulated for each spectrum (resolution, 2 cm<sup>-1</sup>).

*DRIFT spectroscopy.* DRIFT spectra were recorded on a Nicolet 6700 FT-IR spectrometer by using a custom infrared cell equipped with ZnSe windows; the samples were loaded in the cell under inert atmosphere. (glovebox) Typically, 64 scans were recorded for each spectrum (resolution 4 cm<sup>-1</sup>).

*Solid-state NMR.* Spectra were recorded under MAS on a Bruker Avance or Avance II 500 wide-bore or DSX 300 spectrometer with conventional double resonance 4 mm CP-MAS probes. The MAS frequency was set to 10 kHz for the 4 mm probe. The samples were introduced in a zirconia rotor in the glove box and tightly closed. Chemical shifts are reported in ppm downfield from liquid SiMe<sub>4</sub> (0 ppm) for <sup>1</sup>H, <sup>13</sup>C NMR.

*Liquid-state NMR.* Spectra were recorded in CDCl<sub>3</sub> (unless stated otherwise) using a Bruker Spectrospin 300 spectrometer and referenced to the residual protonated solvent peaks of CDCl<sub>3</sub> (<sup>1</sup>H d<sub>H</sub> = 7.26 ppm, <sup>13</sup>C d<sub>C</sub> = 77 ppm ).

*RTP Annealing.* RTP annealing experiments were performed in a JetFirst 200 by Jipelec using BT or HT type optical pyrometer and 2 K type (Chromel/Alumel), Ø 0.127 mm thermocouples.

*ICPMS.* An Agilent 7500cs was used with the following parameters: Analysis hot plasma mode (1600W) under Argon (no He, no H<sub>2</sub> were introduced into the octopole); integration time was 2s on mass 11 for Boron and 5s on mass 31 for Phosphorus.

## 1. Preparation of dehydroxylated silica

---

### 1.1. Silica dehydroxylated at 200°C ( $\text{SiO}_{2-(200)}$ )

---

Silica (Aerosil Degussa,  $200 \text{ m}^2 \cdot \text{g}^{-1}$ ) was compacted using distilled water and dried at  $110^\circ\text{C}$  for 5 days in an oven. The obtained compacted mass was broken down to particles in a mortar and sifted to yield a particle size of 50 meshes.

The obtained powder was then partially dehydroxylated in secondary vacuum ( $10^{-5}$  mbar) for 12h and stored in the glovebox.

### 1.2. Silica dehydroxylated at 700°C ( $\text{SiO}_{2-(700)}$ )

---

Non-dehydroxylated silica powder obtained as described before was put in a quartz reactor and calcined ( $500^\circ\text{C}$  under air) for 2h. It was then partially dehydroxylated by heating up at  $700^\circ\text{C}$  under secondary vacuum ( $10^{-5}$  mbar) for 8h.

### 1.3. $^{18}\text{O}$ -doped silica

---

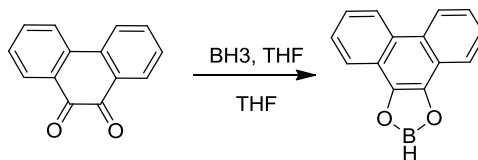
In the glovebox, about 2g from  $\text{SiO}_{2-(700)}$  were inserted into a 50 mL quartz reactor and linked to a high-vacuum line.  $^{18}\text{O}$ -doped from Sigma-Aldrich was distilled to the quartz reactor to yield a vapour pressure of water and then closed. The reactor was then heated up to  $500^\circ\text{C}$  and left at such a temperature for 3h. All volatiles were then evacuated in vacuo and the high-vacuum line was cleaned up to remove any trace of water. This step was repeated 4 times. At the end of the last heating cycle under a vapour pressure of  $\text{H}_2^{18}\text{O}$ , the reactor was heated up to  $700^\circ\text{C}$  in vacuo for 15 min.



## 2. Synthesis of suitable dopant-containing molecules

### 2.1. Synthesis of C2-symmetrical molecules

#### 2.1.1. Synthesis of phenanthro[9,10-d][1,3,2]dioxaborole



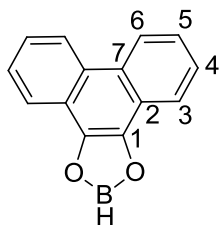
-  $\text{BH}_3$ , THF solution (1M, 11mL) was placed in a three-necked round bottom flask equipped with a bubbler, an argon entry and a magnetic stirrer bar.

- Phenanthrene-9,10-dione (1.95g; 9.3 mmol) was suspended in dry and degassed THF (25 mL) and placed in a dropping funnel fitted to the flask.

- The  $\text{BH}_3$ , THF solution was cooled down to  $0^\circ\text{C}$  and the phenanthrene suspension was added to it over 4 min. The mixture switched colours from orange-ish to dark red transparent then to yellow over stirring for 2h at RT ( $23^\circ\text{C}$ )

- The solvent was evaporated to yield a light yellow solid.

#### NMR (400MHz, $\text{CDCl}_3$ ):



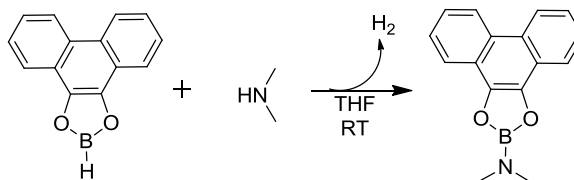
$^1\text{H}$ : 8.2ppm (dd, 5.2Hz, 1H; 1H:  $\text{H}_3$ ); 8.0 ppm (d, 10.8Hz; 1H;  $\text{H}_6$ ); 7.7 ppm (ddd, 6.3 Hz, 2Hz, 1.2 Hz; 1H;  $\text{H}_4$ ); 7.4 ppm (ddd, 5.2 Hz, 1.2 Hz; 1H;  $\text{H}_5$ )

$^{11}\text{B}$ : 26 ppm

$^{13}\text{C}$ : 141 ppm ( $\text{C}_1$ ); 128 ppm ( $\text{C}_2$ ,  $\text{C}_7$ ); 118 ppm ( $\text{C}_4$ ,  $\text{C}_5$ ); 108 ppm ( $\text{C}_3$ ,  $\text{C}_6$ )

## 2.1.2. Synthesis of phenanthrodioxaborole derivatives

### 2.1.2.1. Synthesis of phenanthrodioxaborole-2-amine

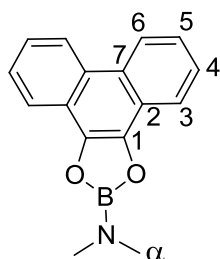


In a glovebox, in a Schlenk flask equipped with a magnetic stirrer bar:

- 0.5360 g (2.44 mmol) of phenanthro[9,10-d][1,3,2]dioxaborole were inserted and the flask was closed and taken out of the glovebox.
- The flask was put under an argon flow and the solid was dissolved with 15 mL of dry and degassed THF.
- 1.22 mL of dimethylamine (2M in THF, 2.44 mmol) were added within 5 min to the mixture at RT (24°C) and left to be stirred at this temperature for 15h.

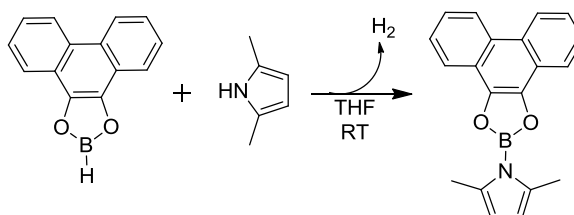
All volatiles were evaporated in vacuo and the resulting solid was washed with 20 mL of pentane and 5 mL of Et<sub>2</sub>O.

#### **NMR (400MHz, CDCl<sub>3</sub>):**



<sup>1</sup>H: 8.2ppm (dd, 5.2Hz, 1H; 1H: H<sub>3</sub>); 8.0 ppm (d, 10.8Hz; 1H; H<sub>6</sub>); 7.7 ppm (ddd, 6.3 Hz, 2H, 1.2 Hz; 1H; H<sub>4</sub>); 7.4 ppm (ddd, 5.2 Hz, 1.2 Hz; 1H; H<sub>5</sub>); 2.5 ppm (s, 6H, H<sub>α</sub>)

### 2.1.2.2. Synthesis of phenanthrodioxaborole-pyrrole

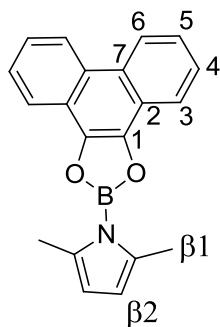


## Experimental Part

The same procedure as described in 1.1.2.1. was used, with 1.12 g (5.09 mmol) of phenanthro[9,10-d][1,3,2]dioxaborole dissolved in 20 mL of THF and 0.53 mL (0.50 g, 5.58 mmol) of 2,5-dimethylpyrrole.

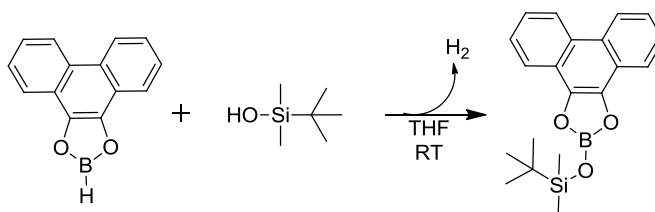
The resulting solid was washed with 20 mL of pentane and 5 mL of Et<sub>2</sub>O.

### **NMR (400MHz, CDCl<sub>3</sub>):**



<sup>1</sup>H: 8.3ppm (dd, 5.2Hz, 1H; 1H: H<sub>3</sub>); 8.0 ppm (d, 10.8Hz; 1H; H<sub>6</sub>); 7.7 ppm (ddd, 6.3 Hz, 2Hz, 1.2 Hz; 1H; H<sub>4</sub>); 7.4 ppm (ddd, 5.2 Hz, 1.2 Hz; 1H; H<sub>5</sub>); 5.5 ppm (s, 2H, H<sub>β2</sub>); 2.2 ppm (s, 6H, H<sub>β1</sub>)

### *2.1.2.3. Synthesis of phenanthrodioxaborole-silane*



The same procedure as described in 1.1.2.1. was used, with 0.19 g (0.86 mmol) of phenanthro[9,10-d][1,3,2]dioxaborole dissolved in 8 mL of THF and 0.20 mL (0.17 g, 1.27 mmol) of 2,5-dimethylpyrrole.

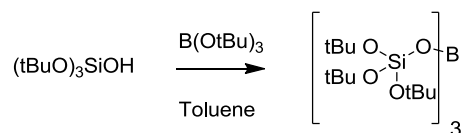
The resulting solid was washed with 10 mL of pentane and 5 mL of Et<sub>2</sub>O.

## 2.2. C<sub>3</sub> tri-coordinated molecules

---

### 2.2.1. Synthesis of tri-tert-butylsilanol borate

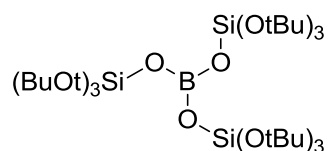
---



In a glovebox, in a Schlenk flask equipped with a magnetic stirrer bar:

- 5 g (20 mmol) of  $\text{HOSi(O}^t\text{Bu)}_3$  were inserted and the flask was closed and diluted in 10mL of toluene.
- 1.89 g (8.2 mmol) of  $\text{B(O}^t\text{Bu)}_3$  were added to the solution and taken out of the glovebox.
- The flask was put under an argon flow and the solid was dissolved with 15 mL of dry and degassed THF. The flask was put under a weak flow of argon and adapted to a condenser. The mixture was then heated up to 80°C and left to react for 24h at 80°C.
- The flask was cooled down to RT (23°C) and all volatiles were taken in vacuo to yield a white solid, which was later recrystallized in toluene/acetonitrile 4:1 (10mL). Colourless needles were formed after cooling down at -30°C

#### **NMR (400MHz, CDCl<sub>3</sub>):**

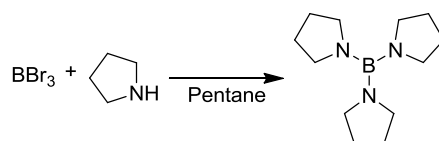


<sup>1</sup>H: 1.50 ppm (s, 12H)

<sup>13</sup>C: 73 ppm (C<sub>4</sub>), 32 ppm (C<sub>1</sub>)

### 2.2.2. Synthesis of tri-pyrrolylborane

---



In a Schlenk flask equipped with a magnetic stirrer bar, under an argon flow:

- 10 mL (8.52 g; 120 mmol) of pyrrolidine were inserted and diluted in 10 mL of dry and degassed pentane. The solution was cooled down to -78°C.
- 2 mL (5.21 g; 21 mmol) of BBr<sub>3</sub> were slowly added to the mixture and was slowly brought back to RT (23°C) to be stirred for 2h.
- All volatiles were taken in vacuo to yield an off-white solid.

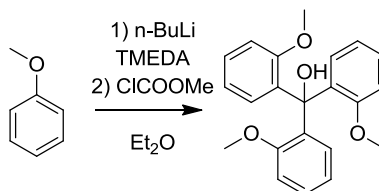
#### **NMR (400MHz, CDCl<sub>3</sub>):**

<sup>1</sup>H: 3.13 ppm (m, 4H), 1.60 (m, 4H)

<sup>13</sup>C: 48 ppm (C<sub>α</sub>), 26 ppm (C<sub>β</sub>)

### 2.2.3. Synthesis of a cage-shaped boron-containing molecule

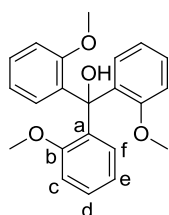
The same reaction as described by Yasuda et al.<sup>[1]</sup> was performed on a different scale.



A 100 mL two-necked round bottom flask was equipped with a condenser, a magnetic stirrer bar and a dropping funnel and was purged with argon.

- 8 mL of a solution of n-BuLi (2.5M) were introduced in the flask and the solvent was exchanged with diethylether to yield 15mL of n-BuLi in Et<sub>2</sub>O. 0.1mL of TMEDA (N,N,N',N'-tetramethylethylenediamine) (0.13g; 1.11mmol) were also added.
- The dropping funnel was charged with 1.8 mL (16.5 mmol) of anisole and 2mL of dry and degassed Et<sub>2</sub>O. The anisole solution was slowly added to the BuLi solution at RT (22°C). The mixture got warmer but no condensation nor reflux of Et<sub>2</sub>O could be perceived. The mixture was left to be stirred at RT (22°C) overnight (12h).
- 0.4 mL (5 mmol) of methylchloroformate were inserted into the dropping funnel and diluted in 4 mL of dry Et<sub>2</sub>O.
- The anisole mixture was cooled down to 0°C, then the formate solution was added dropwise (over 30 min) to yield white chunks that immediately dissolved. The mixture was then allowed to warm up to RT (23°C) and left to be stirred for 3h.
- The reaction mixture was quenched with 20 mL of distilled H<sub>2</sub>O, and the precipitate was filtered and dissolved in 30 mL of dichloromethane to be washed twice with 10 mL of water. The organic phase was dried over MgSO<sub>4</sub> and evaporated in a Schlenk flask to yield a white product.

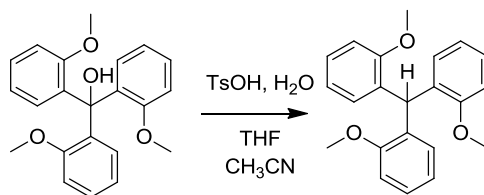
#### NMR (400MHz, CDCl<sub>3</sub>):



<sup>1</sup>H: 7.25-7.16 (m, 6H; H<sub>f</sub>, H<sub>d</sub>), 6.90-6.86 (m, 6H; H<sub>c</sub>, H<sub>e</sub>), 5.48 (s, 1H, OH), 3.45 (s, 9H, OMe);

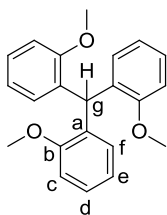
Yield: 64%

## Experimental Part



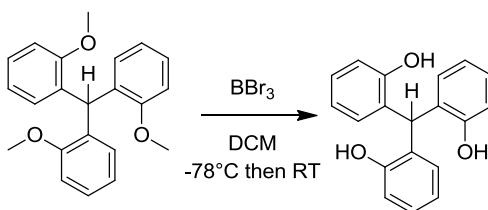
- 1.13g of the previously synthesized product were dissolved in 5 mL of acetonitrile and 7 mL of THF.
- 0.67 g of para-toluenesulfonic acid hydrate (3.53 mmol) were then added to the solution which abruptly changed colours to dark purple. After 15 min of stirring at RT (24°C), the colour changed to transparent orange and the mixture was then left to be stirred overnight at RT (14h at 24°C).
- 30 mL of water were added to the orange mixture: white slurry appeared. The suspension was extracted with 4x20 mL of Et<sub>2</sub>O and the organic phase was dried of MgSO<sub>4</sub>. The solvent was then evaporated in vacuo.

### NMR (400MHz, CDCl<sub>3</sub>):



<sup>1</sup>H: 7.25-7.14 (m, 6H; H<sub>f</sub>, H<sub>d</sub>), 6.86-6.73 (m, 6H; H<sub>c</sub>, H<sub>e</sub>), 4.75 (s, 1H, H<sub>g</sub>), 3.67 (s, 9H, OMe);

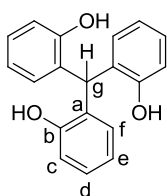
Yield: 87%



- 1.01 g of the previous product (3.04 mmol) were dissolved in 10 mL of dry and degassed dichloromethane. The solution was cooled down to -78°C.
- 1.5 mL of BBr<sub>3</sub> (15.9 mmol) were added to the solution which immediately turned dark brown. The reaction mixture was kept at -78°C for 30 min before it was allowed to warm up to RT (25°C) and left to be stirred for 4h.

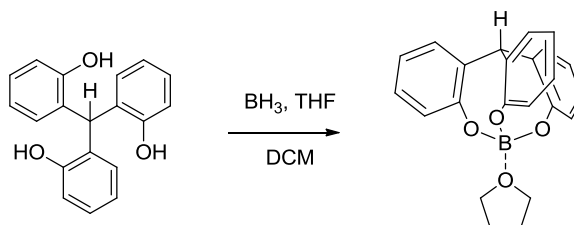
- The mixture was then cooled down to 0°C and quenched with 15 mL of water over 15 min: a yellow solid formed on the walls of the flask.
- The solution was treated with 50 mL of Et<sub>2</sub>O. The organic phase was washed with 3 x 20 mL NaOH (1M). The aqueous phases were gathered and neutralized with 20 mL of HCl (1M) before being extracted with 3 x 25 mL Et<sub>2</sub>O.
- The organic phase was dried over MgSO<sub>4</sub> and evaporated in vacuo to yield an off-white solid that was retaken in Et<sub>2</sub>O/Hexane (4:1) and left in the freezer at -30°C overnight (12h). The white solid was then filtered and dried in vacuo.

**NMR (400MHz, CDCl<sub>3</sub>):**



<sup>1</sup>H: 7.25-7.15 (m, 3H; H<sub>f</sub>, H<sub>d</sub>), 6.90-6.82 (m, 9H; H<sub>c</sub>, H<sub>e</sub>, H<sub>f</sub>), 6.05 (s, 1H, H<sub>g</sub>), 4.96 (s, 3H, OH);

Yield: 55%

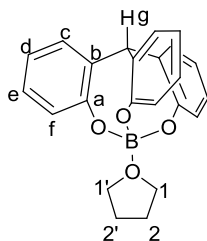


- 0.50 g (1.68 mmol) of the previous triol were dissolved in dry and degassed dichloromethane under an argon flow. To the off-white suspension were added 2 mL of BH<sub>3</sub>, THF (1M in THF): the solution turned transparent yellow within seconds.
- The reaction mixture was left to be stirred at RT (25°C) for 1h.
- All volatiles were removed in vacuo to yield a white solid.



## Experimental Part

### **NMR (400MHz, CDCl<sub>3</sub>):**

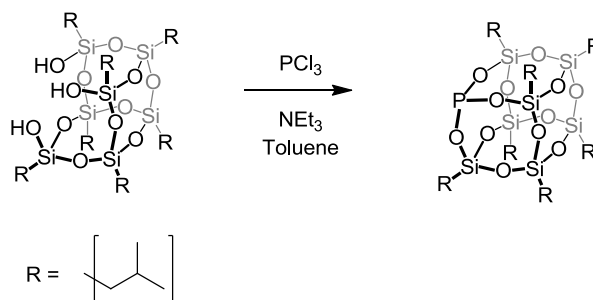


<sup>1</sup>H: 7.29-7.26 ppm (m, 3H, H<sub>f</sub>), 7.17-7.12 (m, 3H, H<sub>d</sub>), 6.95-6.88 (m, 6H; H<sub>c</sub>, H<sub>e</sub>), 5.19 (s, 1H, H<sub>g</sub>), 4.56 ppm (large peak, 2H, H<sub>1,1'</sub>), 2.26 ppm (large peak, 2H, H<sub>2,2'</sub>);

Yield: 98%

### 2.2.4. Synthesis of a POSS-P

The reaction followed was the same as described in literature by Feher et al.<sup>[2]</sup>



In a glovebox, in a Schlenk flask equipped with a magnetic stirrer bar:

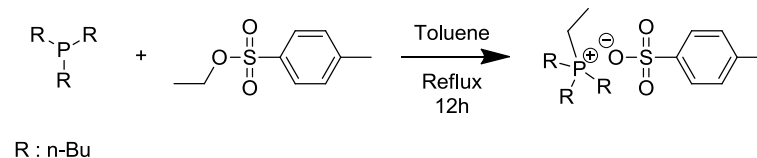
- 1.04 g (1.31 mmol) of POSS-triol were inserted and the flask was closed and diluted in 20mL of toluene and taken out of the glovebox and put under an argon flow.
- 0.68 mL (0.49 g; 4.88 mmol) of Et<sub>3</sub>N were added to the solution.
- 0.11 mL (173.04 mg; 1.26 mmol) of PCl<sub>3</sub> were also slowly added to the reaction mixture.
- The flask was left to be stirred at RT (24°C) for 2h and filtered to remove all Et<sub>3</sub>NHCl. All volatiles were taken in vacuo to yield and the residue was extracted with pentane before being filtered off and dried in vacuo to yield a white-ish slurry.

### **NMR (400MHz, CDCl<sub>3</sub>):**

<sup>1</sup>H: 2.06 ppm (dt, 9.2 Hz; 1H; H<sub>β</sub>); 1.05 ppm (dd, 8.8 Hz, 5.6 Hz; 6 H; H<sub>γ</sub>); 0.79 ppm (dd, 9.2 Hz; 2H, H<sub>α</sub>)  
<sup>31</sup>P: 85 ppm

### 2.3. Synthesis of a phosphonium salt as a weak interaction ligand

The reaction was performed, inspired by other ionic liquids formation: <sup>[3]</sup>

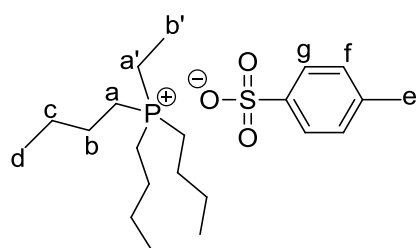


In a 100 mL Schlenk flask blown with argon, 12.223 g of ethyltosylate (61.04 mmol) were diluted in 44 mL of dry and degassed toluene.

Then, 14 mL of tributylphosphine (11.3 g; 56.1 mmol, 1.1 eq) were added to the solution. A water cooler was adapted to the flask and the mixture was heated up and left to be stirred at 90°C overnight (12h).

All volatiles were then taken in vacuo. The flask was cooled down to RT (24°C) and the formed white solid was then suspended in dry diethyl ether and filtered. The product was heated up to 90°C and melted down, and all volatiles were taken in vacuo. The flask was again allowed to cool down to RT (24°C) and stored in the glovebox.

#### NMR (400MHz, CDCl<sub>3</sub>):

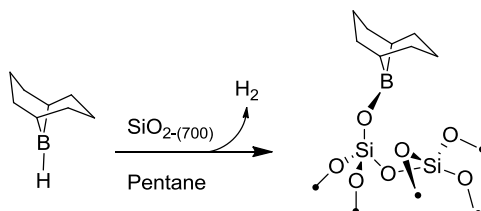


<sup>1</sup>H: 0.97 ppm (m; 9H; H<sub>d</sub>); 1.28 ppm (m; 3 H; H<sub>b'</sub>); 1.52 ppm (large peak; 12H; H<sub>a</sub>, H<sub>a'</sub>); 2.34 ppm (s; 3H; H<sub>e</sub>); 2.45 (m; 8H; H<sub>b</sub>, H<sub>c</sub>); 7.14 ppm (d; 10Hz; 2H; H<sub>f</sub>); 7.81 ppm (d; 10Hz; H<sub>g</sub>)  
<sup>31</sup>P: 35 ppm

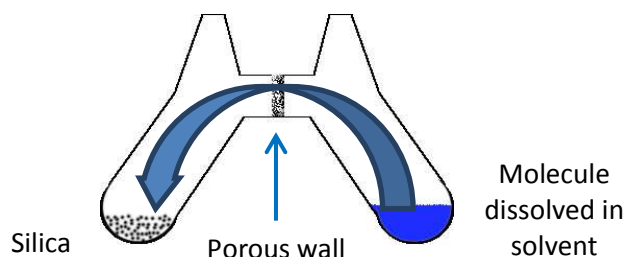
### 3. Silica-supported species

#### 3.1. Boron-containing species

##### 3.1.1. Grafting of 9-BBN on SiO<sub>2</sub>-(700)



The grafting was performed following Schlenk techniques.



**Reaction: 1-2h @ RT**

In a glovebox, in a double Schlenk flask equipped with two magnetic stirrer bars:

- Through the male entry: 250.9 mg of SiO<sub>2</sub>-(700) ( $5.81 \times 10^{-5}$  mol surface silanol) were inserted.
- The flask was closed, brought out of the glovebox, then linked to the hood vacuum line through the female entry tap and put under argon.
- Through the female entry: 0.5 mL of a 9-BBN solution (0.4 M in hexanes) were diluted in 6 mL of pentane.
- The flask was then leaned to have the solution permeate through the porous wall and impregnate silica. The solid in solution was stirred at the minimum spinning rate (100 r/min) and left to react for 2h at RT (22-25°C). Then, the flask was leant the other way to recover all of the initial solution in the female part of the double Schlenk flask. The solvent was then evaporated to the male entry by using a cold point. The reacted silica was rinsed three times. In the case the initial solvent was toluene, the flask was brought into the glovebox, the toluene solution was removed and replaced with pentane. The grafted species was then washed three more times with pentane to eliminate most traces of toluene.
- The flask was then linked to a high-vacuum line through the female entry and all volatiles were removed in a trap. Then, the flask was connected directly though the male entry and

the reacted silica was dried in vacuo. The reacted species was considered dry once the indicated vacuum went back to its initial value ( $1.5 \times 10^{-5}$  mbar).

The grafted species was then stored into the glovebox.

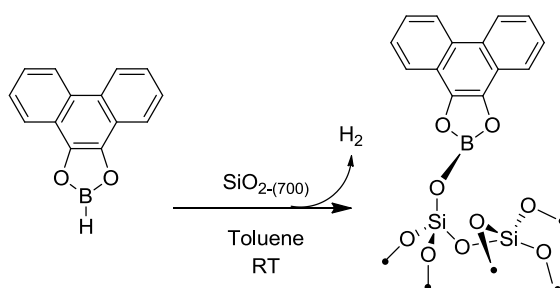
**IR:** 3745, 3700, 3417, 2929, 2898, 2866, 2850  $\text{cm}^{-1}$

### 3.1.2. Grafting of 9-BBN on $\text{SiO}_2$ -(200)

The same procedure as before was used, using 495.1 mg of  $\text{SiO}_2$ -(200) ( $1.15 \times 10^{-4}$  mol OH) and 0.5 mL a 0.4 M solution of 9-BBN in hexanes ( $1.73 \times 10^{-4}$  mol) diluted in 6 mL of pentane.

**IR:** 3746, 3700, 3400, 2929, 2898, 2866, 2850, 1692  $\text{cm}^{-1}$

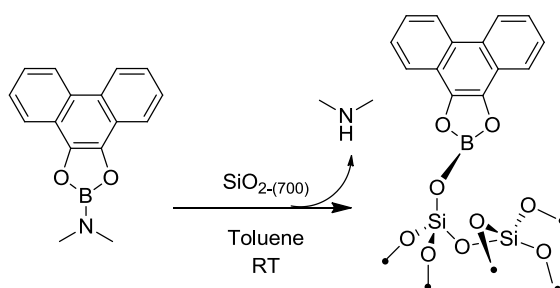
### 3.1.3. Grafting of the $\text{C}_2$ borole



The same procedure as before was used, using 524.9 mg of  $\text{SiO}_2$ -(700) ( $1.22 \times 10^{-4}$  mol OH) and 58.3 mg of  $\text{C}_2$ -borole ( $2.65 \times 10^{-4}$  mol) dissolved in toluene. Toluene was then washed off with pentane in the glovebox.

**IR :** 3746, 3083, 3037, 2962, 1944  $\text{cm}^{-1}$

### 3.1.4. Grafting of the aminodioxaborole



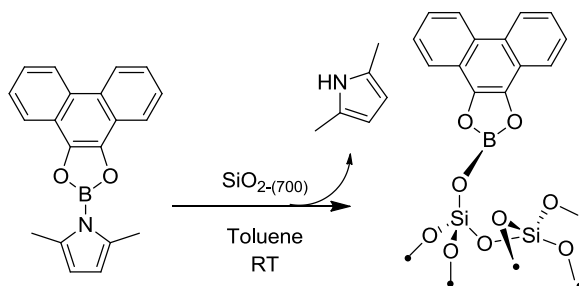
## Experimental Part

The same procedure as before was used, using 499.4 mg of  $\text{SiO}_{2-(700)}$  ( $1.16 \times 10^{-4}$  mol OH) and 39.7 mg of aminodioxaborole ( $1.50 \times 10^{-4}$  mol) dissolved in toluene. Toluene was then washed off with pentane in the glovebox.

**IR:** 3746, 3623, 3235, 3078, 3026, 3008, 2965  $\text{cm}^{-1}$

### 3.1.5. Grafting of the pyrrolyldioxaborole

---

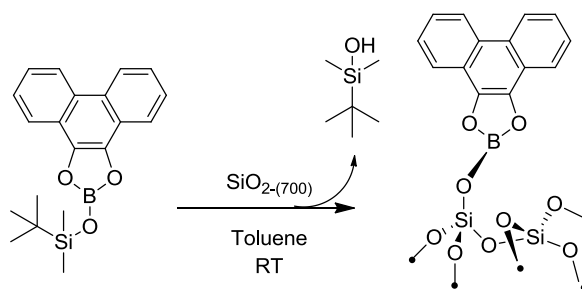


The same procedure as before was used, using 502.8 mg of  $\text{SiO}_{2-(700)}$  ( $1.17 \times 10^{-4}$  mol OH) and 48.3 mg of pyrrolylborole ( $1.50 \times 10^{-4}$  mol) dissolved in toluene. Toluene was then washed off with pentane in the glovebox.

**IR:** 3747, 3601, 3077, 3037, 2968, 2934  $\text{cm}^{-1}$

### 3.1.6. Grafting of the phenanthrodioxaborole-silane

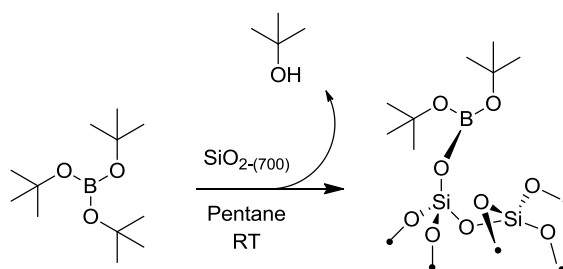
---



The same procedure as before was used, using 502.3 mg of  $\text{SiO}_{2-(700)}$  ( $1.16 \times 10^{-4}$  mol OH) and 52.3 mg of pyrrolylborole ( $1.49 \times 10^{-4}$  mol) dissolved in toluene. Toluene was then washed off with pentane in the glovebox.

**IR:** 3747, 3630, 3079, 3035, 2958, 2936, 2893, 2865  $\text{cm}^{-1}$

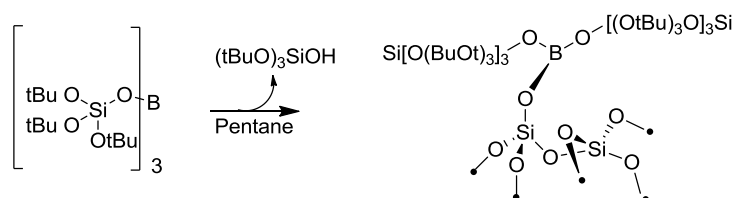
### 3.1.7. Grafting of tri-tert-butylborate



The same procedure as before was used, using 200.5 mg of  $\text{SiO}_{2-(700)}$  ( $4.66 \times 10^{-6}$  mol OH) and 0.2 mL of  $\text{B}(\text{O}^t\text{Bu})_3$  ( $7.05 \times 10^{-3}$  mol) dissolved in pentane.

**IR:** 3347, 2983, 2942, 2909, 2879  $\text{cm}^{-1}$

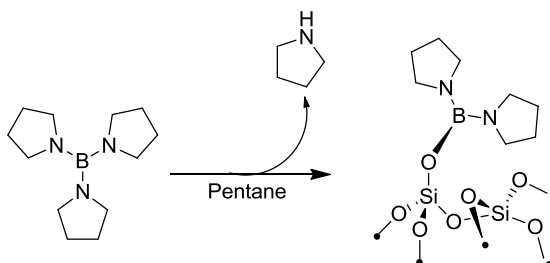
### 3.1.8. Grafting of tri-tert-butylsilanolborate



The same procedure as before was used, using 278.7 mg of  $\text{SiO}_{2-(700)}$  ( $6.00 \times 10^{-6}$  mol OH) and 19.1 mg of  $\text{B}(\text{Si}(\text{O}^t\text{Bu})_3)_3$  ( $2.4 \times 10^{-5}$  mol) dissolved in pentane.

**IR:** 3744, 2980, 2937, 2911, 2877  $\text{cm}^{-1}$

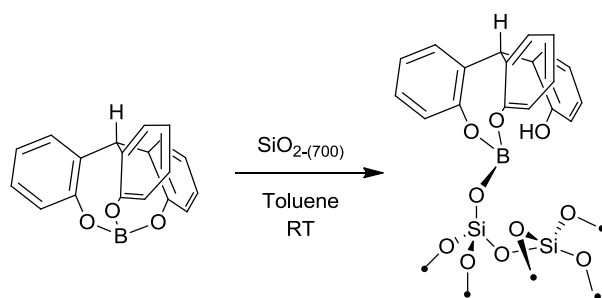
### 3.1.9. Grafting of tri-pyrrolidineborane



The same procedure as before was used, using 257.7 mg of  $\text{SiO}_{2-(700)}$  ( $5.55 \times 10^{-6}$  mol OH) and 16.8 mg of  $\text{B}(\text{C}_4\text{H}_8\text{N})_3$  ( $7.6 \times 10^{-5}$  mol) dissolved in pentane.

**IR:** 3746, 2969, 2949, 2880, 2853  $\text{cm}^{-1}$

### 3.1.10. Grafting of C<sub>3</sub>-borole

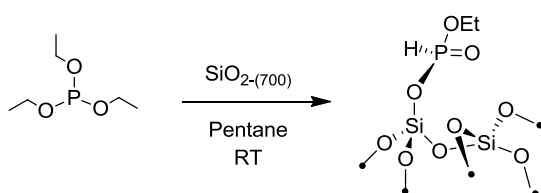


The same procedure as before was used, using 461.7 mg of SiO<sub>2-(700)</sub> ( $1.12 \times 10^{-5}$  mol OH) and 81.3 mg of the C<sub>3v</sub> cage-shaped borole ( $6.17 \times 10^{-4}$  mol) dissolved in toluene. Toluene was then washed off with pentane in the glovebox.

**IR:** 3745, 3570, 3075, 3038, 2964, 2933 cm<sup>-1</sup>

## 3.2. Phosphorus-containing species

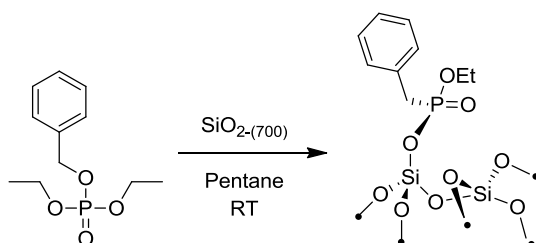
### 3.2.1. Grafting of tri-ethylphosphite



The same procedure as described above was used, using 299.5 mg of SiO<sub>2-(700)</sub> ( $6.42 \times 10^{-5}$  mol OH) and 0.1 mL of tri-ethylphosphite (106.7 mg,  $64.2 \times 10^{-5}$  mol) diluted in pentane.

**IR:** 3222, 2985, 2937, 2905, 2883, 2446 cm<sup>-1</sup>

### 3.2.2. Grafting of diethylbenzylphosphonate

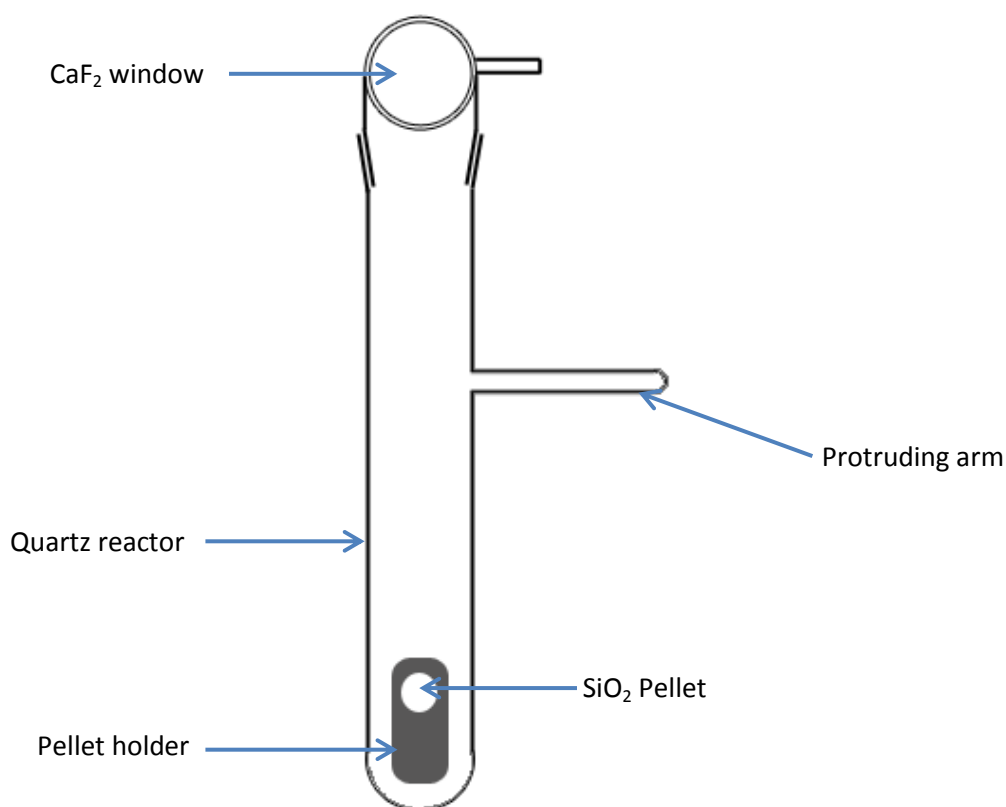


The same procedure as described above was used, using 306.4 mg of  $\text{SiO}_{2-(700)}$  ( $6.56 \times 10^{-5}$  mol OH) and 0.4 mL of diethylbenzylphosphonate (438 mg, 1.92 mmol) diluted in pentane.

IR: 3070, 3037, 2982, 2935, 2914, 2873  $\text{cm}^{-1}$

### 3.2.3. Adsorption of tricyclohexylphosphine

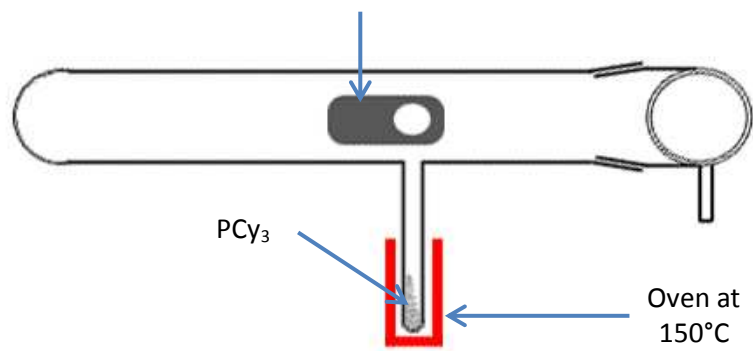
A  $\text{SiO}_2$  pellet was made by pressing some Degussa Aerosil 200  $\text{m}^2 \cdot \text{g}^{-1}$  under 5 t. The pellet was then placed onto a support and into a closed quartz reactor equipped with an adapted UV cell. The reactor was heated up to 500°C for 2h then was taken in vacuo ( $10^{-5}$  mbar) and heated at 700°C overnight (10h).



The reactor was brought into a glovebox and the protruding arm was filled with about 500 mg of  $\text{P}(\text{Cy})_3$ . The reactor was then taken out of the glovebox. The protruding arm of the reactor was heated up to 80°C while the pellet was positioned directly on top of it. The heating was left as is for 3h. Then, the cell holder was heated up for 150°C for 1h to desorb the excess of phosphine that sublimed on deposited onto the pellet.

Pellet holder

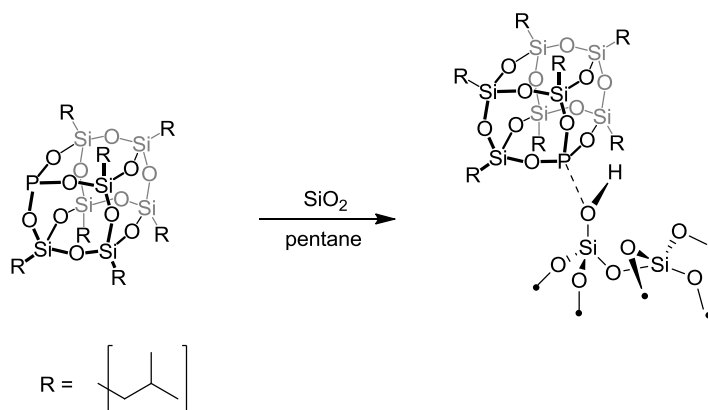




An IR spectrum of the pellet was recorded and the pellet was then heated at 200°C in vacuo for 30 min before another IR spectrum was recorded. Further thermal treatments under vacuum of the solid were performed using 50°C increment until a final temperature of 700°C. The sample was kept under dynamic vacuum for thirty minutes at each temperature.

IR: 3746, 3182, 2939, 2860, 1452  $\text{cm}^{-1}$

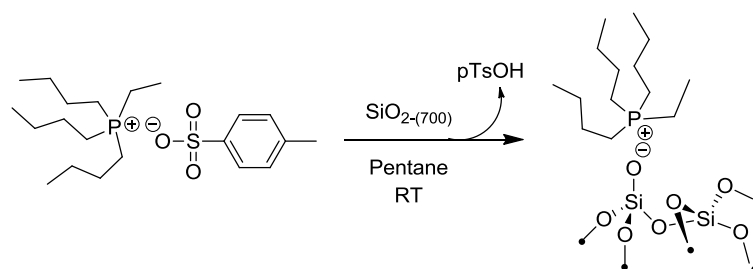
### 3.2.4. Adsorption of POSS-P



The same procedure as described above for boron-containing compounds was used, using 264.0 mg of  $\text{SiO}_{2-(700)}$  ( $6.13 \times 10^{-5}$  mol OH) and 52.3 mg ( $6.49 \times 10^{-5}$  mol) diluted in pentane.

IR: 3746, 3715, 3212, 2964, 2932, 2910, 2875, 2452, 2425  $\text{cm}^{-1}$

### 3.2.5. Adsorption of a phosphonium salt

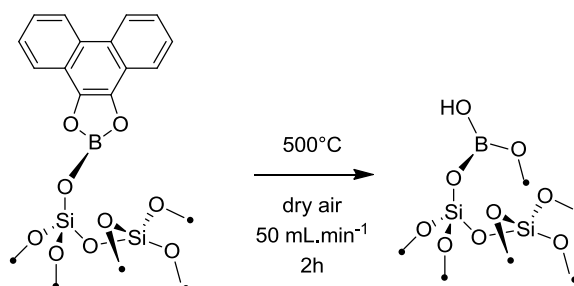


The same procedure as described above was used, using 309.7 mg of  $\text{SiO}_2\text{-(700)}$  ( $6.64 \times 10^{-5}$  mol OH) and 33.8 mg ( $1.09 \times 10^{-4}$  mol) diluted in toluene. Toluene was then washed off with pentane in the glovebox.

**IR:** 3745, 2967, 2932, 2912, 2877  $\text{cm}^{-1}$

## 3.3. Calcination of the supported species

### 3.3.1. Calcination of the supported $\text{C}_2$ -borole



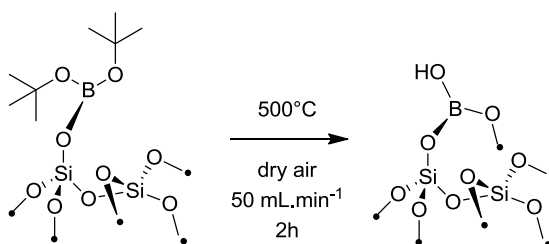
In the glovebox, 249.2 mg from the grafted  $\text{C}_2$ -borole species were inserted in a quartz reactor equipped with a porous wall. The reactor was fitted to a calcination oven, a flow of dry air (50  $\text{mL}\cdot\text{min}^{-1}$ ) was blown through the reactor and the following steps were followed:

- Heating at  $6^\circ\text{C}\cdot\text{min}^{-1}$  until  $500^\circ\text{C}$
- Heating at  $500^\circ\text{C}$  for 2h

The reactor was then taken in vacuo to remove any trace of air and brought into the glovebox to store the obtained species.

**IR:** 3747, 3703  $\text{cm}^{-1}$

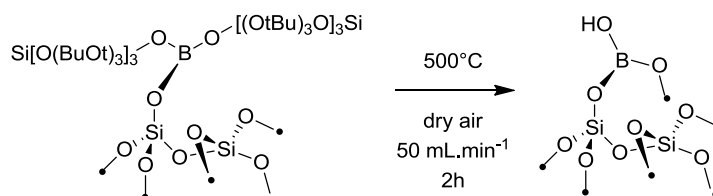
### 3.3.2. Calcination of the supported tri-tert-butylborate



The same procedure as before was used with 200.5 mg of the grafted tri-tert-butylborate species.

**IR:** 3747, 3703  $\text{cm}^{-1}$

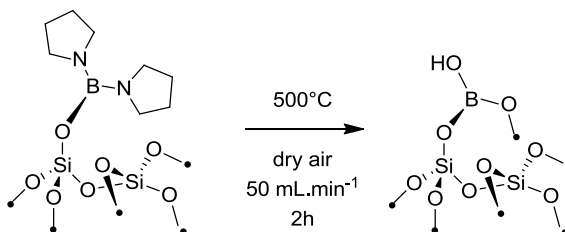
### 3.3.3. Calcination of the supported tri-tert-butylsilylanolborate



The same procedure as before was used with 278.7 mg of the grafted tri-tert-butylsilylanolborate species.

**IR:** 3747, 3703  $\text{cm}^{-1}$

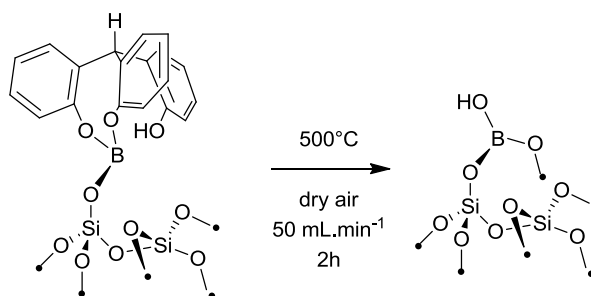
### 3.3.4. Calcination of the supported tri-pyrrolidineborane



The same procedure as before was used with 320.5 mg of the grafted tri-pyrrolidineborane species.

**IR:** 3747, 3703  $\text{cm}^{-1}$

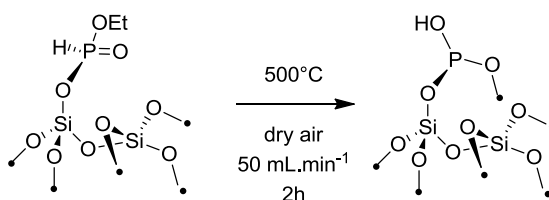
### 3.3.5. Calcination of the supported $C_{3v}$ -borole



The same procedure as before was used with 308.2 mg of the grafted  $C_{3v}$ -borole species.

**IR:** 3747, 3703  $\text{cm}^{-1}$

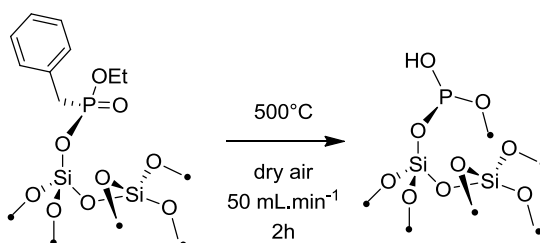
### 3.3.6. Calcination of the supported triethylphosphite



The same procedure as before was used with 329.6 mg of the grafted triethylphosphite species.

**IR:** 3745, 3670, 2984, 2939, 2908  $\text{cm}^{-1}$

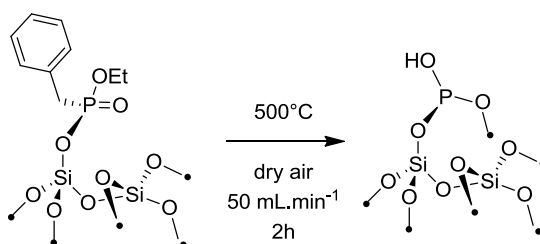
### 3.3.7. Calcination of the supported diethylbenzylphosphonate



The same procedure as before was used with 306.4 mg of the grafted diethylbenzylphosphonate species.

**IR:** 3747, 3636, 3167, 3091, 3069, 3038, 2990, 2936, 2911  $\text{cm}^{-1}$

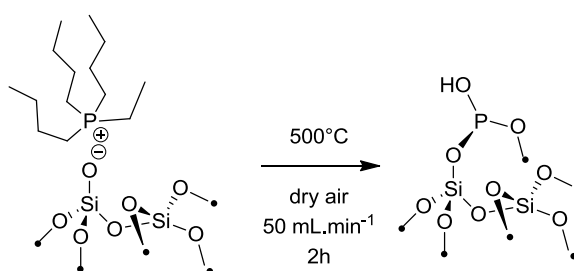
### 3.3.8. Calcination of the supported POSS-P



The same procedure as before was used with 264.0 mg of the grafted POSS-P species.

IR: 3744, 3671, 3332, 2965, 2939, 2908, 2879  $\text{cm}^{-1}$

### 3.3.9. Calcination of the supported phosphonium



The same procedure as before was used with 309.7 mg of the grafted phosphonium species.

IR: 3747, 3670  $\text{cm}^{-1}$

## 4. Wafer-supported species

### 4.1. Grafting of $\text{Ta}(\text{CH}^t\text{Bu})(\text{CH}_2^t\text{Bu})_3$

Silicon wafers were first calcined under air at 500°C then dehydroxylated at 500°C following the procedure used for silica. The tantalum species was then grafted onto the surface in a very simple way: wafers pieces of 20 $\text{cm}^2$  surface area (2.5 x 8  $\text{cm}^2$ ) were dipped into a solution of  $\text{Ta}(\text{CH}^t\text{Bu})(\text{CH}_2^t\text{Bu})_3$  in the glovebox and left to react. (**Fig 87**)

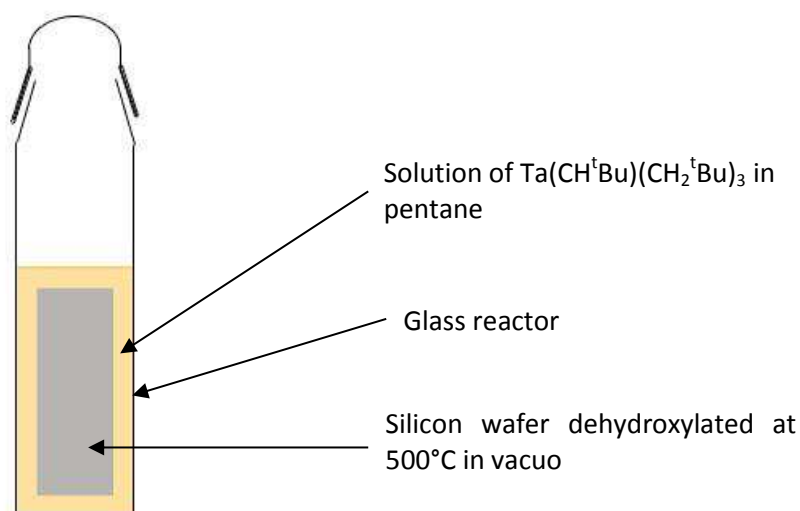
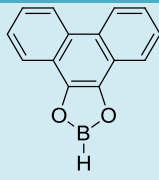
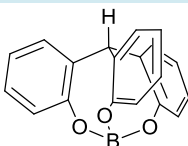
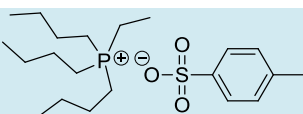


Fig 87. Explanation of the grafting step on silicon wafers

The wafers are then washed and stored in the glovebox before being brought to the CEA.

#### 4.2. Grafting of the dopant-containing molecules on the wafers

The same procedure as before was used with the following values for the grafted species onto wafers:

Species	Weight (mg)	Amount (x 10 <sup>-4</sup> mol)	Solvent
	12.3	0.56	Toluene
	102.5	7.78	Toluene
	127.1	4.1	Toluene

## References

---

- [1] M. Yasuda, S. Yoshioka, S. Yamasaki, T. Somyo, K. Chiba, A. Baba, *Organic Letters* **2006**, *8*, 761.
- [2] F. J. Feher, T. A. Budzichowski, *Organometallics* **1991**, *10*, 812.
- [3] A. Kermagoret, P. Braunstein, *Dalton Transactions* **2008**, 822.





## Experimental Part

## **Appendices**

---

## Appendix 1

---

### Structure of a semi-conductor, a Molecular Orbital approach

---

A good way to describe semiconductors derives from the theory of molecular orbitals (MO).<sup>[1]</sup> According to this theory, one can build a MO diagram based on the atomic orbitals of the atoms involved.<sup>[2]</sup> We shall thus be able to differentiate conductors (Li) from insulators (Be) as extreme models for a better description of semi-conductors (Si).

If two lithium atoms are bonded together, the 1s core orbitals of Li combine to form  $\sigma_{1s}$  and  $\sigma^*_{1s}$ , respectively bonding and antibonding MO. Likewise, the 2s orbitals combine in the same way to form a  $\sigma_{2s}$  and  $\sigma^*_{2s}$ , respectively a bonding and antibonding orbital. Since lithium has only one electron in its 2s orbital, two electrons will fill the bonding MO  $\sigma_{2s}$ .

**Fig A1. Molecular orbital energy levels for  $\text{Li}_2$  (reproduced from <sup>[2]</sup>)**

As the 2s orbitals are farther from the nucleus, their overlap is more efficient. Also, the 1s orbitals of lithium are much lower in energy than the 2s orbitals, resulting in the antibonding  $\sigma^*_{1s}$  being of a lower energy than the bonding  $\sigma_{2s}$ .<sup>[3]</sup>

Using this theory, the number of atoms can be increased to yield n atoms, resulting in the formation of n times the number of atomic orbitals of the atom studied. Moore *et al.* showed an extrapolation of MO theory to n lithium atoms.<sup>[4]</sup> Indeed, adding a third lithium atom will add a third MO as a result of 2s combination to form a triangular  $\text{Li}_3$ , as the overlap of the newly added 3p orbitals will result in 9 resulting empty MO. By increasing the number of Li atoms, the energy spacing

between the MO in the formed cluster are therefore infinitesimal. This is therefore equivalent to a homogeneous energy as an electron jumping amongst these levels could have any energy within such a broad band, therefore an infinitesimal energy is required to excite one electron and send it moving through the metal. This makes lithium a conductor. (Fig A2 Fig hereafter)

**Fig A2. MO energies corresponding to delocalisation of valence electrons with increasing number of lithium atoms (reproduced from [4])**

In the case of lithium, there is an overlap of unfilled 2p band with unfilled 2s band. However, in the case of beryllium, as reported by DeKock *et al.* did, [5] there happens to be an overlap of unfilled 2p band with filled 2s band. Because of this overlap, an infinitesimal amount of energy is required to send electrons into the 2p band, making beryllium a conductor. Had both bands been separated, Be would be an insulator.

**Fig A3. Band-filling diagram for beryllium (reproduced from [5])**

In the case of an insulator, for instance diamond, there happens to be a band gap between the valence band and the conduction band. This band gap is known as the forbidden zone, where no

electron is allowed. In this case, some energy is required to make electrons from the valence band move to the conduction band. (**Fig A4**) Such materials are insulators or semiconductors, the difference between the two being the band gap. Usually, materials with a band gap of 3eV or higher are considered insulators. Materials which behaviour is that of an insulator with a band gap below 3eV are called semiconductors.

**Fig A4. Band-filling diagram of an insulator**

A summary of the band gap energies is displayed in **Table A1** hereafter.<sup>[6, 7]</sup>

**Table A1. Band gaps for some usual materials (from<sup>[6, 7]</sup>)**

Material	Symbol	Band gap (eV) at 302K
Silicon	Si	1.11
Germanium	Ge	0.67
Silicon carbide	SiC	2.86
Aluminium Phosphide	AlP	2.45
Aluminium Arsenide	AlAs	2.16
Aluminium Antimonide	AlSb	1.6
Lead(II) Sulfide	PbS	0.37
Lead(II) Selenide	PbSe	0.27
Lead(II) telluride	PbTe	0.29
Diamond <sup>(a)</sup>	C <sup>(a)</sup>	5.55 <sup>(a)</sup>
Silica <sup>(b)</sup>	SiO <sub>2</sub> <sup>(b)</sup>	9 <sup>(b)</sup>

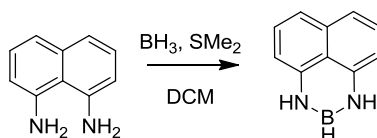
(a) From Surh et al.<sup>[8]</sup>

(b) From Elliott<sup>[9]</sup>

## Appendix 2

### Synthesis of an azaborole

A similar step was to investigate borinines<sup>[10, 11]</sup> which are readily available and which do not provide the possibility for  $\beta$ -H transfer. This compound was obtained in a 70% yield and characterized by NMR. In particular, it is characterized by a single signal at 29.8 ppm in <sup>11</sup>B-NMR.<sup>[10]</sup>



Scheme A1. Synthesis of a borinine

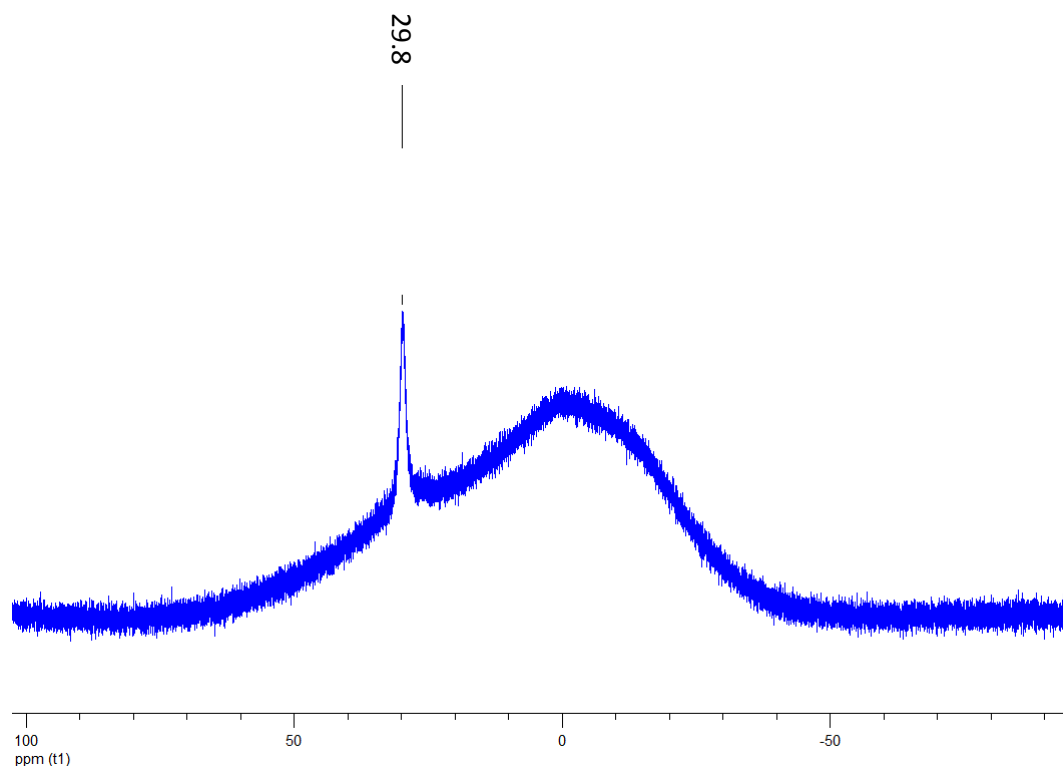
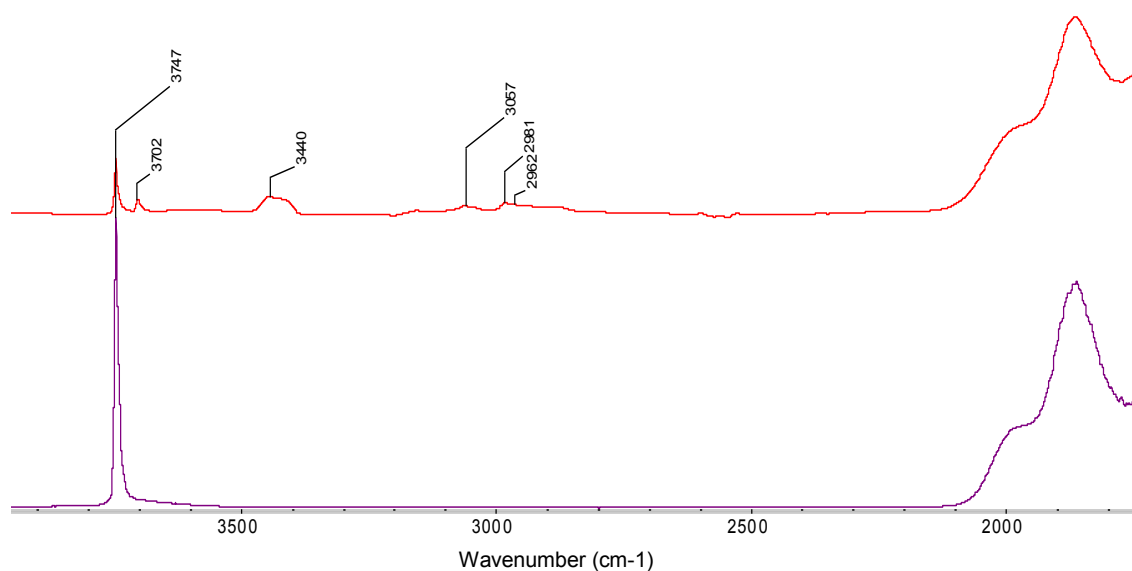


Fig A5. <sup>11</sup>B-NMR spectrum of the borinine

The grafting of the azaborole was then monitored by IR-DRIFT analysis (**Fig A6**).



**Fig A6. IR-DRIFT of the grafted azaborole (red) and of the thermally treated silica before grafting (purple)**

Upon grafting, most of the silanols ( $3747\text{ cm}^{-1}$ ) are consumed. A broad peak appears at  $3440\text{ cm}^{-1}$  and is attributed to N-H stretching of an amine. Additionally, peaks at  $3057\text{ cm}^{-1}$  [ $\nu(\text{C}_{\text{Aromatic}}\text{-H})$ ],  $2981\text{ cm}^{-1}$  [ $\nu_{\text{sym}}(\text{C-H})$ ] and  $2862\text{ cm}^{-1}$  [ $\nu_{\text{asym}}(\text{C-H})$ ] appear, which is in line with the presence of aromatic and alkyl functionalities. While the former is expected, the latter probably arise from the presence of residual adsorbed diethylether, which was used for grafting. The appearance of a peak at  $3702\text{ cm}^{-1}$  is consistent with the formation of  $\text{B-OH}^{[12, 13]}$  species. This would be consistent with the reaction of the B-H bond with water, which would result as previously explained from the condensation of SiOH catalysed by B-containing molecule. This would imply that the kinetic to graft borohydride is competitive with such surface reaction.





## Appendix 4

---

### Circle packing on the silica surface applied to POSS-P

---

In 1773, Joseph Louis Lagrange proved that in order to have the highest density for lattice arrangement of circles of the same size was the hexagonal packing arrangement.<sup>[15]</sup> Lagrange proved that in this state, the centres of the studied circles were set in a hexagonal lattice and surrounded by 6 other circles of the same size.<sup>[16]</sup> Thue's theorem,<sup>[17]</sup> the 2D analog of Kepler's conjecture, shows that the density of such an arrangement is:

$$\eta = \frac{\pi}{\sqrt{12}} = 0.9069$$

Fig A7. Hexagonal lattice of the bee's honeycomb (reproduced from <sup>[16]</sup>)

Therefore, having found that the projected surface of a POSS-P is  $147.77 \text{ \AA}^2$ , and knowing that no  $\text{SiO}_{2-(700)}$ , silanol density is  $0.7 \text{ OH.nm}^{-2}$ , close packing applied for a circle of this area would yield a hexagonal surface of:

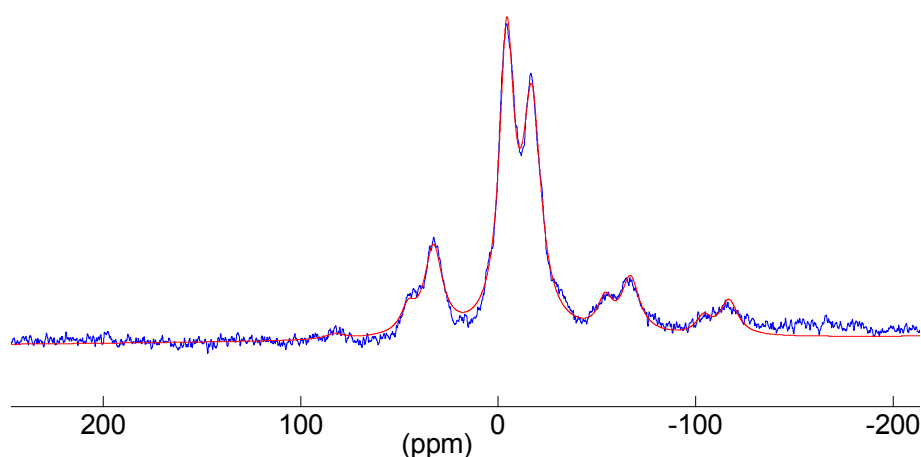
$$A = \frac{147.77}{0.9069} = 162.609 \text{ \AA}^2 \equiv \mathbf{1.14 \text{ SiOH}}$$

Therefore, density of P was **0.88 P/surface SiOH**, i.e. **0.6 P.nm<sup>-2</sup>**.

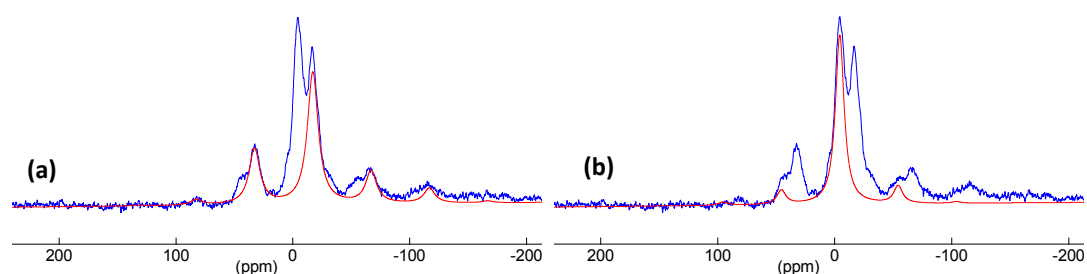
### Calculating tensors of P(OSiMe<sub>3</sub>)<sub>3</sub> compound on SiO<sub>2</sub>-(700)

P(OSiMe<sub>3</sub>)<sub>3</sub> was synthesised and grafted onto silica.

A <sup>31</sup>P-SSNMR of the grafted compound was performed, in the hope to characterize the structure(s) of P-containing surface species. (**Fig A8**)



First, the solid-state phosphorus-31 NMR spectrum display several signals, which can be decomposed into two very different sites with isotropic chemical shifts at -17.5 ppm and -1.9 ppm (**Fig A8** hereafter for the decomposition spectrum). The first site has an isotropic chemical shift  $\delta_{iso}$  of -1.9 ppm, and it is associated with the following chemical shift anisotropy (CSA) :  $\delta_{11} = \delta_{22} = 51.92$  ppm and  $\delta_{33} = -109.56$  ppm, which corresponds in the Haeberlen convention to an asymmetry  $\eta = 0$  and a reduced anisotropy of  $\delta = -107.66$  ppm. This corresponds thus to an axial symmetrical tensor. The CSA static spectra can then be simulated (**Table A2**)



**Fig A8.** Decomposition of the <sup>31</sup>P-SSNMR spectrum using DMFit (as before,  $I_b = 150$ Hz) of each peak: (a) -17.07ppm, (b) -4.29ppm

Table A2. Templating of the calculated tensors for the spectrum at 10kHz

Measured $\delta$ (ppm)	Calculated $\delta_{ii}$ (ppm)	Calculated $\Omega$ and $\kappa$	Tensor shape (no rotation)	Tensor symmetry
-17.07	$\delta_{11} = 47.8$ $\delta_{22} = 17.9$ $\delta_{33} = -116.9$	$\Omega = 164.65$ $\kappa = 0.64$		Asymmetrical
-4.29	$\delta_{11} = 36.9$ $\delta_{22} = 8.43$ $\delta_{33} = -59.18$	$\Omega = 96.06$ $\kappa = 0.43$		Asymmetrical

## Appendix 6

### Verification of calculations on model molecules

Optimisation of the B3LYP / IGLO-II NMR-calculations were undertaken as seen in the following

**Table A3.**

**Table A3. Comparison of the calculated an theoretical NMR shifts for model molecules**

<b>Tricoordinate P</b>	$\delta_{\text{exp}}$	$\delta_{\text{calc}}$	$\delta_{\text{exp}} - \delta_{\text{calc}}$
H <sub>3</sub> P	-266.1	-266.1	0.0
(Me) <sub>3</sub> P	-62.0	-61.2	-0.8
Me-POSS	84.8	72.3	12.5
(Et) <sub>3</sub> P	-20.0	-16.4	-3.6
(n-Propyl) <sub>3</sub> P	-33.0	-26.0	-7.0
(i-Propyl) <sub>3</sub> P	19.3	25.2	-5.9
(t-Bu) <sub>3</sub> P	63.0	102.4	-39.4
Ph <sub>3</sub> P	-5	0.7	-5.7
(MeO) <sub>3</sub> P	137.5	180.2	-42.7
(EtO) <sub>3</sub> P	139.8	178.0	-38.2
(PhO) <sub>3</sub> P	127.0	155.9	-28.9
(Me) <sub>2</sub> HP	-99.0	-100.5	1.5
(Me) <sub>2</sub> FP	186.0	192.0	-6.0
(Me) <sub>2</sub> CIP	96.5	117.4	-20.9
(Me)H <sub>2</sub> P	-163.5	-172.6	9.1
(Me)F <sub>2</sub> P	245.0	262.2	-17.2
(Me)Cl <sub>2</sub> P	192.0	247.3	-55.3
<b>Fourcoordinate P</b>			
(Me) <sub>3</sub> PO	36.0	10.2	25.8
(MeO) <sub>3</sub> PO	0.0	-5.4	5.4
(Et) <sub>3</sub> PO	48.0	25.5	22.5
(EtO) <sub>3</sub> PO	-6.0	-1.0	-5.0
(PhO) <sub>3</sub> PO	-18	-26.0	8.0
Me-POSS oxide	-45.0	-70.4	25.5
Diethylbenzylphosphonate on SiO <sub>2</sub>	26.2	4.5	21.7

A graph showing  $\delta_{\text{exp}}$  vs  $\delta_{\text{calc}}$  was drawn. (Fig A9)

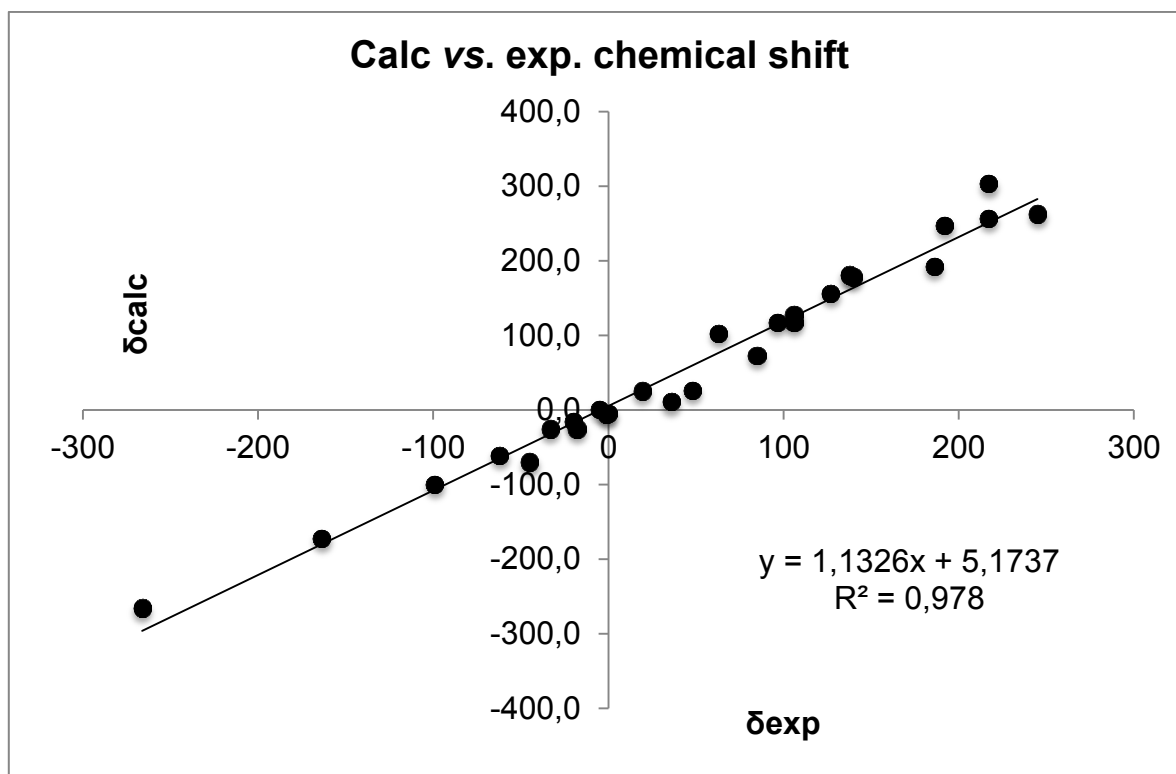


Fig A9. Verification of linear behaviour of  $\delta_{exp}$  vs  $\delta_{calc}$

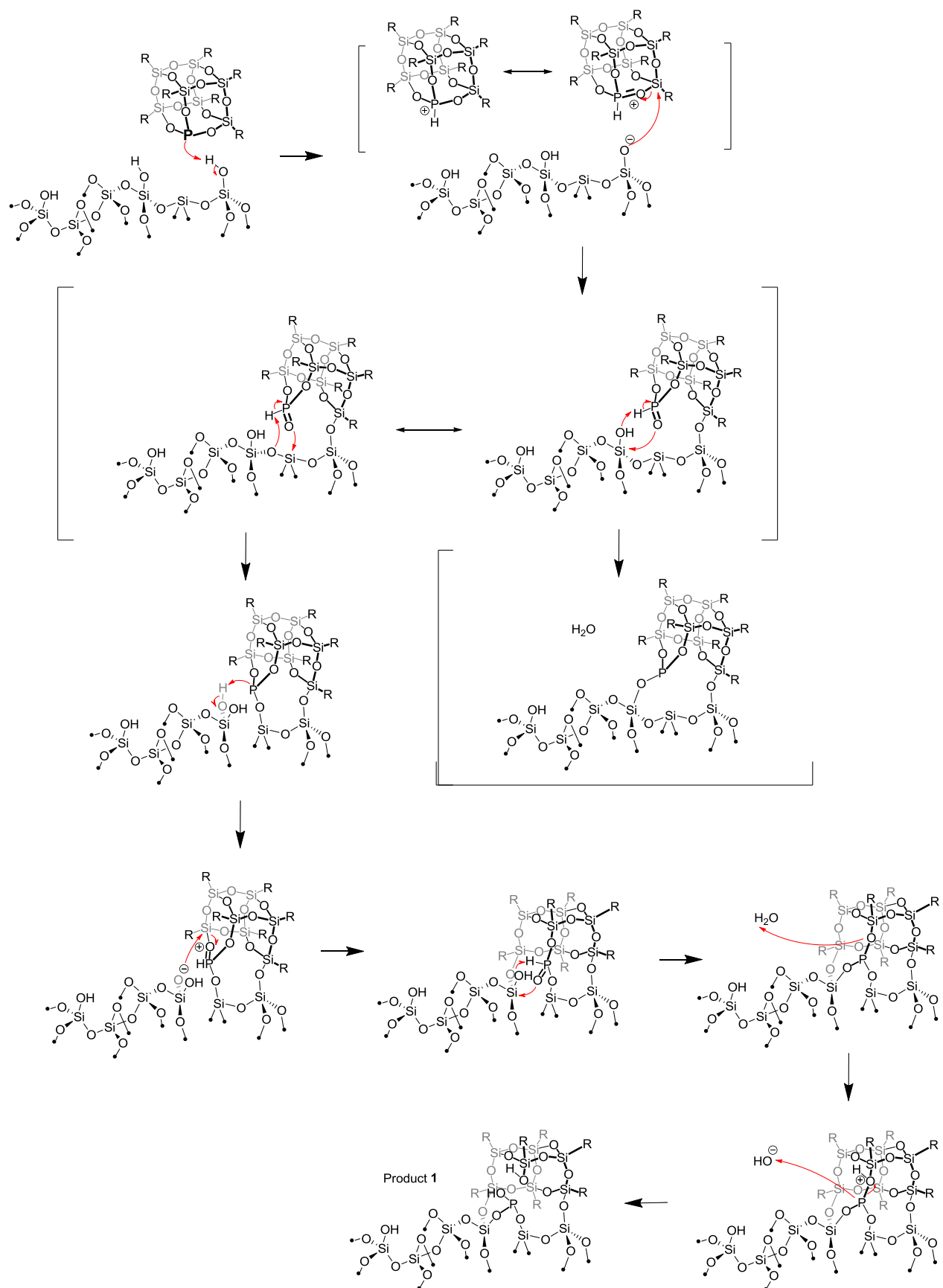


Fig A10. Proposed mechanism of POSS-P on SiO<sub>2</sub>(700)

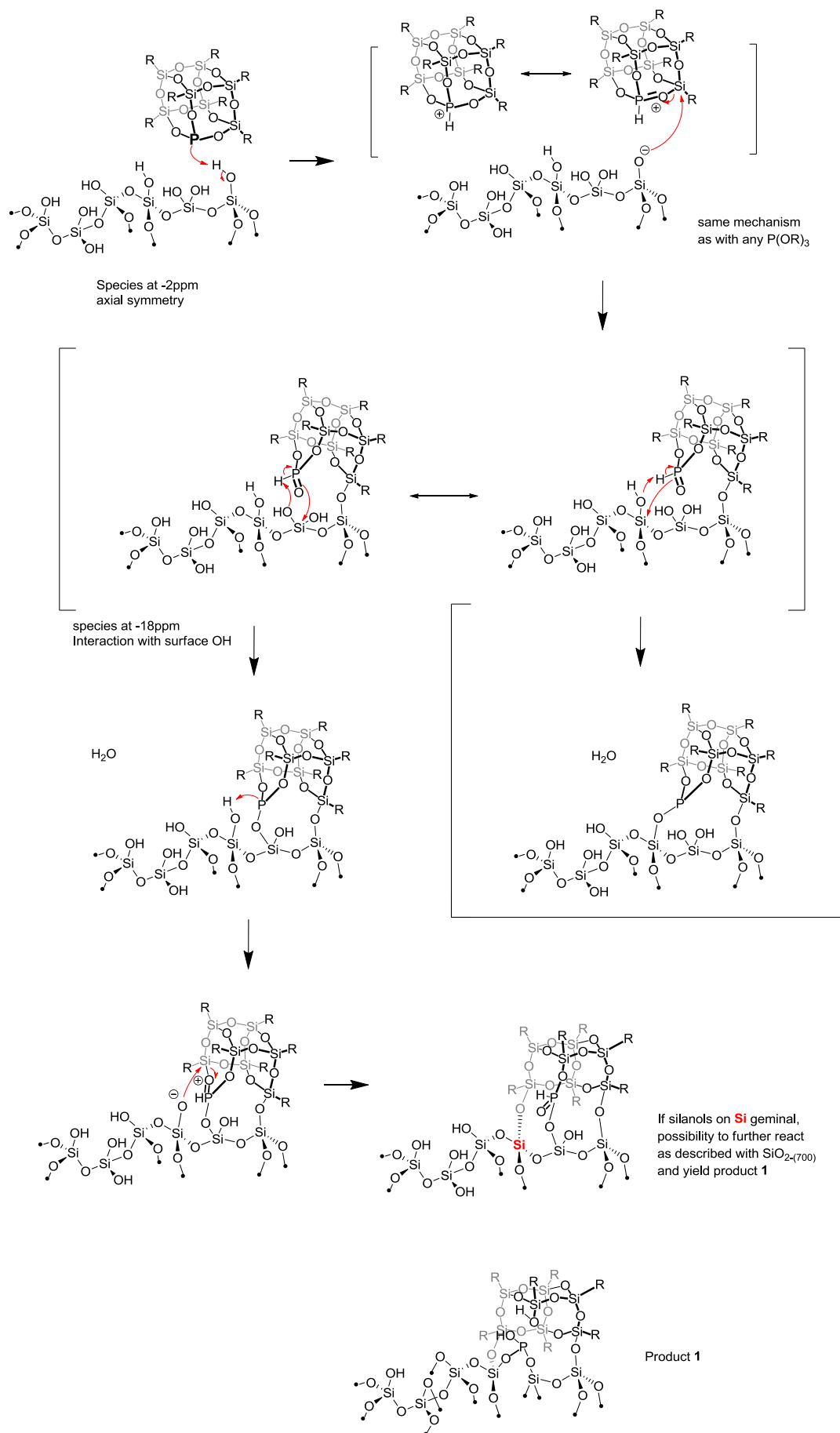


Fig A11. Proposed mechanism of POSS-P on  $SiO_{2(200)}$

### 1.1.Counting the grafted species by ICP-MS analysis

The measurement of metal impurities in silicon wafers is one of the key issues to be tackled in microelectronics as the purity of silicon surfaces are a *conditio sine qua non* for the efficient fabrication of silicon circuits. The importance of clean substrates in microelectronics has indeed been recognised from the early days of microelectronics in the 1950s.<sup>[18]</sup> For instance, severe degradation of generation lifetime, surface generation velocity<sup>[19]</sup> or recombination of charge carriers<sup>[20]</sup> may be some effects of such impurities.

#### 1.1.1. Removal of the oxide layer by VPD

First, the wafer was put in a Teflon reactor in order to have HF vapours condense on it and etch the complete oxide layer. (Vapour Phase Decomposition, VPD) In the VPD method, a silicon wafer is placed on a cooled Teflon support in a Teflon closed box containing a concentrated HF solution.<sup>[21-23]</sup> The cooled plate supporting the silicon wafer permits a condensation of the HF vapour onto the wafer which decomposes the oxide layer and reacts with any trace metal that is included in the latter. (Fig A12Fig ) In this case, the wafer was left for 20 min in the box before being taken out to be washed.

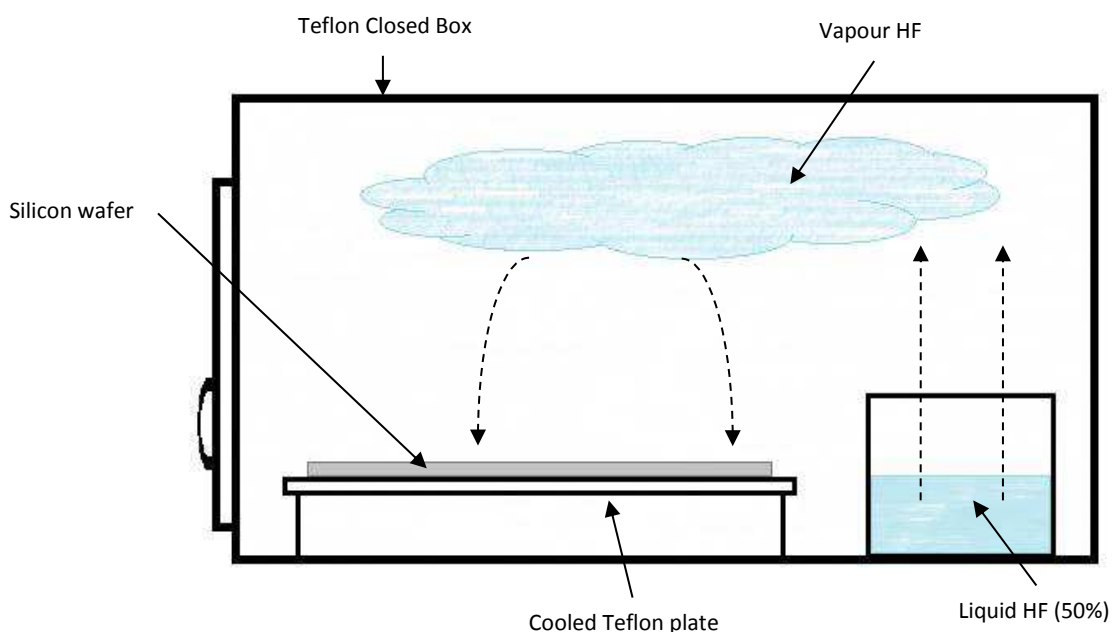


Fig A12. Schematic diagram of decomposition of the oxide of a silicon wafer by VPD method at room temperature



Once the oxide layer is decomposed by HF condensation, the wafer surface turns hydrophobic. Both the condensation and trace metals are collected by a 0.1 mL drop of a solution of HNO<sub>3</sub> 50% rolling on the surface and “sweeping it”.<sup>[24]</sup> All impurities present on the former oxide layer and therefore dissolved in the HF condensation on the wafer are then taken in the HNO<sub>3</sub> droplet.



**Fig A13.** Schematic diagram of the collection of impurities on the surface of silicon wafer by a HNO<sub>3</sub> droplet

The droplet is then dropped into a small Teflon vial and the volume is adjusted to reach a 1 mL solution. The solution is then ready to be analysed by ICP-MS.

### *1.1.2. Atom counting by ICP-MS*

---

The ICP-MS machinery that was used was an Agilent 7500cs ICP-MS system. This machine possesses an on-axis octopole ion guide operating in radio frequency (rf)-only mode, a modified ion lens system and shield torch technology. The rf-field has the effect of not separating masses as what is usually the case with a quadrupole but of focusing the ions that can then collide or react with molecules of the collision/reactant gas, typically hydrogen or helium. The ions were extracted by an omega lens-system, which is made of a dual extraction lens and an omega lens assembly for increased sensitivity, and with an off-axis design allowing a low background. Also, the off-axis design is a way to have photons and neutral compounds not enter the on-axis reaction cell chamber. The whole set-up permits an improved sensitivity.<sup>[25]</sup>

### Rapid Thermal Processing

Rapid Thermal Processing (or RTP) is a common processing in semiconductor manufacturing. In this process, the silicon wafer is heated up to high temperatures (sometimes above 1200°C) on a very short timescale, typically of a few seconds, or more. The cooling step needs to be performed slowly to prevent any break of the wafer due to thermal shock.

This process is widely used for dopant activation<sup>[26-28]</sup> or even chemical vapour deposition.<sup>[29, 30]</sup>

The annealing experiment was performed on a RTP-type oven (JIPELEC). The latter is a multizone oven with infrared lamps. The temperature is regulated by an optical pyrometer, i.e., the temperature is measured by the pyrometer that only receives the substrates infrared radiation. Such a technique allows a temperature measurement without any contact on the substrate, contrarily to thermocouples.

The whole process can be divided into several steps.

First, the atmosphere within the oven is pumped and to eliminate the air from the oven and work in a low-pressure N<sub>2</sub> atmosphere. (200 sccm) Then, the lamps start heating the oven up, at about 300°C until the temperature stabilizes and is detected by the pyrometer. Then, the annealing takes place, the oven is heated up to 985°C at a rate of 10°C.s<sup>-1</sup> and remains at this temperature for 4 s before getting to the actual chosen temperature of 1000°C for 1s. Then, the oven is cooled down until the temperature reaches the atmospheric temperature. As can be seen on **Fig A14** below, the whole process takes about 300s for the 1000°C RTP method.

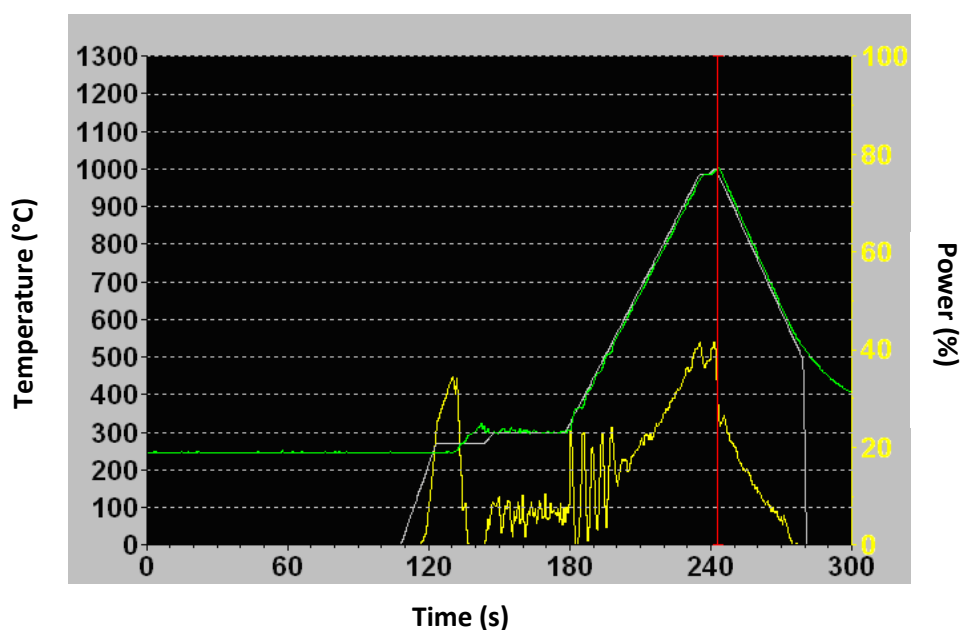


Fig A14. Example of a RTP annealing programme used for one of the wafers

On the graph above, one can see the good accordance between the setting (in grey), the detected temperature by the pyrometer (green) and the heating power (yellow). It is noteworthy that the pyrometer cannot detect temperatures below 270°C, hence the minimum on the corresponding graph from 0 to 120s, time during which the chamber is evacuated then refilled with a low pressure of N<sub>2</sub>. Also, the power needs stabilising at first, which explains the sinusoidal-like behaviour of the power setting at the beginning of the heating.

The same process is applied for any other temperature.

## Appendix 10

---

### Nanoprobe

---

The apparatus used at IEMN, Lille, is called Nanoprobe (Omicron Nanotechnology GmbH). In this system, STM tips that are contacted with a nanostructure are precisely controlled, thanks to a multiprobe scanning tunneling microscope (STM) that works under the supervision of a scanning electron microscope (SEM) in ultra-high vacuum (UHV). Therefore, structural analyses can be simultaneously obtained with the electrical characterisations of a semi-conductor. This device was first developed to characterise nanowires.

A software interface was designed to control the low current Source Measure Units (Keithley 2636) (**Fig A15-c**), to measure the resistivity of a nanostructure. These units are used for simple biasing (**Fig A15-d**) and also for electrical measurements with a specified number of probes (**Fig A15-e**).

**Fig A15. Pictures of the nanoprobe control system for STM and transport measurements (figure and caption reproduced from <sup>[31]</sup>)**

- (a)** Quadruple Nanonis SPM control system for independently operating each probe
- (b)** controller interface with four screens, one keyboard and one mouse allowing one operator to control the whole system
- (c)** switchbox-controlled source measure units (KEITHLEY 2636) for low current transport measurements
- (d)** zoom on the computer interface for the SMU. It is possible to directly set and read the current and voltage for simple biasing
- (e)** Transport measurement interface

## References

- [1] J. P. Dahl, C. J. Ballhausen, in *Advances in Quantum Chemistry, Vol. Volume 4* (Ed.: L. Per-Olov), Academic Press, **1968**, pp. 170.
- [2] T. E. Brown, H. E. LeMay, B. E. B. Murphy, P. Woodward, in *Chemistry: The Central Science, Eleventh Edition*, Prentice Hall, **2009**, p. 368.
- [3] D. B. Lawson, J. F. Harrison, *Journal of Chemical Education* **2005**, *82*, 1205.
- [4] J. W. Moore, W. G. Davies, R. W. Collins, *Chemistry*, McGraw-Hill, New York, **1978**.
- [5] R. L. DeKock, H. B. Gray, *Chemical Structure and Bonding*, University Science Books, **1989**.
- [6] B. Streetman, S. Banerjee, *Solid State of Electronic Devices*, Prentice Hall; 5th Edition, **1999**.
- [7] S. M. Sze, **2001**.
- [8] M. P. Surh, S. G. Louie, M. L. Cohen, *Phys. Rev. B* **1992**, *45*, 8239.
- [9] S. R. Elliott, *Physics of Amorphous Materials*, Longman Marlow, **1984**.
- [10] F. F. J. Caserio, J. J. Cavallo, R. I. Wagner, *Journal of Organic Chemistry* **1961**, *26*, 2157.
- [11] T. Riehm, G. De Paoli, H. Wadepohl, L. De Cola, L. H. Gade, *Chemical Communications* **2008**, 5348.
- [12] H. Michael L, *Journal of Non-Crystalline Solids* **1975**, *19*, 299.
- [13] C. Carteret, A. Burneau, *Physical Chemistry Chemical Physics* **2000**, *2*.
- [14] J. T. Burke, *Journal of Chemical Education* **1997**, *74*, 1213.
- [15] T. Kennedy, *Discrete and Computational Geometry* **2006**, 255.
- [16] H. Steinhaus, in *Mathematical Snapshots, 3rd ed.*, New York: Dover, **1999**, p. 202.
- [17] A. Thue, *Journal für die reine und angewandte Mathematik* **1909**, 284.
- [18] W. Kern, *Journal of The Electrochemical Society* **1990**, *137*, 1887.
- [19] K. Honda, T. Nakanishi, A. Ohsawa, N. Toyokura, *Journal of Applied Physics* **1987**, *62*, 1960.
- [20] S. A. McHugo, A. C. Thompson, G. Lambie, C. Flink, E. R. Weber, *Physica B: Condensed Matter* **1999**, *273-274*, 371.
- [21] S. H. Tan, *Nuclear Instruments and Methods in Physics Research Section B: Beam Interactions with Materials and Atoms* **1995**, *99*, 458.
- [22] M. B. Shabani, Y. Shiina, F. G. Kirscht, Y. Shimanuki, *Materials Science and Engineering: B* **2003**, *102*, 238.
- [23] H.-Y. Chung, Y.-H. Kim, H.-Y. Cho, B.-Y. Lee, H.-D. Yoo, S.-H. Lee, *Analytical Sciences* **2001**, *17*, 653.
- [24] E. Jones Ferrero, D. Posey, *Journal of Analytical Atomic Spectrometry* **2002**, *17*, 1194.
- [25] D. Profrock, P. Leonhard, S. Wilbur, A. Prange, *Journal of Analytical Atomic Spectrometry* **2004**, *19*, 623.
- [26] C.-m. Lin, C.-r. Yang, C.-m. Yang, Vol. US2010/0190274 A1, H01L21/02 B05C11/00 ed. (Ed.: U. P. T. Office), Taiwan Semiconductor Manufacturing Co., Ltd. (Hsin-Chu, TW) United States, **2010**.
- [27] K. Huet, C. Boniface, G. Fiscaro, F. Desse, N. Variam, Y. Erokhin, A. La Magna, V. Privitera, M. Schuhmacher, H. Besaucele, J. Venturing, in *17th IEEE Conference on Advanced Thermal Processing of Semiconductors RTP 2009*, IEEE, Albany Marriott, Albany, NY, **2009**.
- [28] C. Sabatier, M. Py, K. Huet, C. Boniface, J.-P. Barnes, L. Hutin, V. Delayer, D. Morel, M. Vinet, C. Le Royer, J. Venturini, K. Yckache, in *17th IEEE Conference on Advanced Thermal Processing of Semiconductors RTP 2009*, IEEE, Albany Marriott, Albany, NY, **2009**.
- [29] V. Murali, A. Wu, L. Dass, M. Frost, D. Fraser, J. Liao, J. Crowley, *Journal of Electronic Materials* **1989**, *18*, 731.
- [30] A. Theodoropoulou, R. A. Adomaitis, E. Zafiriou, *IEEE Transactions on Semiconductor Manufacturing* **1998**, *11*, 13.
- [31] M. Berthe, C. Durand, T. Xu, J. P. Nys, P. Caroff, B. Grandidier, in *Proceedings of the 1st AtMol European Workshop* (Ed.: C. Joachim), Springer-Verlag Berlin Heidelberg, Singapore, **2012**, pp. 107.

---

**RESUME** : Placement déterministe de dopants sur surfaces pour dispositifs ultimes

En raison de la miniaturisation des dispositifs pour semi-conducteurs, le caractère aléatoire de la distribution de dopants dans un dispositif devient un paramètre critique pour les performances de ce dernier. Le but de ce travail est de valider une stratégie de dopage du silicium par un positionnement contrôlé de molécules, alternatif aux implantations, afin de limiter la variabilité de la tension de seuil. Nous avons choisi de contrôler la densité des sites et le positionnement des dopants en combinant le contrôle de la densité des sites d'ancrage et l'utilisation de molécules à fort encombrement stérique. Ceci a été réalisé en étudiant dans un premier temps le greffage de bore sur les silanols de silice amorphe partiellement traitée en température, à partir de molécules porteuses présentant des ligands de différentes tailles et des symétries ; le modèle de greffage a pu être déterminé en utilisant différentes techniques analytiques (IR-DRIFT, multi-core SSRMN et analyses élémentaires). L'élimination des ligands par un traitement thermique a permis de réaliser la fixation du Bore sur la silice avec un rendement supérieur à 96%. Cette méthode a été transférée avec succès à des wafers de silicium recouverts de silice native. Le recuit à haute température permettant la redistribution du bore dans le silicium a été ensuite validé par l'analyse VPD-ICPMS de l'oxyde greffé couplées aux mesures de profil de dopant dans le silicium obtenues par TofSIMS. Ce traitement a conduit à définir un procédé optimal par greffage sur silice mince, donnant des concentrations de dopant dans le silicium équivalentes à celles rapportées par la littérature sur silicium désoxydé, et sans passivation additionnelle de silice pour éviter la volatilisation du Bore greffé. En effet, la taille des ligands permet de contrôler la volatilisation du bore pendant recuit. Les analyses électriques par spectroscopie à effet tunnel ont confirmé l'activation électrique du dopant apporté par greffage et diffusé dans le silicium.

---

**ABSTRACT**: Deterministic placement of doping atoms on silanol surfaces for ultimate devices

With the everlasting shrinking of semiconductor devices, the randomness of dopant distribution within a device becomes more likely to critically impact the performance of the latter. The aim of this work is to validate a silicon doping strategy through a controlled positioning of molecules in place of conventional implantations in order to limit the variability of the threshold tension. In contrast to previous works, doping atoms were directly grafted onto a thin silica layer and not onto a bare silicon surface. Here, we chose to control both site density and positioning by combining the control of site anchoring density and the use of sterically hindered molecules to yield a finely structured doped surface. This was carried out by first optimizing this approach by studying the grafting of boron compounds with ligands of various sizes and symmetries on the surface silanols of non-porous amorphous silica partially treated at high temperatures (700 °C) as a model system. This allowed obtaining a fully characterization of surface species through combined analytical techniques (IR-DRIFT, solid-state multi-core NMR and elemental analyses).

The ligands were then eliminated by a thermal treatment, yielding surface boronic acids characterized by IR-DRIFT and NMR with optimal density ( $> 96\%$ ,  $6.7 \cdot 10^{13}$  B.cm<sup>-2</sup>). This technology was then successfully transferred to silicon wafers covered with native silica as evidenced by ICPMS analyses of the grafted oxide layer removed in HF droplet (VPD). Subsequent high temperature annealing step without capping in order to trigger diffusion of boron was then validated on silicon wafers using ICPMS in HF-dipped oxide and in silicon by TofSIMS profile measurements. Such treatment led to a dopant concentration in the silicon matrix equivalent to that reported in the literature (e.g. direct grafting on silicon and cap during annealing). Electrical analyses by tunnel spectroscopy showed the efficiency of the annealing step and confirmed the dopant amount in the surface layer of the silicon wafer.

---

**DISCIPLINE**

Chimie

**MOTS-CLES**

Greffage, chimie de surface, bore, phosphore, RMN, micro-électronique, dopant, silicium, silice, spectroscopie, IR, DRIFT, ICPMS, TofSIMS, spectroscopie effet tunnel, diffusion

---

**Laboratoire de Chimie Organométallique de Surface**

C2P2 - CNRS UMR 5265 - CPE LYON